# CLOUD AND MACHINE LEARNING APPLICATIONS FOR HUMAN SILHOUETTE AND GAIT IMAGE FEATURES CLASSIFICATION METHODOLOGY IN SMART HOME

A thesis submitted to the Bharathidasan University in partial fulfilment of the requirements for the award of the Degree of

#### DOCTOR OF PHILOSOPHY IN COMPUTER SCIENCE

By

### Mrs. J. HIRUDHAYA MARY ASHA

(Ref.No: 6119/Ph.D. K3/Computer Science/Full Time/April 2018/Date: 04.04.2018)

Under the supervision and guidance of

Dr M. DURAIRAJ, M.C.A., Ph.D.

Assistant Professor & Research Supervisor School of Computer Science and Engineering, Bharathidasan University, Tiruchirappalli - 620 023



School of Computer Science and Engineering,

Bharathidasan University Tiruchirappalli - 620 023,

Tamil Nadu, India

January 2022

Mrs. J. Hirudhaya Mary Asha

Full-Time Research Scholar

Bharathidasan University

Tiruchirappalli – 620023

India.

**DECLARATION** 

I hereby declare that the work done in this thesis entitled, "CLOUD AND

MACHINE LEARNING APPLICATIONS FOR HUMAN SILHOUETTE

AND GAIT IMAGE FEATURES CLASSIFICATION METHODOLOGY

**IN SMART HOME**", is a research work done by me under the supervision and

guidance of Dr M. DURAIRAJ, M.C.A., PhD, Assistant Professor, School of

Computer Science and Engineering, Bharathidasan University, Tiruchirappalli

- 620 023, India.

I also declare that this work has not been done or submitted partially or

fully on the basis for the award of any other degree or diploma in any university.

Date:

Place: Tiruchirappalli

(J. Hirudhaya Mary Asha)

Dr M. DURAIRAJ

Research Supervisor and Assistant Professor Bharathidasan University

Tiruchirappalli - 620 023, India.

Mobile: +91 948 754 2202

Email: durairaj.bdu@gmail.com

**CERTIFICATE** 

This is to certify that the thesis entitled "CLOUD AND MACHINE

LEARNING APPLICATIONS FOR HUMAN SILHOUETTE AND GAIT

IMAGE FEATURES CLASSIFICATION METHODOLOGY IN SMART

HOME", is a bonafide work done by Mrs J. Hirudhaya Mary Asha (Ref. No:

6119/Ph.D.K3/Computer Science/Full-Time/April 2018/ Date:04.04.2018), in the

School of Computer Science, Applications and Engineering, Bharathidasan

University, Tiruchirappalli - 620 023, for the award of the degree of Doctor of

Philosophy in Computer Science, as a record of original work carried out by her

under my supervision and guidance.

The thesis has fulfilled all the requirements as per the regulations of the

University and in my opinion, the thesis has reached the standard required for

submission. The data included in this thesis have not been submitted to any other

University or Institute for the award of any degree or diploma.

Date:

Dr M. DURAIRAJ

Place: Tiruchirappalli

(Research Supervisor & Guide)

Dr M. DURAIRAJ

Research Supervisor and Assistant Professor Bharathidasan University

Tiruchirappalli -620 023, India.

Mobile: +91 948 754 2202

regard which has been attached here.

Email: durairaj.bdu@gmail.com

**CERTIFICATE OF PLAGIARISM-FREE** 

This is to certify that the thesis entitled, "CLOUD AND MACHINE LEARNING APPLICATIONS FOR HUMAN SILHOUETTE AND GAIT IMAGE FEATURES CLASSIFICATION METHODOLOGY IN SMART HOME", submitted by Mrs J. Hirudhaya Mary Asha (Ref. No: 6119/ Ph.D.K3/Computer Science /Full-Time /April 2018 /Date:04.04.2018), in the School of Computer Science, Applications and Engineering, Bharathidasan University, Tiruchirappalli - 620 023, the report was checked for plagiarismfree using Ouriginal tool and found 0% of the content from other sources. The Librarian and Head, Department of Library and Information Science, Bharathidasan University, Tiruchirappalli - 620 024, has also reported in this

Date: Dr M. DURAIRAJ

**Place: Tiruchirappalli** (Research Supervisor & Guide)



#### **Document Information**

J. HIRUDHAYA MARY ASHA.pdf (D125799624) Analyzed document

> 2022-01-22T11:48:00.0000000 Submitted

Submitted by Srinivasa ragavan S Submitter email bdulib@gmail.com

> Similarity 0%

Analysis address bdulib.bdu@analysis.urkund.com

#### Sources included in the report

URL: https://www.math.toronto.edu/undergrad/projects-undergrad/Project01.pdf Fetched: 2022-01-22T11:48:06.2230000

3

Acknowledgements

### **ACKNOWLEDGEMENT**

Showing my thankfulness is not a formality at this juncture. It is the right time to think and thank all the people who stood behind me to make me step forward. I am very much pleased and blessed to do my research under the guidance of Dr M. Durairaj, Research supervisor and Assistant Professor, School of Computer Science, Engineering and Applications. His enlightening words inspires me to finish my work in time.

I am also grateful to Dr M. Selvam, Honourable Vice-Chancellor and Dr Gopinath Ganapathy, Registrar of Bharathidasan University, and Dr M. Balamurugan, Professor and Head, Department of Computer Science and all the faculty members of the Computer Science department, Bharathidasan University, Tiruchirappalli for the opportunity given to do my research work.

I also extend my sincere thanks to the members of the Doctoral Committee members Dr B. Smitha Evelin Zoraida, Assistant Professor, School of Computer Science, Applications and Engineering, Bharathidasan University and Dr P. Thanga Raju, Assistant Professor, Department of Computer Science, Bishop Heber College, for their guidance and suggestions during the research journey.

My gratitude and salutes go to my seniors Dr A. Alagu Karthikeyan, Dr T.S. Poorna Priya and Dr S. Alonsiya, for their timely replies and comments. I continue my thankfulness to My paternal and maternal family members for their love and respect towards my passion for studies.

I also extend my cheers and heartful thanks to my kids, J. Stefy Joashna and J. Stany Jherson who wiped my tears when I was felt broken. My faithful love and sincere

thanks to My Financier, My husband Adv. M. John Paul M.A., L.L.B for his love, encouragement and motivation in my life.

More than all, I thank God Almighty, for His blessings and strength showered upon me during all the endeavours of the research.

J. Hirudhaya Mary Asha



S.No	TABLE OF CONTENTS	PAGE No
	List of Tables	
	List of Figures	
	List of Abbreviations	
	Abstract	1
CHAPTER 1	INTRODUCTION	4
1.1	Research Context and Motivation	4
1.2	Existing system	4
1.3	Proposed System	5
CHAPTER 2	RELATED WORKS	13
2.1	Introduction	13
2.2	Need for gait recognition	13
2.3	Review of literature	14
2.4	Summary	27
CHAPTER 3	IMAGE COMPRESSION AND ENHANCEMENT	29
	FOR INCREASING QUALITY OF THE IMAGE	
3.1	Introduction	29
3.2	Image Compression	30
	3.2.1 Chrominance components – a sub-sampling	30
	process	
	3.2.2 Block Splitting	31
	3.2.3 Discrete Cosine Transformation	31
	3.2.4 CLAHE Transformation on Images	32
	3.2.5 Pseudocode for EQI-AC Algorithm for Image	33
	Compression with Enhanced Quality	
3.3	Experimental results	35

3.4	Summary	41
CHAPTER 4	THRESHOLDING OF SILHOUETTE FROM THE	43
	BACKGROUND USING BINARIZATION AND	
	TOP-BOTTOM AGGLOMERATIVE	
	CLUSTERING HIERARCHY (BTTBACH)	
4.1	Introduction	43
4.2	Preliminaries of Image Thresholding work	45
	4.2.1 Binarization thresholding	45
	4.2.2 Top-Bottom Agglomerative Clustering Hierarchy	47
	(TBACH)	
	4.2.3 Improved Fuzzy C-means Clustering	49
4.3	Performance Metrics	50
4.4	Summary	54
CHAPTER 5	SILHOUETTE EXTRACTION AND FEATURES	56
	CLASSIFICATION USING NEAREST SUPPORT	
	CLASSIFICATION USING NEAREST SUITORI	
	FEATURE VECTOR	
5.1		56
5.1	FEATURE VECTOR Introduction	56 57
	FEATURE VECTOR Introduction	
	FEATURE VECTOR  Introduction  Image Averaging or Silhouette Detection Using the	
	FEATURE VECTOR  Introduction  Image Averaging or Silhouette Detection Using the Frame Difference method	57
	FEATURE VECTOR  Introduction  Image Averaging or Silhouette Detection Using the Frame Difference method  5.2.1 Pseudocode for Frame Difference Average Image	57
5.2	FEATURE VECTOR  Introduction  Image Averaging or Silhouette Detection Using the Frame Difference method  5.2.1 Pseudocode for Frame Difference Average Image (FDAI) function denoted by F <sub>d</sub>	57 57
5.2	Introduction  Image Averaging or Silhouette Detection Using the Frame Difference method  5.2.1 Pseudocode for Frame Difference Average Image (FDAI) function denoted by F <sub>d</sub> Features detected from FDAI Silhouette	57 57 59
5.2	Introduction Image Averaging or Silhouette Detection Using the Frame Difference method 5.2.1 Pseudocode for Frame Difference Average Image (FDAI) function denoted by F <sub>d</sub> Features detected from FDAI Silhouette 5.3.1 Area	57 57 59 60
5.2	Introduction Image Averaging or Silhouette Detection Using the Frame Difference method 5.2.1 Pseudocode for Frame Difference Average Image (FDAI) function denoted by F <sub>d</sub> Features detected from FDAI Silhouette 5.3.1 Area 5.3.2 Bounding box	57 57 59 60 60
5.2	Introduction  Image Averaging or Silhouette Detection Using the Frame Difference method  5.2.1 Pseudocode for Frame Difference Average Image (FDAI) function denoted by F <sub>d</sub> Features detected from FDAI Silhouette  5.3.1 Area  5.3.2 Bounding box  5.3.3 Eccentricity	57 57 59 60 60 60
5.2	Introduction Image Averaging or Silhouette Detection Using the Frame Difference method 5.2.1 Pseudocode for Frame Difference Average Image (FDAI) function denoted by F <sub>d</sub> Features detected from FDAI Silhouette 5.3.1 Area 5.3.2 Bounding box 5.3.3 Eccentricity 5.3.4 Euler Number	57 57 59 60 60 60

	5.3.8 Solidity	62
5.4	Feature Extraction using Gray Level Co-Variance	66
	Matrix	
	5.4.1 Pseudocode for Best Feature Selection and	66
	Optimization using GLCMPSO	
5.5	Classification of Optimized Feature Subset	68
	5.5.1 Pseudocode for Nearest Support Feature Vector	70
	(NSFV) algorithm	
5.6	Summary	72
CHAPTER 6	ACCUMULATED GAIT ENERGY IMAGE (AGEI)	73
	FEATURE OPTIMIZATION, SELECTION AND	
	CLASSIFICATION USING BAYESIAN FILTERS	
6.1	Introduction	73
6.2	The preliminaries of the AGEI Feature Classification	76
	6.2.1 Infrared Sensors	76
	6.2.2 RGB-depth Camera	76
	6.2.3 Gait Energy Image – GEI (real)	77
	6.2.4 Augmented Gait energy Image-AGEI (artificial)	78
6.3	Feature representation in AGEI using the Spatial	78
	Dependence Matrix of the Pixels	
	6.3.1 Pseudocode for Feature representation in AGEI	79
6.4	Feature Optimization and Feature Prediction using CSA	83
	and PPFT	
	6.4.1 Pseudocode for Feature Optimization and Feature	83
	Prediction	
6.5	Classification of the Optimized Features	87
	6.5.1 Support Vector Machine (SVM)	87
	6.5.2 K-Nearest Neighbor (KNN)	87
	6.5.3 Ada Boost (AB)	88
	6.5.4 Random Forest (RF)	88

	6.5.5 Naive Bayes (NB)	88
	6.5.6 Quadrant Discriminant Analysis (QDA)	89
	6.5.7 Pseudocode for Classification of Predicted	89
	Features Using NB algorithm	
6.6	DBNetwork Layers	92
	6.6.1 Pseudocode for RBM training phase	93
	6.6.2 Pseudocode for DBNetwork training	94
6.7	Summary	97
CHAPTER 7	FUZZY PROBABILITY DECISION ON FPR AND	98
	FRR FOR HUMAN RECOGNITION	
7.1	Introduction	98
7.2	Preliminaries of Fuzzy probability	98
7.3	Selection of Best Match Score based on PDF	99
7.4	XGBoost (Extreme Gradient Boosting)	102
	7.4.1 K fold validation	106
7.5	Summary	106
CHAPTER 8	THE ENCRYPTION AND DECRYPTION OF THE	107
	SILHOUETTE AND ACCUMULATED GAIT	
	ENERGY IMAGE USING A CHAOTIC	
	ALGORITHM- P-FIBONACCI EXCLUSIVE OR-	
	DISCRETE COSINE TRANSFORM	
8.1	Introduction	107
8.2	P-Fibonacci transform function	108
	8.2.1 Proof: The Fibonacci sequence is a recursive	108
	function	
	8.2.2 Proof: Fibonacci sequence generator is formed by	110
	Fn	
	8.2.3 Proof: Golden Spiral Ratio is continued	110
8.3		111

	8.3.1 Pseudocode for Encryption using XORDCT algorithm	115
	8.3.2 Pseudocode for Decryption using Inverse-	115
	XORDCT algorithm	113
8.4	Statistical Result Analysis	116
0.4	, and the second	
	8.4.1 Net Pixel Change Ratio (NPCR)	116
	8.4.2 Unified Average Changing Intensity (UACI)	117
	8.4.3 Correlation Coefficient Analysis	117
	8.4.4 PSNR and MSE analysis	119
8.5	Summary	119
CHAPTER 9	RESULTS AND DISCUSSION	120
9.1	Introduction	120
9.2	Pre-processing Phase – Compression and Enhancing	121
9.3	Thresholding the Compressed and Enhanced Image	125
9.4	Silhouette Feature extraction and Classification using	129
	Nearest Support Feature Vector	
	9.4.1 ROC (Receiver Operating Characteristic) curve	130
	9.4.2 DET (Detection Error Trade-off) graph	130
9.5	Feature Extraction from Accumulated Gait Energy	134
	Image (AGEI)	
9.6	Comparison of NSFV and NBDBNetwork for Feature	142
	Classification	
9.7	XGBoost Strength for NBDBNetwork	143
9.8	Encryption and Decryption of Input Images for	143
	Protecting from Unauthorized Access	
9.9	Summary	146
CHAPTER 10	CONCLUSION AND FUTURE ENHANCEMENTS	147
	References	150

CNO	TEADLE C	DACE NO.
Table 3.1	TABLES  The compression table shows the name of the rayy image.	PAGE NO
Table 5.1	The compression table shows the name of the raw image,	36
	its actual size, the compressed image with its shrunk file	
	size	
Table 3.2	The PSNR difference between the compressed image and	38
	enhanced image	
Table 3.3	The structure similarity index measure of the compressed	39
	image and Enhanced image	
Table 4.1	The image name table	52
Table 5.1	The texture-based features extracted from the silhouette	67
	using GLCM	
Table 5.2	Optimized features list using PSO	69
Table 5.3	The metrics used for evaluating the performance of the	71
	optimized silhouette feature classification algorithms	
Table 6.1	Feature description values of the walking gait calculated	81
	using the spatial dependency matrix	
Table 6.2	Spatio-temporal based AGEI Features	85
Table 6.3	The features extracted using the RFE algorithm from	86
	AGEI after optimization	
Table 6.4	The metrics used for evaluating the predicted AGEI	91
	features classification algorithms	
Table 6.5	The t-test and p-value for the classified AGEI features	96
	were calculated based on the Conditional Probability	
	Value (CPV) of the walking speed	
Table 7.1	EP, SSIM, PSNR, CQM measures of the compared	105
	methods used for Gait classification	
Table 9.1	The Structure Similarity Index difference between the	122
	compared methods EQIAC, SIFT and DCT	
L		<u>1</u>

Table 9.2	The PSNR difference between the compared methods	123
	EQIAC, SIFT and DCT	
Table 9.3	CDR, FAR, FRR measure comparison for image1	127
Table 9.4	CDR, FAR, FRR measure comparison for image2	127
Table 9.5	CDR, FAR, FRR measure comparison for image3	128
Table 9.6	CDR, FAR, FRR measure comparison for image4	128
Table 9.7	Jaccard Index and Dice Coefficient of the given images	129
	thresholded into 10 clusters using BTTBACH method	
Table 9.8	The Precision, Accuracy and F-rate metrics calculated for	131
	evaluating the silhouette feature classifiers	
Table 9.9	The Precision, Recall, Accuracy and F-rate metrics	135
	calculated to differentiate the AGEI classifiers	
Table 9.10	The Accuracy value of the AGEI Feature classifiers	136
Table 9.11	The Mean Absolute Error of the AGEI Feature classifiers	137
Table 9.12	The Root Relative Squared Error (RRSE) of the AGEI	137
	Feature classifiers	
Table 9.13	The Relative Absolute Error of the AGEI Feature	138
	classifiers	
Table 9.14	The Relative Mean Squared Error of the AGEI Feature	138
	classifiers	
Table 9.15	Performance Comparison of NSFV and NBDBNetwork	142
Table 9.16	The overall performance between the NBDBNetwork	143
	with Fuzzy Probability and XGBoost	
Table 9.17	The correlational coefficient of the encrypted image and	144
	decrypted image	
Table 9.18	The NPCR, UACI, MSE and PSNR of the encrypted	145
	image	

S.NO	FIGURES	PAGE NO
Fig. 1.1	Conceptual Framework of the Cloud and Machine	7
	Learning Applications for Human Silhouette and Gait	
	Image Features Classification Methodology in Smart	
	Home	
Fig. 1.2	Silhouette extracted using BTTBACH method from the	8
	actual image	
Fig. 1.3	a) Selected phase of the gait cycle	8
	b) Silhouette for the selected phase	
	c) Augmented silhouette image	
	d) GEI for the augmented image	
Fig. 1.4	Gait energy image with the Walking frequency and phase	8
Fig. 3.1	Clip limit of the histogram value	33
Fig. 3.2	Shows how the image is compressed from 182.9 kb size	37
	to 41.3 kb size	
Fig. 3.3	Image Compressed and Enhanced using EQI-AC	40
Fig. 4.1	Steps involved in Binary Thresholding Top Bottom	48
	Agglomerative Clustering Hierarchy (BTTBACH)	
Fig. 4.2	a) Input images	53
	b) Histogram of the Input images	
	c) Top Bottom Binary Thresholded Image	
Fig. 5.1	Block diagram of proposed work	58
Fig. 5.2	Angles marked on the Silhouettes for segmenting	61
Fig. 5.3	The model silhouettes with different dresses	63
Fig. 5.4	Model Image and its corresponding Silhouettes of the	64
	captured video	
Fig. 5.5	Covariance matrix saved in GLCM table	65
Fig. 6.1	The gait cycle with multiple phases	75

Fig. 6.2	The gait energy image with the Walking frequency and	75
115. 0.2		, 5
TI (2	phase	
Fig. 6.3	Angle to be noted on the Accumulated Gait Energy	80
	Image (AGEI)	
Fig. 6.4	Spatial Dependence Matrix of the GEI and the artificial	82
	AGEI calculated based on the angles noted in Fig.3.	
Fig. 7.1	Probability of Misidentification	101
Fig. 7.2	show the Probability of Correct Identification	101
a and b		
Fig. 7.3	show the Probability of Misidentification by the integral	103
a and b	of $f(x)FPR(x)$	
Fig. 8.1	The golden spiral representation of an equation	109
Fig. 8.2	Golden ratio spiral representation of the taken inputs	112
Fig. 8.3	Flowchart for XORDCT method	115
Fig. 8.4	a) The compressed image	118
	b) The encrypted image	
	c) Histogram of the compressed image	
	d) Histogram of the encrypted image	
Fig. 9.1	Image compressed with JPEG standards and CLAHE	121
Fig. 9.2	The graph for the SSIM difference between EQIAC,	124
	SIFT, DCT has drawn using Table 9.1	
Fig. 9.3	The graph for the PSNR difference between EQIAC,	124
	SIFT, DCT has drawn using Table 9.2	
Fig. 9.4	The foreground and background difference of the input	126
	image	
Fig. 9.5	Segmentation of image1 using Binarization Thresholding	126
	and Top-Bottom Agglomerative Clustering Hierarchy	
	(BTTBACH) algorithm	

Fig. 9.6	The clustered chart shows the F-rate performance of the	132
	NEAREST SUPPORT FEATURE VECTOR (NSFV)	
	classifier compared with SVM and KNN methods	
Fig. 9.7	The performance of the NEAREST SUPPORT	133
	FEATURE VECTOR (NSFV) classifier through the	
	ROC curve	
Fig. 9.8	The Performance of Nearest Support Feature Vector	133
	(NSFV) classifier through DET graph	
Fig. 9.9	The accuracy graph of the AGEI Feature classifier	139
Fig. 9.10	The Mean Absolute error graph of the AGEI Feature	140
	classifier	
Fig. 9.11	The Relative mean squared error graph of the AGEI	140
	Feature classifier	
Fig. 9.12	The Root relative squared error graph of the AGEI	141
	Feature classifier	
Fig. 9.13	The Relative absolute error graph of the AGEI Feature	141
	classifier	

# LIST OF ABBREVIATIONS

AB	Ada Boost
AGEI	Augmented Gait energy Image
AHE	Adaptive Histogram Equalization
BPN	Back Propagation Neural Network
ВТТВАСН	Binary Thresholding Top Bottom Agglomerative Clustering
	Hierarchy
CD	Cadence
CDF	Cumulative Distribution Function
CDR	Cumulative Distance Ratio
CLAHE	Contrast Limited AHE
CPV	Conditional Probability Value
CSA	Crow Search Algorithm
DBNetwork	Dynamic Bayesian Network
DCT	Discrete Cosine Transform
DET	Detection Error Trade-off graph
EQIAC	Enhanced Quality Image After Compression
EX-OR	Exclusive OR
FAR	False Accept Ratio

FDAI	Frame Difference Average Image method
FRR	False Reject Ratio
GEI	Gait Energy Image
GLCM	Gray Level Co-Variance matrix
IOT	Internet of things
JPEG	Joint Photographic Experts Group
KNN	K-Nearest Neighbor
KSVM	K-Nearest Support Vector Machine
LAJA	Left ankle joint angle
LKJA	Left knee joint angle
MSE	Mean Square Error
NB	Naive Bayes Algorithm
NLPR	National Laboratory of Pattern Recognition
NPCR	Net Pixel Change Ratio
NSFV	Nearest Support Feature Vector
PPFT	Principal Polynomial Feature Transform ().
PSNR	Peak signal noise ratio
PSO	Particle Swarm Optimization
QDA	Quadrant Discriminant Analysis
RAJA	Right ankle joint angle
RBM	Restricted Boltzmann Machine
RF	RANDOM FOREST

RFE	Recursive Feature Elimination
RKJA	Right knee joint angle
ROC	Receiver operating Characteristic curve
SIFT	Scale In Variant Feature Transform
SLL	Stride length left
SLR	Stride length right
SSIM	Structure Similarity Index Measure
SVM	Support Vector Machine
ТВАСН	Top-Bottom Hierarchical Agglomerative Clustering
UACI	Unified Average Changing Intensity
WT	Wavelet Transform
XGBoost	Extreme Gradient Boosting

#### **ABSTRACT**

Smart Home is an environment built with ensured security and luxury to the residents. The locator would feel comfortable and convenient by living there. Using smart technology, the monitoring system is engineered with the smart home to ensure security. In order, to enhance security, the human entering into the smart homes must be analysed at distance. Identification of every individual entering into smart homes with analysis gives more predictions about the entering human. Using the Gait, the human can be identified at a distant location without the human's co-operation. But, in Face, Iris and Fingerprints recognition the human may try to fool the monitoring systems with some attachments or else needs co-operation. The proposed work was aimed to construct a Cloud and Machine Learning Applications for Human Silhouette and Gait Image Features Classification Methodology in Smart Home.

To analyse the human, the gait or walking pattern of the human recorded using the RGB-depth camera ensured the arrival of the human by the grid eye sensor setup fixed in the smart home premises. The Gait Energy Image (GEI) was the image that collate both the frequency and phase of the walking state. Consider the situation, if a human carries properties like bag (shoulder bag, back bag), raincoat, cap while entering or the human wore dresses like a dhoti, saree etc., shows the different silhouette and hence the features extracted from the silhouettes would also differ. Thus, the varied features may slow down the recognition process. So, the recognition of the human is done in 2 scenarios to find the best one out of the two. The proposed work was established in 6 layers. They are, 1) Image Compression and Enhancement for increasing quality of image, 2) Thresholding of silhouette from the background using

Binarization and Top-bottom Agglomerative Clustering Hierarchy (BTTBACH), 3) Silhouette feature extraction and Classification using Nearest Support Feature Vector, 4) Accumulated Gait Energy Image (AGEI) feature extraction and Classification using NBDBNetwork, 5) Fuzzy probability decision on FPR and FRR for Human Recognition, and 6) The Encryption and Decryption of the Silhouette and AGEI using a Chaotic algorithm P-Fibonacci Exclusive OR-Discrete Cosine Transform (XORDCT).

In the first scenario, the GEI sliced from the captured videos are averaged using the Frame Differencing method and converted as Frame Difference Average Image (FDAI). From the FDAI, the Silhouettes are the black pixel representation considered for feature extraction, from that the texture-based (appearance) features are extracted using Grey Level Covariance Matrix (GLCM) and got 33 features as output. The Particle Swarm Optimization (PSO) algorithm filtered 20 features which were lesser than the compared Chi-Square test and Unsupervised Learning method. The algorithms like SVM, KNN, Nearest Support Feature Vector (NSFV) methods are employed to classify the optimized features based on True Positive (TP), True Negative (TN), False Positive (FP), False Negative (FN) values. From the experiment, NSFV produces 95% of accuracy than the compared classifiers.

In the second scenario, the features extracted from the Accumulated Gait Energy Image (AGEI) are considered. It is the coupling of normal GEI and augmented GEI. The augmentation method was called to fit the captured image for the extraction process. Consider a situation, if a human walking position is not recorded or else the human may be limping or else the human wore dresses like saree, dhoti, nighty etc., There were 23 Spatio-temporal features from the AGEI are captured using Recursive

Feature Elimination (RFE) based on the spatial dependence matrix of the feature pixel. The Crow-Search Optimization Algorithm (CSA) optimize the captured features and 12 new features are predicted from the optimized features using Principal Polynomial Feature Transform (PPFT). Thus, the predicted features give more information about the dataset and are used for classification. The classifier algorithms like SVM, KNN, QDA, AB, RF, NB are used for classification, and the Naive Bayes (NB) algorithm provides higher accuracy than the comparison.

The Dynamic Bayesian Network (DBNetwork) model was trained to classify the gait with the Conditional Probability Value (CPV) of the features. The Naive Bayes DBNetwork (NBDBNetwork) model with PPFT shows greater accuracy than the comparison. The Fuzzy probability method is followed to approve the human as Authentic (genuine user) or Reject (impostor user) based on the features matching score level. This level is also known as confidence level or measurement level. Matching score level is a measure of similarity between features derived from an incoming sample and a stored template. Thus the Naive Bayes DBNetwork was deployed with Fuzzy probability using XGBoost (Extreme Gradient Boosting) wrapper class for human recognition. The wrapper class strengthen the model with its gradient architecture.

As a security measure, the matrix representation of the Silhouette image feature extracted using Gray Level Co-Variance Matrix (GLCM) and the matrix representation of the Accumulated Gait Energy Image (AGEI) feature extracted using RFE Spatial dependency matrix is encrypted using P-Fibonacci XORDCT transform with masking coefficients and decrypted by applying the inverse transform for ensuring safety.

Research Supervisor

# **CHAPTER 1**

#### **INTRODUCTION**

#### 1.1 Research Context and Motivation

Smart Home is an environment built with ensured security and luxury to the residents. Thus, the locator feels comfortable and convenient by living there. Using smart technology, the environment is engineered as a monitoring system to ensure security. The Internet of Things (IoT) is a new platform that makes it impracticable into practicable. It can process a large amount of data with fewer human interventions [1]-[6]. Apartments like the gated community organised with various advantages and Amenities, comparatively higher than the individual houses in the streets. So, people preferred apartments. Like advantages, there are some disadvantages in the gated community, as a coin has two sides. Two-layer security must be provided for the apartments. One type of security is provided by security guards and the second type of security must be provided by the technology [7]-[10]. So, securing the apartments by the security guards is not only enough to avoid crimes in the living area, identification of every individual entering into the apartments is necessary. Biometric surveillance systems with gait analysis give more predictions about the entering human. Using the gait, the human can be identified at a distant location without human co-operation [11]-[12]. But, in Face, Iris and Fingerprints recognition the human has to co-operate and may try to fool the monitoring systems with some attachments. Finally, the identification of a human with his gait is useful and knowledgeable [13].

#### 1.2 Existing system

The human can be identified using biometric features like Face, Iris, Fingerprints, Speech, Gait etc. But in those types of recognition, the monitoring system

needs the full-fledged cooperation of the human need to be identified [14]-[18]. In iris recognition, the human can fool the system by wearing contact lenses, spectacles, coolers etc. In face recognition, make-ups, the injuries or the newly arrived moles or warts can decrease the accuracy level. In fingerprint recognition, the human can hide imprints with gloves or any solutions. By the gait recognition, the human can be identified at a distant location, but the carrying conditions like bags, overcoats, dresses they wore like saree, dhoti, nighty, shoes or the leg injuries will change the gait shape and decrease the recognition rate [19]-[22].

# 1.3 Proposed System

In the proposed work, the human can be identified by combining the gait features and face image. Every human has a unique style of walking and walking speed. For this research work, some initial hardware setups are experimented and trained using the National Laboratory of Pattern Recognition (NLPR) gait database CASIA gait database and celebrity images. Human recognition for smart home safety is done in a hierarchical process. They are,

The gait profile is captured through the Grid-eye sensor fixed with RGB-depth virtual camera fixed at the main entrance of the apartments, and ensure that no one can enter without capturing [21]-[39]. The gait profile is nothing but the mobility of the human captured within a certain period. The Grid-eye Infrared thermopile sensor is used to detect humans. The silicon lens is attached with a sensor for image formation. It detects humans using infrared radiation. Grid-eye extends its view to 60° in both horizontal and vertical directions up to 5 meters. Grid-eye sensor and RGB-depth camera are used to capture the gait based on the movement and estimate the 3-D view

of the human body joints. If anybody walks before the camera, the infrared radiations detect the human and wake up the camera to capture the pose depth. The camera is placed at 1 meter from the floor distance to capture all parts of the body [31]-[40]. The gait cycle (gait profile) consists of human gait details captured in the 11 views of focus.

The captured gait image or gait profile video is compressed to get non-redundant information called image compression. After compression, the image gains high visual quality with a reduced bit rate compared to the raw image. In the Internet of Things (IoT) environment, efficient transmission and storage of images are required for security purposes [41]-[50]. Block Splitting (BS) and Discrete Cosine Transform (DCT) is applied initially on the raw images to reduce the actual bit rate which minimizes the Mean Square Error (MSE) and the noise in the near-constant region. In this paper, EQI-AC (Enhanced Quality Image After Compression) algorithm is used to enhance contrast, intensity and brightness of the compressed image, which is balanced, for visualization.

The compressed images or videos are shielded from disrupting while transporting them in a shared link for security reasons. The security levels are increased by chaotic methods [51]-[58]. The input image is scrambled in a pixel-by-pixel limit using P-Fibonacci XOR transform with the masking coefficients and Discrete Cosine Transform (DCT). Later, the scrambled images got unscrambled by applying the inverse of the applied function. As a result, Chaotic concepts avoid iteration of the image data by the unintended humans. The human entering into the house environment must be analysed at distance. Thus, the identification of every individual passing

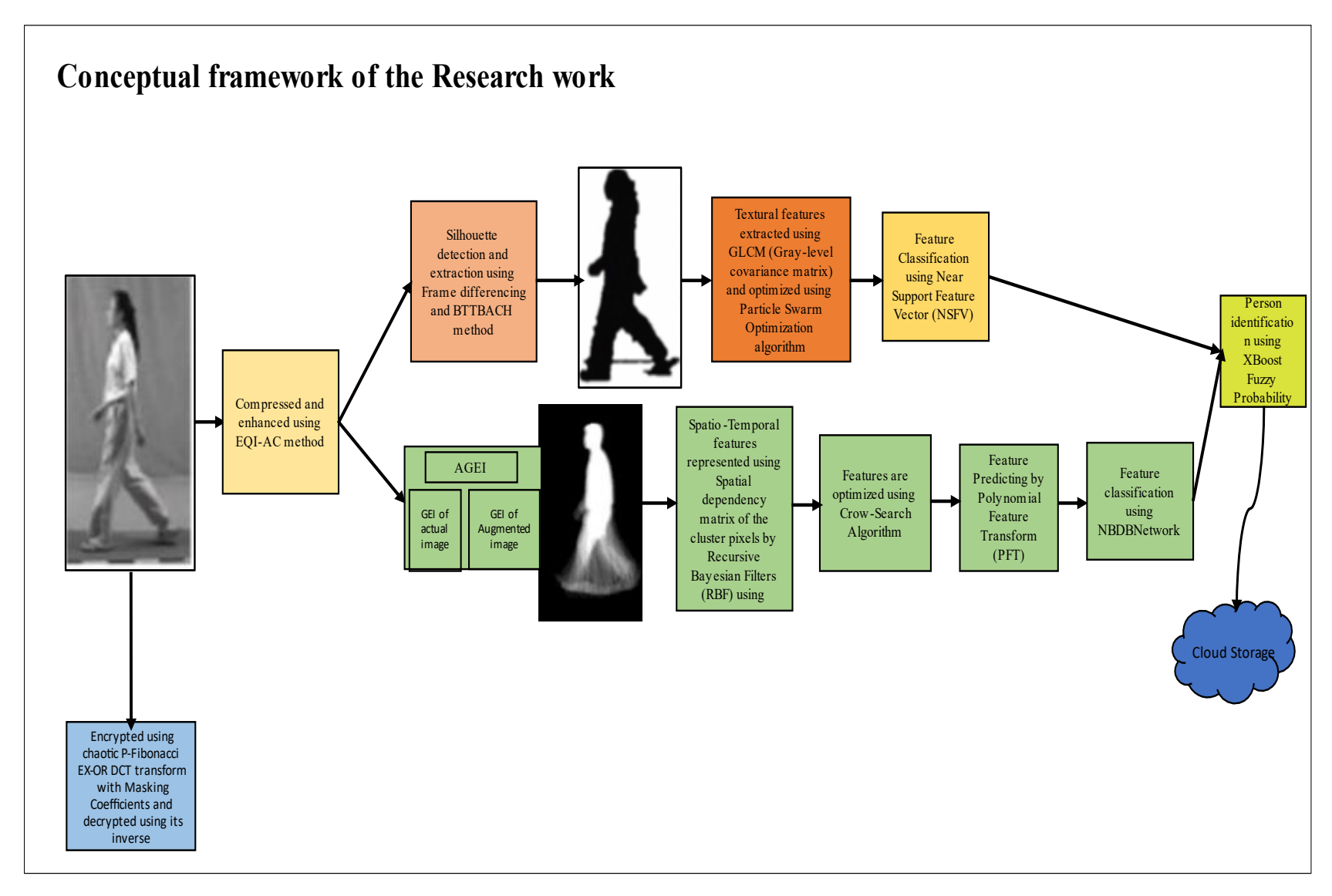


Fig. 1.1 Conceptual Framework of the Cloud and Machine Learning Applications for Human Silhouette and Gait Image Features Classification Methodology in Smart Home

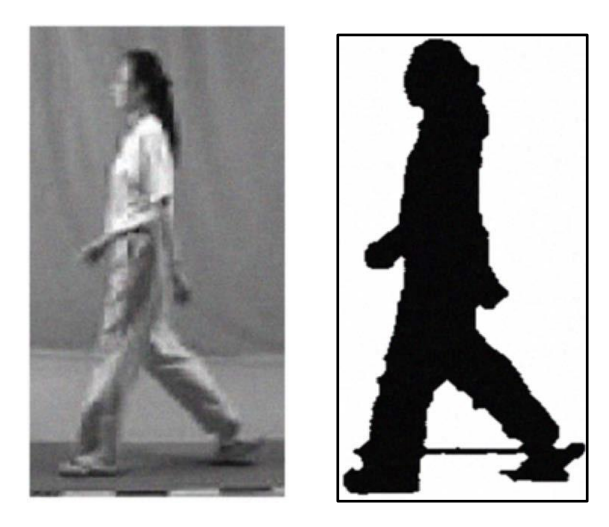
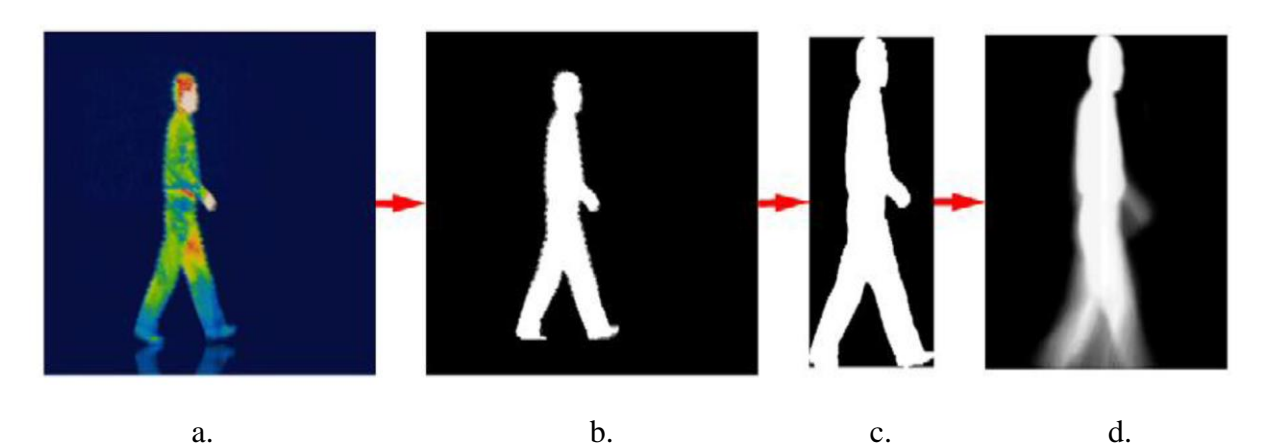


Fig. 1.2 Silhouette extracted using BTTBACH method from the actual image



a.b.c.d.Fig. 1.3 a) Selected phase of the gait cycle b) Silhouette for the selected phasec) Augmented silhouette image d) GEI image for the augmented image



Fig. 1.4 Gait energy image with the Walking frequency and phase

through the recognition set-up gives more predictions about the entering human without the human's co-operation [59]-[70].

The gait or walking pattern of the human recorded using the RGB-depth camera with the help of grid eye sensors fixed at smart home premises are used as the source. The gait images sliced from the captured videos are compressed and enhanced using the EQI-AC algorithm. The silhouettes are the black pixel representation (see in Fig. 1.2.) of the human located in the enhanced video image segmented using Binary Thresholding Top Bottom Agglomerative Clustering Hierarchy (BTTBACH) algorithm. The texture (appearance) based features such as Area, Eccentricity, Extent, Convex Area, Orientation, Bounding Box, Euler number, Solidity from the silhouettes are extracted using the Grey Level Co-Variance Matrix (GLCM). The Particle swarm optimization (PSO) algorithm was called to optimize the features list. The classification of optimized features is done using Nearest Support Feature Vector (NSFV) method. Next, the Accumulated Gait Energy Image (AGEI) is the output of the addition of normal Gait Energy Image (GEI) and the Augmented GEI (see in Fig. 1.2 and Fig. 1.3 and Fig. 1.4).

Where GEI is the average image that stores the static and dynamic representation of a gait cycle (the frequency and phase of the walking gait) [71]-[78]. The Spatio-temporal based features of the Accumulated Gait Energy Image (AGEI) are represented using the Recursive Feature Elimination (RFE) factor based on the Spatial dependency matrix of the feature pixels. Totally 23 Spatio-temporal features are recorded from those 20 features are optimized by the Crow Search Optimization Algorithm (CSA). The Principal Polynomial Feature Transform (PPFT), a feature prediction algorithm was

called to predict a few more features from the optimized feature list. The features such as Head, Cadence or Walk length (CD), Shoulder Left Angle (SLA), Shoulder Right Angle (SRA), Left Ankle Joint Angle (LAJA), Left Knee Joint Angle (LKJA), Right Ankle Joint Angle (RAJA), Right Knee Joint Angle (RKJA), Stride Length Left (SLL), Stride Length Right (SLR), Left Hand Elbow Angle (LHEA), Right Hand Elbow Angle (RHEA) are predicted to analyse the human. Finally, the classification of the optimized features is done using Naïve Bayes Dynamic Bayesian Network (DBNetwork) [79]-[83]. The Dynamic Bayesian Network (DBNetwork) is trained with the Conditional Probability Value (CPV) found for each feature.

The recognition of a human is possible based on the features matching score level. This level is also known as confidence level or measurement level. Matching score level is a measure of similarity between features derived from a presented sample and a stored template. The Fuzzy probability method is followed to take the decision of approving the human as Authentic (genuine user) or Reject (impostor user). As a resultant work, the Naive Bayes Dynamic Bayesian Network is recommended to deploy with Fuzzy Probability to get the human identified through the gait. Thus, no human can be escaped from the identification process [84]-[89].

The matrix representation of the Silhouette features extracted using the Grey Level Co-Variance Matrix (GLCM) and the Accumulated Gait Energy Image (AGEI) features extracted using the Spatial dependency matrix are encrypted using P-Fibonacci EX-OR DCT transform with masking Coefficients and decrypted using the Inverse transform [90]-[118]. The XGBoost (Extreme Gradient Boosting) is the wrapper class that combines all the weak learners using gradient architecture and strengthens the gait

models through system optimization and algorithmic improvements [119]-[122]. Finally, the NBDBNetwork can be deployed with the Fuzzy Probability module to analyse the human features more accurately. The dataset for the entire work is taken from [123].

Chapter 1 titled "Introduction", describes the gait based feature extraction motivation, issues, and objective of the research work.

Chapter 2 titled "Related Literature", lists the basic requirements methodologies, results of based human recognition.

Chapter 3 titled "Image Compression and Enhancement for increasing quality of image", explains the use of compression and enhancement of image as a pre-processing.

Chapter 4 titled "Thresholding of silhouette from the background using Binarization and Top-bottom Agglomerative Clustering Hierarchy (BTTBACH)", explains the importance of thresholding in the recognition concept.

Chapter 5 titled "Silhouette extraction and Features Classification using Nearest Support Feature Vector", explains the feature extraction from silhouettes and its classification

Chapter 6 titled "Accumulated Gait Energy Image (GEI) Feature Optimization, Selection and Classification using Bayesian Filters", explains the feature prediction and classification algorithms terminology and Dynamic Bayesian Network concepts Chapter 7 titled "Fuzzy Probability decision on FPR and FRR for Human Recognition", helps the NBDBNetwork to make the prediction based on the probability value by wrapping it with the XGBoost method

Chapter 8 titled "The Encryption and Decryption of the Silhouette and Accumulated Gait Energy Image using A Chaotic algorithm- P-Fibonacci Exclusive OR-Discrete Cosine Transform", explains the importance of cryptographic concepts for security purposes

Chapter 9 titled "Result and Discussion", summarizes the results obtained from the experiment of the proposed recognition system.

# CHAPTER 2

#### **RELATED WORKS**

#### 2.1 Introduction

Traditional devices of all kinds are turned into smart and capable devices. This promotion turns the experts towards home security concepts. Smart homes are connected with an interface to build surveillance setups for home monitoring [1]. Smart homes are living places that would be filled with information processing technology which is expected to respond and record the happenings to promote the home occupant's security. As an advantage, Smart sensors are designed to sense gases leakage, temperature, recognize the face, energy consumption finding, humidity, control television, door lock status, doorbell, refrigerator storage sensors, light intensity, smoke etc., continuously in regular intervals within range and send alerts to the authorized user-initiated by [2]-[8]. To make the smart home security, the protective measures taken must be strong and static, so that no one can intrude.

# 2.2 Need for Gait recognition

The gait is a biometric feature that no one can replicate. From the previous research, it was found that every individual has a unique walking style (gait), fingerprints and iris. In fingerprint recognition, the intruder can fool the system by using any solutions in the fingers for avoiding the matching of prints. In Iris recognition, the intruder can avoid the matching by using contact lenses, to escape from the featured recording. From the aforementioned, biometric systems, the co-operation of the person is required for successful recognition. In the case of gait recognition, the person co-operation is not

necessary, at the same time, the recognition system is alerted to record the person's arrival video without the person's knowledge. After the video got recorded, the images are segmented for the next processing [9]-[10].

#### 2.3 Review of Literatures

In the color optical images, aberration occurs in the borders of the images in the form of abrasive color fringes, which is termed chromatic aberration. Due to the smaller digital camera with the maximization of picture elements, this issue tends to rise as a critical problem. A novel method has been implemented by Alaa Jabbar Qasim et al, [11] for the detection and elimination of aberration in the images. The refractive effects of the lens tend to affect the optical systems by causing aberration. The algorithm proposed by Shaik Anwar et al., [12] will separate the data for processing in both the vertical and in the horizontal direction. Then the color fringes are eliminated directly from the given image. This algorithm also reduces the computation of parameter estimation process complexity.

Soon-Wook Chung et al., [13] analyzed the influence of chroma sub-sampling on the apparent video quality that had been analyzed subjectively. The video codecs used in this paper belongs to H.264/AVC and H.265/HEVC (High-Efficiency Video Coding) that is commonly used. The process of image encoding with the implementation of lower resolution for chroma information is termed chroma subsampling (the concentration is provided more to chroma information rather than luma). The visual systems of humans have a minimum sensitivity to color details. The evaluation of the video quality depends on two important factors. The perceived quality of an image obtained from the observers

or people, who rate the quality of the video by watching them is termed as subjective quality assessment. This is the most fundamental way in determining the quality of the video which is termed as Quality of Experience (QoE). The duration is the drawback of this method but the accuracy quality could be enhanced. This method is further divided into single and double stimulus methods.

The objective quality assessment is not concentrated when compared to the subjective type. For the test sequence, the Mitsu tool had been used in [13] for the Spatial (SI) and Temporal Information (TI) of full HD and Ultra HD video sequences. Then the coding procedure is carried out with the MPEG tool, where the chroma sub-sampling is done at the test video sequence with the change in the resolution carried out from UHD to FHD. This procedure is carried out at all the test sequences. Then, the encoding process takes place and all the sequences are encoded to H.264/AVC and H.265/HEVC standard for the compression. "Bund Nightscape" and the "Construction Field" are denoted as the sequences with low SI and TI values that have low MOS scores and bit rates. The MOS score along with the difference between the resolution of H.265 and H.264 codec has also been estimated in [13]. The difference between the sub-sampled and unsub-sampled videos could not be recognized by the observers.

This recommends that the data could be saved if the sub-sampled video is preferred. The modification of the luminance quantization table with the enhanced JPEG compression algorithm was presented by Miroslav UHRINA et al, [14]. The two most important components are considered in the quantization table namely chrominance and luminance. As stated in the previous work [14], luminance table changes could not be

detected by the human visual system easily it chooses the different image color that utilizes Baboon, Pepper, Brick-house etc. The modified performance JPEG is assessed by peak signal and noise ratio (PSNR), compression ratio (CR) and mean square error (MSE). Due to the modification of the quantization table, the PSNR, CR and MSE values had been improved by the proposed JPEG algorithm [14] when compared to the standard JPEG methodology and the lowest frequency DCT coefficients have considerable amplitude values. The most important process of capturing, storing, sharing, rendering and utilizing the images belongs to the standards that include JPEG, JPEG 2000, JPEG XT and JPSearch.

Suman Kunwar, [15] proposed the archiving and digitization application with these standards that had been presented with certain efforts of ongoing standard. The author had also stated the advancement of each of these standards. Among these, JPEG 2000 has good compression efficiency with versatility and good rate-distortion control. This standard could be adapted in the field of satellite imaging, medical imaging, digital cinemas and many more due to their wavelet-based compression technique. By piggybacking with the other standards, JPEG XT finds its application into the widened consumer markets with advanced functionalities.

JPEG standards play a role in the portability of images, searching and accessing the image along with the metadata handling. The images are stored in personal devices, social media and online repositories, and due to this wide growth of image data, interoperability should be supported among the systems. This could be possible with the JPSearch that helps in the search and retrieval of still images. Certain ongoing activities

include JPEG PLENO and JPEG-LS that supports low-latency along with the new image modalities. The reduction of data correlation is the basic idea behind the development of data compression techniques. Discrete Cosine Transform (DCT), is used that transfers the data from the time domain to the frequency domain. But the image at a higher frequency is not visible to the human vision due to the low sensitivity. In the case of video captured with the 3-D space, reduction of time correlation along with the spatial correlation is necessary. Histogram equalization by estimating the motion had been proposed by Zhipeng Chen et al, [16] in which the past and the new evolving image frames are compared to get similar parts. Then the time correlation factor is reduced by replacing the image with the Motion Vector (MV). The compression standard in this paper includes JPEG and MPEG respectively.

The detection of Contrast Enhancement (CE) with the laundering attacks is said to be a very difficult task. The CE detectors had been misled by the compression standard JPEG that is found to be a detrimental laundering attack. Barni Mauro et al, [17], selected the compression standard JPEG that had been utilized along with the adaptive histogram (AH) to determine the CE using training a JPEG-aware SVM detector with the color SPAM feature. Results have also been estimated based on this SVM trained detector and this works well with the imposed Quality Factor (QF) along with the compressed images under tests. If this QF factor could not be determined from the image then the idempotency properties of JPEG compression for extracting QF could be adapted. The enhancement in the contrast is done by local descriptor blocks of AHE in [18] by David Cozzolino et al, with 1372 dimensional features that are determined from the color images. The parameters of the Gaussian kernel were obtained by 5-fold cross-validation.

This approach could also be adapted with the Convolutional Neural Networks (CNN) that could provide higher significant results in many applications. To detect the presence of histogram equalization, a novel machine learning concept had been proposed in this paper [19]-[21] and the statistical parameters of DC Discrete Cosine Transform (DCT) coefficients are considered. The features used for the classification of original and histogram equalized image is done by the Gaussian Mixture Model (GMM) statistical parameters. The accuracy is obtained with the SVM classifier that classifies the original and histogram equalized images. Enhancing the contrast of the image could be possible with the Contrast-Limited implementation of AHE (CLAHE).

In Adaptive Histogram Equalization (AHE), an image will be sub-divided into several tiles and the enhancement will be carried out by applying HE to every individual tile that concentrates on every small detail by improving the image local contrast. Sometimes, AHE could increase the amplification noise factor that could be prevented by CLAHE in the relatively homogenous region. Before the cumulative distribution function (CDF) computation, the above procedure will be carried out that could clip the histogram at the particular value.

The function of slope transformation will be limited, which obtains the contrast amplification. This slope transformation function will be estimated by the CDF [22]-[24]. Clip limit is said to be the clipped value of the histogram and this will rely on the histogram normalization value as well as the default neighborhood region size 8×8. The RGB image will be converted to HSV color space despite applying the CLAHE directly for each channel that color results in the improper color balance and also produces unbalanced image presentation. By converting the image to HSV color space, the above

cons could be avoided and the CLAHE could be applied focusing on the luminance channel. After this process, the image will be converted again back to the original RGB domain image forgeries are highly possible due to the contrast enhancement inconsistency.

A Novice method had been introduced by De Rosa et al, [25] to analyse the contrast enhancement for the particular image. According to this method, mapping is done among the pixel values and also a distinct characteristic is introduced to the histogram of the image pixel. The method is said to be highly robust that considers the additive noise perturbations that affect the contrast enhancement. Thus, the enhancement of the captured image is needed for input consideration. Gowtham Bhargavas et al, [26] argues that the human image is considered for recognizing the person by converting image into silhouettes. The Biometric system was classified as either anatomical or behavioural. Anatomy corresponds to the shape of the body. Behaviour corresponds to the activity of a person.

In this paper, the gait of the person is considered as input. The walking of a person process is cyclic and unique. The unique gait can be used for differentiating every person from a distant location without the person's knowledge too. The identification of humans using biometric features has been a wide centric technique followed in the security, surveillance, and forensic department. The movement of the person such as gait and facial features are authentic and unique for every person, especially used for personal identification, discussed by Strukova et al, in [27]. The unalterable gait model can be used for identifying a person from distance by Veronica Cimolin et al, [28]. The silhouettes are the portraits used to recognize the person based on its similarity score by

Nahid A Makhdoomi et al [29]. The special case like the silhouettes with unique features like clothes and the properties carried in Haralick features are used to extract it. The gait energy image (GEI) is the average image of all the images calculated based on the frame difference after the segmentation. The horizontally or vertically divided GEI uses the K-Nearest Neighbor method for classifying the features read from the silhouettes. Signal to Noise Ratio value is used for ranking by Ait O.Lishani et al, in [30] and SVM, decisiontree and K-Nearest Neighbor are united to produce 98% accuracy as stated in the segmentation process is done either Region-based or Edge-based segmentation method by Anu J Nair et al, [31]. The features are the noticeable fragments. It remains static to the transformation operation like rotation, translation and scaling. Texture features are selected by regions of interest and specified by the scattering of the energy level of neighborhood pixels. Whether it is a human image or a medical image, extracted features only helps to differentiate between the original and fake. In [32], the image segmentation method called the hybrid technique proposed by Dilpreet Kaur et al, used for segmentation which improves the feature matching performance of the recognition phase. A method called Object Seeds Estimation Model [33] is designed by Muthahir O et al, for detecting the face using the image segments, where segmentation and merging are done using the grab cut method.

The infrared image thresholding method is the segmentation method executed based on a 1-D histogram approximation of the image by the first-order linear circuit. An imperial competitive algorithm [34] with the K-means clustering algorithm objective function is used for Nanofibers image thresholding. The Canny edge detector is used for edge detection and the FCM algorithm is modified related to the distant value for the

segmentation process. Here intensity corrupted noised images are used as an input and achieve a good trade-off than the compared methods. The human face can be recognized by segmenting the images using Enhanced SPCA and KNN method used for person analysis was described by Savitha et al [36]. Grey-Level Covariance Matrix energy information [36], is designed for retinal image segmentation with higher sensitivity, accuracy rates and time-efficient than the compared. A review of segmentation techniques explained and suggested intensity and texture-based segmentation. The edges, the level set is compared with the parental clustering algorithms and get the best results. PSO and Cat PSO [37], is used to find the optimal threshold for segmenting and binarization thresholding value is used as the fitness function of algorithms and the performances are compared using PSNR by Qu S et al. Where, filtration methods are initiated with changing probability values to segment a new region and classify with the features selected.

Euclidean distance is used for calculating the neighbor data distance for forming clusters [38]. The Gaussian and Bayesian algorithm is used to classify the data to form a cluster framework for person recognition by locating the object. The silhouettes features are focused on recognition of human action by the learning model and training model. The pre-phases of recognition concepts are discussed in-deep which promotes better knowledge for focusing on thresholding [39]. As per the prior paper, the hierarchical methods help to build the database profile and parameters initiated for training the operation is suggested, which shows the future idea of this current work and selecting the feature based on the requirement is discussed [40]. Krill Herd Optimization [41] is proposed with the objective function of Otsu which reduces the time complexity of

multilevel thresholding which is compared with biological aspects thresholding techniques. Gait recognition may be Model-based or Model-free based. Learning enthusiasm-based teaching—learning-based optimization (LebTLBO) [42] is designed by combining Otsu and Kapur's entropy for image segmentation by Asrul Adam et al, using PSNR, mean, threshold values, Iterations number proves the image segmentation quality. 3D-MET an optimum threshold with minimum error method is used to threshold the noisy images and proposed a relative method to reduce the time complexity of 3D-MET. Using SVM, the accuracy of the gait recognition through the gait with varying clothing and carrying properties status using public figures are tested.

The deep belief networks are used to analyze the pose of the gait with or without carrying properties in low-resolution gait captured in surveillance is worked out. The gait recognition concept can capture information from gait for identification with carrying conditions such as bad, coat or clothes wearing with normal walk enhancing the recognition accomplishment. Feature descriptors including Local Binary Pattern and Spectral Regression Analysis are followed to extract features from GEI [43].

The Accumulated Frame Difference Energy Image (AFDEI) reflects the time characteristics taken for walking or complete gait. The invariants of GEI and invariants of AFDEI are added to get the gait feature. The factors such as shoe, carrying properties, the surface they walk, angle view, and clothing affects the recognition while the other static parts are also considered for recognition. The technique followed defines the most effective part and least effective parts [44]. After the segmentation process is completed, the features from the segmented part would be read by using various practices. The backpropagation method is used to learn the face features to recognize the person with

an accuracy of acceptance ratio. The extracted features are classified to ease the next level process like storing in the database or assigning a rank to the features etc. Although various algorithms are suggested for the classification procedure, the reliability of the classification part solely depends on the feature segmentation method and extracted features discussed in [45]. To increase the chance of reliability in the appearance-based feature extraction and recognition model, the co-occurrence matrix values of the features are calculated from the silhouette images.

As an extension, the framework for recognizing the object has been done by classification of each object data and made as a cluster using the Gaussian and Bayesian algorithm in [46]. Detecting an object in real-time using correlation coefficient video surveillance is the algorithm that uses DCT for compression of video, correlational coefficients are used for detection of the object and Bayesian rule is followed for locating the object. Finally, the video surveillance image is used as a toss for the detection of human activity by the supervised learning model using the extracted features [47].

The silhouette feature-based human action recognition method was built using the learning phase and training phase. The learning phase was constructed by the extracted features and the training phase was initiated using the unique walking pose patterns required for human action recognition [48]. The stages involved in the biometric recognition system are discussed. These stages are comprised of levels of tasks united to provide better sensing. The parameters required for personal identification at the front end and the database profile at the back end are united hormonally to build a sequential platform. It is possible to find the percentage of body fat by the sequential sensing platforms, using, the feature selection methods. Thus, the ability to optimize features that

satisfies the requirement of the recognition task was very challenging [49]. For example, the Kinect sensor was used nowadays to record the joints of the gait. The Gaussian mixture model is used to segment the person image and Principal Component Analysis (PCA) is used for averaging the video frames and classification was done using SVM vectors and Fisher component was used to recognize the person, LIBSVM is a software used to query the database, as discussed in [50]. Techniques such as EMG inside the skin, Chips, Kinect sensors, are used to watch the person. Kinect techniques need the cooperation of the person for identification that produces results not so good compared to the other methods discussed. The joint coordinates are the temporal feature relations marked to plot the gait signature pattern. The gait signature profile for every individual can be compared for person identification and person recognition [51].

An empirical evaluation of various constraints such as cross-view and cross-walking-condition of the person with different processing approaches such as augmentation is followed and bags, glass, hat, dress the model wore also affect the recognition accuracy. So, the extra aspect other than the person body in the image is augmented in [52]. Gait captured in 11 views with three variations such as viewing angle, clothes worn by the gait and the carrying properties of the gait are considered. The person detection and extraction of the mobility of the person is done in the captured video sequence by applying the normalization factor to reduce the dimension of the selected frames for the classification of features [53]. The variance in the human gait is calculated using the deep convolutional features and Bayesian network. Data augmentation is the solution for overfitting which refers to the feature with high variance. The augmentation technique helps to enhance the size and quality of the features used for building Deep

Learning models [54]. Biological aspects of the gait are optimized using algorithms such as the Crow Search algorithm and SVM is used for feature selection. Gabor filters extract spatial features to make the CNN eligible for classification of images and solve the overfitting crisis using batch normalization [55]. Support Vector Machine and Gabor filters are used to extract texture features by calculating the standard deviation of the input image [56].

Naive Bayes and Support Vectors are combined to classify the Tokopedia data and users' opinions where Support Vectors develop hyperplane equations [57]. The features of the text documents are extracted using the improved nearest neighbor K-means (KSVM) method and classification of the features after optimization using the crow search algorithm [58]-[61]. The Particle Swarm Optimization (PSO) algorithm is the most widely used metaheuristic technique for feature optimization because it is simple and able to tend in any application [62]-[64]. SVM and KSVM are the kernel function of the Twitter data classification. The data may be divided into training and testing data using the random distribution and normal distribution [65]-[69]. Biometric systems are deployed for safety and security purposes using the features of face or gait used for detection and recognition [70]-[74]. In [75]-[79], five filtration methods various probabilities are united to form a new filter with selected features, classified features and the time needed for execution.

The average distance of the selected region data to the neighbor is calculated and classified. The data with minimum distance is found using the Euclidean measure. Each data is formed as a single class [80]-[84]. The Fuzzy Probability Distribution [85]-[91] is explained how the preliminaries are helpful to find the probability of the random variable

assumed. The probability value of the random variables must be filtered upon interests. Due to the in-determinant rise in digital communication, manifold technologies are used to transfer private particulars like images and videos. Every individual, companies and officials use encryption methods. Encrypting or transforming the data into an altered format is a constructive method to protect images or videos. The authorized users can decode encrypted objects [89]-[91].

Many applications require security as a basement for shielding confidential commercial matters. Authorization is allocated to others via fingerprint matches, iris matches etc., which are such types of security applications. Depending upon the expecting security, the data can be either partially or fully altered by following different Technologies [92]. Fresnel Transform (Fr-T) was used to transform the input image [93]-[94]. Fractional and Fourier Transform (Fr-FT) is followed to scramble the image input [95]-[97]. Spatial domain calculus is used to protect data with high security and high quality. Naive-based algorithms assume the data stream to encrypt the data [98].

DES (Data Encryption Standard) encrypts data part of the sequence [99]. Without scrambling the input, AES (Advanced Encryption Standard) method performs expandable output [100]-[102]. Chaos or mathematical systems use numeric data and provide results with real numbers which guide the algorithm for scrambling [103]-[108]. Recursive routines like Fibonacci sequences encrypt images with less security [109]-[110]. The efficiency and security of the encryption process are improved using the P-Fibonacci transform sequence and P-recursive function [111]-[112]. Permutation changes the pixel values of image blocks vulnerable to plain-text attacks [113]-[114]. Exclusive-OR functions followed for bit plane encryption [115]. In handheld devices,

transforms are done using Asynchronous standards for encryption (AES). Images are arranged with a matrix of pixels of Red Green Blue color. Each color value starts from 0 to 255 for each bit.

Base Picture based method is similar to the random matrix-based methodology. Here, instead of generating the random matrix, we take a base picture extract the pixel values from it and use it to XOR each value in the other picture matrix. If the size of the base picture is smaller than the size of the original picture, we repeat the same values from the start of the loop to the end in a loop [118]. A scalable endthe to-end boosting model called XGBoost was studied. The important factor behind the high demand for XGBoost is its scalability. The XGBoost system runs faster on a single machine and scalable up to billions of examples in distributed shrinked memory [119]-[120]. XGBoost accepts a large number of input features by learning the missing values on its own depending on the training loss and can solve the real-time problems in the world using only limited resources [121]-[122].

#### 2.4 Summary

From the review of literature, it was shown that the gait cycles are used for human recognition. The movement of the body parts and their angles are very much considered for gait analysis. The CASIA A database, CASIA B database and UCI repository have been used in the literature for gait feature analysis. In many reviews and researches Gabor filters, discrete wavelets, PCA, Fuzzy concepts, Probability values of the features are used. The existing works are carried out both in the laboratory and in real-time applications. The feature selection, feature optimization methods possess importance

over other methods in the reviewed literature. In a conclusion, Gait Energy Image (GEI) has been used by many researchers for gait analysis. Hence, in this research work, KSVM, SVM, Naïve Bayes classification algorithms are considered for comparison and implementation. The DBNetwork model and XBoost method are also analysed and used in the recognition work.

#### **CHAPTER 3**

### IMAGE COMPRESSION AND ENHANCEMENT FOR INCREASING QUALITY OF THE IMAGE

#### 3.1 Introduction

The person can be recognized using the dataset containing person images taken at different poses, different angles, different climatic conditions etc., which helps to train the algorithm for person recognition work. Before entering into the recognition process, the compression is the pre-processing work done to compress the image captured from the video using the EQI-AC algorithm, the amalgamation of JPEG (Joint Photographic Experts Group) and CLAHE methods. Initially, the captured images are larger with unwanted noise, so the Lossy compression algorithm is used to compress the input image and makes the input dataset eligible for recognition work [3]-[9]. Every image should be represented in the appropriate value of brightness and contrast for human eye visualization. Brightness refers to the limited darkness needed to visualize the image. If the brightness value of the image is high as usual, the white color ratio of pixels is dripped, if the brightness value of the image is low, the black color ratio of the pixels is dripped and hence the actual details of the image will be destroyed. Contrast means the percentage of color or grayscale representation that exists in images which helps to differentiate the object.

If the contrast value of the image is set high as compared to average, the black color in the pixels become too black and the white color in the pixels become too white. If the contrast value is set as low, the pixels of the image fades. So, contrast and

brightness are the parameters used to measure the intensity of the image. The proposed system of this paper focuses more on the contrast and brightness level of the compressed image compared to the raw image.

#### 3.2 Image Compression

The clarity and certain features of the images are not guaranteed during the image compression technique done by JPEG standard. Hence the below technique should be carried out to enhance the quality and control over the image that could be better than the source image. I converted in the form of Luminance (Y) and Chrominance (Cb & Cr) to achieve the delicacy and for interpret the spatial content better for an image since the human visual system is more sensitive to luminosity [14]. This methodology is done by the JPEG compression standard to limit the amount of information stored in the image. Usually, the color of the image could be represented by RGB and the transformation to Y, the luminosity component will enhance the intensity and the brightness of the pixels in the image. Cb and Cr represent the chrominance of the colors blue and green respectively. Through this conversion, high compression could be achieved and this is mathematically represented as,

$$[y \text{ Cb Cr}] = [RGB] = \begin{bmatrix} 0.299 & 0.169 & 0.499 \\ 0.587 & 0.331 & 0.418 \\ 0.114 & 0.500 & 0.081 \end{bmatrix}$$
3.1

#### 3.2.1 Chrominance Components - Sub-Sampling Process

Our human visual system is composed of rods and cones. Rods indicate the brightness and cons detect the color sensitivity [13]. The density of the rods is very high

when compared to the cons, which make them go well with the brightness rather than the color. This concept had been utilized by the JPEG standard in reducing the spatial resolution of the chrominance components. The subsampling process takes place on the Cb and Cr chrominance components formed due to the color transformation. The advantage of this method is that humans do not have effective diligence to find chrominance changes [13]. Every horizontal and vertical component will be removed from the image with the JPEG standard that results in the subtraction of 3/4 of the information from each of these components [14]. In simple words, certain pixels could be merged that have the same chrominance values done at a factor of 2 in both the vertical and horizontal directions.

#### 3.2.2 Block Splitting

The entire matrix will be sub-divided into the smaller individual matrix of 8 x 8. These sub-matrices are said to be known as the blocks. After this splitting process, it is necessary to fill the empty block with pixel edge data.

#### 3.2.3 Discrete Cosine Transformation

The redundancy in the image data is removed by applying DCT in every pixel block. For lossy image compression, DCT is the best-adapted method due to their robust energy compaction [16]. DCT will store a large amount of data with the low-frequency component and the rest of the smaller data will be stored at a low bit rate level. DCT transformation formula is given as:

$$F_{u,v} = \frac{c(u)c(v)}{4} \sum_{x=0}^{7} \sum_{y=0}^{7} f(x,y) \cos \frac{(2x1)u\pi}{16} \cos \frac{(2x1)v\pi}{16},$$
3.2

u, v – spatial frequencies in both horizontal and vertical direction and the integers should be in the range of  $0 \le u \le 8$ 

 $F_{u}$ , – DCT coefficient at the coordinates (u,v)

f(x,y) – the value of the pixel at the coordinates (x,y)

The information regarding the image file should be obtained before performing the DCT transformation [14]. The information file consists of the pixel value in terms of integers ranging from 0 - 255 that is divided in 8X8 matrix block and then DCT is applied in every block of data. Before transforming the image to the frequency domain, JPEG should subtract 128 from all the pixel values of the image to minimize the DC coefficient size. After DCT transformation it is found that 90% of the data will fall below the lower frequency component. To enhance the compressed image, the CLAHE metric is applied to the images using the Eqn. 3.1 to Eqn. 3.3.

#### 3.2.4 CLAHE Transformation on Images

To reduce noise in the near-constant region Contrast Limited AHE (Adaptive Histogram Equalization) (CLAHE) is adapted that works better with adaptive histogram equalization by limiting the contrast amplification factor thereby reducing the noise factor. The contrast amplification in CLAHE is given by the transformation function slope for the sufficient pixel value. This will be proportional to the slope of the

neighborhood Cumulative Distribution Function (CDF) and hence to the histogram of that particular pixel value. Before the CDF computation, the histogram amplification

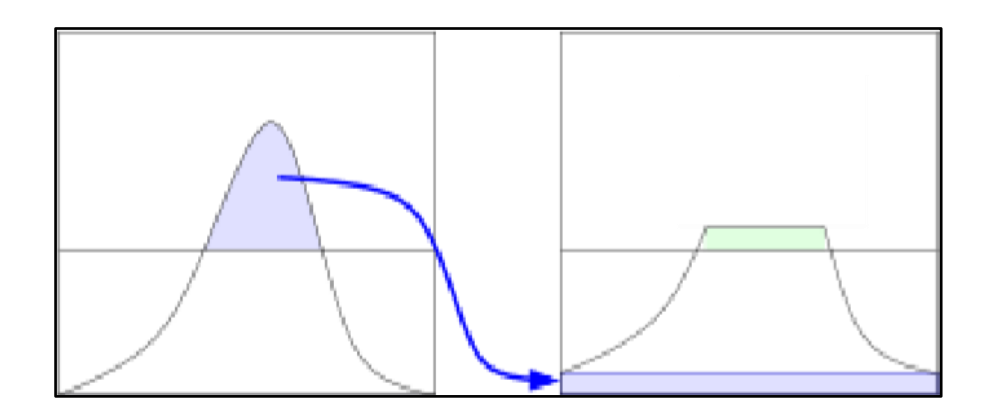


Fig. 3.1 Clip limit of the histogram value

will be clipped at a predefined value thereby limiting the transformation function and CDF slope. This clip limit value depends on the size of the neighborhood region. The clip limit amplified value lies at a range of 3 and 4. This does not eliminate the histogram value rather it will distribute the values to the histogram bins. In Fig. 3.1, it is seen that the range above the clip limit will be pushed to the bin through the redistribution process (shaded in green color) which results in the effective clip limit of an exact value. This redistribution process could be repeated until the prescribed effective value is obtained.

## 3.2.5 Pseudocode for EQI-AC Algorithm for Image Compression with Enhanced Quality

Input: Raw images with .png extension

Output: Compressed images with enhanced color, brightness and intensity

Step1: Take an image and divide it up into 8-pixel blocks. If the image cannot be divided into 8-by-8 blocks, then you can add empty pixels around the edges, essentially zero-padding the image.

Step 2: For each 8-by-8 block, get image data such that you have values to represent the color at each pixel.

Step 3: Take the Discrete Cosine Transform (DCT) of each 8-by-8 block.

Step 4: After taking the DCT of each block, multiply the block by a mask called matrix value that will zero out certain values from the DCT matrix.

Step 5: Finally, to get the data for the compressed image, take the inverse DCT of each block. All these blocks are combined back into an image of the same size as the original.

Step 6: Now we have the compressed Images.

Step 7: Calculate a grid size based on the maximum dimension of the image. The minimum grid size is 32 pixels square.

Step 8: If a window size is not specified chose the grid size as the default window size.

Step 9: Identify grid points on the image, starting from the top-left corner. Each grid point is separated by grid size pixels.

Step 10: For each grid point calculate the CDF of the region around it, having an area equal to window size and centered at the grid point.

Step 11: After calculating the mappings for each grid point, repeat steps 6 to 8 for each pixel in the input image.

Step 12: For each pixel find the four closest neighboring grid points that surround that pixel.

Step 13: Using the intensity value of the pixel as an index, find its mapping at the four grid points based on their CDFs.

Step 14: Interpolate among these values to get the mapping at the current pixel location.

Map this intensity to the range [min: max] and put it in the output image.

Step 15. Thus, output images formed are of high quality when compared to the JPEG Compressed Images.

#### 3.3 Experimental results

The raw images of varying sizes are selected automatically stored in the temporary folder and considered for compression. For compressing the raw images, the folder which contains ns the raw images are imported as an input to the source codes. For example .png files are compressed and saved with the .jpg extension. The dataset of nearly 98 images is given as an input to the source codes for compression. From Table 3.1, it is easy to visualize the extension of the input file and its actual file size and what is the extension of the saved output file and its compressed file size. Using the EQI-AC algorithm, the file size is reduced and the quality of the image is also improved In this paper, EQI-AC (Enhanced Quality Image After Compression) algorithm is used to enhance contrast, intensity and color of the compressed image, which is balanced, for visualization. Peak Signal Noise Ratio (PSNR) and Structure Similarity Index Measure (SSIM) is also calculated to prove that there is only a slight degrade in the quality of the compressed image compared to the original image.

Table 3.1 The Compression table shows the name of the raw image, its actual size, the compressed image with its shrunk file size

	-		-	
		Raw		Compressed
S.No	Raw Image Name	Image Size	Compressed Image Name	Image Size
			Compressed Image Name	
1	mag-06firstwords-t_CA0-article large-v2.png	182.9 KB	mag-06firstwords-t_CA0-article large-v2.jpg	41.3 KB
2	forest4_612251.png	435.0 KB	forest4_612251.jpg	155.0 KB
3	Untitled-design-9-796x417.png	189.9 KB	Untitled-design-9-796x417.jpg	136.1 KB
4	forestsmain.png	2.7 MB	forestsmain.jpg	742.9 KB
5	csm_Finland_forest_by_Ninara_flickr_42b14a06aa.png	669.9 KB	csm_Finland_forest_by_Ninara_flickr_42b14a06aa.jpg	184.3 KB
6	when-will-little-people-big-world-return-	320.4 KB	when-will-little-people-big-world-return-	86.7 KB
	1546445203.png		1546445203.jpg	
7	ThinnedForest_UnthinnedForest_background.png	826.8 KB	ThinnedForest_UnthinnedForest_background.jpg	275.2 KB
8	Bianca-devins.png	2.0 MB	Bianca-devins.jpg	765.6 KB
9	inner_slider.png	2.1 MB	inner_slider.jpg	637.0 KB
10	FOD.png	1.1 MB	FOD.jpg	351.5 KB
11	denis5-1-400x400.png	180.7 KB	denis5-1-400x400.jpg	37.1 KB
12	theni%20forest.png	767.0 KB	theni%20forest.jpg	202.9 KB
13	Ron-golden-1.png	275.8 KB	Ron-golden-1.jpg	208.1 KB
14	river.png	429.8 KB	river.jpg	102.1 KB
15	About us-our-people-tab-careers.png	132.4 KB	About us-our-people-tab-careers.jpg	127.0 KB

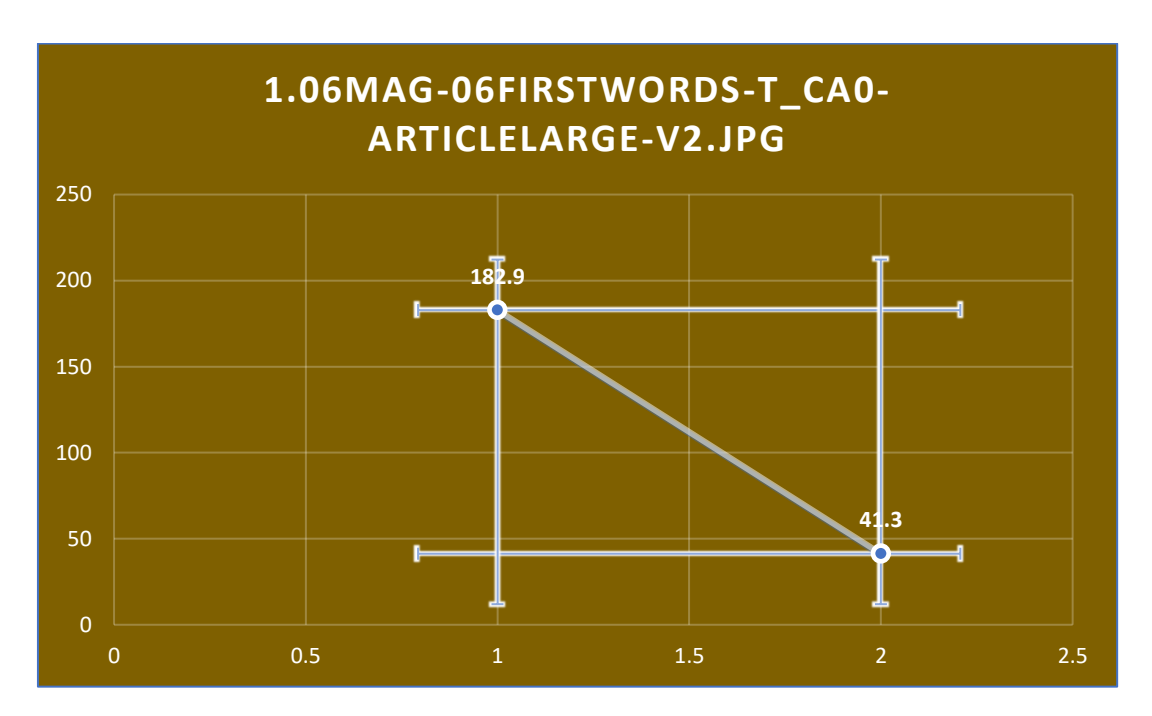


Fig 3.2 shows how the image is compressed from 182.9 kb size to 41.3 kb size

Table 3.2 The PSNR difference between the Compressed image and Enhanced image

S.No	Compressed Image Name	Compressed Image Size	PSNR for Compressed image	PSNR for image Enhanced using EQI-AC
1	mag-06firstwords-t_CA0-article large-v2.jpg	41.3 KB	42.015724	33.592275
2	forest4_612251.jpg	155.0 KB	31.034558	28.372946
3	Untitled-design-9-796x417.jpg	136.1 KB	37.538788	28.675094
4	forestsmain.jpg	742.9 KB	39.031124	28.150498
5	csm_Finland_forest_by_Ninara_flickr_42b14a06aa.jpg	184.3 KB	32.277014	28.210030
6	when-will-little-people-big-world-return-1546445203.jpg	86.7 KB	36.295363	29.166638
7	ThinnedForest_UnthinnedForest_background.jpg	275.2 KB	32.250588	28.553793
8	Bianca-devins.jpg	765.6 KB	49.482729	28.378726
9	inner_slider.jpg	637.0 KB	34.099730	28.354852
10	FOD.jpg	351.5 KB	31.601226	28.162941
11	denis5-1-400x400.jpg	37.1 KB	40.550236	30.594078
12	theni%20forest.jpg	202.9 KB	38.958962	28.21869
13	Ron-golden-1.jpg	208.1 KB	33.831556	28.440464
14	river.jpg	102.1 KB	42.871738	28.499099
15	About us-our-people-tab-careers.jpg	127.0 KB	37.698569	30.453635

Table 3.3 The Structure Similarity Index Measure of the compressed Image and enhanced image

		SSIM value of	SSIM value of
S.No	Compressed Image	Compressed image	EQI-AC applied image
1	mag-06firstwords-t_CA0-article large-v2.jpg	0.993276488	0.967669013
2	forest4_612251.jpg	0.980494321	0.831007905
3	Untitled-design-9-796x417.jpg	0.976760044	0.818730254
4	Forestsmain.jpg	0.988178904	0.723306708
5	csm_Finland_forest_by_Ninara_flickr_42b14a06aa.jpg	0.97671113	0.808361255
6	when-will-little-people-big-world-return-1546445203.jpg	0.97784198	0.863056503
7	ThinnedForest_UnthinnedForest_background.jpg	0.970369237	0.794251695
8	Bianca-devins.jpg	0.99559195	0.86142213
9	.inner_slider.jpg	0.992146256	0.85905047
10	FOD.jpg	0.964105035	0.762102643
11	.denis5-1-400x400.jpg	0.991242482	0.899955901
12	theni%20forest.jpg	0.992998901	0.842987241
13	.ron-golden-1.jpg	0.944776986	0.776488431
14	.river.jpg	0.990599087	0.828948821
15	.aboutus-our-people-tab-careers.jpg	0.970074594	0.881192121



raw image. 6th image in the dataset



EQI-AC algorithm applied enhanced image

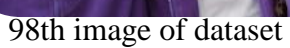


12th raw image of the dataset



EQI-AC algorithm applied enhanced image







EQI-AC algorithm applied enhanced image

Fig. 3.3 Image Compressed and Enhanced using EQI-AC algorithm

For measuring the quality of the compressed image, MSE (Mean Square Error) and PSNR values are calculated. Peak Signal Noise Ratio (PSNR) is the rational value calculated between the signal or original data and the noise or error which corrupts or affects the quality of the image after compression. The PSNR value of the raw image and compressed image are tabulated to show how the compressed image is enhanced see Table 3.2. Structure Similarity Index is the quality measure used to find the similarity quality between two same images, the raw image and the compressed image see Table 3.3. The images seen in Fig.3.3 shows how the raw images and the enhanced images are differed in contrast, brightness and intensity before and after applying the EQI-AC algorithm for compression. Here the enhanced output of the 6th image, 12th image and 98th image of the dataset is displayed for the reference

#### 3.4 Summary

JPEG (Joint Photographic Experts Group) is an international standard for continuous-tone still image compression both the color and the grayscale help with a large variety of applications. This standard is now in progress with the JPEG XS that forms a solution for the interoperable solution for visually lossless compression, low-latency and light-weight compression of video and image. Based on the novel structure addressing image compressing, the EQI-AC algorithm is found for compressing and enhancing the raw image. Every horizontal and vertical component will be removed from the image with the JPEG standard that results in the subtraction of 3/4 of the information from each of these components. Certain pixels could be merged that have the same chrominance values

done at a factor of 2 in both the vertical and horizontal directions. The entire matrix will be sub-divided into the smaller individual matrix of 8X8. These sub-matrices is said to be known as blocks. After this splitting process, it is necessary to fill the empty block with pixel edge data. The redundancy in the image data is removed by applying DCT in every pixel block. After DCT transformation, CLAHE metrics are applied. The following EQI-AC algorithm is used to improve the color, brightness and intensity of the compressed image. The Scale In-Variant Feature Transform (SIFT) method and Discrete Cosine Transform (DCT) are the image compression method compared with the Proposed EQIAC algorithm and found that the SSIM and the PSNR value of EQIAC are better.

#### **CHAPTER 4**

# THRESHOLDING OF SILHOUETTE FROM THE BACKGROUND USING BINARIZATION AND TOP-BOTTOM AGGLOMERATIVE CLUSTERING HIERARCHY (BTTBACH)

#### 4.1 Introduction

To avoid direct contact with the person and the devices, distant locating gaits are used as input for recognition. Capturing the gait from the video sequences and differencing the foreground and the background of the image. The thresholding or Image segmentation is an interesting topic in the image analysis and the expected outcome of this paper too. Binarization and the TBACH (Top-Bottom Hierarchical Agglomerative Clustering) unsupervised Thresholding method [38]-[41] is created to segment the selected region using the boundary information until all clusters are dealt one by one. Cumulative similarity measures are optimized and applied to the image. The resultant segments are the expected thresholding output. The proposed method is applied to test the performance of the method. There are 4 steps of performance followed in this work.

- 1. The average energy image is formed for the image profile using the frame differencing method.
- 2. Binarization thresholding is used to find the histogram normalization
- 3. Clusters are formed for the average energy image using the TBACH method
- 4. The TBACH method is used to analyze each cluster individually and changes the cluster structure by merging the neighboring clusters to iterate the structure and form hierarchical clusters.

- 5. Cumulative similarity scores are optimized with min and max values so that the maximized threshold value is chosen as the perfect cluster.
- 6. The minimum distance between the clusters is also calculated for the thresholded results.

Frame differencing method is used to find the average de-noised image of the gait profile. The average de-noised image of each cluster becomes the energy image. FDEI [29] is formed by adding the frame difference between the previous frame and the current frame with the cluster. The final FDEI image is considered for segmentation. The Wavelet Transform (WT) method is used to detect the edges of the average image. Using the histogram of the image, the image details are highlighted. The difference between the white and grey values of the image pixels are used to calculate the gradient value. The gradients are calculated in all four directions without missing the edge points. Binarization [30]-[31] and Top-bottom Agglomerative clustering hierarchy (BTTBACH) is proposed for thresholding by considering each data point in the input image as one cluster. Euclidean Distance metric is used to measure the distance between the two groups. Then the clusters are paired and merged to make a single cluster containing all the data points of the 2 clusters. This method allows pixels of one cluster present in every other cluster also.

A proximity matrix is created to store the distances between each point. So, the membership function of the pixels is maintained for every cluster to minimize the processing. Currently, clustering is one of the unsupervised learning methods, used for segmenting large-scale images. The membership function of the pixels is stored and used

to minimize the complex processing. In this paper, the Frame differencing method is used then Binarization Thresholding and Top-Bottom Agglomerative Cluster Hierarchy (BTTBACH) are combined to frame the cluster hierarchy of the image.

#### 4.2 Preliminaries of Image Thresholding work

The images are segmented based on clustering concepts. The input for the method is an image found using the frame difference method. Frames are the patterns captured and grouped as one gait cycle. A gait cycle is the full walking pattern of an individual. Frame rate depends on the number of frames captured in the specific duration. Frame differencing is the method used to detect the moving object by finding the difference between two consecutive frames in a cluster. Average energy image (G) is found by converting the image pattern into a grey image. Where,

$$G(x, y) = \frac{1}{N} \sum_{t=1}^{N} D(x, y, t)$$
4.1

Frame Difference Energy Image (FDEI) is calculated by

$$F_d(x, y, t) = F_s(x, y, t) + D_3(x, y)$$
 4.2

Using the FDEI, the unique differences noted in the silhouette frames are normalized and described. Feature description is the prior step of feature extraction [24], 36]-[39].

#### 4.2.1 Binarization thresholding

The automatic thresholding method selects the threshold value 't' to be optimal by maximizing the variance between the groups and minimizing the variance within the groups [23],[26]-[31]. Therefore, the sum of the variances remains constant for every segment.

Thresholding 
$$t = arg \begin{cases} max \\ 0 \le t \le N-1 \end{cases} arg \begin{cases} min \\ 0 \le t \le N-1 \end{cases}$$
 4.3

The binarization thresholding method can also be applied for multi-level thresholding. If the grey level value reaches M-1 then the threshold t [t1, t2, ...t<sub>M-1</sub>] then the group may be  $\{c1, c2, ...c_{M-1}\}$ . The algorithm uses two thresholds  $t_{max}$  and  $t_{min}$  to describe the image gradients to highlight the edge of the cluster region.

If the image gradients >  $t_{\text{max}}$ , then definitely the pixels are on the edge of the cluster region

If the image gradients > low then the pixels are on the background

Here X(i,j) be the pixels on the image cluster. The maximum value of the image threshold is assumed as  $P_x(x)$ , and the minimum value is  $Q_x(X)$ . The degree of membership value  $d_x(X)$  of the cluster image X is found by,

$$d_{x}(X) = \frac{1}{\sum_{k=1}^{\max} \left(\frac{||P_{x}(X) - P_{y}(X)||}{||P_{x}(X) - P_{k}(X)||}\right)^{\frac{1}{\alpha}}}}$$
4.4

$$d_{y}(X) = \frac{1}{\sum_{k=1}^{\min(\frac{||P_{x}(X) - P_{y}(X)||}{||P_{x}(X) - P_{k}(X)||})}^{\alpha}}$$
4.5

Where  $d_x(X)$ ,  $d_y(X)$  are the max and min values of the degrees of membership function. The modified degree of image gradients are found by,

$$DIG = \frac{1}{Q} \sum_{\min}^{\max} d(x) [d_x(x) - d_y(x)]$$

$$4.6$$

Where Q is the total degree of image gradients, min and max are the maximum and minimum values of a Euclidean distance of the cluster d(x).

#### **4.2.2** Top-Bottom Agglomerative Clustering Hierarchy (TBACH)

The top-bottom hierarchical clustering algorithms treat each data point as an individual cluster at the initial stage. It merges pairs of clusters until you have a single group containing all data points. Hence, it is also known as Hierarchical Agglomerative Clustering (HAC). Compare it to a tree where the root is the unique cluster that gathers all samples with the leaves as the clusters with a single sample [31]-[41]. The following graph (see in Fig. 4.1 a and b) displays how the image clusters are formed.

The probability P of grey level k P<sub>k</sub> represented by,

$$P_k = n_k / N, P_k \ge 0, \sum_{k=0}^{N-1} P_k = 1$$
 4.7

In this thresholding, the pixels of images are divided into two groups, B1 and B2. Where B1 has grey levels [0, 1...t] and B2 has grey levels [t+1, N-1] by the threshold t. The weighted average of the probability of the two groups or clusters are,

$$w1 = P(B1) = \sum_{j=0}^{t} P_k$$
 4.8

$$w2 = P(B2) = \sum_{i=t+1}^{N-1} P_k$$
 4.9

The mean of the weighted averages of B1 and B2 is calculated by,

$$u1 = \sum_{j=0}^{t} j P_k / w1$$
 4.10

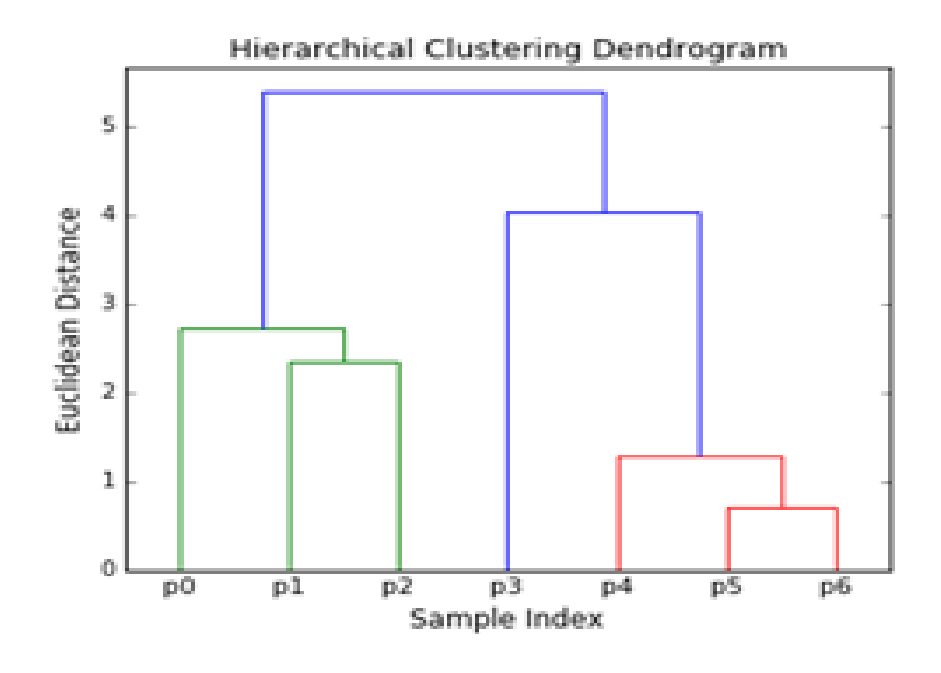
$$u2 = \sum_{j=t+1}^{N-1} j P_k / w2$$
 4.11

The average weighted mean of two groups together is denoted by Ut.

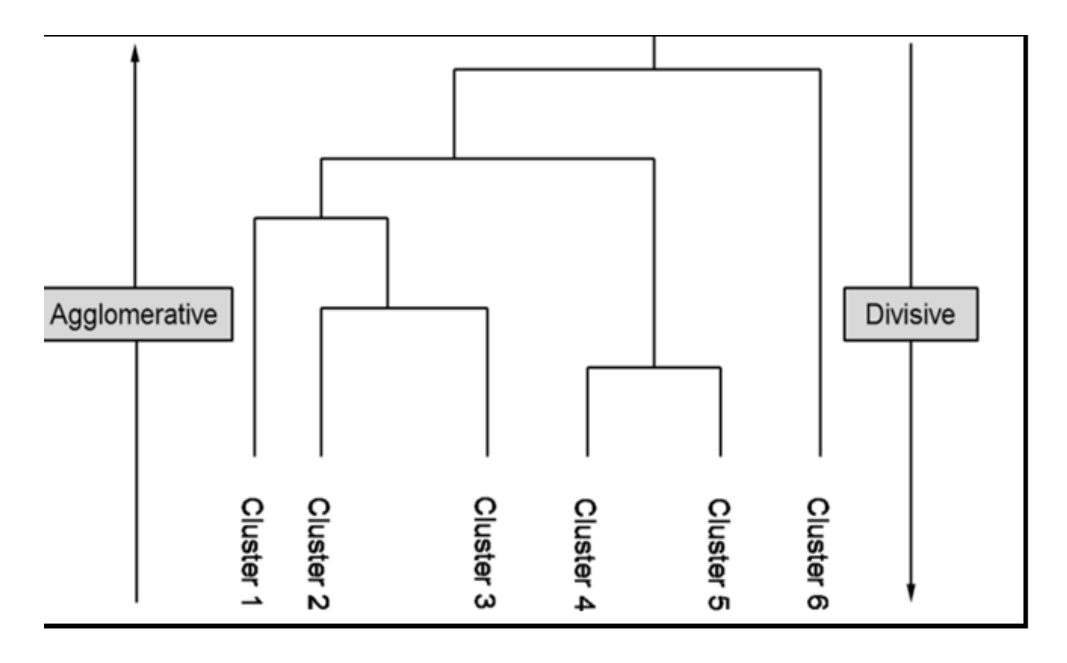
$$uT = u1w1 + u2w2$$
 4.12

The variance of the two groups are represented by,

$$\sigma_1^2 = [w1(u1-uT)]^2 + w2[(u2-uT)]^2$$
4.13



a. shows the clusters of image



b. shows the formation of clusters either top-down or bottom-up of the image

Fig. 4.1 Clustering steps involved in Binary Thresholding Top Bottom Agglomerative Clustering Hierarchy (BTTBACH)

$$\sigma_2^2 = \sum_{j=t+1}^{N-1} (j - u^2)^2 P_j / w^2$$
 4.14

The variance within the group is calculated by,

$$\sigma_{\mathbf{w}}^2 = \sum_{\mathbf{k}=1}^{\mathbf{M}} \mathbf{w}_{\mathbf{k}} \sigma_{\mathbf{k}}^2 \tag{4.15}$$

The variance between the group is calculated by,

$$\sigma_b^2 = w1(u1 - uT)^2 + w2(u2 - uT)^2$$
4.16

The sum of the variance of the two groups are,

$$\sigma_{\rm S}^2 = \sigma_{\rm w}^2 + \sigma_{\rm b}^2 \tag{4.17}$$

#### 4.2.3 Improved Fuzzy C-means Clustering

Fuzzy C-means is a clustering method [26]-[30], used to process the local data that belongs to various clusters. Fuzzy attempts to increase the recognition ratio by applying some decision variables and constraints. The value of the constraints will solve the solution. Fuzzy set maintains the cluster center and membership values as their data points are updated in regular intervals until the cluster center becomes stable, whereas the membership functions are used in recognition problems to handle the situation with experience. Here,  $\mu$ mf equals any real number such as  $1 \ge mf > \infty$ ,  $\mu$ jk equals membership value of  $X^j$  in the cluster named 'j' and  $C^k$  denotes the cluster center. In Fuzzy C-Means, the membership matrix MM have values ranging from the 0 to 1 to satisfy the following cluster constraint, the input images are clustered based on the interest to achieve the good results in the segmentation output. The cluster center decides the segmentation output.

$$\sum_{j=1}^{C} \mu j k = 1$$
 4.18

$$\mu_{mf} = \sum_{j=1}^{N} \sum_{k=1}^{C} \mu \frac{mf}{jk} ||X^{j} - C^{k}||^{2}$$

$$4.19$$

where C is the cluster center and j be the cluster and the values of k = 1, ..., n.  $\mu$  denotes the mean value of the data points in the cluster.

$$\mu j k = \frac{1}{\sum_{p=1}^{c} \frac{xj - ck}{xj - cp}}$$
 4.20

$$C_{k} = \frac{\sum_{j=1}^{N} \mu_{jk}^{mf}.xk}{\sum_{j=1}^{N} \mu_{jk}^{m}}$$
 4.21

Dividing the given dataset and forming a cluster is done using optimization of the objective function using fuzzy partitioning. The membership matrix  $\mu$ jk and cluster center are the  $C_k$ . The output of the compressed and enhanced algorithm is considered for thresholding. Here Frame Differencing (FD) method is applied to the input images and found the difference between the foreground and background images focused on thresholding. Wavelet Transform (WT) is applied for detecting the edges, and, binarization thresholding is applied to detect the min and max value for thresholding. Finally, Top-Bottom Agglomerative Clustering hierarchy has been applied for thresholding the interesting parts from the input image. The following images are the output of the compressed and enhanced algorithm considered for thresholding.

#### **4.3 Performance Metrics**

The Jaccard Index, Dice Coefficient, CDR, FAR, FRR are the performance metrics calculated for the thresholding methods used for segmenting the given image

into clusters. As per the clustering size, the performance value of the images are varied, Eqn. 4.1 to Eqn. 4.21 are used to threshold the given images into clusters and Eqn. 4.22 to Eqn. 4.26 are used to calculate the performance metrics such as Cumulative Distance Ratio (CDR) between the clusters, False Accept Ratio (FAR) of the clusters and False Reject Ratio (FRR) of the clusters of each image are calculated. In this proposed work, the Frame differencing method is used to segment the cluster from the captured image. The comparison took place between the clustering methods like Binarization thresholding, Improved Fuzzy C-Means clustering and Top-Bottom Agglomerative Clustering Hierarchy. The calculation of CDR, FAR and FRR and the time taken to cluster the images are kept in mind to find the thresholding model.

Binarization and the TBACH (Top-Bottom Hierarchical Agglomerative Clustering) unsupervised Thresholding method is created to segment the selected region using the boundary information until all clusters are dealt with one by one. Cumulative similarity measures are optimized and applied to the image. The resultant segments are the expected thresholding output. The gait profile contains the number of images captured within a certain period. Using the histogram of the image, the image details are highlighted. The difference between the white and grey values of the image pixels are used to calculate the gradient value. The gradients are calculated in all four directions without missing the edge points. Later, the Automatic thresholding method is used to calculate the threshold of the image histogram. The ratio of the total number of pixels in a block is used to set the initial threshold. The area located on the sides of the selected threshold is fixed as the max and

Table 4.1 the image name table

S.No	Image Name	
Image1	img-people-Abha-Mishra.jpg	
Image2	ron-golden-1.jpg	
Image3	Lena.jpg	
Image4	ashford-oaks-primary-8.jpg	



Fig. 4.2 a) Input images b) Histogram of the Input images c) Top Bottom Binary
Thresholded Image. Refer Table 4.1 for Input image names

min values. Here, the immediate thresholding method is employed for silhouette segmentation.

$$Jaccard Index = \frac{cluster1 \cap cluster2}{cluster1 \cup cluster2}$$
4.22

Dice Coefficient = 
$$2 * \frac{|\text{cluster1} \cap \text{cluster2}|}{|\text{cluster1}| + |\text{cluster2}|}$$
 4.23

$$CDR = \frac{Number of pixels correctly grouped as clusters}{Total number of pixels in clusters}$$
4.24

$$FAR = \frac{\text{Number of pixels falsely accepted in the clusters}}{\text{Total number of pixels in the clusters}}$$
4.25

$$FRR = \frac{\text{Number of pixels falsely rejected in the clusters}}{\text{Total number of pixels in the clusters}}$$
4.26

The Jaccard Index of the images are calculated using Eqn. 4.22 and Dice Coefficient of the given images are calculated using Eqn. 4.23. CDR, FAR, FRR is calculated using Eqn. 4.24 to Eqn. 4.26.

### 4.4 Summary

Thresholding is an important aspect of the image analysis part. Thresholding helps to focus on the interesting parts of the image. The features extracted from the interesting parts helps to variate the parts and are used for recognition. In this paper, Binarization

thresholding and Top-bottom Agglomerative Clustering Hierarchy (BTTBACH) and frame differencing Method is proposed for person recognition. Frame Differencing method is used for averaging the image profile and from the averaged image, the interesting parts are focused individually using the TBACH method and gets an optimized cluster containing all the data parts. Thus, there will be no parts of the image missed while using the proposed thresholding method.

### **CHAPTER 5**

### SILHOUETTE FEATURE EXTRACTION AND CLASSIFICATION USING NEAREST SUPPORT FEATURE VECTOR

### 5.1 Introduction

Every human has their style of walking and walking speed. For this research, gait cycles stored in the National Laboratory of Pattern Recognition (NLPR) gait database and CASIA gait database are used. Human recognition for smart home safety is planned in 5 steps. The block diagram of this proposed work is displayed in Fig. 5.1. This initial step was modelled by collecting human gait through the Grid-eye sensor fixed with the RGB-depth camera. The gait profile contains the number of images captured within a certain period as like in [26]. The Grid-eye Infrared thermopile sensor is used to detect humans. The silicon lens is attached with a sensor for image formation. It detects humans using infrared radiation. The thermopile sensors consist of numerous thermocouples arranged in 8\*8 series of the grid without contact with each other for measuring temperature. Every thermopile records temperature value.

Thus overall, 65 temperature values are stored. Grid-eye extends its view to 60° in both horizontal and vertical directions up to 5 meters. The Grid-eye sensor is used to detect humans at a stationary position. A Grid-eye sensor is attached with an RGB-depth camera to capture the gait based on the movement and estimate the 3-D view of the human body joints without any locating bounding boxes. If anybody walks before the camera, the infrared radiations detect the human and wake up the camera to capture the pose depth.

The camera is placed at 1 meter from the floor distance to capture all parts of the body.

The gait cycle (gait profile) consists of human gait details captured in 11 focus views based

on variations such as angle, clothes wearing and carrying properties [25]-[28].

5.2 Image Averaging or Silhouette Detection Using the Frame difference

Method

Frames are the patterns captured and grouped as one gait cycle. A gait cycle is the

full walking pattern of an individual. A walking pattern is the oscillation of the legs from

the floor to up marching. Frame rate depends on the number of frames captured in the

specific duration. Frame differencing is the method used to find the average image from

all the captured images. Frame Difference Average Image method (FDAI), fills the

incomplete pixels in the silhouette pattern using the membership values of the clusters [29]-

[30].

5.2.1 Pseudocode for Frame Difference Average Image (FDAI) function denoted by

 $\mathbf{F_d}$ 

Frame Difference Average Image method (FDAI) fills the incomplete pixels in the

silhouette pattern using the membership values of the clusters [29]-[31].

**Input:** All the captured images are given as input

**Output:** Average image

Step 1: Each image is split into two parts. Pixels occupied in the object and pixels outside

the object within the image. Silhouette models are represented as D (x, y, t). So, D  $\in$  I and

57

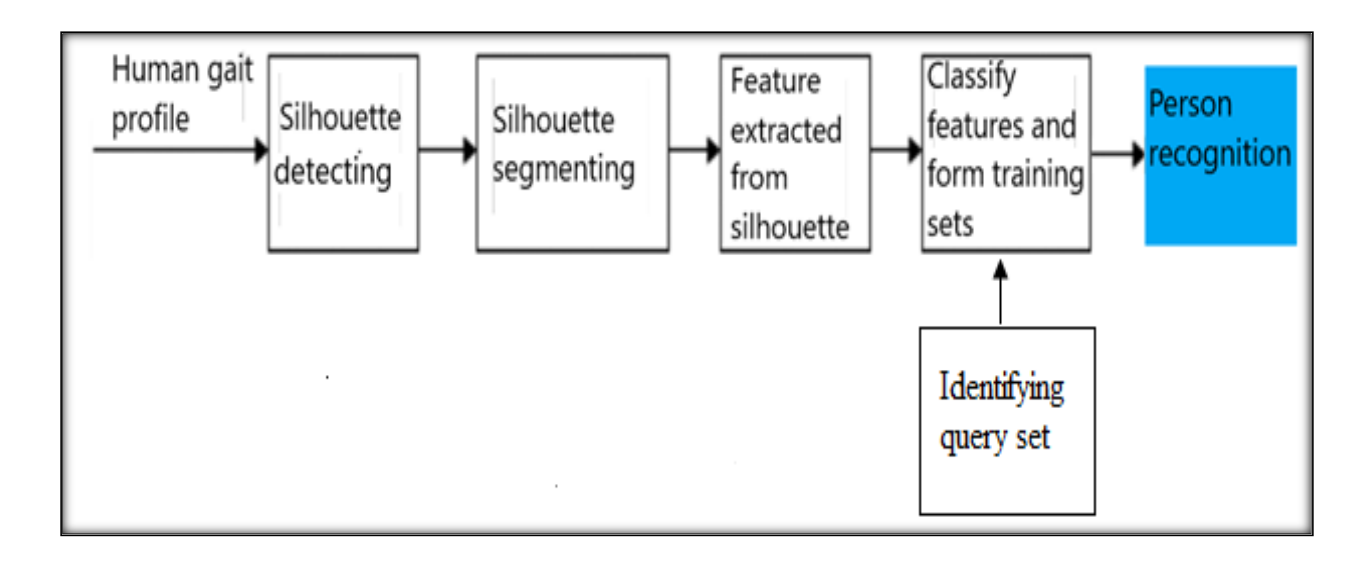


Fig. 5.1 Block diagram of Silhouette feature extraction and classification

x and y are the coordinates of the image, and t is the index of the frames.

Step 2: Average energy image (A) finding: It converts the silhouettes into the 2D-grey image. It is computed by

A 
$$(x, y, t) = \frac{1}{N} \sum_{t=1}^{N} D(x, y, t)$$
, Where N is the total number of frames captured

Step 3: If the segmented silhouette is not smooth, because of the noise or uneven edges and fake spots, the normalization factor q is applied to the exacted silhouettes for smoothing the edges. Then q is computed by,

$$q = \frac{1}{n^2} \sum_{i=1}^{n} \sum_{j=1}^{n} |P_i - P_j|$$
, Where n is the number of points normalizing the pixels P,

Step.4: The smooth silhouettes  $F_s(x,y,t)$  are calculated by

$$F_s(x, y, t) = \begin{cases} 0 \text{ if } A(x, y, t) \ge A(x, y, t - 1) \\ A(x, y, t - 1) - A(x, y, t), \text{ Otherwise} \end{cases}$$

Step 5: Using Eqn. (2) and Eqn. (3), FDAI is calculated by

$$F_d(x, y, t) = F_s(x, y, t) + q(x, y)$$

Using FDAI (F<sub>d</sub>) the unique differences noted in the images are averaged and normalized.

### 5.3 Features detected from FDAI Silhouette

Features are special notable fragments. For images, edges, corners, blobs and ridges are the types of features practised for years. Features remain static to the transformation operation like rotation, translation and scaling. Texture features are split by regions of interest and specified by the scattering of the energy level of neighborhood pixels. For the

features noted from the given silhouettes refer to Table 5.1. Some of the features selected are described below.

### 5.3.1 Area

The area is the number of pixels in the specified image region [30], [52].

### **5.3.2** Bounding box

The height and width of the silhouette are calculated by the rectangular box bounded over the silhouette. The height of the box is directly proportional to the height of the silhouette and vice-versa of the width [30],[52].

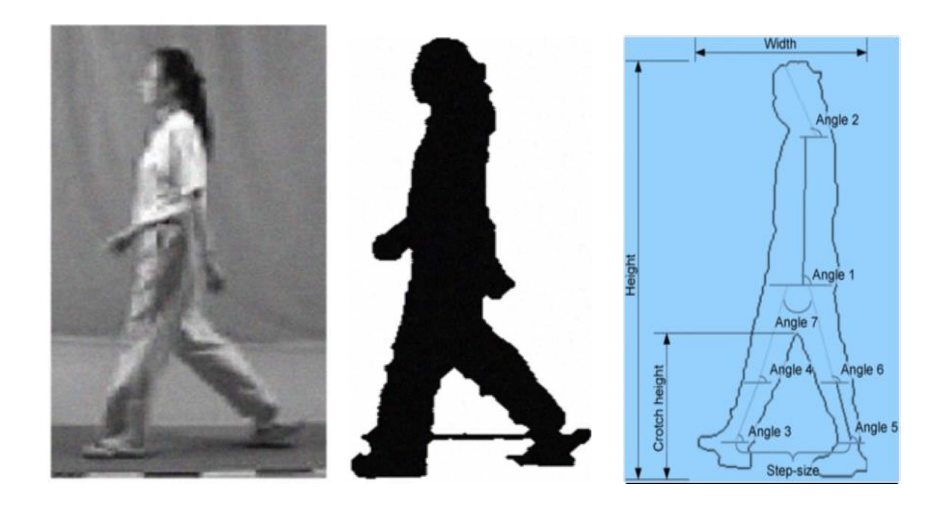
### **5.3.3** Eccentricity

It refers to the correlational distance between the centroid and its major axis length (see in Fig 5.2 a). For example, the foot-step length is the distance between the left leg and right leg while walking [30],[52] (see in Fig, 5.2)

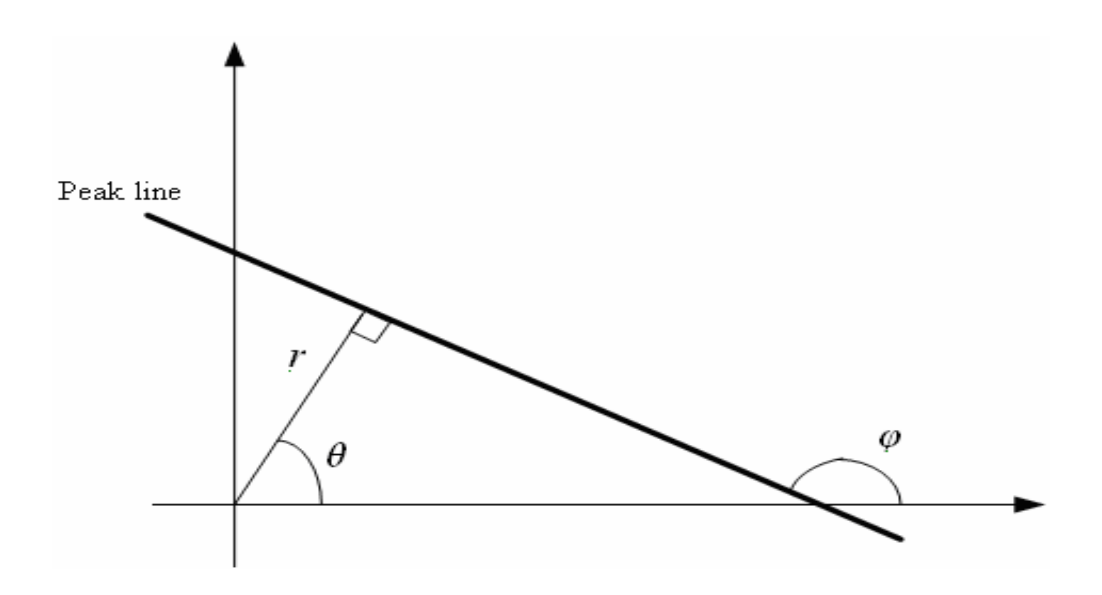
Angle 
$$7 = \text{Angle } 6 - \text{Angle } 5$$

### **5.3.4 Euler Number**

It refers to the difference between the number of segments and the number of joints in the image region. For example, dividing the silhouettes based on anatomy. So, silhouettes are segmented into 10 body segments based on the human anatomy. Based on the centroid, the upper human parts that appeared above the centroid is the head, neck



a. Model silhouette is marked with angles for extracting features



b. The angle of the silhouettes

Fig. 5.2 a and b shows Angles marked on the Silhouettes for segmenting

and torso. The lower human parts that appeared below the centroid is the hip, legs and feet [52].

### **5.3.5** Extent

It refers to the correlation of the pixels in the image region to the pixels in the total bounding box. For example, if the targeted region is the human face, quality silhouettes of facial profiles are referred to as duplicating the captured silhouette by shifting the targeted region to left, up and then down relatively proportional to the actual area of the template silhouette [52].

### 5.3.6 Convex Area

The total number of pixels present in the image outcurve. For example, the property the human carries along with him [52].

### 5.3.7 Orientation

It refers to the angle between the x-axis and sits corresponding to the y-axis [52]. For example, the foot-step length of the human, marching length, marching speed, pulse and hip angles are used for gait analysis (see in Fig. 5.2).

### 5.3.8 Solidity

It specifies the proportion of the pixels in the skeletal outcurve of the image region. It is calculated as the ratio of the total area and the convex area (see in Fig. 5.2).

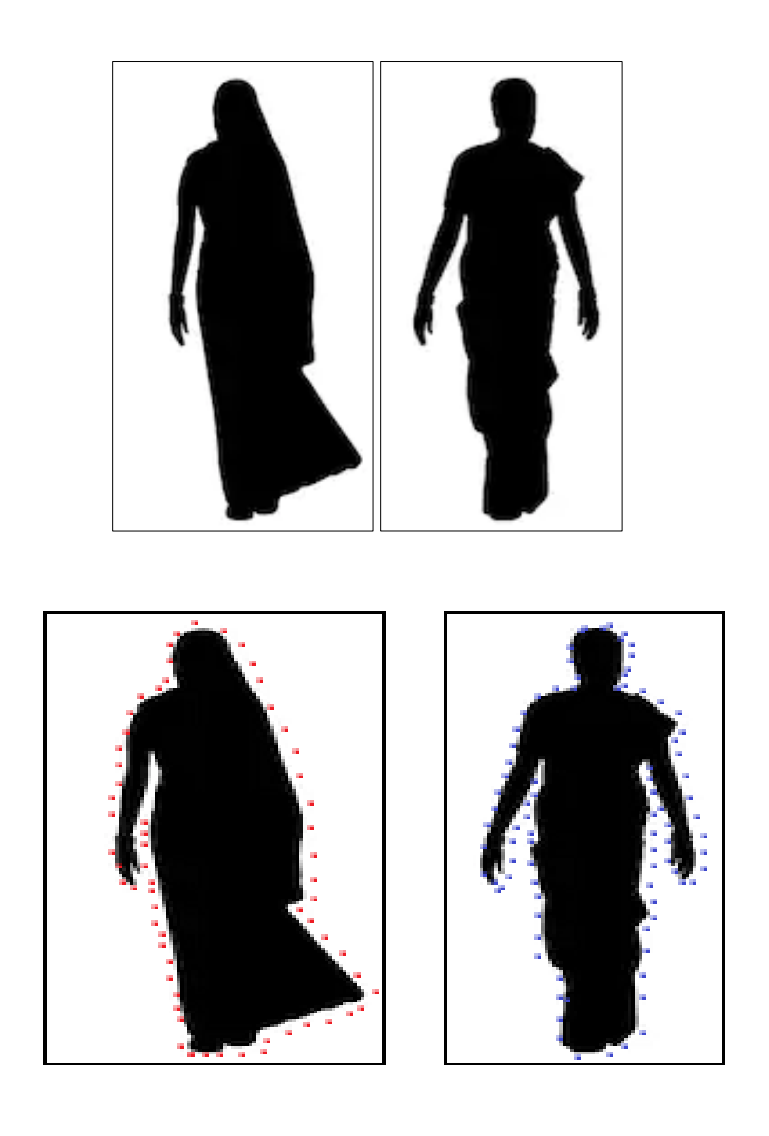


Fig. 5.3 The model silhouettes with different dresses

(The gait features cannot be captured correctly in some clothes worn by the human)



- a) Model image carrying barrel bag
- b) Model image wearing Coat



c) Human wearing shoulder bag

Fig. 5.4 a), b), c) Model Image and its corresponding Silhouettes of the captured video

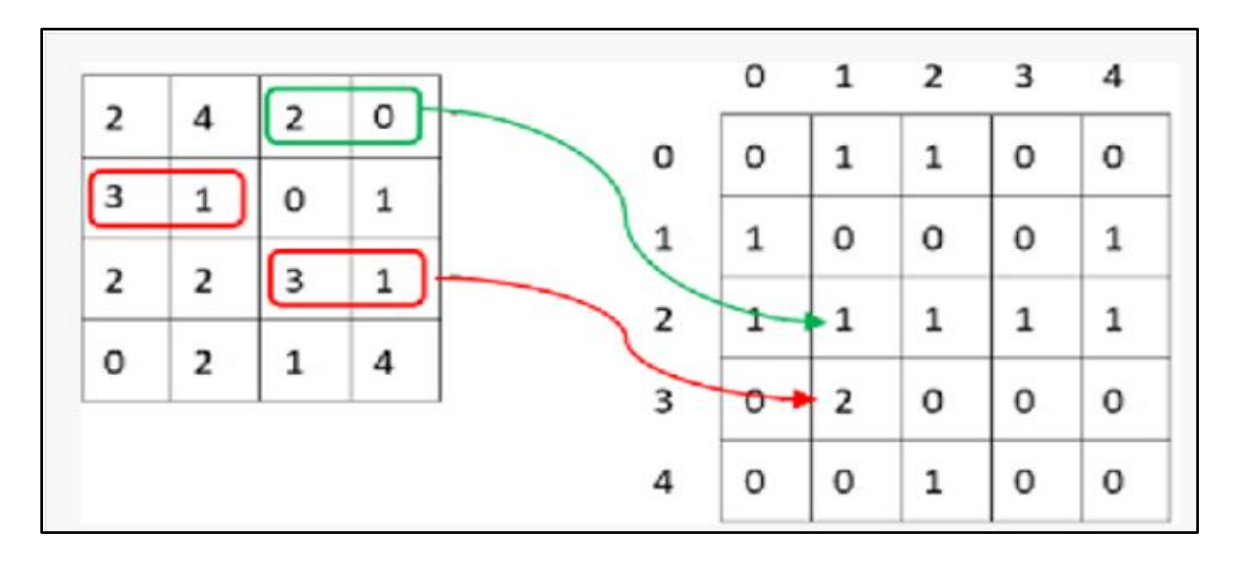


Fig. 5.5 Covariance matrix saved in GLCM table

(the output of the silhouette image pixel values stored in the left side table and its corresponding GLCM table)

5.4 Feature Extraction using Gray Level Co-Variance Matrix

Texture-based features are described from the silhouette image using edge

histogram descriptor. The feature subsets are extracted using Grey level Covariance Matrix

(see in Fig. 5.5) and reduced by Particle Swarm Optimization (PSO) algorithm. The

GLCM is used to find the distance between the blocks of the image, the location angle

relationship of blocks and to calculate the occurrence of the grey-level pixel in all the

directions either horizontal, vertical, diagonal or adjacent. The image features or blocks

are composed of individual particles or pixels. Each particle has an attribute value which

is directly or indirectly depends on the behaviour and location of the particle [55]-[57].

5.4.1 Pseudocode for Best Feature Selection and Optimization using

**GLCMPSO** 

**Input**: Features extracted and optimized from the image

**Output**: Best features are filtered

Step 1: Define each block in terms of i, j matrix using GLCM and find the number of

times the pixel occurs in a specific location of blocks.

Step 2: Make the GLCM symmetric by adding the matrix with its transpose

Step 3: Normalize the GLCM by dividing each element by the sum of all elements

 $\sigma(x,y) = \frac{1}{n-1} \sum_{i=1}^{n} (x - \bar{x})(y - \bar{y})$ 

Table 5.1 The texture-based features extracted from the silhouette using GLCM

66

S.NO	FEATURE	FEATURE NAME	CALCULATED VALUE
1	Shape	Area	737
2	Shape	Centroid	114.5726
3	Shape	Bounding Box	84.5
4	Shape	Major Axis Length	70.592
5	Shape	Minor Axis Length	46.2697
6	Shape	Eccentricity	0.7552
7	Shape	Orientation	-67.802
8	Shape	Convex Hull	142.5
9	Shape	Convex Area	1839
10	Shape	Filled Area	1703
11	Shape	Euler Number	-7
12	Shape	Extrema	142.5
13	Shape	Solidity	0.4008
14	Shape	Extent	0.2955
15	Shape	Perimeter	180.4092
16	Texture	Autocorrelation	1.211
17	Texture	Contrast	0.034
18	Texture	Correlation	0.878
19	Texture	Cluster Prominence	32.13
20	Texture	Cluster Shade	0.92
21	Texture	Dissimilarity	0.017
22	Texture	Energy	0.968
23	Texture	Entropy	0.126
24	Texture	Homogeneity	0.993
25	Texture	Sum of Square: Variance	1.1968
26	Texture	Sum Average	2.0841
27	Texture	Sum Variance	4.4117
28	Texture	Sum Entropy	0.116
29	Texture	Difference Variance	0.0348
30	Texture	Difference Entropy	0.0694
31	Texture	Information measure of correlation	-0.6087
32	Texture	Inverse difference normalized	0.9982
33	Texture	Inverse difference moment normalized	0.9995

Step 4: Initialize each feature with random position and their velocity within the block

Step 5: Define the feature subset f and its boundary as min and max, where f = 1, 2, ..., nStep 6: For best feature selection:  $P_f$ ,  $V_f$ , the local feature  $L_f$ , global feature  $G_f$  and nearest neighbor  $N_f$  are combined together to get  $U_f$ . Where,

$$U_f = WV_f + \rho 1r1(G_f - P_f) + \rho 2r2(L_f - P_f)$$

The coefficients W,  $\rho 1$ ,  $\rho 2$  adds weightage to the global feature and local feature which determines the new velocity. The parameters r1 & r2 are the random vectors with values lies between 0 & 1.

Step 7: Update the new position of the particle, Hence  $NP_f = P_f + V_f$ 

If  $NP_f < P_f$  then

resume the local feature as  $Np_f \leftarrow P_f$ 

If  $P_f < G_f$  then

resume the global feature as  $G_f \leftarrow NP_f$ 

Step 8: Continue the steps 6 and 7 until the best position found for selecting the feature.

### **5.5** Classification of Optimized Feature Subset

Images are made up of numerous pixels with the various colour combination. The correlation value and locational relationship angles are considered for grouping the features. The features are classified for ease of the recognition part. In the feature learning method, K-Nearest Neighbor (KNN) method is used to train noisy large data. For every new block, an objective function called distance D is generated, approximated and applied

Table 5.2 Optimized features list using PSO

S.No	Features found using GLCM	Unsupervised Learning	Chi-Square Method	Proposed Swarm optimized feature set
1	Area	Area	Area	Area
2	Solidity	Autocorrelation	Autocorrelation	Autocorrelation
3	Bounding Box	Bounding Box	Bounding Box	Bounding Box
4	Centroid	Centroid	Centroid	Centroid
5	Autocorrelation	Cluster Prominence	Cluster Prominence	Cluster Prominence
6	Contrast	Cluster Shade	Cluster Shade	Cluster Shade
7	Extent	Contrast	Contrast	Contrast
8	Orientation	Convex Area	Convex Area	Convex Area
9	Eccentricity	Convex Hull	Convex Hull	Correlation
10	Perimeter	Correlation	Correlation	Difference Entropy
11	Sum Average	Difference Entropy	Difference Entropy	Dissimilarity
12	Sum of Square: Variance	Difference Variance	Difference Variance	Eccentricity
13	Correlation	Dissimilarity	Dissimilarity	Energy
14	Major Axis Length	Eccentricity	Eccentricity	Entropy
15	Cluster Prominence	Energy	Energy	Extent
16	Cluster Shade	Entropy	Entropy	Filled Area
17	Convex Area	Euler Number	Euler Number	Orientation
18	Extrema	Extent	Extent	Solidity
19	Filled Area	Extrema	Extrema	Sum Average
20	Convex Hull	Filled Area	Filled Area	Sum Entropy
21	Dissimilarity	Homogeneity	Homogeneity	
22	Sum Variance	Information measure of correlation	Orientation	
23	Sum Entropy	Inverse difference normalized	Perimeter	
24	Minor Axis Length	Orientation	Solidity	
25	Equiv Diameter	Perimeter	Sum Average	
26	Euler Number	Solidity	Sum Entropy	
27	Energy	Sum Average	Sum Variance	
28	Homogeneity	Sum Entropy		
29	Entropy	Sum Variance		
30	Difference Variance			
31	Difference Entropy			
32	Information measure of correlation			
33	Inverse difference normalized			
34	Inverse difference moment normalized			

to the neighborhood. The disadvantage of the Support Vector algorithm is used to find the distance of each training block or feature. In the feature classification part, the distance of the N-vectors of the blocks is grouped and formed, a similarity function k which would be nearly closer to the feature vector. The average distance between the newly arrived features and the support feature vectors are also calculated [57]-[71]. Based on the distances, the features are grouped as a single class. The accuracy of the classification method proposed is found that SVM (Support Vector Machine) and KNN (K-Nearest Neighbor) are together deployed to achieve better accuracy than using alone. SVM and KSVM are called NSFV (Nearest Support Feature Vector).

### 5.5.1 Pseudocode for Nearest Support Feature Vector (NSFV) algorithm

**Input:** Set of features as S, proportional values of each feature as M, classification definition as  $\epsilon$ , training set as R, support vectors as  $SV_i$ . where  $SV_i \in R$  (i = 1, 2, ..., m) and Difference D,

**Output:** multiple features are classified based on their support vector values.

For each feature set do

```
For i, j= 1 to m do  If \ D \ (SVi, SV_j) < \epsilon  SV_j \leftarrow SV_i;   Update \ SV_j;  SVj = Pi   end if  end \ for
```

The performance of the classification methods is calculated using Table 5.3.

Table 5.3 The metrics used for evaluating the performance of the optimized silhouette feature classification algorithms

Metrics	Calculating formula
Accuracy	TP+TN
	TP+FP+FN+TN
Precision or Positive Predictive	TP
Value (PPV)	TP+FP
F-rate	(Precision * Recall) 2 (Precision + Recall)
Specificity or True Negative Rate	TN
(TNR)	TN+FP
Sensitivity or Recall or True	TP
Positive Rate (TPR)	TP+FN
False Positive Rate (FPR)	FP
	TN+FP
False Negative Rate (FNR)	FN
	FN+TP
True Positive (TP)	No of the pixels correctly identified as silhouettes
	selected for averaging
True Negative (TN)	No of the pixels correctly identified as non-
E.L. D. W. (ED)	silhouettes
False Positive (FP)	No of pixels incorrectly identified as silhouette features
Ealso Nagative (EN)	No of pixels incorrectly identified as non-silhouette
False Negative (FN)	features
	reatures

### **5.6** Summary

From the proposed work, the human would be recognized by the features extracted from the silhouette. The Grey level Co-Variance Matrix extracts nearly 30 features from the silhouettes using the wavelet transform and the Particle Swarm Optimization method, decreasing the features list. The fuzzy probability concepts are coupled with NSFV to perform the recognition process. The relationship between the CMS, TPR, TNR and F-rate of the classifiers are calculated and the Nearest Support Feature Vector (NSFV) algorithm was found to be better than the compared classification algorithms. If the classification part will be done clearly, the template matching from the gallery setting will also be good during the recognition part.

### CHAPTER 6

# ACCUMULATED GAIT ENERGY IMAGE (AGEI) FEATURE OPTIMIZATION, SELECTION AND CLASSIFICATION USING BAYESIAN FILTERS

### **6.1 Introduction**

In the technology field, biometrics is used as an automation input for identifying or authenticating a human. The objective of this paper is to extract the feature from the gait for recognition. The gait model is captured by the cameras installed in the surrounding, targeting the corresponding human. The walking process of a human process is cyclic and unique used for differentiating every human without human knowledge from distant locations [50]-[51]. Grid-eye sensors are installed in the nearby places to capture the human gait from distance, not only sensor chips inside the skin for recording the human data [52], whereas some method needs the cooperation of the human for recognition, some don't. To analyse the gait data, methods like fisher [53], CNN [54], PCA and SVM [55] are used. The joint movements of the human are uniquely identifiable, so the analysis is done based on the movements of the body parts [58]. The movements of the human captured in the image are called GEI. The GEI is the average image of the gait profile widely used to retrieve the gait knowledge. It stores the static and dynamic representation of a gait cycle. The static representation contains, the outer appearance and shape of the human and the dynamic representation contain, the walking frequency and phase variation [56]-[66].

Using the augmentation [67] concept, the augmented GEI is calculated. Gait captured in 11 views with three variations such as viewing angle, clothes worn by the

gait and the carrying properties of the gait are considered in [68]. The human detection and extraction of the mobility of the human in the captured video sequence by applying the normalization factor are to reduce the dimension of the selected frames for the classification of features [69]. The Spatio-temporal features are the variations of the AGEI calculated using the linear regression and GLCM. The features are the special noticeable space in the image, so the filtration methods like Gabor filters [70]-[71], optimization algorithms like Particle Swarm Optimization, Crow Search Algorithms [53] are used to decrease the feature list. After all, the optimized features are classified to make the recognition process easy, by applying the normalization rules to the network models [73]-[80].

The contributions of this proposed work are done in the following manner:

- 1. The GEI of the static image and the GEI of the augmented image are merged to find the Accumulated Gait Energy Image (AGEI).
- 2. By closely observing the AGEI and walking speed value, the features are represented from AGEI using Recursive Feature Elimination (RFE). The represented features are optimized using the Crow Search Optimization Algorithm (CSA). The new features are predicted from the optimized features using Principal Polynomial Feature Transform (PPFT). Thus, the predicted features give more information about the dataset and are used for classification.
- 3. The SVM, KNN, RF, QDA, AB, NB are the classifiers used to classify the AGEI features. From that the best feature classifier algorithm is found by calculating Precision, Recall, Accuracy and F-rate using the True Positive (TP), False.

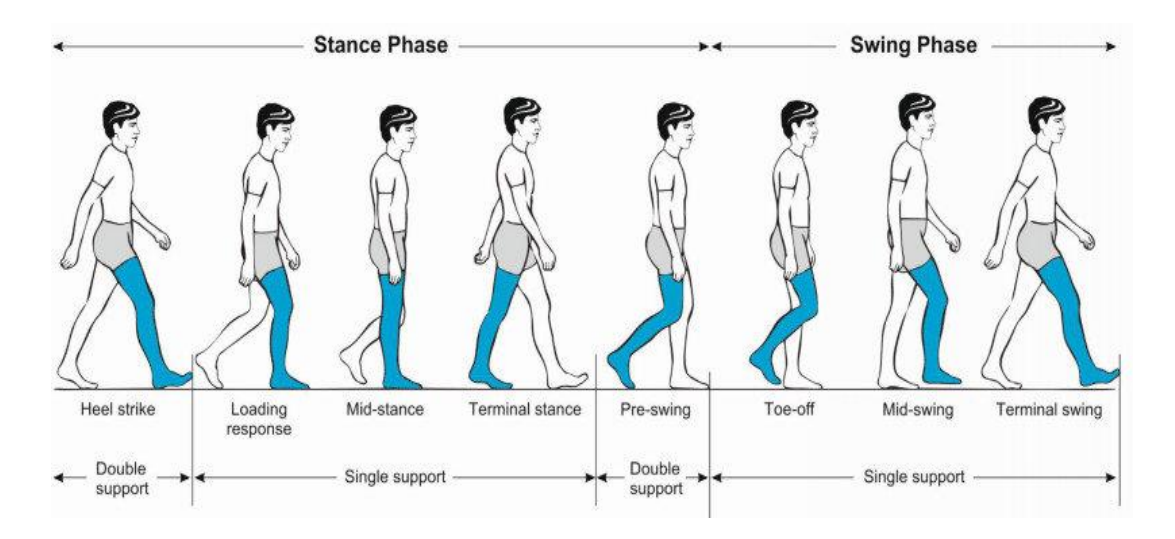


Fig. 6.1 The gait cycle with multiple phases



Fig. 6.2 The Gait Energy Image (GEI) with the Walking frequency and phase

Positive (FP), True Negative (TN) and False Negative (FN) based on the selected features

4. An improved DBNetwork model is trained with the Conditional Probability Value (CPV) of the predicted features to deploy with the best feature classification algorithm primarily needed for human recognition.

### 6.2 The preliminaries of the AGEI Feature Recognition

The gait model is captured by the cameras installed in the surrounding, targeting the corresponding human. The walking process of a human process is cyclic and unique used for differentiating every human without human knowledge from distant locations.

### **6.2.1 Infrared Sensors**

The Infrared thermopile sensors consist of the number of thermocouples that detects the human at a distance of up to 5 metres without any contact. Every thermopile records the human temperature value. For detecting the human Grid-eye sensor is used.

### 6.2.2 RGB-depth Camera

The RGB-depth cameras are attached with Grid-eye sensors to capture the 3-D view of the human body joints without any locating bounding boxes walking in front of the camera. The gait cycle was captured irrespective of the walking angle, clothes wearing and carrying properties [51]-[63]. It is difficult to recognize individuals under various conditions like humans with carrying bags, humans with wearing dresses like saree, nighty etc are included in this recognition task. The features of the gait models

obtained under similar conditions are learned to fit with the training set. To study the problem, augmented gait energy images are used as input.

### **6.2.3** Gait Energy Image – GEI (real)

The GEI is the average image of the gait profile widely used to retrieve the gait knowledge. It stores the static and dynamic representation of a gait cycle. The static representation contains the outer appearance and shape of the human and the dynamic representation contains the walking frequency and phase variation (see in Fig. 6.2). The gait cycle consists of multiple phases as in Fig. 6.1. The time taken for the switch over from one phase to another phase in the gait cycle cannot be easily calculated, because it may be varied between human to human. The phase of gait is A (x, y, t). By applying the running average, In order to calculate the GEI Eqn. 6.1 is called for considering the AGEI

$$GEI = \frac{1}{N} \sum_{t=1}^{N} A(x, y, t)$$
 6.1

Where x be the horizontal axis, y be the vertical axis, and t be the temporal axis. The correlation between the original GEI and the augmented image is used as the feature of gait. The AGEI is calculated by adding the frame difference of the augmented image (Fig. 2. c) and GEI of the augmented image [64-]-[73] (Fig. 6.2)

$$AI(x,y,t) = \begin{cases} 0 \text{ if } A(x,y,t) \ge A(x,y,t-1) \\ A(x,y,t-1) - A(x,y,t), \text{ Otherwise} \end{cases}$$
 6.2

GEIA 
$$(x, y, t) = \begin{cases} 0 \text{ if } B(x, y, t) \ge B(x, y, t - 1) \\ B(x, y, t - 1) - B(x, y, t), \text{ Otherwise} \end{cases}$$
 6.3

### **6.2.4** Augmented Gait energy Image-AGEI (artificial)

The classification of Features selected from the feature list is the proposed work. The input GEI image may be less appropriate to extract the features, so, it is necessary to augment the GEI image to get a perfect input GEIA. Zooming the image to some extent is the spatial change augmentation done. In the training process, the height and width of the GEI image are chosen with the interval [w/3, 1], where w is the width of the GEI image and [1, h/3], here h is the height of the image box. The resulting image is then resized to  $52 \times 52$ . The image looks the same but changed the pixel location inside the frame [62]-[70], [71]-[72].

## **6.3** Feature Representation in AGEI using the Spatial Dependence Matrix of the Pixels

The Features are the notable representation in the gait and its descriptor values are calculated using the Spatial Dependency Matrices (N x M) formed from the angle (see in Fig. 6.3)  $\Delta p_r$  of the pixel pairs ( $\Delta p_1$ ,  $\Delta p_2$ ). Then x and y be the pixel values and  $\Delta p_1$ ,  $\Delta p_2$  reverts the relationship of the pixel value pairs. The gait points are marked as P (p1, p2, p3,...,pn). The angle between the two gait points are calculated by p1 and p2 and a reference point pr (see in Fig. 6.3). The reference point connects the gait points or joints calculated using the Recursive Feature Elimination (RFE). The factor N stores the number of features and the factor M stores the number of frames of the features. Here, N = 27 and M = 120 [11] (see in Fig. 6.4). Consider a wrist, which is a

reference point or joint that connects the hand and the palm. Then the next step was to establish the connections between the selected features to frame a complete model to recognize. Let R be the AGEI and C be the connection between the selected features calculated by the descriptions shown in Table 6.1.

$$C_{\Delta x \Delta y}(i,j) = \sum_{x=1}^{m} \sum_{y=1}^{n} \begin{cases} 1, & \text{if } C(x,y) = i \text{ and } A(x + \Delta x, y + \Delta y) = j \\ 0, & \text{otherwise} \end{cases}$$
 6.5

To compute the joint angles from any given frame,

$$\Delta(p_1, p_r) = \sqrt{(x_1 - x_r)^2 + (y_1 - y_r)^2 + (z_1 - z_r)^2}$$

$$6.6$$

$$\Delta(p_2, p_r) = \sqrt{(x_2 - x_r)^2 + (y_2 - y_r)^2 + (z_2 - z_r)^2}$$
6.7

$$\emptyset(p_1, p_2, p_r) = \frac{\cos^{-1}\vec{p}_1 \cdot \vec{p}_2}{\Delta(p_1, p_r)\Delta(p_2, p_r)}$$
6.8

### **6.3.1** Pseudocode for Feature representation in AGEI using RFE

**Input:** the Probability density function Value of the Features are calculated using Eqn 6.1 to 6.10

Output: Features represented in Gait

Step 1: Normalization: Given the input state p(x) and the output state p(y|x), the posterior state p(x|y) is obtained by dividing by the normalization factor p(y).

$$p(X/y) = \frac{p(\frac{y}{x})p(x)}{\int X p(\frac{y}{y})p(x)dx}$$
 6.3.1 (a)

Step 2: Marginalization: By giving the joint posterior, the marginal posterior of the gait is found by,

$$p(X/y) = \int Zp(x, (Z/y)dz$$
 6.3.1 (b)

Step 3: Expectation: The expected or the output posterior is calculated by

$$\operatorname{Ep}(X/y)[f(x)] = \int Xf(x)p(X/y) \, dy \tag{6.3.1 (c)}$$

Step 4: Let p(xn|yn:0) be the conditional pdf of xn, calculated using 6.3.1(a), 6.3.1(b), 6.3.1 (c) and formed the equation,

$$p\left(\frac{x_n}{y_{n:0}}\right) = \frac{\frac{p\left(\frac{y_{n:0}}{x_n}\right)p(x_n)}{p(y_{n:0})}}{\frac{p(y_n, y_{n-1}/x_n)p(x_n)}{p(y_n, y_{n-1:0})}}$$
6.9

Step 5: Using the angles of the joints, the features are labeled.

Step 6: Consider each Feature in terms of i, j matrix using spatial dependency in order to find the number of times the pixel occurs in specific location of blocks

Step 7: Let  $\sigma$  be the spatial dependence matrix, calculated by,

$$\sigma(x,y) = \frac{1}{n-1} \sum_{i=1}^{n} (x - \bar{x})(y - \bar{y})$$
6.10

Step 8: End

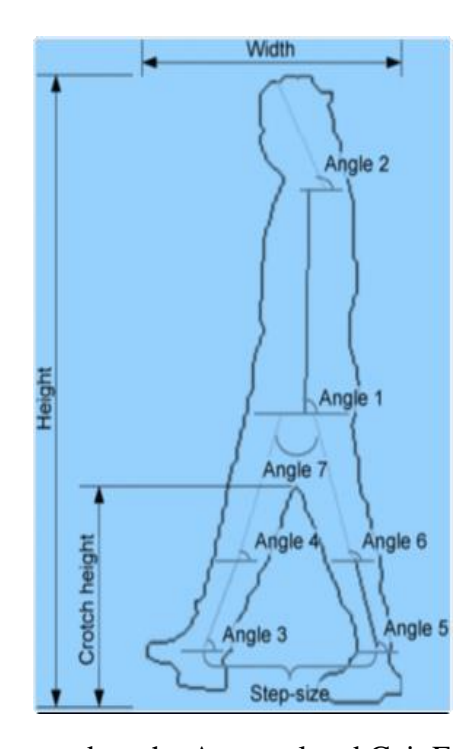


Fig.6.3 Angle to be noted on the Accumulated Gait Energy Image (AGEI)

Table 6.1 Feature description values of the walking gait calculated using the Spatial dependency Matrix

Feature descriptions	Normal gait	Abnormal gait or limping	Gait with carrying properties	Gait with saree, dhoti or skirt
Contrast	15.9206	112.1709	61.7209	58.4289
Correlation	0.6488	0.9297	0.8643	0.7732
Dissimilarity	0.0797	0.7566	0.5156	0.6453
Energy	0.9987	0.9547	0.9789	0.9745
Entropy	0.0069	0.2490	0.1250	0.1299
Homogeneity	0.9994	0.9796	0.9900	0.8976
Mean	1.1015	2.4098	5.1603	5.1603
Variance00	22.6651	227.4835	797.8255	25.8744
Standard Deviation	4.7608	15.0826	28.2458	9.7867
Area	9.456	136.5000	492.88	12.455
Perimeter	766	132	488	955
Circularity	0.0260	1.1784	2.0984	1.8824

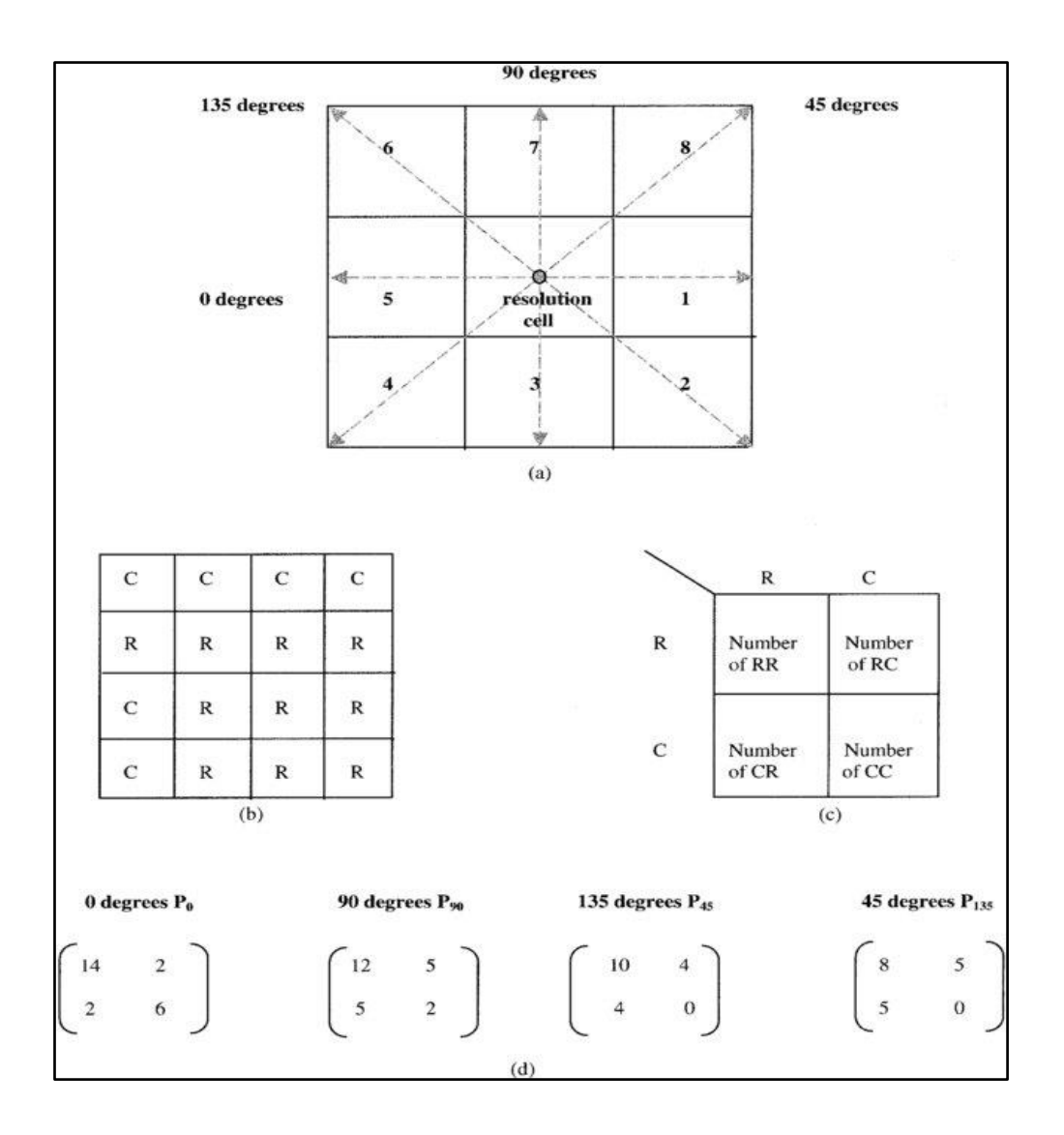


Fig. 6.4 Spatial Dependence Matrix of the GEI and the artificial AGEI calculated based on the angles noted in Fig. 6.3

### 6.4 Feature Optimization and Feature Prediction using CSA and PPFT

The Crow Search Algorithm (CSA) is a metaheuristic Swarm intelligence algorithm used for feature optimization. The real crow hides the whole food and remembers the location and retrieves when needed. In the optimization theory, the algorithm is the searcher, the selected feature list is the search place, the feature match is achieved from the feature list, the mostly matched features are differentiated as the global optimal solution [53]-[87]. The total feature list is initialized as D. Using the traditional crow search algorithm, consider several crows needed for search as M and D. The probability of search be P, the flight length of the crow are assumed as F, T<sub>max</sub> represents the travel times or iterations and the memory of the crow is assumed as Memo to store the feature details. The crow knows the actual feature list based on the constraints, the crow uses the input features seen in Table 6.2. The prediction is the finding of new features and leaving the existing features using the Principal Polynomial Feature Transform method. The polynomial features are created by raising the existing optimized features to an exponent. The algorithm for feature optimization using crow search is implemented in Python 3.6.9.

### **6.4.1** Pseudocode for Feature Optimization and Feature Prediction

**Input:** 19 input features (D), the total number of crows needed for search as M, the search Probability P, the flight length of crow as F,  $T_{max}$  represents the travel times

Output: Reduced and Optimized feature set

Step 1: Explore each considered Feature to automatically select the number of features

Step 2: There will be the choice of selecting features from the list by initialising the crow position and memory of crow Memo with a random value

Step 3: For  $F \leftarrow 1$  to  $T_{max}$  do

Step 4: For  $j \rightarrow 1$  to D do

Step 5: Count  $\rightarrow$  0

Step 6: For  $I \rightarrow 1$  to M do

Step7:. If Memo [I, j] == 1 and I in Selected features then

Step 8: Count  $\rightarrow$  Count + 1

Step 9: Print (Count)

Step 10: If F← fitness (Memo)

Step 11: If len (F) < len (F+1) then

Step 12: Initialize  $F \leftarrow F + 1$ 

Step 13: Initialize accuracy  $\leftarrow \frac{\text{len(F)}}{M} * 100$ 

Step 14: Print (accuracy)

Step 15: The accuracy of the various feature subsets are considered and mean of the average subset is final

Step 16: End

The input features are a total of 23 listed in Table 6.2, from that 20 Features are optimized. In the Principal Polynomial Feature Transform (PPFT), the 12 new features are predicted from the optimized features and proved to be sufficient to identify every human uniquely, from a distance.

Table 6.2 Spatio-temporal based AGEI Features

S. No	Input Features		
1	Head		
2	Neck		
3	Spine Shoulder		
4	Elbow Left		
5	Elbow Right		
6	Wrist Left		
7	Wrist Right		
8	Thumb Left		
9	Thumb Right		
10	Hand Left		
11	Hand Right		
12	Hand Tip Left		
13	Hand Tip Right		
14	Spine Mid		
15	Spine Base		
16	Hip Left		
17	Hip Right		
18	Knee Left		
19	Knee Right		
20	Ankle Left		
21	Ankle Right		
22	Foot Left		
23	Foot Right		

Table 6.3 The features extracted using the RFE algorithm from AGEI after optimization

		After Feature	
G M	I (F)	Optimization	Feature predicted from the Optimized
S. No	Input Features	using CSA	features using PPFT
1	Head	Head	Head
2	Neck	Neck	Cadence or Walk length (CD)
3	Spine Shoulder	Spine Shoulder	Shoulder Left Angle
4	Elbow Left	Elbow Left	Shoulder Right Angle
5	Elbow Right	Elbow Right	Left Ankle Joint Angle (LAJA)
6	Wrist Left	Wrist Left	Left Knee Joint Angle (LKJA)
7	Wrist Right	Wrist Right	Right Ankle Joint Angle (RAJA)
8	Thumb Left	Hand Left	Right Knee Joint Angle (RKJA)
9	Thumb Right	Hand Right	Stride Length Left (SLL)
10	Hand Left	Spine Mid	Stride Length Right (SLR).
11	Hand Right	Spine Base	Left Hand Elbow Angle (LHEA)
12	Hand Tip Left	Hip Left	Right Hand Elbow Angle (RHEA)
13	Hand Tip Right	Hip Right	
14	Spine Mid	Knee Left	
15	Spine Base	Knee Right	
16	Hip Left	Ankle Left	
17	Hip Right	Ankle Left	
18	Knee Left	Ankle Right	
19	Knee Right	Foot Left	
20	Ankle Left	Foot Right	
21	Ankle Right		
22	Foot Left		
22	Foot Right		

### **6.5** Classification of the Optimized Features

Classification is the process of grouping objects based on category. The correlation value and locational relationship angles are considered for grouping the features. So, the DBNetwork model was integrated with the classification algorithms to classify the multilabel features (see Table 6.3) based on the Conditional Probability Value of the Features.

### **6.5.1 Support Vector Machine (SVM)**

It is the popular Supervised Learning algorithm used for Classification and Regression. Here, the gait features are classified to ease the recognition part. SVM can able to classify multiple, continuous and categorical variables. SVM minimizes the out of sample error (generalization error) and maximizes the geometric margin if there was any lowest relative confidence between two clusters. Radial Basis Function (RBF) is used as a kernel function to map the input features into high-dimensional feature space to find an optimal feature using CSO to divide the feature as optimized and unoptimized. Moreover, selecting the necessary feature vectors from the features list to train SVM. The SVM is trained to classify the feature vectors to train the SVM, the user should select a suitable kernel function and also optimal amounts for kernel parameter and penalty factor [75]-[77].

### **6.5.2** K-Nearest Neighbor (KNN)

It is the simplest learning and classification algorithm, which works by assuming the similarity between the newly arrived feature and the test case feature and settles the new feature into the category that is most similar to the available feature set. It is also called a lazy learner because it stores the dataset and starts processing in the training set later. In the feature classification part, the distance of the N-vectors of the features within the clusters is grouped and formed a similarity function k which would be nearly closer to the feature vector. The average distance between the newly arrived features is calculated. Based on the distances, the features are grouped as a single class. The classification algorithms are trained to classify the predicted features as TP, TN, FP, FN [78]-[79].

### **6.5.3** Ada Boost (AB)

Here Ada boosting algorithm was used to learn the dataset to make predictions with high accuracy. It combines the average findings of all the weak features to build a strong feature [80].

### 6.5.4 Random Forest (RF)

The decision trees are collectively called. This algorithm is designed to identify a new feature based on its descriptor value, the cluster tree is formed with votes. The forest chooses the cluster with more votes. The dataset is selected at random number m to set the training set N, from the starting to end, the value of m must be constant during this process [80].

### 6.5.5 Naïve Bayes (NB)

A Naive Bayes classifier initially considers one feature unrelated to any other feature in the same cluster. In the feature classification work whether the features are

related or not, the Naïve Bayes classifier considers the properties of every feature individually by calculating the probability of every feature [81]-[83].

# **6.5.6** Quadrant Discriminant Analysis (QDA)

QDA allows the covariance matrix of each feature estimated for every cluster of the image. The neighbor features show related covariances and the distant feature shows distinct covariances. But the QDA cannot allow reducing the feature set [83].

# 6.5.7 Pseudocode for Classification of Predicted Features Using NB algorithm

**Input:** vroot: root of the trained tree,

R: features to predict,

M: Feature List

w:descriptor value

x:Slow, fast, medium

v:CPV

**Output:** Predict (x, R)

procedure GetFeat(f)

Step 1: if f is Feat then

Step 2: FeatList.push(f)

Step 3: for  $m \in 1 \dots M$  do

else if f.w> mx > 0.5

print ("normal gait)

else if f.w>mx > 0.8

print ("abnormal gait")

```
else if f.w>mx>0.95 && <1.05
print ("Gait with carrying properties")
GetFeat(vm)
sent ← true
end if
end for
if not sent then
m \leftarrow \operatorname{argmax} \ m \in \{1, 2, ..., M\}
GetFeat(vm)
end if
end if
leafList \leftarrow \emptyset % list of leaves reached by example xGetFeat(vroot)
hist ← \emptyset for vl ∈ FeatList do
sum \leftarrow P \ k \in vl.Lhist \ vl \ .Lhist[k]
for k \in vl .Lhist do
hist[k] += vl .Lhist[k]/sum
end for
end for
labels \leftarrow select R top entries from hist
return labels
```

The classification algorithms are inputted with the gait features such as 19, 17, 15, 12 trained to classify the features. The performance metrics tabulated in Table 6.4 are executed to know the performance difference of the Naïve Bayes classification algorithm.

Table 6.4 The metrics used for evaluating the predicted AGEI features classification algorithms

Metrics	Calculating formulae		
Accuracy	TP + TN		
	$\overline{TP + FN + TN + FP}$ $\overline{TP}$		
Recall or True Positive Rate (TPR)	TP		
	TP + FN FP		
False Positive Rate (FPR)	FP		
	FP + TN TP		
Precision	TP		
	$\overline{\text{TP} + \text{FP}}$		
F-rate	Procision * Pocall		
	2 Precision + Recall		
Mean Absolute Error (MAE)	1 \( \sum_{N} \)		
	$\frac{1}{N} \sum\nolimits_{i=1}^{N}  \widehat{\sigma_i} - \sigma $		
Root Mean Squared Error (RMSE)			
	$\frac{1}{N}\sum_{i=1}^{N}(\widehat{\sigma}_{i}-\sigma)^{2}$		
	\ \ \ \ \ \ \ \ \ \ \ \ \ \ \ \ \ \ \		
Relative Absolute Error (RAE)	$\sum_{i=1}^{N}  \widehat{\sigma_i} - \sigma $		
	$\frac{\sum_{i=1}^{N}  \widehat{\sigma}_i - \sigma }{\sum_{i=1}^{N}  \widehat{\sigma}_i - \sigma }$		
Root Relative Squared Error (RRSE)	∇N 1≎ -1		
_	$\frac{\sum_{i=1}^{N}  \widehat{\sigma}_{i} - \sigma }{\sum_{i=1}^{N}  \widehat{\sigma}_{i} - \sigma }$		
	$\sqrt{\sum_{i=1}^{N}  \widehat{\sigma}_i - \sigma }$		
True Positive (TP)	No of features from the optimized feature set are		
	selected for classification		
True Negative (TN)	No of features from the omitted features are not		
	used for classification		
False Positive (FP)	No of features from the omitted features are		
, ,	used for classification		
False Negative (FN)	No of features from the optimized feature set are		
	not used for classification		

Here  $\sigma$  indicates the positive value of the feature and  $\hat{\sigma}$  denotes the value calculated by the proposed algorithm.

# 6.6 DBNetwork Layers

As per the feature representation work, the Bayesian filters classify the gait as normal, abnormal and limping based on the spatial dependency matrix representation of pixels in the AGEI. The network model called Dynamic Bayesian Network is designed with RBM (Restricted Boltzmann Machine) sub-ordinates and a supervisor Back Propagation Neural (BPN) Network. The supervisor BPNN utilized the Probability distribution of the feature subset produced by RBM (Restricted Boltzmann Machine) to initialize the RBM layer models. The DBNetwork nodes are constructed as RBM1, RBM2, using the CPV values tabulated in Table 6.4. The RBM1 is the parent node and RBM2 is the child node. The Conditional Probability Value of each RBM node is calculated using the probability distribution function of the selected features. The correlational value and CPV of the features are required to train the model. The correlation value  $C_R$  is calculated by

$$C_{R} = \frac{1}{n-1} \sum \frac{(x-\bar{x})}{S_{x}} \frac{(y-\bar{y})}{S_{y}}$$

The Cadence or walk length range of a normal adult will be between 90 and 120 steps/min. The feature description metrics (see in Table 6.2) are calculated for example M is calculated as 99.1 steps/min and Standard deviation SD = 10.4. The abnormal gait or gait with carrying bags or gait wearing a dress like saree, skirt or dhoti records the value low in cadence, mean and standard deviation compared to the normal. While training the network, the dataset was inputted to the node sequentially, so, the network can be adapted to the learning phase [82]-[93]. The initial cadence was set by considering the standard deviation marked in the left or right side of the normal walk length map

using M, SD, Cadence relativeness [26]-[27]. To find the abnormality in the walk, the threshold cut off lower than the stated mean and standard deviation must be noted separately to train the RBM layer. The primary conditional probability value of Cadence (CD), Stride Length Right (SLR), Stride Length Left (SLL), Left Ankle Joint Angle (LAJA), Left Knee Joint Angle (LKJA), Right Ankle Joint Angle (RAJA), Right Knee Joint Angle (RKJA)

To find the abnormality in the walk, the initial consideration is,

If slow < 90 and fast > 110 then

$$\mu$$
(normal) + 1 $\sigma$ , where ( $\mu$  = M and  $\sigma$  = SD)

### 6.6.1 Pseudocode for RBM training phase

**Input:** In terms of RBM, the hidden bias of initial phase is  $a_i$ , the visible bias of initial phase is  $b_j$ , and the amplitude or the weight of the nodes are  $W_{ij}$ , the learning rate of the initial phase is  $\delta_0$ , the iteration number is R and the lowest learning rate is  $\delta_{min}$ .

**Output:** weight of the node  $W_{ij}$ , the final bias  $a_{ij}$  and  $b_{ij}$  and the highest learning rate  $\delta^{new}_{ij}$ 

Step 1: For  $\alpha = 1,2,3, .... R$  do

Step 2: Calculate the status of the hidden layer and visible layer of the randomly selected node of the RBM

Step 3: Calculate the probability of the slope of initial weight Wij and bias a<sub>i</sub> and b<sub>i</sub>

Step 4: Calculate the probability of the incremented weight and bias

Step 5: The reconstruction error is calculated as  $\Delta e_n = e_n - e_{n-1}$ 

Step 6: The updated weight and bias after reconstruction is calculated as,

$$W_{ij}^{next} = W_{ij} + \Delta W_{ij}$$
 and  $a_i^{next} = a_i + \Delta a_i$  and  $b_i^{next} = b_i + \Delta b_i$ 

where  $\Delta$  represents the reconstruction error

Step 7: Using the updated values, each and every layer of the RBM is calculated so  $\delta_{ij}^{next}$  value is set as the learning rate.

Step 8: End for

# 6.6.2 Pseudocode for DBNetwork training

**Input:** Consider T as the training dataset, the amplitude or weight of the node is  $W_{ij}$ , the hidden bias  $a_i$  and visible bias  $b_j$ , the learning rate of the initial phase is  $\delta_0$ , the number of iterations are R, and the number of hidden layers are H

Output: the weight  $W_{ij}$ , the hidden bias  $a_i$  and visible bi

as b<sub>i</sub> achieved through training

Step 1: training phase:

Step 2: For  $\beta = 1, 2, ..., H-1, ...$  do

Step 3: For  $\alpha = 1, 2, ..., R, ...$  do

Step 4: If  $\beta = 1$ , then

Step 5: Now call the RBM training phase and get the weight  $W^1_{ij}$ , the hidden bias is  $a^1_i$ ,

the visible bias is  $b_j^1$ , and the next learning rate is  $\delta_{ij}^1$ 

Step 6: End if

Step 7: End for

Step 8: End for

Step 9: Tuning phase:

Step 10: Consider the weight, hidden bias, visible bias and the learning rate got from all the RBM layers training.

Step 11: For  $\alpha = 1, 2, ..., R, ..., do$ 

Step 12: Call the Crow search algorithm to get the optimized spatial parameters or

features image using the trained RBM layers.

Step 13: End for

The DBNetwork is trained to classify the image as normal gait, abnormal gait, gait with carrying properties, dress worn by the human gait by the CPV. The NB is the highly accurate classifier deployed with DBNetwork to differentiate the newly entering image using the CPV. The NBDBNetwork model is trained with the conditional probability value to identify the human (see in Table 6.4).

Table 6.5 The t-test and p-value for the classified AGEI features calculated based on Conditional Probability Value (CPV) of the walking speed

S.No	Predicted Features	Normal Gait (mean± standard error)	Abnormal Gait (Mean± standard error)	Gait with Carrying Properties (Mean ± standard error)	Dress worn by the Human gait	t-test	p-value
1	Head	0.701+4.507	1.765+0.043	3.556+0.043	0.701+4.507	4.261	1.012
2	Cadence or Walk length (CD)	134.7+3.564	94.56+5.356	74.23+7.578	-0.887+3.564	3.651	0.132
3	Shoulder Left Angle(SLA)	112.78+0.98	95.78+2.76	88.78+3.672	-12.68+0.9	-2.675	0.178
4	Shoulder Right Angle(SRA)	115.46+0.86	98.23+2.45	77.23+1.56	-15.69+0.6	-2.675	0.178
5	Left Ankle Joint Angle (LAJA)	5.342+0.653	9.456+2.335	13.621+2.9	50.342+0.653	-3.768	<1.011
6	Right Ankle Joint Angle (RAJA)	5.322+0.567	9.567+2.577	13.458+2.37	50.322+0.567	4.293	<1.011
7	Left Knee Joint Angle (LKJA)	46.23+0.987	48.22+2.789	50.78+3.122	68.3+0.87	2.366	<0.988
8	Right Knee Joint Angle (RKJA)	49.23+0.355	51.74+2.674	53.21+1.678	97.23+0.5	2.593	<0.988
9	Stride Length Left (SLL)	45.887+1.78	41.34+1.897	37.23+1.121	85.887+1.78	-0.033	0.732
10	Stride Length Right (SLR).	96.344+2.78	94.34+1.465	91.12+1.82	86.344+2.78	0.873	0.453
11	Left Hand Elbow Angle (LHEA)	9.34+1.785	7.26+2.876	11.26+2.16	11.34+1.785	1.342	0.022
12	Right Hand Elbow Angle (RHEA)	9.67+1.789	7.34+2.567	11.34+3.76	11.67+1.789	2345	0.123

### 6.7 **SUMMARY**

In this work, the feature from the Accumulated Gait Energy Image (AGEI) are used as an input for Feature detection, Feature optimization and Feature prediction, From the AGEI, the Spatio-temporal features of the images are represented using Recursive Bayesian filters based on the spatial dependency matrix of the feature pixel. The represented features are optimized using CSA. From the Optimized feature set, new features predicted using the Principal Polynomial Feature Transform (PPFT) method. Finally, the Classification algorithms such as Support Vector Machine (SVM), K- Nearest Neighbor (KNN), Ada Boost (AB), Random Forest (RF), Naïve Bayes (NB), Quadrant Discriminant Analysis (QDA), are used to classify the predicted features. As a result, the NB shows higher classification accuracy than the other classifiers show the better difference in TPR, Accuracy, F-rate, Precision, Recall. The Dynamic Bayesian Network (DBNetwork) model is trained with the Conditional Probability Value (CPV) of the classified features to be deployed with the NB classifier to match the newly arriving image feature set. The model is trained with the calculated RRSE, RMSE, RAE, RME metrics. Finally, the NBDBNetwork model with PPFT produces the best result.

# **CHAPTER 7**

# FUZZY PROBABILITY DECISION ON FPR AND FRR FOR PERSON RECOGNITION

### 7.1 Introduction

Fuzzy logic is a logic with many values ranging the value between 0 and 1. The uses of Fuzzy logic is deployed to dig the partial truth lies in the person recognition concept, where the truth value of the recognition procedure lies between completely true and completely false. The Probability Distributive Function (PDF) of the human features in moving conditions along with carrying properties are calculated using the Fuzzy probability. For example, if a person is walking with carrying bags (shoulder bag, back bag). Cap, Person wearing dresses such as dhoti, saree, nighty would produce an abnormal gait and hence the accuracy and rate of recognition would be difficult [84]-

### 7.2 Preliminaries of Fuzzy Probability

Let P be the probability measure for the Fuzzy set X.  $P(x_i)$  denotes the probability of  $x_i$ , where  $x_i \in X$ . Likewise A be the fuzzy set representing the fuzzy event. A ={x,  $\mu_A(x) \mid x \in X$ }. The degree of membership of  $x_i$  is represented by  $\mu_A(x_i)$  [10].

### **Definition 7.2.1**

Let A, B be two fuzzy sets.

a) The complement of A is denoted by A<sub>c</sub>.

$$A_c(x) = 1 - A(x)$$
 where  $x \in X$ .

- b) The intersection of fuzzy sets will also be a fuzzy set defined by  $(A \cap B)(x) = T(A(x), B(x))$
- c) The union of fuzzy sets will also be a fuzzy set defined by  $(A \cup B)(x) = S(A(x), B(x)) \text{ as defined in [10]}.$

where A and S are associative in each argument.

### **Definition 7.2.2**

Let X, Y are the two Fuzzy random variables. If X and Y are independent then each random variable in the set are also independent.

$$P(Y=y|X=x) == P(Y=y)$$
, for all x, y. where P be the probability

# 7.3 Selection of Best Match Score using PDF

Using the proven Naive Bayes DBNetwork model the classified features are initialized as Pi. The database G with m samples (i = 1, 2, ...m). The newly entered image is Q with unknown features Qj(j = 1, 2, ..., n) having more than one feature not stored before in G. For gaining the Probability, every image must undergo the initial stages of processing such as feature extraction, feature optimization, feature classification and Qj is formed. For estimating the cumulative match score every Qj, must have the t-test and p-value. The cumulative match score S is calculated by,

$$S = \{s(Qj...P1), s(Qj.P2), P'_{j}.P3\}, ..., s(P'_{j}.Pm)$$
7.1

The query Qj is assigned the rank  $k_j = K$ . Then the matching feature from G is  $P_i(K)$ . There are K set of n rank estimates and must be one estimate for each query

feature Qj. For each query there is one estimate likewise every feature is ranked only if there is correct identity  $C_m$  from the sorted list of galleries.

$$C_{m} = C_{m}(Qj;G)$$
 7.2

The probability of rank estimation is Pr(k)(k=1, ..., m). For the query set and the gallery data. the  $P_r(k)$  of the matcher is estimated by,

$$P_r(k) = \frac{1}{n} (\# k_j = k) \text{ where } k \in K$$
 7.3

That is, the Cumulative match score(CMS) is calculated by the sum of P(k). So,

$$CMS(k \sum_{r=1}^{k} P(r))$$
7.4

where k=1, 2, ..., m. To identify new features from the features Qi in the gallery set G, fuzzy rule chooses the highest-ranking feature,

$$C_m(Qj, G) = \{P_{(1)}, P_{(2), \dots, s_{(m)}}\}$$
7.5

$$I_d(Qj)=I_d(d1)$$
 7.6

Then

 $I_d(Qj)$  is "Identified" if  $Qj \in C_m(Qj,\ G)$  and

$$I_d(Qj)$$
 is "Identified" if rank  $K_j$  of  $Qj < K$  7.7

for every new search the authentic scores of the correctly matching feature can be found as better threshold on the imposter scores  $s(Qj,\ P_i)$  and  $I_d(P_i)\neq I_d(Qj)$  from the database. To select m random match from the gallery of size m:

- 1. The authentic score  $X = s(P_i, Q_j)$  where  $P_i \in G$  where  $P_i$  and  $Q_j$  are same set
- 2. Imposter score is Y.

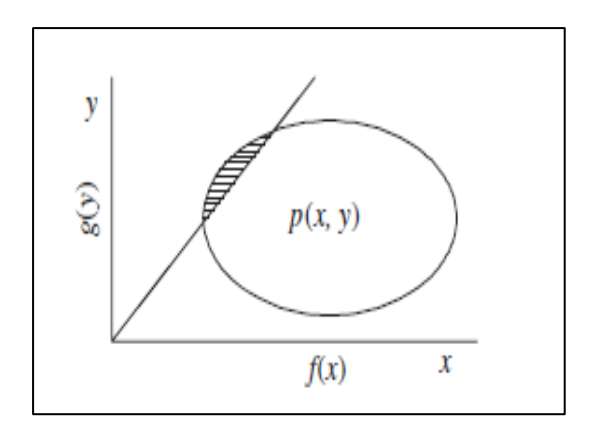
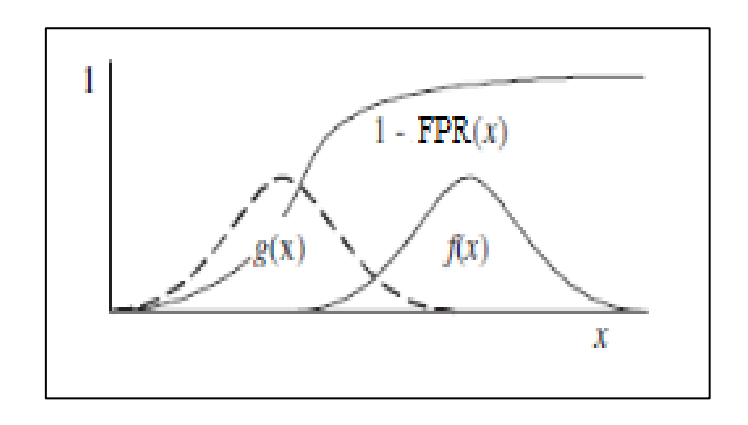
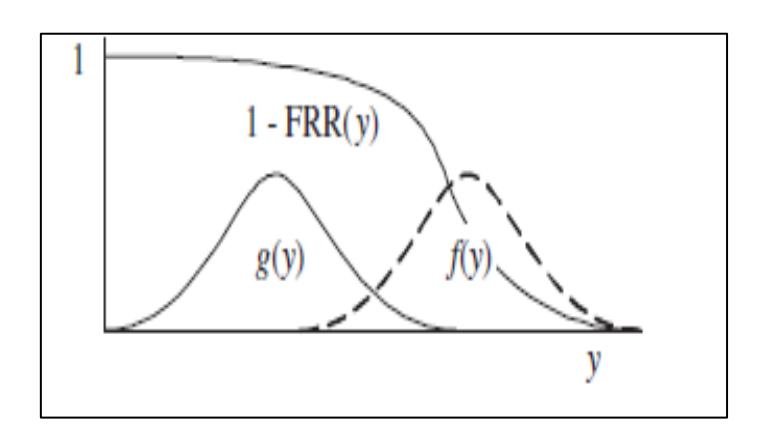


Fig. 7.1 Probability of Misidentification (When the size of the database m=2)



a.



b.

Fig. 7.2 a and b show the Probability of Correct Identification (When database size is m=2 is the integral of f(x)[1-FPR(x)] and g(y)[1-FRR(y)])

From the size gallery, there are m-1 imposter scores  $\{Y_1, ..., Y_{m-1}\}$ , where.  $\{s(P_i, Q_j), i=1, ..., (-1), (+1), ..., n \text{ and } j=1, ..., (-1), (+1), ..., m \}$ , Though Qj is listed in the gallery but Qj not matching to  $P_i$ . In a fuzzy system, input, output with two corresponding membership values are derived. Authentic score X and imposter score Y are the two membership values used in fuzzy probability.

### • If the database size m equals 2(m = 2)

The newly arriving unknown query feature starts with j = 1(Qj) gives the XY value with an authentic score as  $X=s(Qj, P_1)$  and imposter score  $Y=s(Qj, P_2)$ . The probability density function of X is f(x) and the probability density function of Y is g(y). Finally, the probability density function of (X, Y) for 1:1 matcher will be p(x, y)=f(x).g(y).

The rank probability of X and Y is calculated as,

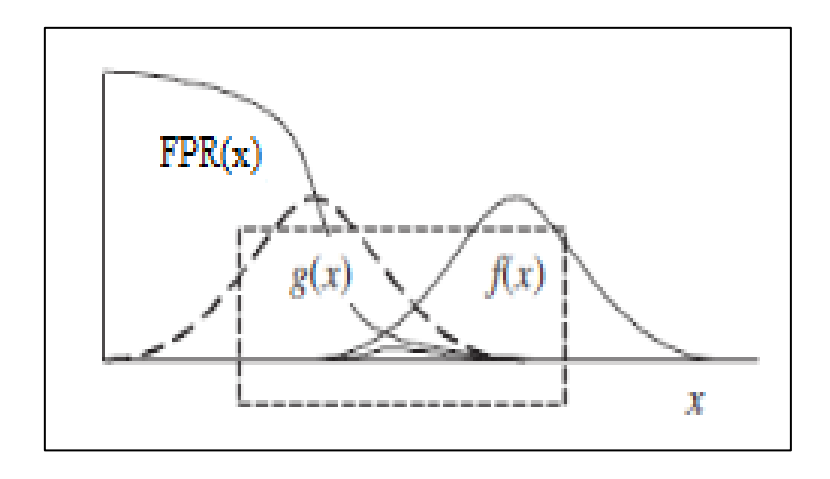
$$P(1) = P_r(rank \ Qj \ is \ 1) = P_r(X \ge Y),$$

$$P(2) = P_r(rank Qj is 2) = P_r(Y > X)$$
 7.8

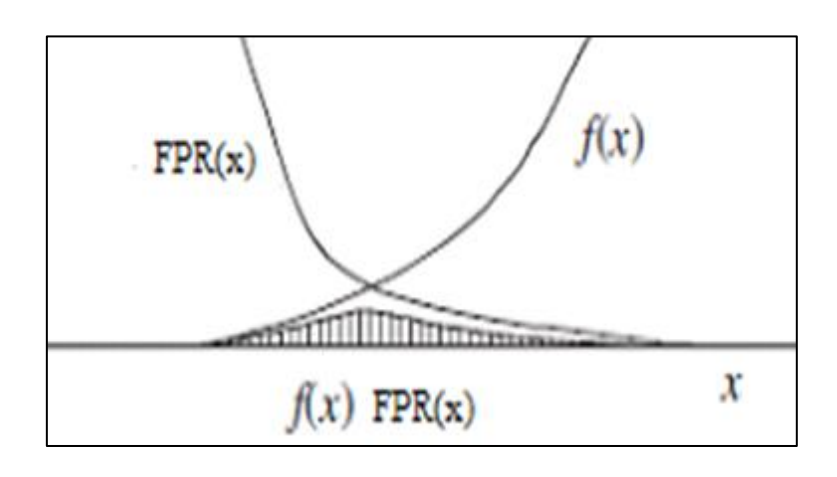
The Fuzzy probability values of the silhouette images are chosen for selecting the perfect match from the gallery set. Using Eqn. 7.1 to Eqn 7.8, the probability of correct identification and probability of misidentification are found.

# **7.4** XGBoost (Extreme Gradient Boosting)

With the development of Artificial Intelligence (AI) technology, a Gait recognition procedure is deployed to ensure security. Firstly, captured images are compressed and thresholded. The new features are predicted from the previous one and loaded into the XGBoost model using the Fuzzy probability values of the features.



a.



b.

Fig. 7.3 a and b show the Probability of Misidentification by the integral of f(x)FPR(x)

The algorithm was designed for increasing the efficiency of computing time and memory utilities. XGBoost supports gradient descent architecture by strengthening the weak learners through system optimization and algorithmic improvements. In the Gait Feature classification methodology framework. the XGBoost model is followed to add all the weak classifiers to fit the data to improve the performance of the current model, without making any change in the proposed classifier.

The features classified using NBDBNetwork model is fused with the Fuzzy probability for PDF calculation using XGBoost wrapper class. Each new classifier would be considered where the previous classifiers were not performing well. First, we estimate P(x, y) by considering f(x) and g(x). by fitting the data to a decision tree using FAR, and the second tree is fitted based on the residual from the previous step which is FRR and this process continues. Where, n is the number of samples, m is the number of features by denoting the features and the target variable of the dataset.

The UCI repository dataset contains nearly 200 observations and finally, 12 features are predicted as necessary for gait recognition. XGBoost objective function helps to choose the targeted predictive functions that control the complexity by Considering the rejection rate and constraints together. The recognition rate of the model depends on the FRR.

Table 7.1 EP, SSIM, PSNR, CQM measures of the compared methods used for Gait classification

Performance of the human recognition model	EP	SSIM	PSNR	CQM
NBDBNetwork	0.0147	0.9009	43.6937	34.0028
NBDBNetwork with PPFT	0.0287	0.9933	34.8725	54.5813
NBDBNetwork XGBoost Fuzzy Probability	0.0041	0.9982	45.9202	57.1044

### 7.4.1 K fold validation

As per the XGBoost advantages. the features list are split into k number of folds. Each fold is used at the testing stage at some point. Hence. 4 folds of datasets are used in this proposed work,

- 19 features are considered as a test set
- 17 features are considered as a test set
- 15 features are considered as a test set
- 12 features are considered as a test set

### 7.5 Summary

Fuzzy logic is a concept used in this proposed work for making decisions based on FPR and FRR. Here unknown or unrecognizable FPR and FRR are the two truth values of the Fuzzy logic capable of probability. Fuzzy probability is a many-valued attribute logic with more than two truth values. Initially, it allows two possible values either True or False. But in-person recognition condition there are three case studies, such as normal gait, abnormal gait, Person with carrying conditions are passed as an argument in the proposed work. Thus, the proposed system allows all the person except the unregistered or newly arrived persons. If there is any value loss in the recognition rate, the XGBoost is the wrapper class that binds all the constraints together as one objective function helps to find the result in minimal time with limited resources. The performance of the classifiers used for Gait feature classification is measured using Entropy (EP), Structure Similarity Index Measure (SSIM), Peak Signal Noise Ratio (PSNR), Cumulative Quality Measure (CQM) and tabulated in Table 7.1.

# **CHAPTER 8**

# THE ENCRYPTION AND DECRYPTION OF THE SILHOUETTE AND ACCUMULATED GAIT ENERGY IMAGE USING A CHAOTIC ALGORITHM- P-FIBONACCI EXCLUSIVE ORDISCRETE COSINE TRANSFORM

### 8.1 Introduction

Secret storage of enhanced input images is necessary for future reference. Though, unintended persons may intercept our images to be aware of them or to destroy them. Smart homes are places where numerous people live together in a gated community. The surveillance systems are set up to monitor the people now and then entering and leaving the apartment. The videos captured every day in the monitoring set-up would be processed in the personal system or the cloud-based on customer satisfaction and future references. The cryptographic algorithms are used to protect the data from intrusion. In the proposed work, the captured images are encrypted and decrypted using Exclusive OR (XOR) and Discrete Cosine Transform. The P-Fibonacci method is applied for scrambling the image, then XOR encrypts the image data using mathematical parameters for making the encryption stronger by combining matrix data of an image with a random key to make the process highly efficient and unbreakable [90]-[93].

The scrambling gives more permutation to re-align the pixels of the image which can be non-recognizable and dis-order. These mathematical or chaotic P-Fibonacci XOR techniques are called scrambling techniques which follows randomization using numerical data of the image by unchanging the actual representation of the image data.

The encryption process is formulated by giving the hash value of the raw image and compressed image as input. Transformation in the image data is done using DCT (discrete cosine transform) [93]-[99]. The encryption process encodes the original image using the cipher key and the decryption process reverses the encryption to get the original image back. There are two methods, Confusion and Diffusion to perform encryption. The masking key and image is confused and rearranged in the distribution process [92]. High redundant pixels in the image have strong correlations in the encrypted image and also Chaos or mathematical based iterations are applied [100]–[103]. Chaotic systems have two types of integer order, the proper fractional-order and improper-fractional order. Parameters of the matrix image data are arranged in fractional orders. While transferring secret images or text, the density of the image pixel and the security of the data are interrelated [104]-[105].

### 8.2 P-Fibonacci transform function

The P-Fibonacci Transform method is used to select an initial sequence from the inputted image matrix. Consider some of the properties of the P-Fibonacci transform series for selecting the input sequence. To encrypt the image, the pixel location of the image is scrambled initially using the P-Fibonacci Transform series.

### **8.2.1:** Proof: The Fibonacci sequence is a recursive function

$$f(p) = \begin{cases} 0 & p < 0 \\ 1 & 1 \\ f(p-1)^{n}(p-2)^{2} & p > 0 \end{cases}$$
8.1

Where p is an indexing parameter of the Fibonacci XOR transform sequence. This The parameter is used to mark the distance vector. From Eq. (1), the Fibonacci sequence

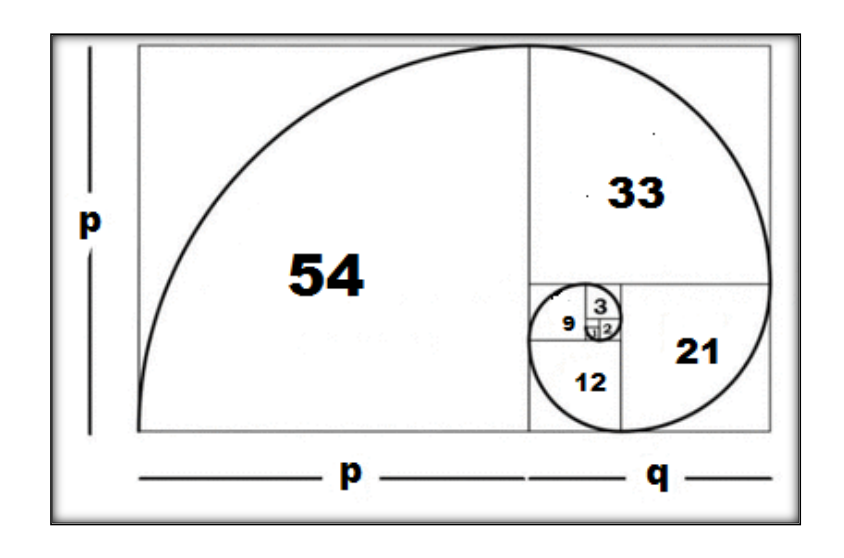


Fig.8.1 The golden spiral representation of an equation

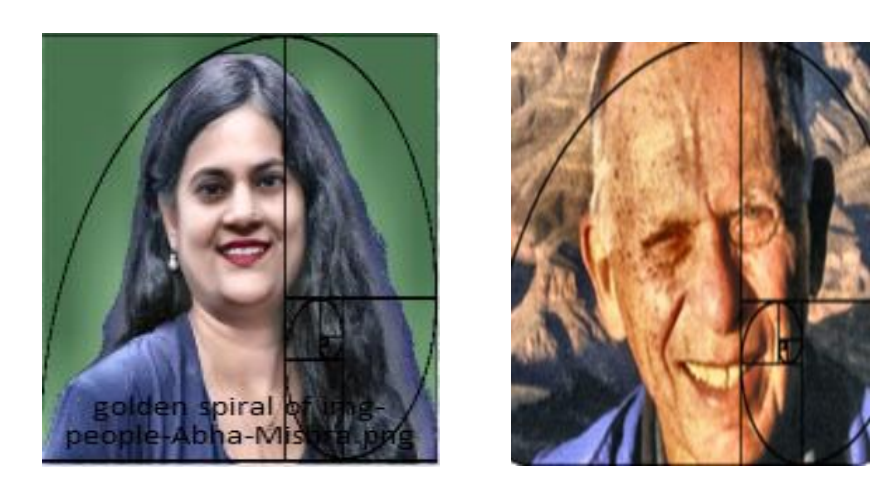




Fig. 8.2 Golden ratio spiral representation of the taken inputs

changes with the difference in the values of p and is calculated by representing the image data in binary form, the result will be true or 1 if either bit of data is 1 otherwise false [106]-[107].

### **8.2.2:** Proof: Fibonacci sequence generator is formed by Fn

$$Fn = Fn-r + .... + Fn-s \pmod{q}$$
 where  $r > s > 0$  8.1

Initially, two elements are needed to find the next element in the sequence. From the previous expression, the value of r and s must be set greater than 0. Adding all the terms, the nth term of the function is calculated. The interest of function Fn is calculated by the power of two that is,

### **8.2.3:** Proof: Golden Spiral Ratio is continued

Based on Eqn. 8.2, to select the next term of the Fibonacci series. The Fibonacci sequence varies depending on the p and q values. Fibonacci series is an infinite series of integer numbers, where each term is the sum of the two previous terms. The total pixel ratio of an image is found by summing the pixel values of the whole image called the Fibonacci-golden ratio. It is represented mathematically with p and q where p > q > 0,

$$q = 2q$$
 8.3

$$p/q = (p+q)/p = 1.6180339887498948420 ...$$
 8.4

If p = 0, the Fibonacci coding sequence is a power sequence of 2 that 1, 2, 4, 8, 16,

If p = 1, the Fibonacci-1 coding sequence is the classical Fibonacci sequence 1, 1, 2, 3, 5, 8, 13, 21, ...

If p > 1, the Fibonacci-2 coding sequence is a recursive function [108]-[111].

# 8.3 Proposed methodology-XORDCT Transform

XOR cipher is an encrypting method used to make cipher images and is hard to find by intruders. Every character of the image can be scrambled by applying the XOR operation using a given cipher key. To descramble the encrypted image, reapply the XOR function along with the cipher key.

Let the secret image be represented as I. Based on the Fibonacci series concept, an image is split into a sequence of images such as I1, I2, I3,....In. The XOR operator on the source side transforms the inputted single secret image into a subset of clusters before transmitting it to the destination side. The masking coefficients are discovered by performing discrete cosine transform (DCT) on the input image [99]-[103]. The XOR-ed result of the input images are,

$$R \le \sum \{I1 \oplus I2 \oplus I3,... \oplus In\}$$
8.5

Where R and  $\Sigma$ {.} denotes the coefficients for masking the input images. The masked image is represented as Mi and

$$Mi = M1, M2, M3,...Mn$$
 8.6

The masked image Mi is XOR-ed using the Ii and R. Likewise,

$$Mi = Ii \oplus R$$
 8.7

Where i = 1,2,3,...n. Then the masked images Mi are formed and transmitted to the destination side. After receiving,

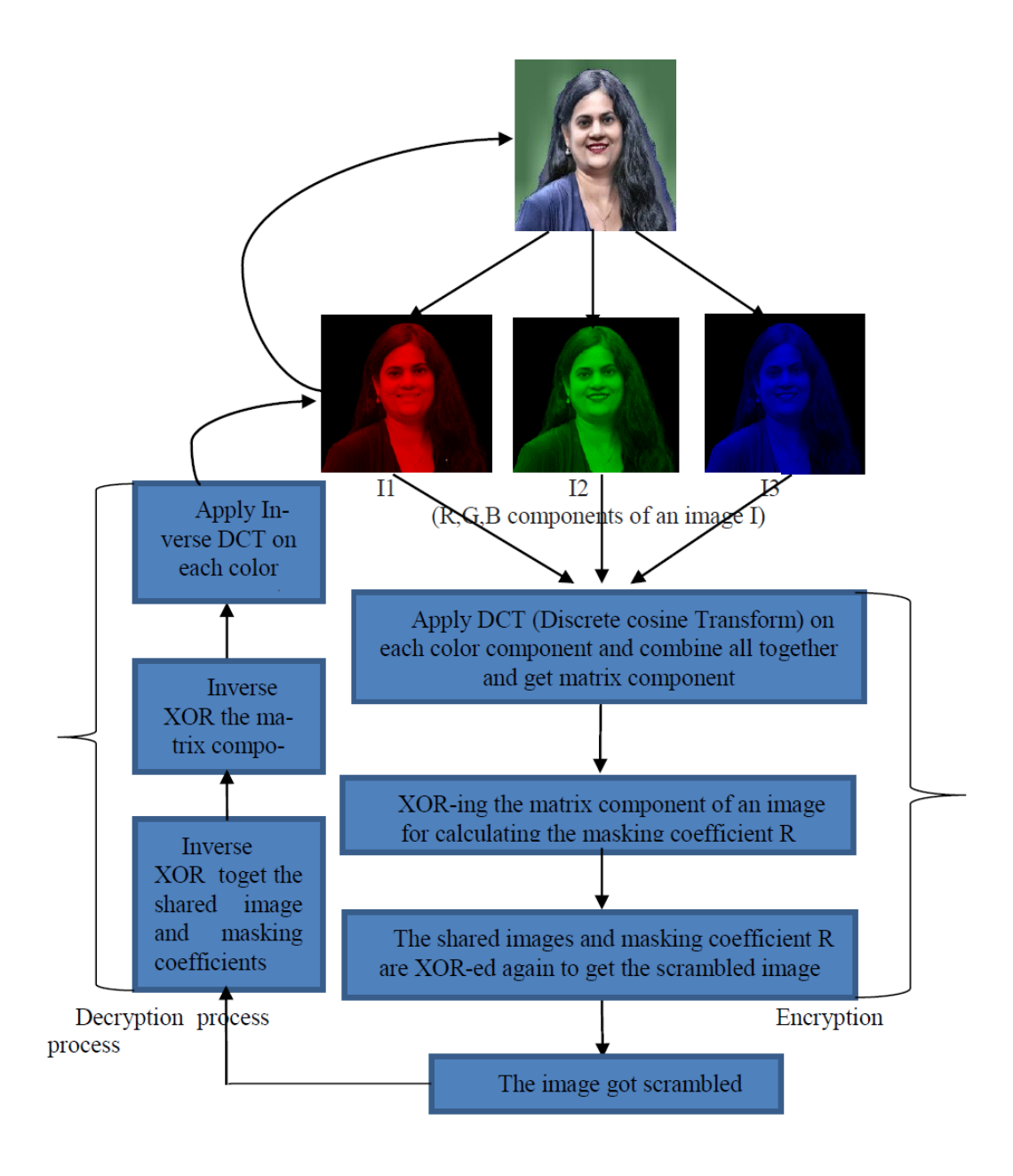


Fig. 8.3 Flowchart for XORDCT method

the destination part joins all the masked images M1, M2,...., Mn and perform the XOR to recover the original input image.

$$\overline{I}_{I} = Mi \oplus \overline{R}$$
 8.8

### **Theorem 1:**

The XOR sequence is reversible if and only if  $R = \overline{R}$ 

**Proof:** The P-Fibonacci XOR sequence is reversible if it satisfies  $\text{Ii} = \overline{I}i$ , where  $\text{i} = 1, 2, \ldots$ n. This condition is solved when  $\text{Ii} = \overline{I}i$  then  $\overline{I}i = \text{Mi} \oplus \overline{R}$ . From the above equation know that,  $\text{Mi} = \text{Ii} \oplus R$ , where  $\text{i} = 1, 2, \ldots$ n then

$$\overline{I}_1 = I_1 \oplus R \oplus \overline{R}$$
 (substitute eq.(9) here) 8.2

whereas Ii  $\bigoplus 0 = \overline{I}i$ 

By using the XOR property  $\mathbb{R} \oplus \overline{\overline{R}} = 0$  multiply both side by  $\overline{R}$ 

$$R \oplus \overline{R} \oplus \overline{R} = 0 \oplus \overline{R} \text{ and } 0 \oplus \overline{R} = \overline{R},$$
 8.10

The above equation is simplified as  $R = \overline{R}$ . Now the value of

$$\overline{R} = \sum \{ I1 \oplus I2 \oplus \dots In \oplus \underline{R} \oplus \underline{R} \oplus \underline{R} \}, \quad \text{n is odd}$$
 8.11

Finally  $R \oplus \overline{R} = 0$  equals  $R = \overline{R}$ . If the masking coefficients are identical for both encryption and decryption, the process is reversible.

### **Theorem 2:**

The process is reversible, if n is an even number.

**Proof:** If n is even number, the masking coefficient is

$$\overline{R} = \sum \{M1 \oplus M2 \oplus \dots \oplus Mn\}$$
 By fact 8.3

 $Mi = Ii \oplus R$  (Mi-masking coefficient) Where R can be written as

$$\overline{R} = \sum \{I1 \oplus I2 \oplus .... \oplus In \oplus Rn\}$$
 By regrouping of R 8.4

$$\overline{R} = \sum \{I1 \oplus I2 \oplus .... \oplus In \oplus R \oplus R \oplus ...... \oplus R\} \quad \text{n is even}$$
 8.5

$$\overline{R} = \sum \{I1 \oplus I2 \oplus ... \oplus In \oplus 0\}$$
8.15

Where  $R \oplus R \oplus .... \oplus R = R \oplus R = 0$ } it can be rewritten as  $\Sigma \{I1 \oplus I2 \oplus ... \oplus In\}$ 

The value of  $\bar{R}$  is equal to the value of R. (i.e)  $\bar{R} = R$ . If n is an odd number, the recovered masking coefficient  $\bar{R}$  is calculated as,

$$\overline{R} = \sum \{M1 \oplus M2 \oplus .... \oplus Mn\}$$

Initially M1 = Ii  $\bigoplus$  R then  $\bar{R}$  can be rewritten as

$$\overline{R} = \sum \{I1 \oplus R \oplus I2 \oplus R \oplus \dots In \oplus 8.6\}$$

By using XOR property  $\underbrace{R \oplus R \oplus ..... \oplus R}_{} = R \oplus R \oplus R \oplus R = 0 \oplus R = R$ , n is odd

The value of  $\bar{R}$  can be formed by  $\bar{R} = \sum \{I1 \oplus I2 \oplus ... ... \oplus In \oplus R \oplus R \oplus .... \oplus R\}$ 

$$\overline{R} = \sum \{ I1 \oplus I2 \oplus \dots \oplus In \oplus R \}$$
8.17

The  $\bar{R}$  is not identical to original R. From comparing Eqn. 8.11 to Eqn. 8.17 it is clear that  $\bar{R}$  is identical to R when the inputted images are scrambled into even number of images. Thus, scrambling the image is an alternative choice for enhancing the security of the image. The images are altered in unreadable mode. The original image of the

jpeg format is transformed using a Discrete Cosine Transform (DCT). The coefficients

of the clusters are formed by the 2D P-Fibonacci XOR Transform. The parameters of

P-Fibonacci XOR transform are p and i. The lossless image scrambling method is built

using the P-Fibonacci XOR transform.

8.3.1 Pseudocode for Encryption using XORDCT algorithm

Input: Compressed and enhanced image

Output: The encrypted image

Step 1: Based on the Fibonacci series, The image Ii is converted to three color

components: R, G, B such as 'n' number of shared images I1, I2, I3,...In, before sending

to the destination.

Step 2: Apply DCT to each color component and combine together all components.

 $(Ii=I1 \oplus I2 \oplus I3 \oplus ... \oplus In)$ 

Step 3: XOR-ing the matrix component of an image for calculating the masking

coefficient R (R<=XOR(Ii))

Step 4: The shared images Mi are scrambled by XOR-ing the Ii and R. (Mi $\leq$  Ii  $\bigoplus$  R)

Step 5: If the scrambled images have 'n' odd shared images then the original image is

irreversible otherwise reversible.

Step 6: The scrambled images are got.

8.3.2 Pseudocodes for Decryption using Inverse-XORDCT algorithm

Input: Encrypted image

115

Output: RGB components of the image

Step 1: The destination module XOR-ed the scrambled image with the masking coefficient Mi.

Step 2: Calculate the XOR inverse function for the masking coefficient matrices of an image  $\overline{R}$ . ( $\overline{R} \le (M1 \oplus M2 \oplus M3 \oplus .... \oplus Mn)$ )

Step 3: After that apply inverse DCT to each color component and combining together all components. ( $\overline{Ii} = Mi \oplus \overline{R}$ )

Step 4: Recover the color components together to get the original R:G:B image.

Step 5: The actual image is reconstructed.

### 8.4 Statistical Result Analysis

Here more than 95 images are considered. First of all, consider an image that we want to encrypt. Initially convert the image into binary data which want to encrypt. The image with .png format is taken for compression. The iteration made in the images is seen visually. To quantify the encryption process two metrics are used.

### 8.4.1 Net Pixel Change Ratio (NPCR)

Change in the rate of the pixel number comparing the he original and the encrypted image.

NPCR = 
$$\frac{1}{M \times N} \sum_{i=1}^{M} \sum_{j=1}^{N} D(i, j) \times 100 \%$$

where 
$$D(i,j) = 0$$
 when  $C1(i,j) = C2(i,j)$ 

$$D(i,j) = 1$$
 when  $C1(i,j) \neq C2(i,j)$ 

The parameters C1 be the original image and C2 be the modified image, D be the array used for storing the image size before and after encryption M and N are the height and width of the images. NPCR is used to analyze the image and find the bit change by comparing pixel by pixel.

### **8.4.2** Unified Average Changing Intensity (UACI)

This metric is used to measure the average of the intensity differences in pixels of the raw image and the original images.

UACI = 
$$\sum_{i=1}^{M} \sum_{j=1}^{N} \left[ \frac{|(C1(i,j)-C2(i,j))|}{255} \right] x \frac{100 \%}{M \times N}$$

### 8.4.3 Correlation Coefficient Analysis (CCA)

The pixels of the encrypted image is intercorrelated with others. The correlation exists in the adjacent pixels can be used by the intruder for creating the sequence of the image. The range of the correlation coefficient lies within -1 and +1.

$$Cov(\alpha, \beta) = \frac{1}{N} \sum_{i=1}^{N} (\alpha i - E(\alpha))(\beta i - E(\beta))$$

$$r\alpha\beta = \frac{Cov(\alpha, \beta)}{\sqrt{D(\alpha)} \sqrt{D(\beta)}}$$

$$D(\alpha) = \frac{1}{N} \sum_{i=1}^{N} (\alpha i - E(\alpha))2$$

$$E(\alpha) = \frac{1}{N} \sum_{i=1}^{N} \alpha i$$

The correlation covariance of the original image and the encrypted image is calculated using  $Cov(\alpha,\beta)$  and  $D(\alpha)$  is the variance range value of the image and  $E(\alpha)$  is assumed as the mean deviation of the image pixel values.

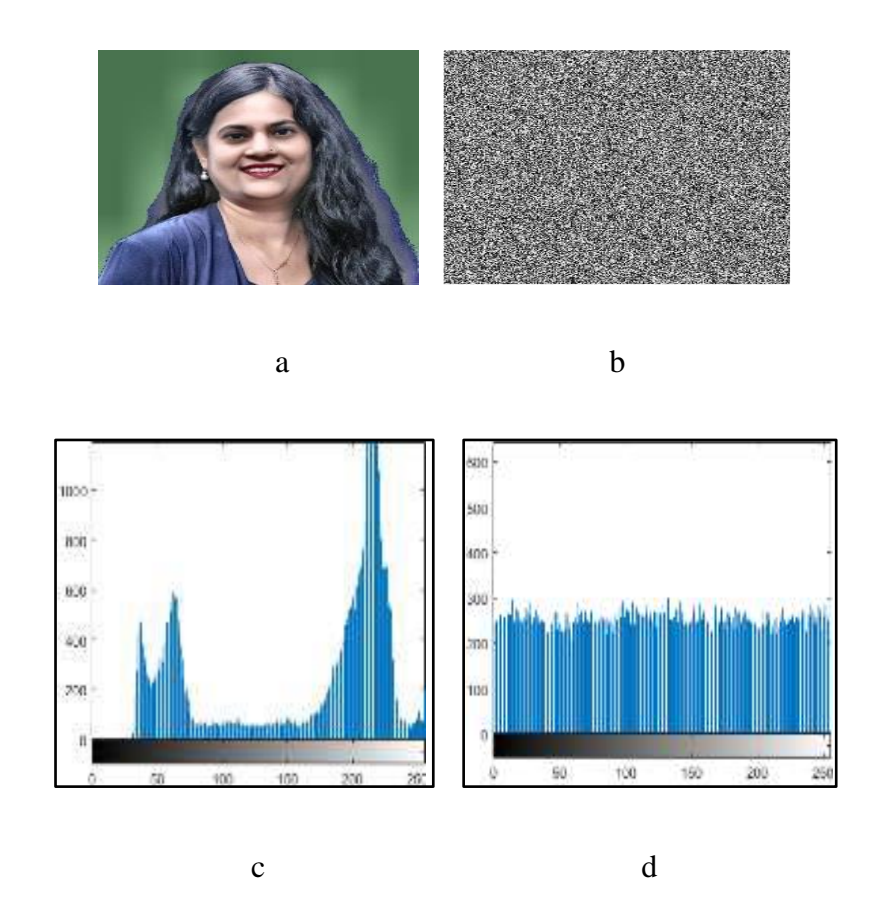


Fig. 8.4 a) The compressed image b) The encrypted image c) Histogram of the compressed image d) Histogram of the encrypted image

### 8.4.4 PSNR and MSE analysis

It is the ratio between the original image(signal) and the encrypted image (noise).

PSNR scale is used to represent the signal. It is calculated by

PSNR=20 x 
$$\log_{10} \left( \frac{255}{\sqrt{MSE}} \right) dB$$

Where *MSE* is the average of the errors  $MSE = \sum_{i=1}^{M} \sum_{j=1}^{N} \frac{[R(i,j) - S(i,j)]}{M \times N}$ 

Where R(i,j) is the pixel value of the taken input image, S(i,j) is the pixel value of the encrypted image.

# 8.5 Summary

An image is scrambled using the Fibonacci series and Exclusive OR (XOR) and masking coefficients of the Discrete Cosine Transform (DCT). As a next step, XORing the matrix value of the image makes changes in the input and also brings drastic variation in the encrypted image. The masking coefficients used in this experiment is also XORed to bind more with the input data. The working feature of the encryption and decryption algorithm is experimented with and described in this literature. The Experimental results of all the images (image A, image B, image C) are tabulated (see in Fig. 8.4) in this literature. It is clear that the XORDCT algorithm is suitable for encryption and avoids attacks that violate security like brute-force attacks.

# **CHAPTER 9**

### RESULTS AND DISCUSSION

### 9.1 Introduction

This chapter comprises the results obtained from the previous chapters 3, 4, 5, 6, 7 and 8. The overall work comprises the comparative study of the classification of features extracted from the silhouettes and Accumulated Gait Energy Image (AGEI). The Textural features extracted from the silhouettes using Grey level Co-variance Matrices are optimized by the Particle Swarm Optimization algorithm and classified by the Nearest Support Feature Vector (NSFV) and the Spatio-temporal features represented from the AGEI are optimized by the Crow Search optimization algorithm and selected by Recursive Feature Elimination algorithm and classified using Naïve Bayes Dynamic Bayesian Network. The classifiers are compared on Accuracy, Precision, Recall and F-rate values found by the feature classification work. From that, the Naïve Bayes DBNetwork gives better accuracy results compared to the NSFV. The False Positive Rate (FPR) and False Rejection Rate (FRR) probability found using Fuzzy Probability was deployed with Naive Bayes DBNetwork model for better recognition in the smart environment. The Gait Energy Image dataset was chosen from the CASIA-A and CASIA-B Gait datasets and UCI repositories.

The output was programmed and implemented in Python Tensorflow and Keras library in the Jupyterlab IDE then the outcomes are tabulated and displayed in the coming sections.

# 9.2 Pre-processing Phase – Compression and Enhancing

After the image is captured in real-time, the raw image may be rough, distorted and unclear. If we extract the features from the unclear image, the results got may also not be good. Initially, the raw image has to undergo a pre-processing stage called compression and enhancement. After the initial pre-processing step, the images are Compressed and Enhanced (see in Fig 9.1).

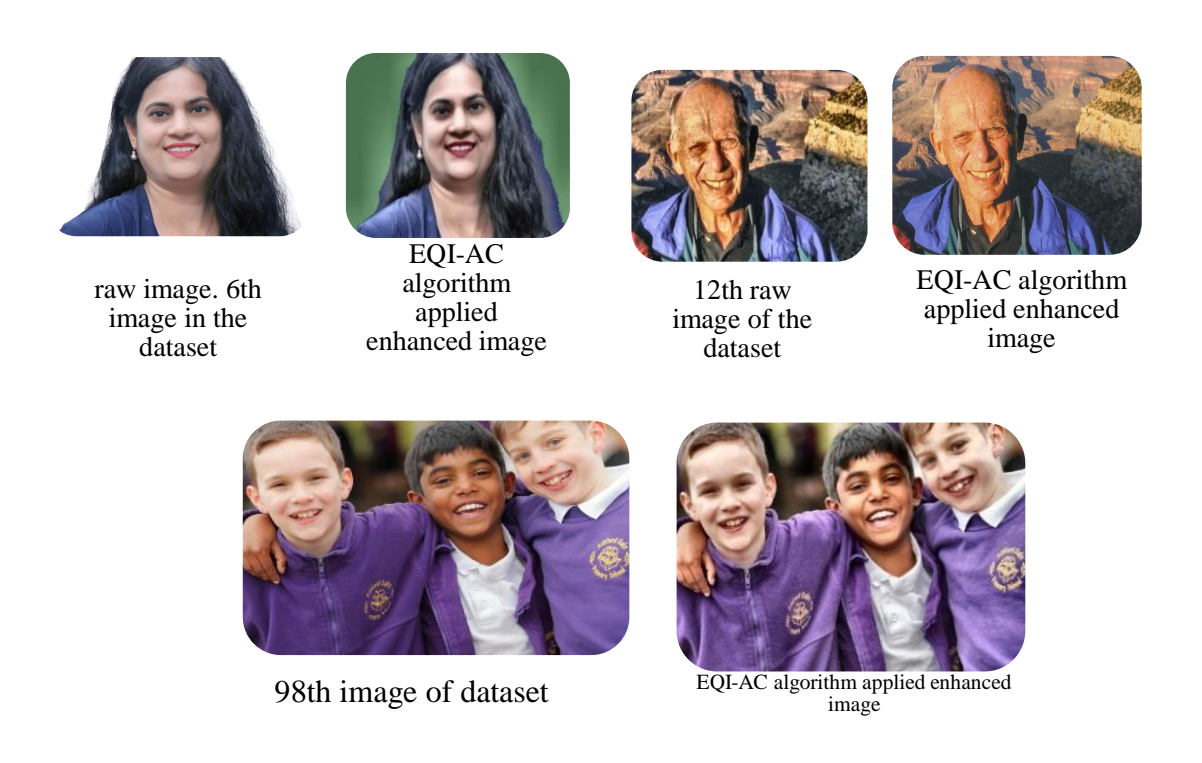


Fig. 9.1 Image compressed with JPEG standards and CLAHE

In this work, Compression algorithms like SIFT, DCT and the proposed EQIAC are compared by SSIM and PSNR. The size of the file was compressed and the result of that was tabulated in (Table 9.1 and Table 9.2). The graphical difference between the SSIM and PSNR can be seen in Fig. 9.2 and Fig. 9.3.

Table 9.1 The Structure Similarity Index difference between the compared methods EQIAC, SIFT and DCT

				SSIM	
S.No	Raw Input Image	EQIAC	SIFT	DCT	
1	mag-06firstwords-t_CA0-article large-v2.png	0.967669013	1.5872639	1.446664	
2	forest4_612251.png	0.831007905	3.7879878	2.774987	
3	Untitled-design-9-796x417.png	0.818730254	3.7879276	2.35555	
4	forestsmain.png	0.723306708	2.7788888	2.222668	
5	csm_Finland_forest_by_Ninara_flickr_42b14a06aa.png	0.808361255	2.5875786	1.587578	
6	when-will-little-people-big-world-return-1546445203.png	0.863056503	1.76976945	1.242469	
7	ThinnedForest_UnthinnedForest_background.png	0.794251695	1.69862988	1.233559	
8	Bianca-devins.png	0.861422138	1.6786734	1.624222	
9	inner_slider.png	0.859050475	3.3523546	2.278554	
10	FOD.png	0.762102643	2.7689462	1.774524	
11	denis5-1-400x400.png	0.899955901	3.7877894	1.926673	
12	theni%20forest.png	0.842987241	2.6598465	1.659847	
13	ron-golden-1.png	0.776488431	2.6594698	1.12339	
14	river.png	0.828948821	1.6579356	1.234984	
15	About us-our-people-tab-careers.png	0.881192121	3.5237427	2.74827	

Table 9.2 the PSNR difference between the compared methods EQIAC, SIFT and DCT

		PSNR		
S.No	Compressed image	EQIAC	SIFT	DCT
1	mag-06firstwords-t_CA0-article large-v2.jpg	28.56440	32.90772	35.63525
2	forest4_612251.jpg	28.50308	33.02903	35.78893
3	Untitled-design-9-796x417.jpg	28.44176	33.1503	35.94261
4	forestsmain.jpg	28.38044	33.27163	36.09629
5	csm_Finland_forest_by_Ninara_flickr_42b14a06aa.jpg	28.31912	33.39294	36.24997
6	when-will-little-people-big-world-return-1546445203.jpg	28.25779	33.51424	36.40365
7	ThinnedForest_UnthinnedForest_background.jpg	28.19647	33.63555	36.55732
8	Bianca-devins.jpg	28.13515	33.75685	36.71100
9	inner_slider.jpg	28.07383	33.87816	36.86468
10	FOD.jpg	28.01251	33.99946	37.01836
11	denis5-1-400x400.jpg	27.95118	34.12076	37.1720
12	theni%20forest.jpg	27.88986	34.24207	37.3257
13	ron-golden-1.jpg	27.82854	34.36337	37.4794
14	river.jpg	27.76722	34.48468	37.6330
15	aboutus-our-people-tab-careers.jpg	27.7059	34.6059	37.7867

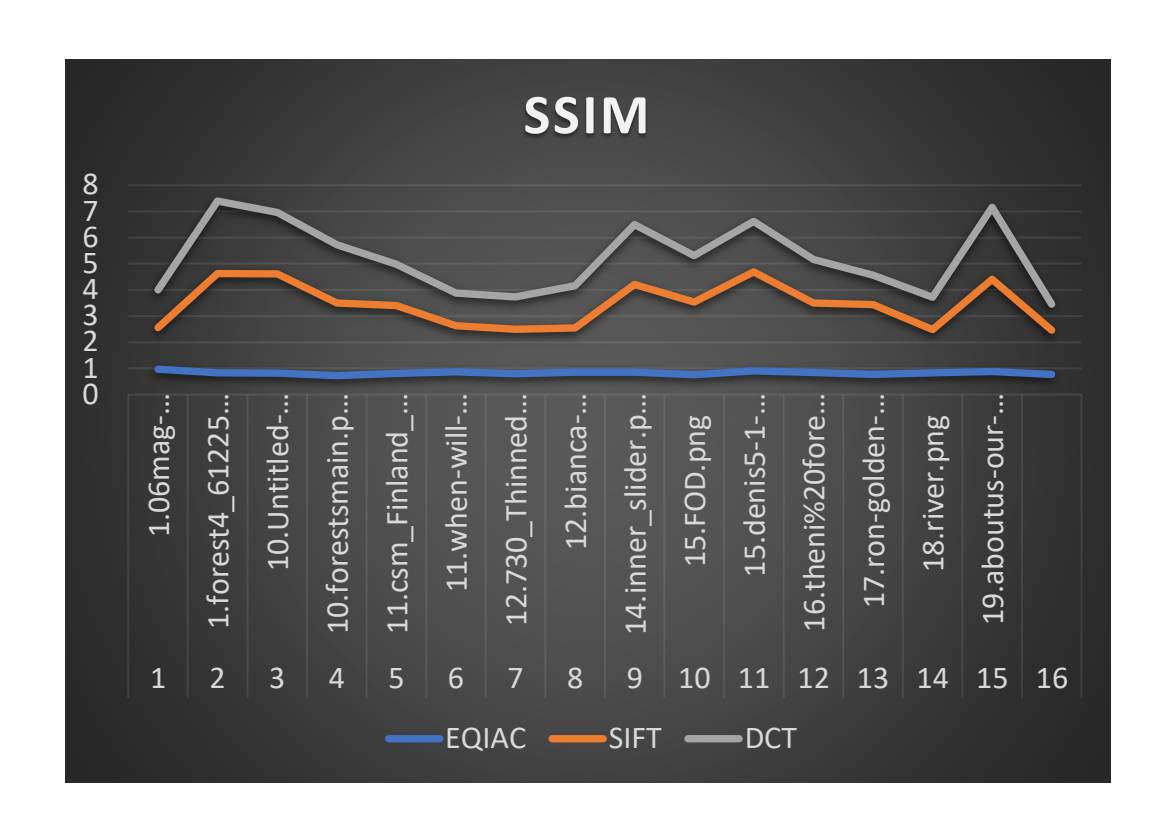


Fig. 9.2 The graph for the SSIM difference between EQIAC, SIFT, DCT has drawn using Table 9.1

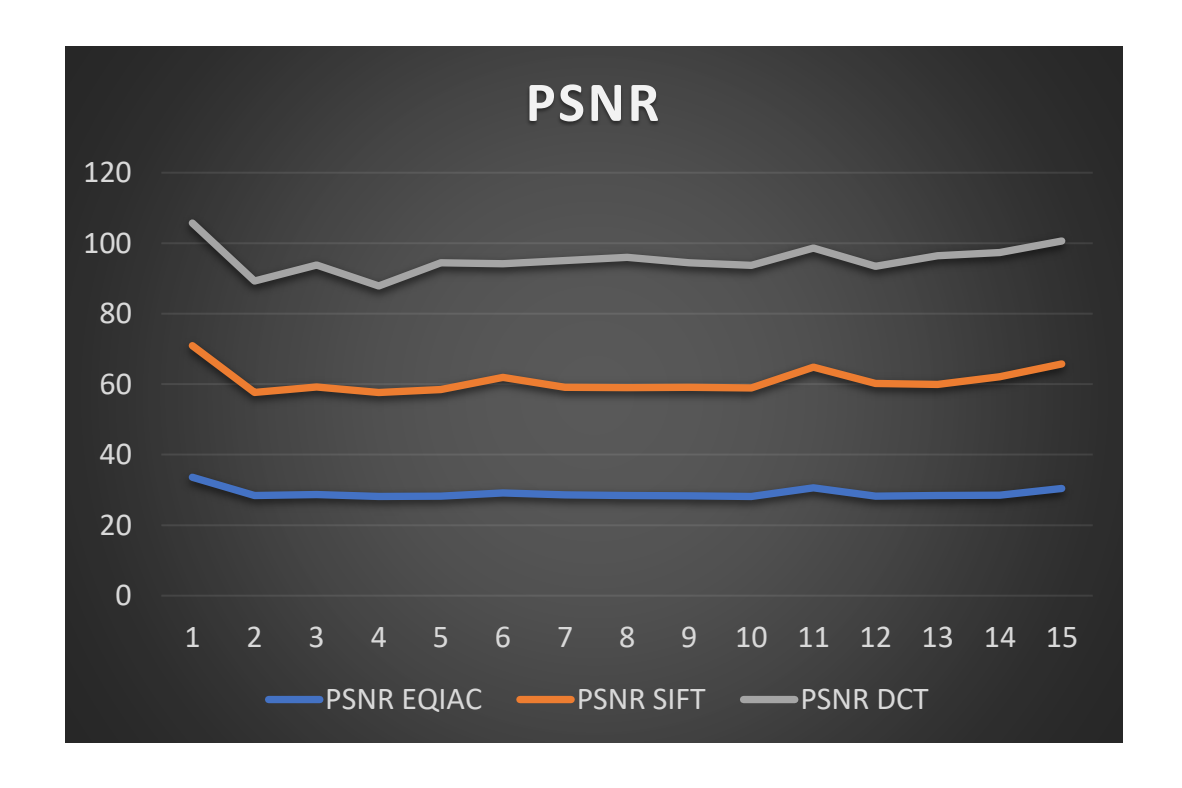


Fig. 9.3 The graph for the PSNR difference between EQIAC, SIFT, DCT has drawn using Table 9.2

By comparing Table 9.1 and Table 9.2 and also viewing Fig 9.2 and 9.3, it is clear that EQIAC works well than the compared SIFT and DCT. Thus EQIAC is proposed for compressing and enhancing the raw image in the pre-processing stage.

#### 9.3 Thresholding the Silhouette from the Compressed and Enhanced Image

Based on the expectation, every initial raw image undergoes into EQIAC algorithm for compression and enhancement. The Silhouettes are thresholded or segmented from the compressed image by differentiating the human from the background by clustering process. The Binary Thresholding Top-Bottom Agglomerative Clustering Hierarchy (BTTBACH) algorithm was applied to segment the Silhouette. Then the clusters are paired and merged to make a single cluster containing all the data points of the clusters. The proposed cluster Hierarchy methods perform well with less computing time than structural or stochastic methods and differentiate the foreground from the background (see in Fig. 9.4). The given input image is divided into 20 segments and 50 segments (see in Fig. 9.5) and the performance results of the clusters or segments are compared using the Jaccard Coefficient and Dice Coefficient (see in Table 9.7).

The comparison took place between the clustering methods used for thresholding the Silhouettes like Binarization thresholding, Improved Fuzzy C-Means clustering and Top-Bottom Agglomerative Clustering Hierarchy. The Cumulative Distance Ratio (CDR) between the clusters, False Accept Ratio (FAR) of the clusters and False Reject Ratio (FRR) of the clusters of each input image and the time taken to complete the clustering process are calculated and tabulated as Table 9.3., Table 9.4, Table 9.5, Table 9.6.



Fig. 9.4 The foreground and background difference of the input image

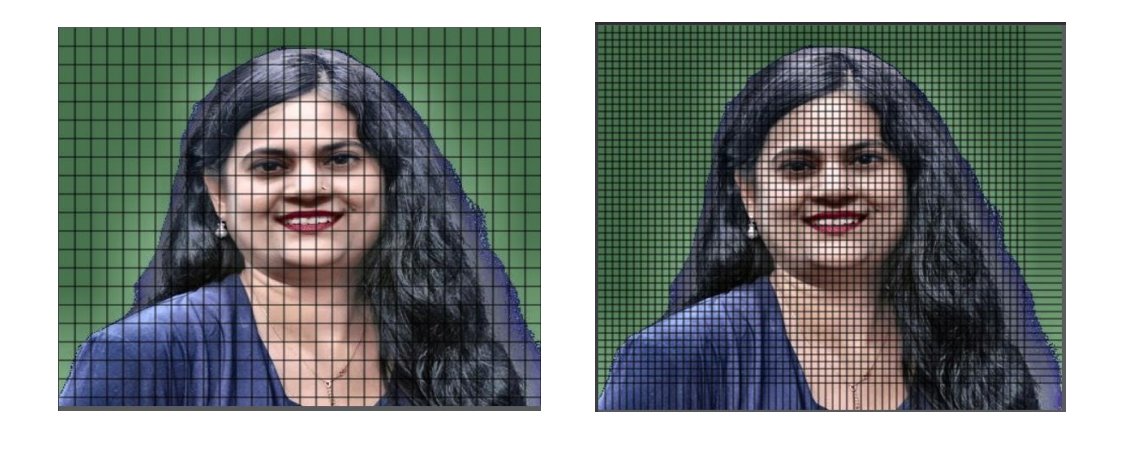


Fig. 9.5 Segmentation of image1 using Binarization Thresholding and Top-Bottom

Agglomerative Clustering Hierarchy (BTTBACH) algorithm

Segmented with row = 50 and col = 60

Segmented with row = 20 and col = 30

Table 9.3 CDR, FAR, FRR measure comparison for image1 segments

Performance Measures	Frame differencing And Binarization thresholding	Frame differencing and Improved Fuzzy C-means clustering	Frame differencing and Top- Bottom Agglomerative clustering hierarchy	Binarization thresholding and Improved Fuzzy C-means	Frame differencing and Top-bottom Agglomerative hierarchy	Proposed Method Frame differencing and Binarization thresholding and Top- Bottom Agglomerative clustering hierarchy (BTTBACH)
CDR%	34.09	44.44	40.4	77.18	88.63	93.18
FAR%	43.18	13.63	16.82	14.44	8.82	4.44
FRR%	22.72	16.82	14.44	12.27	4.44	2.27
Time is taken in sec	120	107	98	81	74	68

Table 9.4 CDR, FAR, FRR measure comparison for image2 segments

Performance Measures	Frame differencing And Binarization thresholding	Frame differencing and Improved Fuzzy C-means clustering	Frame differencing and Top- Bottom Agglomerativ e clustering hierarchy	Binarization thresholding and Improved Fuzzy C-means	Frame differencing and Top-bottom Agglomerativ e hierarchy	Proposed Method Frame differencing and Binarization thresholding and Top- Bottom Agglomerative clustering hierarchy (BTTBACH)
CDR%	31.09	48.44	43.4	79.44	70.12	92.21
FAR%	44.44	20.63	18.46	16.23	14.11	8.41
FRR%	24.72	20.86	17.82	14.44	13.47	4.27
Time is taken in sec	128	112	108	94	92	64

Table 9.5 CDR, FAR, FRR measure comparison for image3 segments

Performance sures	Frame differencing And Binarization thresholding	Frame differencing and Improved Fuzzy C-means clustering	Frame differencing and Top- Bottom Agglomerative clustering hierarchy	Binarization thresholding and Improved Fuzzy C-means	Frame differencing and Top-bottom Agglomerative hierarchy	Proposed Method Frame differencing and Binarization thresholding and Top- Bottom Agglomerative clustering hierarchy (BTTBACH)
CDR%	36.09	44.44	40.4	77.18	73.33	94.27
FAR%	42.18	13.63	16.82	14.44	12.22	7.4
FRR%	20.44	22.24	14.44	13.27	10.44	6.27
Time is taken in sec	132	117	98	96	87	63

Table 9.6 CDR, FAR, FRR measure comparison for image4 segments

Perform ance Measure s	Frame differencing And Binarization thresholding	Frame differencing and Improved Fuzzy C-means clustering	Frame differencin g and Top- Bottom Agglomerat ive clustering hierarchy	Binarization thresholding and Improved Fuzzy C-means	Frame differencing and Top-bottom Agglomerative hierarchy	Proposed Method Frame differencing and Binarization thresholding and Top- Bottom Agglomerativ e clustering hierarchy (BTTBACH)
CDR%	38.09	44.44	40.4	77.18	68.71	92.71
FAR%	40.18	13.63	16.82	14.44	8.44	4.44
FRR%	23.72	19.22	17.44	12.27	11.21	7.27
Time is taken in sec	134	120	118	106	99	72

Table 9.7 Jaccard Index and Dice Coefficient of the given images thresholded into 10 clusters using BTTBACH method

S.No	Images	Clusters	Jaccard Coefficient	Dice
				Coefficient
1	1.img-people-Abha-Mishra.jpg	10	0.257926	0.308178
2	2.ron-golden-1.jpg	10	0.288336	0.417308
3	3.Lena.jpg	10	0.263516	0.372908
4	4.ashford-oaks-primary-8.jpg	10	0.267144	0.381148

# 9.4 Silhouette Feature Extraction and Classification using Nearest Support Feature Vector

For this proposed work, Silhouettes are considered as input. The black and white images are called Silhouettes. The Silhouettes are formed from the Gait Energy Image (GEI). For this work, 34, textural features are extracted from Silhouettes using Grey Level Co-Variance Matrix (GLCM), thus the increasing number of features would decrease the rate of accuracy. The Chi-square method, Unsupervised learning method and PSO are called to perform optimization. By then, the Particle Swarm Optimization (PSO) method performs well and reduces the features list as 20. After optimization, classification of features is done based on TP, TN, FP, FN using Nearest Support

Feature Vector (NSFV), SVM and KNN classifier. The NSFV shows good results than the compared KNN and SVM classifiers on their TPR, TNR, FPR, FNR, Accuracy, Frate, Precision and found that the increase of the dataset for training produces the best result in the output (see Table 9.8). The visual output of Table 9.8 is drawn as the graph seen in Fig. 9.6.

#### 9.4.1 Receiver Operating Characteristic (ROC) curve

It plots with the True Positive Rate (TPR) on X-axis and False Positive Rate (FPR) on the Y-axis. The best recognition performance occupies the top of the plot (see in Fig. 9.8).

#### 9.4.2 Detection Error Trade-off (DET) graph

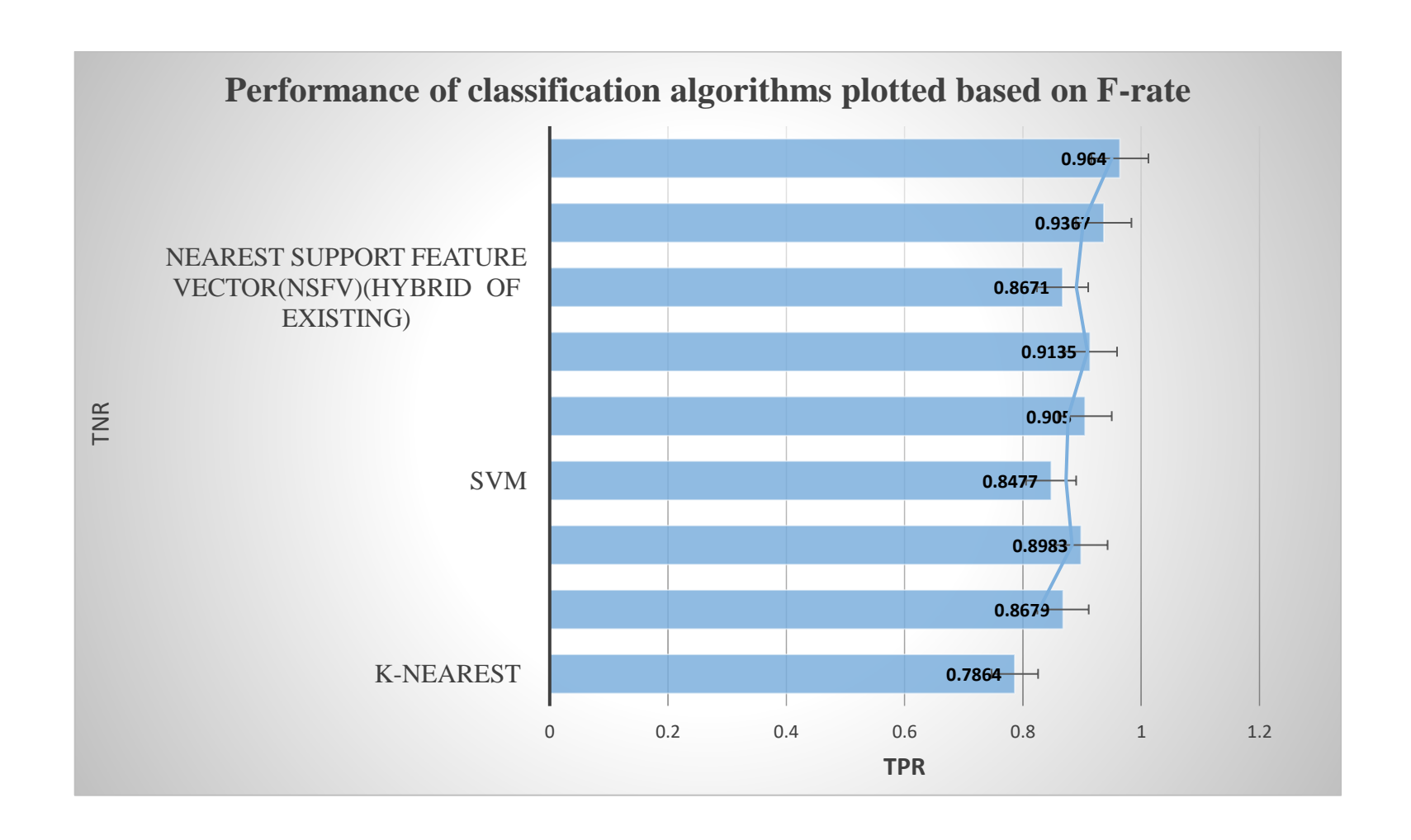
It plots with FPR in X-axis and FNR as Y. The curve slants closure to the bottom of the graph to show the best recognition performance (see in Fig. 9.7).

The performance of the classifiers is displayed by plotting the DET graph and ROC curve. The best classifier will occupy the bottom position in the DET graph and the topmost position in the ROC curve.

Table 9.8 The Precision, Accuracy and F-rate metrics calculated for evaluating the silhouette feature classifiers

Classifiers	Total images used	True Positive (TP)	True Negat ive (TN)	False Positive (FP)	False Negative (FN)	Precisio n	TPR	TNR	FPR	FNR	Accuracy	F-rate
K-nearest	45	35	10	10	9	0.7777	0.7954	0.5	0.5	0.2045	0.7031	0.7864
	80	69	11	13	10	0.8625	0.8734	0.4583	0.5416	0.1265	0.7766	0.8679
	100	90	10	6	6	0.9	0.9375	0.625	0.375	0.0625	0.8928	0.8983
SVM	45	39	6	10	8	0.8666	0.8297	0.375	0.0625	0.1702	0.7142	0.8477
	80	74	6	9	6	0.925	0.925	0.4	0.6	0.75	0.8421	0.905
	100	92	8	8	3	0.92	0.9684	0.5	0.5	0.031	0.9009	0.9135
NEAREST SUPPORT	45	41	4	10	8	0.9	0.8367	0.2857	0.0714	0.1632	0.7142	0.8671
FEATURE VECTOR	80	74	6	4	4	0.925	0.9487	0.6	0.4	0.0521	0.9090	0.9367
(NSFV) (a hybrid of existing)	100	94	6	3	1	0.94	0.9894	0.666	0.333	0.0163	0.9615	0.964

Fig. 9.6 The Clustered chart shows the F-rate performance of the NEAREST SUPPORT FEATURE VECTOR (NSFV) classifier compared with SVM and KNN methods



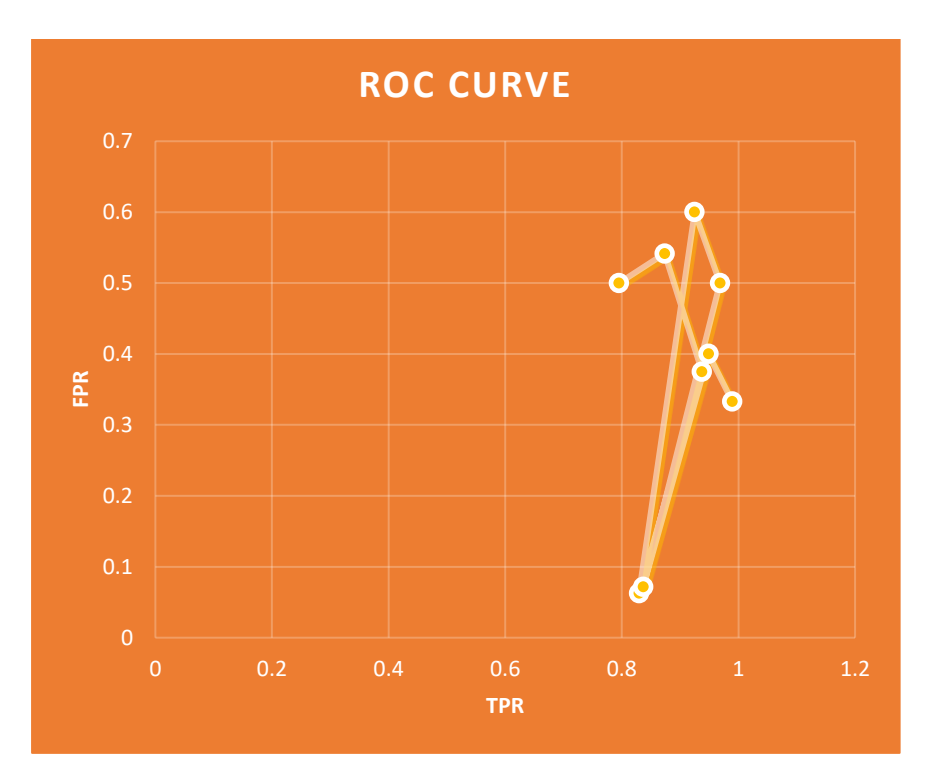


Fig. 9.7 the performance of the Nearest Support Feature Vector (NSFV) classifier through the ROC curve

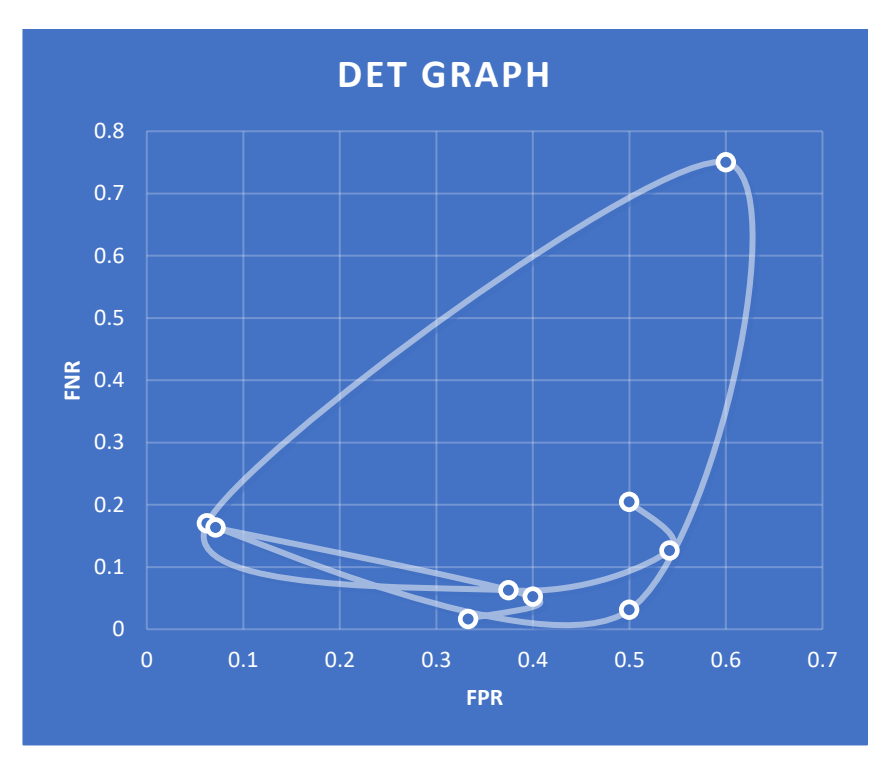


Fig.9.8 shows the performance of the Nearest Support Feature Vector (NSFV) classifier through the DET graph

### 9.5 Feature extraction from Accumulated Gait Energy Image (AGEI)

Gait Feature detection and extraction is an interesting process in gait image analysis. The walking (cadence) speed of the human captured from the video was marked by the Recursive Feature Elimination (RFE) and categorized as fast, slow and medium by DBNetwork based on time series and the Conditional Probability Value (CPV). From the captured video, a normal gait phase is cut down and an augmented image of that phase are merged to form the Augmented Gait Energy Image (AGEI). From the AGEI, the Spatiotemporal features of the images are filtered across time and space terms optimized by CSA. The PPFT was called to predict new features from the existing one forgets the existing one and proceeds with the newly created features list. The Naïve Bayes Dynamic Bayesian Network (DBNetwork) is a classifier model trained to classify the gait based on the Conditional Probability Value (CPV).

In the experiments, a varying number of features such as 19, 17, 15, 12 are given as input for the classification algorithm to find the performance difference (see in Table. 9.9). Finally, 12 features are predicted from the optimized features using PPFT. As per, the aim of this research work, the classification of predicted features are necessary. The feature classification algorithms like SVM, KNN, QDA, RF, NB, AB are called for classification purposes. The results of the classifiers are compared using Precision, Recall, Accuracy, F-rate, Mean Absolute Error (MAE), Root Mean Squared Error (RMSE), Relative Absolute Error (RAE), Root Relative Squared Error (RRSE).

Table 9.9 The Precision, Recall, Accuracy and F-rate metrics calculated to differentiate the AGEI classifiers

Classifiers	Total gait features used	True Positive (TP)	True Negative (TN)	False Positive (FP)	False Negative (FN)	Precision	TPR or Recall	Accuracy	F-rate
SVM	19	10	9	6	3	0.8	0.75	0.72	0.954198
	17	10	7	4	7	0.84146	0.8734	0.79646	0.857143
	15	9	6	9	6	0.92105	0.9052	0.857143	0.913043
	12	7	5	2	8	0.9542	0.9542	0.925926	0.774194
KNN	19	13	6	2	5	0.93939	0.9509	0.909091	0.945122
	17	10	7	9	6	0.89157	0.925	0.857143	0.907975
	15	11	4	4	6	0.89655	0.9398	0.895522	0.917647
	12	12	0	8	4	0.94118	0.9771	0.931677	0.958801
NB	19	15	4	2	1	0.97143	0.9827	0.957447	0.933011
	17	12	5	4	3	0.94937	0.9494	0.918367	0.949367
	15	11	4	6	4	0.91803	0.9573	0.888889	0.937238
	12	9	3	5	5	0.91837	0.9574	0.892857	0.977375
AB	19	11	8	8	6	0.85938	0.9483	0.882353	0.901639
	17	10	7	7	7	0.89394	0.831	0.825688	0.861314
	15	11	4	8	7	0.85821	0.8984	0.789474	0.877863
	12	10	2	9	7	0.84375	0.9122	0.797872	0.876623
	19	12	7	10	8	0.6875	0.8462	0.72	0.758621
QDA	17	6	11	4	10	0.6	0.7059	0.580645	0.648649
	15	9	6	9	9	0.64748	0.7317	0.594059	0.687023
	12	7	5	5	8	0.78125	0.7813	0.681818	0.78125

After the classification result was obtained, the DBNetwork model was designed with the Conditional Probability Value (CPV) of the normal gait, abnormal gait or limping, gait with carrying properties and the dress-wearing style.

In Table 9.10, the accuracy of the classifiers after being deployed with DBNetwork are listed. In Table 9.11, the Mean Absolute Error (MAE) of the NBDBNetwork model is listed. The Root Relative Squared Error (RRSE) is calculated and listed in Table 9.12 and the Relative Absolute Error (RAE) of the proposed are calculated and listed in Table 9.13. Finally, in Table 9.14, the Relative Mean Squared Error (RMSE) is calculated and displayed. From the observations of Table 9.10 to Table 9.14, it was clear that the NBDBNetwork with PPFT shows a much better output with minimal errors than the comparison.

Table 9.10 shows the Accuracy value of the AGEI Feature classifiers

Classification methods	Accuracy						
	SVM	KNN	NBDBNetwork				
Chi-Square (CS)	80.67%	49.33%	73.66%				
Information Gain (IG)	75.22%	50.33%	69.77%				
Crow Search Optimization (CSO)	85.21%	51.34%	85.30%				
Principal Polynomial Feature Transform (PPFT)	85%	89%	96%				

Table 9.11 shows the Mean Absolute Error of the AGEI Feature classifiers

	Mean Absolute Error (MAE)						
Classification methods	SVM	KNN	NBDBNetwork				
Chi-Square (CS)	0.2854	0.4825	0.2668				
Information Gain (IG)	0.2689	0.3786	0.1699				
Crow Search Optimization (CSO)	0.2587	0.4769	0.2135				
Principal Polynomial Feature Transform PPFT)	0.1687	0.2667	0.0988				

Table 9.12 Root Relative Squared Error (RRSE) of the AGEI Feature classifiers

	Ro	oot Relative Squar	red Error (RRSE)
Classification methods	SVM	KNN	NBDBNetwork
Chi-Square (CS)	109.5564	166.2211	125.3481
Information Gain (IG)	107.3421	183.3864	120.456
Crow Search Optimization (CSO)	98.4489	135.832	75.2398
Principal Polynomial Feature Transform (PPFT)	68.7332	74.2348	73.2612

Table 9.13 Relative Absolute Error of the AGEI Feature classifiers

	]	Relative Absolu	te Error (RAE)
Classification methods	SVM	KNN	NBDBNetwork
Chi-Square (CS)	149.231	59.672	69.5671
Information Gain (IG)	154.239	68.224	74.2649
Crow Search Optimization (CSO)	128.231	58.812	63.8563
Principal Polynomial Feature Transform (PPFT)	110.876	52.8564	61.2387

Table 9.14 Relative Mean Squared Error of the AGEI Feature classifiers

	Relati	ve Mean Squa	red Error (RMSE)
Classification methods	SVM	KNN	NBDBNetwork
Chi-Square (CS)	0.5464	0.5623	0.5521
Information Gain (IG)	0.3412	0.3254	0.2989
Crow Search Optimization (CSO)	0.2671	0.2976	0.2713
Principal Polynomial Feature Transform(PPFT)	0.2533	0.2456	0.2145

The virtual representation of the output is highly helpful to visualize the output and make the analysis easier. From the graph, the Principal Polynomial Feature Transform (PPFT) performs well than the compared classifiers. The graphical representation of the outputs is drawn using Table 9.10, Table 9.11, Table 9.12, Table 9.13 and Table 9.14, from the graph the less error produced classifier reaches the lower height in the graph (see in Fig. 9.9 to Fig. 9.13) The PPFT shows higher accuracy and less error value than the compared classifiers. So, the NBDBNetwork with Principal Polynomial Feature Transform (PPFT) shows good results than the compared classifiers and is recommended for gait feature classification.

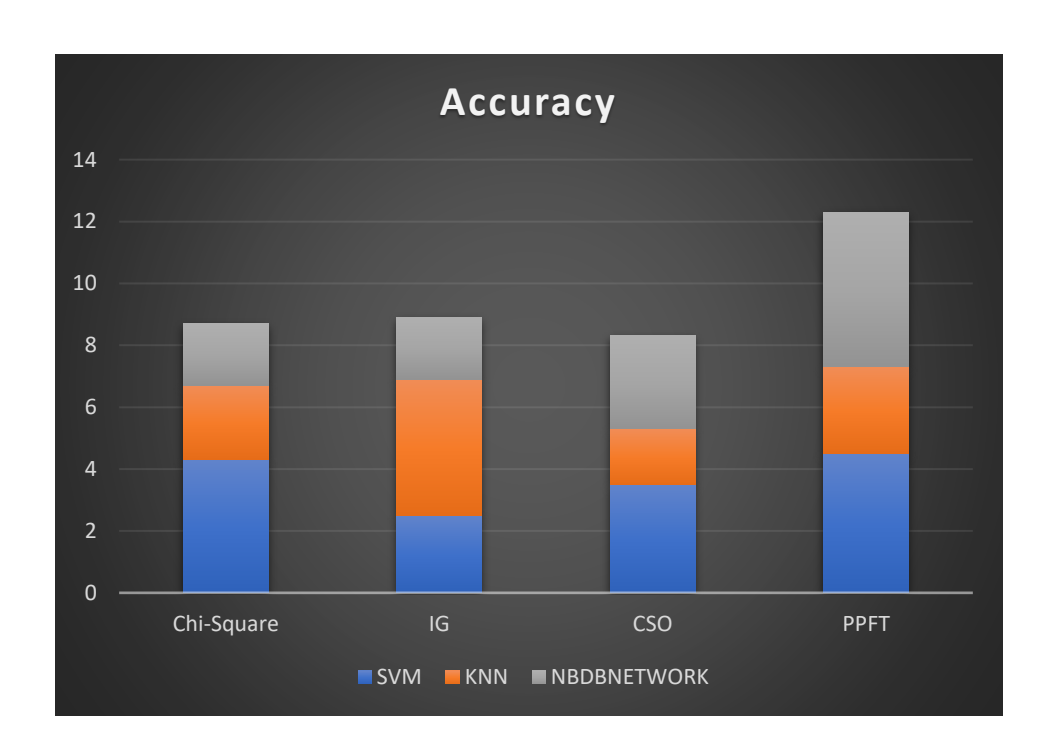


Fig. 9.9 The accuracy graph of the AGEI Feature classifiers

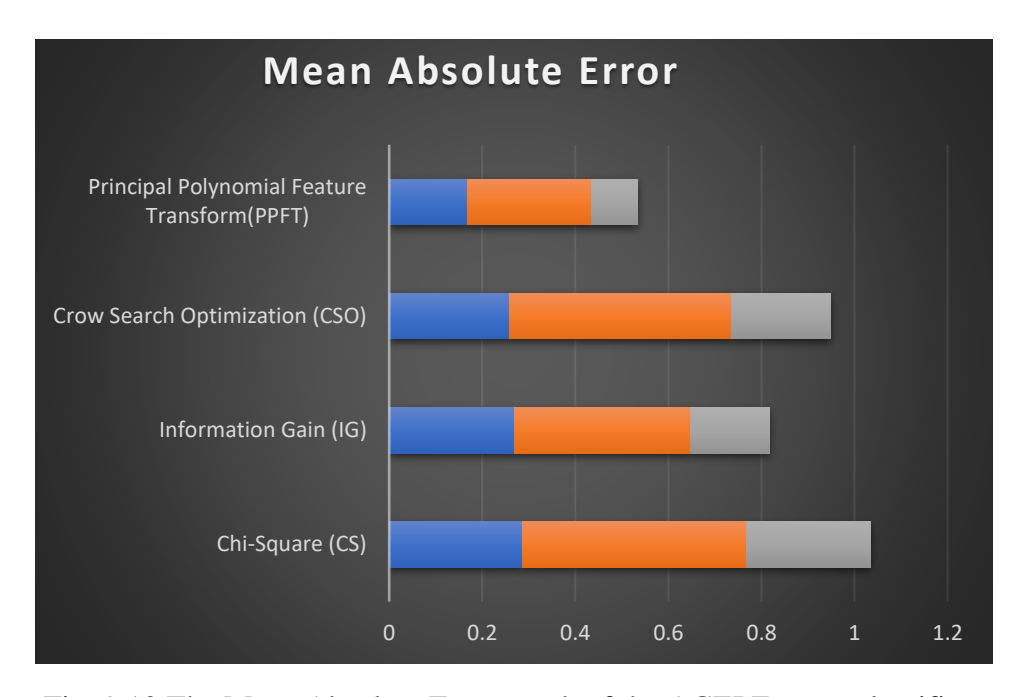


Fig. 9.10 The Mean Absolute Error graph of the AGEI Feature classifiers

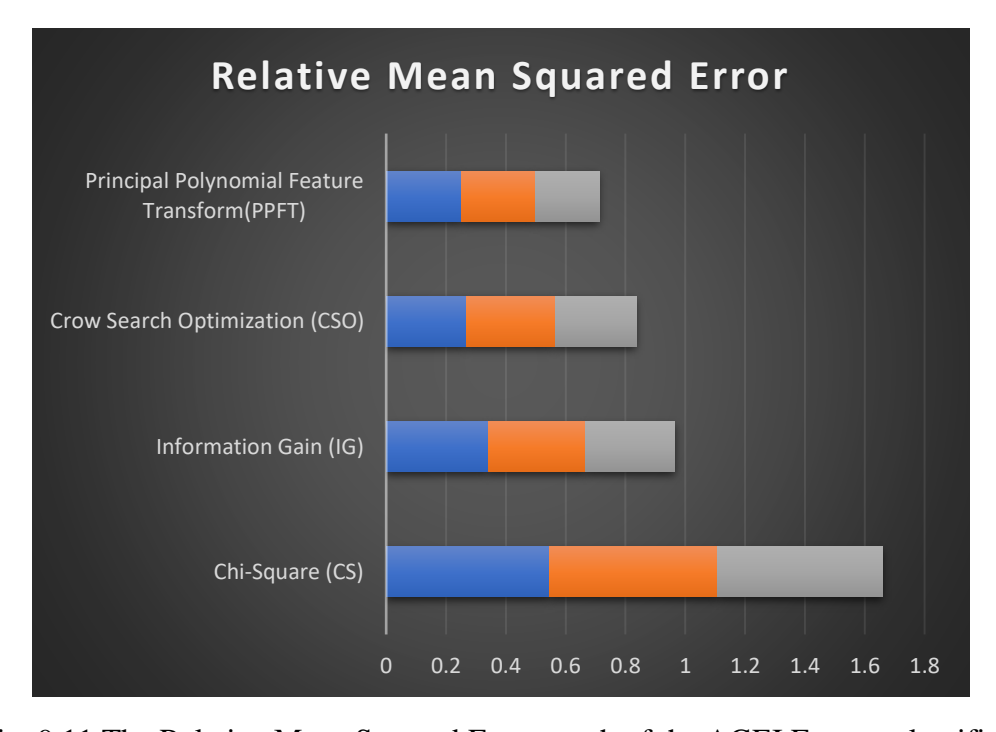


Fig. 9.11 The Relative Mean Squared Error graph of the AGEI Feature classifiers

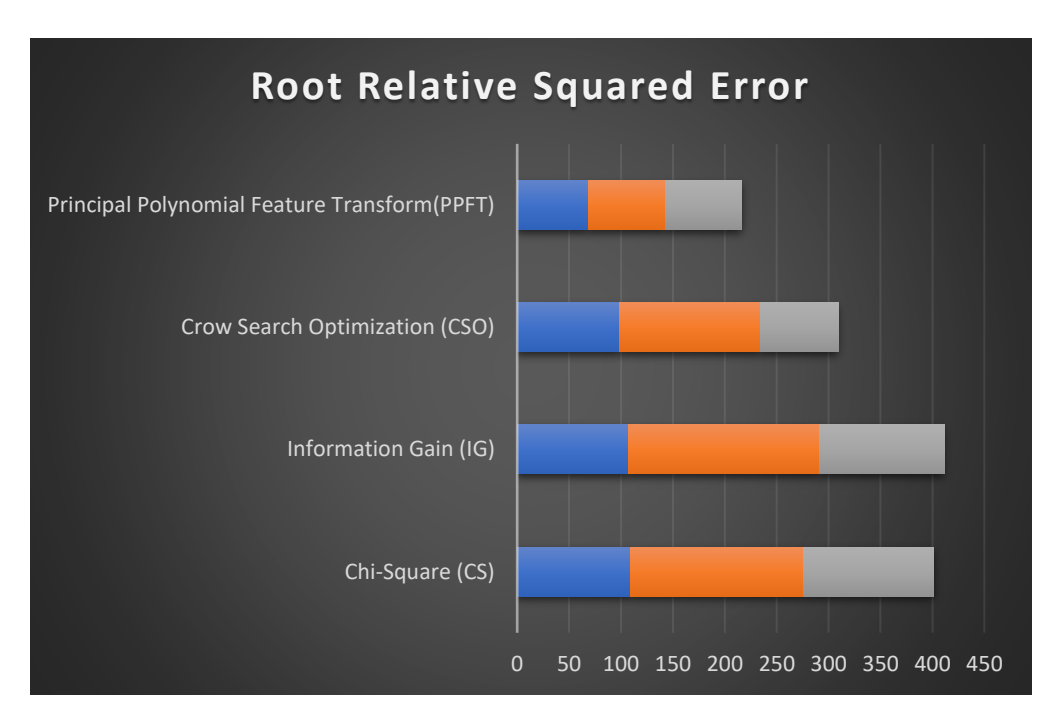


Fig. 9.12 the Root Relative Squared Error graph of the AGEI Feature classifiers

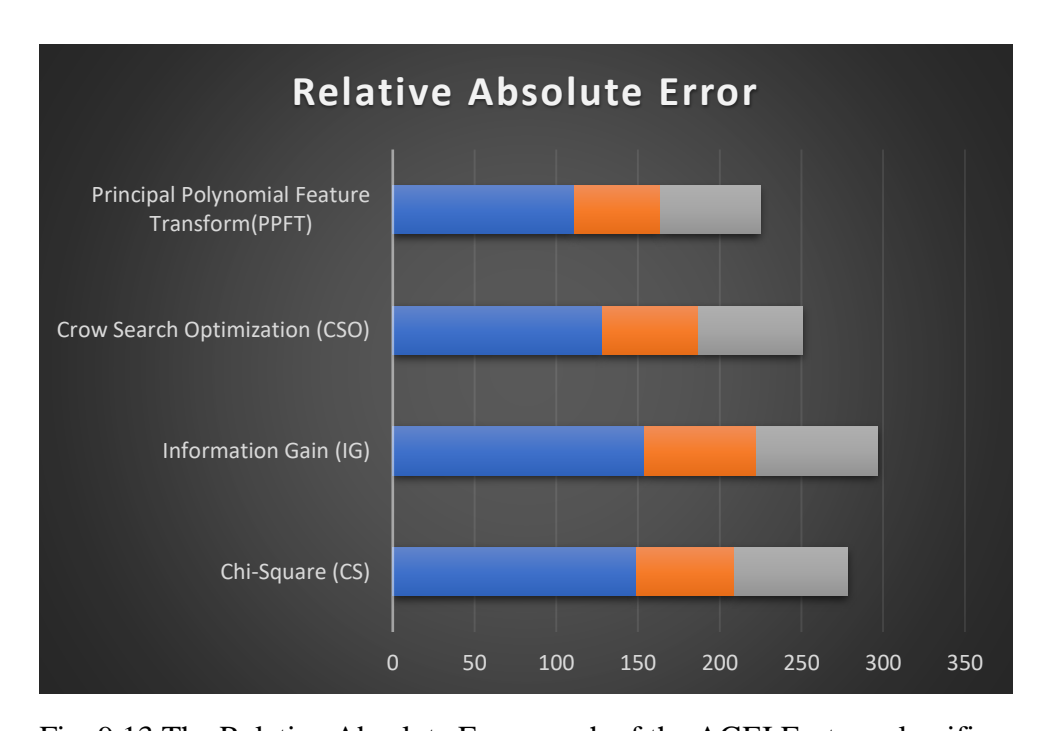


Fig. 9.13 The Relative Absolute Error graph of the AGEI Feature classifiers

# 9.6 Comparison of NSFV and NBDBNetwork for Feature Classification

Based on the previous results tabulated in Table 9.8, Table 9.9, it was clearly defined that Features extracted from AGEI using NBDBNetwork produces acceptable results than the Features extracted from Silhouette. Hence, NBDBNetwork was recommended for feature classification. The CPV constraints are executed by the term of Fuzzy Probability to improve the classification accuracy. The performance difference between NSFV and NBDBNetwork was calculated by the terms Accuracy, Kappa Statistic, TPR, FPR, Precision, Recall, F-rate, MAE, RMSE, RAE, RRSE see in Table 9.15.

Table 9.15 Performance Comparison of NSFV and NBDBNetwork

Performance Metric	NBDBNerwork	NSFV	
Accuracy	92.37%	87.98%	
Kappa Statistic	0.712	0.452	
TPR	0.892	0.741	
FPR	0.112	0.351	
Precision	0.896	0.751	
Recall	0.892	0.741	
F-rate	0.893	0.739	
MAE	0.0536	0.421	
RMSE	0.1641	0.8652	
RAE	51.811	78.961	
RRSE	67.1468	114.523	

# 9.7 XGBoost Strength for NBDBNetwork

The XGBoost is the wrapper class introduced in the recognition process to recognize the human in accurate manner. The XGBoost wrapper class acts as a container to deploy with the proposed NBDBNetwork Fuzzy probability concepts. It works well in gradient descent architecture by strengthening the proposed system through system optimization and algorithmic improvements. The XGBoost wrapped recognition system performance was measured by the Entropy, SSIM, PSNR and Cumulative Quality Measure and the results are tabulated (see Table 9.16).

Table 9.16 The overall performance between the NBDBNetworkwith Fuzzy Probability and XGBoost

Feature Classification				
methods	EP	SSIM	PS	CQM
NBDBNetwork	0.0147	0.9009	43.6937	34.0028
NBDBNetwork Fuzzy				
Probability	0.0287	0.9933	34.8725	54.5813
XGBoost NBDBNetwork				
Fuzzy Probability	0.0041	0.9982	45.9202	57.1044

# 9.8 Encryption and Decryption of input Images for Protecting from

#### **Unauthorized access**

The Energy Image generated from the Silhouette and Gait is protected by encrypting that using Exclusive OR Discrete cosine Transform and decrypted the image by applying the inverse

of the Exclusive OR to get the value of the image. The Correlation Coefficient for the input images is calculated. Based on the Coefficient value, NPCR, UACI, MSE and PSNR metrics for the encrypted and decrypted images are found.

The encryption and decryption of the image features are proved by the quality metrics such as Net Pixel Change Ratio (NPCR), Unified Average Changing intensity(UACI), Correlation coefficient analysis, Peak Signal Noise Ratio and MSE of the encrypted images are calculated and found to be protective to use on images (see in Table 9.17 and Table 9.18)

Table 9.17 The correlational coefficient of the encrypted image and decrypted image

(img-people-Abha-Mishra.jpg)					
	Horizontal	Vertical	Diagonal	Counterdiagonal	
Original image	0.972953	0.970462	0.916925	0.938441	
Encrypted image	-4.097226 × 10−5	1.158832 × 10-4	4.620716 × 10-5	4.539076 × 10−4	
(ron-golden-1.jpg)					
	Horizontal	Vertical	Diagonal	Counterdiagonal	
Original image	0.915352	0.922622291	0.868221	0.857255	
Encrypted image	−3.811868 × 10−6	-7.131676 × 10-4	-9.372164 × 10−4	-3.496642 × 10-4	
(ashford-oaks-primary-8.jpg)					
	Horizontal	Vertical	Diagonal	Counterdiagonal	
Original image	0.94514	0.950725	0.919702	0.937272	
Encrypted image	-0.001678	3.514572 × 10−4	-9.329940 × 10−4	-4.626904 × 10−5	

Table 9.18 The NPCR, UACI, MSE and PSNR of the encrypted image

Image	Image Name	NPCR (in %)	UACI (in %)	MSE for encrypted image	PSNR for decrypted image
	Image A-img- people-Abha- Mishra.jpg	99.585	28.621	0.2698	28.621
	Image B-ron-golden-1.jpg	99.6078	50.1931	0.2711	50.1931
	Image C-ashford- oaks-primary-8.jpg	99.6094	27.4092	0.2013	27.4092

# 9.9 Summary

In the proposed gait based human recognition system, the algorithms like SVM, KNN, Ada Boost, Random Forest classifiers are used to classify the features. Finally, XGBoost Fuzzy Probability-based NBDBNetwork shows better results than the compared NSFV. Thus Features extracted from AGEI provides more information about the human gait. Hence, the features extracted from AGEI helps to analyze the human at the distance whether the human walking with a bag, cap or else wear dresses like saree, dhoti, nighty, skirts. The proposed system is a customized model suitable to smart homes which contains feature selection, feature extraction, feature classification process.

## **CHAPTER 10**

#### CONCLUSION AND FUTURE ENHANCEMENTS

#### **10.1 Conclusion**

The following observations are made in this work are stated as follows;

- 1. Frame differencing method is used to consider the Average Energy Image (FDEI). The Textural features of the Silhouettes are considered and extracted from the FDEI. Binary thresholding with Top-Bottom Agglomerative Clustering is done to read the features. Gray Level Covariance Matrix (GLCM) is used to extract features. These features are optimized using Swarm optimization algorithm and the features are classified as True Positive, True Negative, False Positive and False Negative using Nearest Support Feature Vector (NSFV). The Accuracy, TPR, FPR, F-Rate, Precision, Recall are calculated and found that the Nearest Support Feature Vector classifier shows better results than the compared classifiers.
- 2. The Spatio-temporal based features from the augmented GEI are represented using Recursive Bayesian Filters (RFE) based on the spatial dependence matrix of the feature pixel. By closely observing the AGEI and walking speed value, the features are represented from AGEI using Recursive Bayesian Filters (RBF). The represented features are optimized using Crow Search Optimization (CSO) algorithm. The new features are predicted from the optimized features using

Principal Polynomial Feature Transform (PPFT). Thus the predicted features give more information about the dataset and are used for classification.

- 3. The Naïve Bayes Classifier algorithm provides higher accuracy than the comparison. The Dynamic Bayesian Network (DBNetwork) model was deployed with the Naïve Bayes Classifier trained to classify the gait with the Conditional Probability value (CPV) of the features. The Naïve Bayes-DBNetwork model classifier shows greater than 95% of accuracy. Now the third stage of the proposed work begins, the recognition of a person is possible based on the features matching score level. This level is also known as confidence level or measurement level. Matching score level is a measure of similarity between features derived from a presented sample and a stored template. The Fuzzy probability method is followed to take the decision of approving the person as Authentic (genuine user) or Reject (impostor user). So, the Naïve Bayes DBNetwork was deployed with Fuzzy Probability for person recognition. The XGBoost is a wrapper class used to strengthen the weak learners and helps to identify the person in a time-efficient manner.
- 4. As a security measure, the matrix representation of the silhouette feature extracted using Gray Level Co-Variance Matrix and the matrix representation of the Accumulated Gait Energy Image (AGEI) feature extracted using Spatial Dependency Matrix are encrypted using P-Fibonacci EX-OR DCT transform with

masking coefficients and decrypted by applying the inverse transform for ensuring safety.

Hence the proposed system helps to identify the person with carrying back bag, a person with carrying shoulder bags, a person wearing dresses like saree, nighty, a person with normal and abnormal gait or limping using the cadence (walking speed with the stipulated time)

#### **10.2** Future Enhancements

Though there were sophisticated algorithms customized over some time, still a lot of studies and research is mandatory to identify, authorize and admit persons through video using gait and additional features. From the reviewed literature, it would be noted that all experiments of gait analysis are cost-effective and laboratory oriented. There are surveillance cameras fixed in the busy streets of the important city. In the recent Survey, in India, Delhi is the first city installed with more than 1800 cameras. In future, the proposed XGBoost Fuzzy NBDBNetwork can be deployed with the behaviour recognition system to analyze the person emotion as well before admitting into the smart home environment as authorized to provide utmost safety to the house locators

#### REFERENCES

- 1. S. F. Kak, F. M. Mustafa, "Smart Home Management System Based on Face Recognition Index in Real-time", Conference on Advanced Science and Engineering (ICOASE), 2019, Pp. 40-45, DOI: 10.1109/ICOASE.2019.8723673.
- 2. Nor Syazwani Md Noh, Haryati Jaafar, Wan Azani Mustafa, Syed Zulkarnain Syed Idrus and A. H. Mazelan, "Smart Home with Biometric System Recognition", Journal of Physics: Conference Series, DOI: 10.1088/1742-6596/1529/4/042020.
- 3. Du, Yegang, Yuto Lim, Yasuo Tan, "A Novel Human Activity Recognition and Prediction in Smart Home Based on Interaction", Sensors 19, 2019, Vol. 20, Issue: 4474, DOI: 10.3390/s19204474.
- 4. S. Pawar, V. Kithani, S. Ahuja, S. Sahu, "Smart Home Security Using IoT and Face Recognition", Fourth International Conference on Computing Communication Control and Automation (ICCUBEA), 2018, Pp. 1-6, DOI: 10.1109/ICCUBEA.2018.8697695.
- 5. Xiao Guo, Zhenjiang Shen, Yajing Zhang, Teng Wu, "Review on the Application of Artificial Intelligence in Smart Homes", Smart Cities, 2019, Vol.3, Pp. 402–420, DOI:10.3390/smartcities203002.
- 6. Yao L, Kusakunniran W, Wu Q, Zhang J, "Gait Recognition using a few Gait Frames", PeerJ Computer Science, 2021, Vol.7, DOI:/10.7717/peerj-cs.382.
- 7. Angel Peinado-Contreras, Mario Munoz-Organero, "Gait-Based Identification Using Deep Recurrent Neural Networks and Acceleration Patterns", Sensors, 2020, Vol. 20, Issue. 6900, DOI:10.3390/s20236900.
- 8. Mohd Muntjir, Mohd Rahul, Hesham A. Alhumyani, "An Analysis of Internet of Things (IoT): Novel Architectures, Modern Applications, security Aspects and Future Scope with Latest Case Studies", International Journal of Engineering Research & Technology (IJERT), 2017, Vol. 6, Issue.06.

- 9. Kevin Ashton, "That internet of things thing RFID journal", 1991.
- 10. Saman Fatima, Naila Aiman Aslam, Iqra Tariq, Nouman Ali, "Home Security and Automation Based on Internet of Things: A Comprehensive Review", 2020, 3rd Pak-Turk International Conference ETSE2020, 2020, Vol. 899, Issue. 012011, DOI: 10.1088/1757-899X/899/1/012011.
- 11. Alaa Jabbar Qasim, Roshidi Din, Farah Qasim Ahmed Alyousuf, "Review on techniques and file formats of image compression", Bulletin of Electrical Engineering and Informatics, 2020, Vol. 9, Issue. 2, Pp. 602-610, ISSN: 2302-9285, DOI: 10.11591/eei.v9i2.2085.
- 12. Shaik Anwar D, Kishore, "IOT based Smart Home Security System with Alert and Door Access Control using Smart Phone", International Journal Of Engineering Research & Technology (IJERT), 2016, Vol. 05, Issue. 12, DOI: 10.17577/IJERTV5IS120325.
- 13. Soon-Wook Chung, Byoung-Kwang Kim, Woo-Jin Song, "Removing chromatic aberration by digital image processing", Optical Engineering, 2010, Vol.49, Issue. 6, DOI:10.1117/1.3455506.
- 14. Miroslav UHRINA, Juraj BIENIK, Tomas MIZDOS, "Chroma Subsampling Influence on the Perceived Video Quality for Compressed Sequences in High Resolutions", Digital Image Processing and Computer Graphics, 2017, Vol. 15, Issue. 4, DOI: 10.15598/aeee.v15i4.2414.
- 15. Suman Kunwar, "Image Compression Algorithm and JPEG Standard", International Journal of Scientific and Research Publications, 2017, Vol. 7, Issue. 12, ISSN 2250-3153, DOI: 10.13140/RG.2.2.12178.76482.
- 16. Zhipeng Chen, Yao Zhao, Rongrong, "Detection for operation chain: Histogram equalization and dither-like operation. KSII Transactions on Internet and Information Systems", KSII TRANSACTIONS ON INTERNET AND INFORMATION SYSTEMS, 2015, Vol. 9, Issue. 9, Pp. 3751–3770, ISSN 1976-7277, DOI: 10.3837/tiis.2015.09.026.

- 17. Mauro Barni, Ehsan Nowroozi, Benedetta Tondi, "Detection of adaptive histogram equalization robust against JPEG compression", 2019, 10.1109/IWBF.2018.8401564.
- 18. Davide Cozzolino, Diego Gragnaniello, Luisa Verdoliva, "Image forgery detection through residual-based local descriptors and block-matching", Image Processing (ICIP), 2014, Pp. 5297–5301.
- 19. Tikoo S and Malik N, "Detection, Segmentation and Recognition of Face and its Features Using Neural Network, Journal of Biosensors & Bioelectronics, Vol.7, Issue. 210, DOI:10.4172/2155-6210.1000210.
- 20. Shiji Kumar P.S, Dharun V.S, "Extraction of Texture Features using GLCM and Shape Features using Connected Regions", International journal of engineering and technology, 2016, Vol. 8, Issue. 6, ISSN: 2319-8613, DOI:10.21817/IJET/2016/V8I6/160806254.
- 21. Stephen M. Pizer, E. Philip Amburn, John D. Austin, Robert Cromartie, Ari Geselowitz, Trey Greer, Bart ter Haar Romeny, John B. Zimmerman, Karel Zuiderveld, "Adaptive histogram equalization and its variations, Computer Vision, Graphics, and Image Processing", 1987, Vol. 39, Issue. 3, Pp. 355-368, ISSN 0734-189X, DOI:10.1016/S0734-189X(87)80186-X.
- 22. Gang Cao, Yao Zhao, Rongrong Ni, "Forensic estimation of gamma correction in digital images", 2010 IEEE International Conference on Image Processing, 2010, Pp. 2097–2100, DOI: 10.1109/ICIP.2010.5652701.
- 23. Gang Cao, Yao Zhao, Rongrong Ni, "Contrast enhancement-based forensics in digital images", IEEE transactions on information forensics and security, 2014, Vol. 9, Issue. 3, Pp. 515–525, DOI: 10.1109/TIFS.2014.2300937.
- 24. M. Barni, M. Fontani, and B. Tondi, "A universal technique to hide traces of histogram-based image manipulations", 2012: Proceedings of the Multimedia and security, 2012, Pp. 97–104, DOI:10.1145/2361407.2361424.

- 25. De Rosa, M. Fontani, M. Massai, A. Piva, and M. Barni, "Second-order statistics analysis to cope with contrast enhancement counter-forensics", IEEE Signal Processing Letters, 2015, Vol. 22, Issue. 8, Pp. 1132–1136, DOI: 10.1109/LSP.2015.2389241.
- 26. Gowtham Bhargavas M, Harshavardhan K, Mohan G C, Nikhil Sharma A and Prathap C, "Human Identification using Gait Recognition", International Conference on Communication and Signal Processing, 2017, ISBN: 978-1-5090-3800-8, DOI: 10.1109/ICCSP.2017.8286638.
- V Strukova, LV Shiripova, E V Myasnikov, "Gait analysis for person recognition using principal component analysis and support vector machines", IV International Conference on "Information Technology and Nanotechnology (ITNT-2018), 2018, Vol. 2210.
- 28. Veronica Cimolin, Manuela Galli, "Summary measures for clinical gait analysis: A literature review", Gait & Posture, 2014, Vol. 39, Issue. 4, Pp. 1005-1010, https://DOI.org/10.1016/j.gaitpost.2014.02.001.
- 29. Nahid A Makhdoomi, Teddy S Gunawan, Mohamed H Habaebi, "Human Gait Recognition And Classification Using Similarity Index for various conditions", IOP Conf. Series: Materials Science and Engineering, 2013, Vol. 53, Issue. 012069, DOI:10.1088/1757-899X/53/1/012069.
- 30. Ait O. Lishani, Larbi Boubchir, Ahmed Bouridane, "Haralick Features for GEI-based Human Gait Recognition", 26th International Conference on Microelectronics (ICM), ISBN:978-1-4799-8153-3/1, DOI:10.1109/ICM.2014.7071800.
- 31. Anu J Nair, Rizwana Rasheed, Maheeshma KM, "An Ensemble-Based Feature Selection and Classification of Gene Expression using Support Vector Machine, K-Nearest Neighbor, Decision Tree", 2019 Proceedings of the Fourth International Conference on Communication and Electronics Systems, 2019, Pp. 1618-1623, ISBN: 978-1-7281-1261-9, DOI: 10.1109/ICCES45898.2019.900204.

- 32. Dilpreet Kaur, Yadwinder Kaur Dilpreet Kaur, "Various Image Segmentation Techniques: A Review", International Journal of Computer Science and Mobile Computing, 2014, Vol.3, Issue.5, Pp. 809-814, ISSN 2320–088X,
- 33. Muthahir O, Oloyode, Gerhad P, Hancke, "Unimodal and Multimodal Biometric Sensing Systems: A Review", Sensors 2016, Vol. 4, Pp. 2169-3536, DOI: 1109/ACCESS.2016.2614720
- 34. Shafagat Mahmudova, "The Ways of Increasing Quality of Human Recognition in Biometric Network Environment", International Journal of Intelligent Information Systems, 2017, Vol. 6, Issue. 5, Pp. 56-61, DOI: 10.11648/j.ijiis.20170605.11.
- 35. Asrul Adam, Zuwairie Ibrahim, Norrima Mokhtar, Mohd Ibrahim Shapiai, Marizan Mubin and Ismail Saad, "Feature selection using angle modulated simulated Kalman filter for peak classification of EEG signals", Springerplus, 2016, Vol.5, Issue.1580, DOI 10.1186/s40064-016-3277.
- 36. J.Savitha, A.V.Senthil Kumar, "Image Segmentation Based Face Recognition Using Enhanced SPCA-KNN Method", International Journal of Computer Science and Information Technologies, 2015, Vol. 6, Issue.3, Pp. 2115-2120, DOI: 10.1186/s40064-016-3277-z.
- 37. Qu S., Li Q, "The Human Image Segmentation Algorithm Based on Face Detection and Biased Normalized Cuts", CCCV 2015. Communications in Computer and Information Science, 2015, Vol. 546, Pp 134-143, DOI:10.1007/978-3-662-48558-3\_14.
- 38. Manikanta Prahlad Manda, Hi Seok Kim, "A Fast Image Thresholding Algorithm for Infrared Images Based on Histogram Approximation and Circuit Theory", Algorithms 2020, 2020, Vol. 13, Issue. 207, DOI:10.3390/a13090207.
- 39. P. Karampelas, T. Bourlai, "A Survey of Using Biometrics for Smart Visual Surveillance: Gait Recognition", Surveillance in Action, Advanced Sciences and Technologies for Security Applications, 2018, Pp. 3-23, DOI:10.1007/978-3-319-68533-5\_1.

- 40. Sayana Sivanand, "Adaptive Local Threshold Algorithm and Kernel Fuzzy C-Means Clustering Method for Image Segmentation", International Journal of Latest Trends in Engineering and Technology (IJLTET), 2013, Vol.2, Issue.3, Pp.38.
- 41. Simrandeep Singh1, Nitin Mittal, Harbinder Singh, "A multilevel thresholding algorithm using LebTLBO for image segmentation", Neural Computing and Applications, 2020, Vol. 32, Pp. 16681–16706 DOI:10.1007/s00521-020-04989-2.
- 42. Jin Liu, Jianhong Zheng, Quanhua Tang, Weidong Jin, "Minimum Error Thresholding Segmentation Algorithm Based on 3D Grayscale Histogram", Mathematical Problems in Engineering, 2014, Vol. 2014, Article ID. 932695, DOI: 10.1155/2014/932695.
- 43. Temitope Mapayi, Serestina Viriri, Jules-Raymond Tapamo, "Adaptive Thresholding Technique for Retinal Vessel Segmentation Based on GLCM-Energy Information", Computational and Mathematical Methods in Medicine, 2015, Vol. 2015, Article ID. 597475, DOI: 10.1155/2015/597475.
- 44. Akshay Upadhyay, Ramgopal Kashyap, "Fast Segmentation Methods for MedicalImages", International Journal of Computer Applications, 2016, Vol. 156, Issue. 3, Pp. 18-23, DOI: 10.5120/ijca2016912399.
- 45. Murat Karakoyun, Nurdan Akhan Baykan, Mehmet ibeyoglu "Multi-Level Thresholding for Image Segmentation With Swarm Optimization Algorithms", International Research Journal of Electronics & Computer Engineering, 2017, Vol. 3, Issue.3, ISSN: 2412-4370, DOI: 10.24178/irjece.2017.3.3.01.
- 46. EISSA D. HABIL, TAGHREED Z. NASR, "THE TWO SCOPES OF FUZZY PROBABILITY THEORY", Algebras Groups and Geometries, 2010, Vol.27, Issue.2.
- 47. F. Koumi, M. Aldasht, H. Tamimi, "Efficient Feature Selection using Particle Swarm Optimization: A hybrid filters-wrapper Approach", 2019 10th International

Conference on Information and Communication Systems (ICICS), 2019, Pp. 122-127, ISSN: 2573-3346, DOI: 10.1109/IACS.2019.8809133.

- 48. Gulnaz Alimjan, Tieli Sun, Yi Liang, Hurxida Jumahun, and Yu Guan, "A New Technique for Remote Sensing Image Classification Based on Combinatorial Algorithm of SVM and KNN", International Journal of Pattern Recognition and Artificial Intelligence, 2018, Vol. 32, Issue. 7, Article ID. 1859012, DOI: 10.1142/S0218001418590127.
- 49. Nii Longdon Sowah, Qingbo Wu, Fanman Meng, "A Classification and Clustering method for tracking multiple objects", proceeding of IEEE conference on Computing and communication workshop and conference (cows), 2018, Pp. 537-544, DOI: 10.1109/CCWC.2018.8301626.
- 50. Shakir F. Kak, Firas Mahmood Mustafa, Pedro Valente, "A Review of Person Recognition Based on Face Model", Eurasian Journal of Science & Engineering, 2018, ISSN: 2414-5602, DOI: 10.23918/eajse.v4i1sip157.
- 51. K. Kalirajan, M. Sudha, "Moving Object Detection for Video Surveillance", The Scientific World Journal, 2015, Vol. 2015, Article ID. 907469, DOI:10.1155/2015/907469.
- 52. Alexandros Andre Chaaraoui, Francisco Flórez Revuelta, "A Low-Dimensional Radial Silhouette-Based Feature for Fast Human Action Recognition Fusing Multiple Views", International Scholarly Research Notices, Vol. 2014, Article ID. 547069, DOI: 10.1155/2014/547069.s
- 53. Akshaya D. Shetty, Disha, Shubha B, Suryanarayana K, "Detection of intruders in warehouses using Infrared based Thermopile Sensor Array", IOP Conference Series Materials Science and Engineering, 2018, Vol. 376, Article ID: 012087, DOI:10.1088/1757-8.
- 54. Ghalleb AEK, Amara NEB, "Soft and hard biometrics for the authentication of remote people in front and side views", International Journal of Applied Engineering Research, 2016, Vol. 11, Issue.14, Pp.8120–8127.

- 55. Kozlow P, Abid N, Yanushkevich S, "Gait Type Analysis Using Dynamic Bayesian Networks", Sensors, Vol. 18, Issue. 10, Article ID: 3329, DOI:10.3390/s18103329.
- 56. Lee J., Phan C.B., Koo S, "Predicting Three-Dimensional Gait Parameters with a Single Camera Video Sequence", International Journal of Precision Engineering and Manufacturing, 2018, Vol. 19, Pp.753–759, DOI: 10.1007/s12541-018-0090-3.
- 57. Strazza A., Mengarelli A., Fioretti S., Burattini L., Agostini V., Knaflitz M., Di Nardo F, "Surface-EMG analysis for the quantification of thigh muscle dynamic co-contractions during normal gait", Gait Posture, 2017, Vol.51, Pp.228–233, DOI: 10.1016/j.gaitpost.2016.11.003.
- 58. Zhang Y, Huang Y, Wang L, Yu S, "A comprehensive study on gait biometrics using a joint cnn-based method", Pattern Recognition, 2019, Vol.93, Pp. 228–236, DOI:10.1016/J.PATCOG.2019.04.023.
- 59. Jiande Sun, Yufei Wang and Jing Li, "Gait Recognition", Motion Tracking and Gesture Recognition, 2017, DOI: 10.5772/68119.
- 60. B. Jawed, O. O. Khalifa, S. S. Newaj Bhuiyan, "Human Gait Recognition System", 7th International Conference on Computer and Communication Engineering (ICCCE), 2018, Pp. 89-92, DOI: 10.1109/ICCCE.2018.8539245.
- 61. P. Nithyakani, A. Shanthini and G. Ponsam, "Human Gait Recognition using Deep Convolutional Neural Network", 2019 3rd International Conference on Computing and Communications Technologies (ICCCT), 2019, Pp. 208-211, DOI: 10.1109/ICCCT2.2019.8824836.
- 62. Strukova O, Shiripova L, Myasnikov E, "Gait analysis for person recognition using principal component analysis and support vector machines", Image Processing and Earth Remote Sensing. Information Technology and Nanotechnology 2018, 2018, Vol. 2210, Pp.170–176, DOI: 10.18287/1613-0073-2018-2210-170-176.

- 63. Lee CP, Tan AW, Tan SC, "Gait probability image: an information-theoretic model of gait representation", Visual Communication image representation, 2014, Vol.25, Issue.6, Pp.1489-1492, DOI: 10.1016/j.jvcir.2014.05.006.
- 64. Arora P, Srivastava S, "Gait Recognition Using Gait Gaussian Image, In: 2nd IEEE International Conference on Signal Processing and Integrated Networks (SPIN)", 2015, Pp.791-794.
- 65. Guodong Zhang, Peilin Jiang, Kazuyuki Matsumoto, Minoru Yoshida, and Kenji Kita, "Reidentification of Persons Using Clothing Features in Real-Life Video", Machine Learning and Visual Computing, 2017, Vol. 2017, Article ID:5834846, DOI:10.1155/2017/5834846.
- 66. Zou Q, Wang Y, Wang Q, Zhao Y, Li Q, "Deep learning-based gait recognition using smartphones in the wild", IEEE Trans Inform Forensics Security, 2020, Vol. 15, Pp. 3197–3212.
- 67. Shiji Kumar P.S, Dharun V.S, "Extraction of Texture Features using GLCM and Shape Features using Connected Regions", International journal of engineering and technology, 2016, Vol.8, Issue,6, Pp.2926-2930, DOI:10.21817/IJET/2016/V8I6/160806254.
- 68. C. Li, S. Sun, X. Chen, and X. Min", Cross-view gait recognition using joint Bayesian", In Proc. SPIE 10420, Ninth International Conference on Digital Image Processing (ICDIP 2017), 2017, DOI:10.1117/12.2281536.
- 69. Y. Makihara, A. Suzuki, D. Muramatsu, X. Li, and Y. Yagi, "Joint intensity and spatial metric learning for robust gait recognition" 2017 IEEE Conference on Computer Vision and Pattern Recognition (CVPR), 2017, Pp. 6786-6796, DOI: 10.1109/CVPR.2017.718.

- 70. Anna Sokolova1, Anton Konushin", Pose-based deep gait recognition", Institute of Engineering and Technology, 2019, Vol. 8, Issue. 2, Pp. 134-143, https://DOI.org/10.1049/iet-bmt.2018.5046.
- 71. Binu M Nair and Kimberly D Kendricks, "Deep network for analyzing gait patterns in low resolution video towards threat identification", Society for Imaging Science and Technology, 2016, Vol.8, Pp.1-8, DOI: 10.2352/ISSN.2470-1173.2016.11.IMAWM-471.
- 72. Lishani, A.O., Boubchir, L., Khalifa, E, "Human gait recognition using GEI-based local multi-scale feature descriptors", Multimed Tools Applications, 2019, Vol. 78, Pp. 5715–57, DOI: 10.1007/s11042-018-5752-8.
- 73. Jing Luo, Jianliang Zhang, Chunyuan Zi, Ying Niu, Huixin Tian, and ChunboXiu, "Gait Recognition Using GEI and AFDEI", International Journal of Optics, Hindawi Publishing Corporation, Vol. 2015, Article ID: 763908, Pp. 1-5, DOI:10.1155/2015/763908.
- 74. M. Rokanujjaman, M. Islam, M. A. Hossain, M. Rezaul Islam, Y. Makihara, Y. Yagi, "Effective part-based gait identification using frequency-domain gait entropy features", In Multimedia Tools and Applications, 2013, Vol. 74, Issue.9, Pp. 1-22, DOI: 10.1007/s11042-013-1770-8
- 75. Z. Wu, Y. Huang, L. Wang, X. Wang and T. Tan, "A Comprehensive Study on Cross-View Gait Based Human Identification with Deep CNNs", in IEEE Transactions on Pattern Analysis and Machine Intelligence, 2017, Vol. 39, Issue. 2, Pp. 209-226, DOI: 10.1109/TPAMI.2016.2545669.
- 76. Shiqi Yu, Daoliang Tan and Tieniu Tan, "A Framework for Evaluating the Effect of View Angle, Clothing and Carrying Condition on Gait Recognition", 18th International Conference on Pattern Recognition (ICPR'06), 2006, Pp. 441-444, DOI: 10.1109/ICPR.2006.67.
- 77. Strukova O, Myasnikov E, "The choice of methods for the construction of PCA-based features and the selection of SVM parameters for personidentification by

- gait" Journal of Physics: Conference Series, 2019, Vol. 1368, Issue. 032001, DOI:10.1088/1742-6596/1368/3/032001.
- 78. Chao Li, Xin Min, Shouqian Sun, Wenqian Lin, Zhichuan Tan, "DeepGait: A Learning Deep Convolutional Representation for View-Invariant Gait Recognition Using Joint Bayesian", DOI: 10.5281/zenodo.321246.
- 79. Shorten C, Khoshgoftaar TM, "A survey on image data augmentation for deep learning", Journal of Big Data, 2019, Vol. 6, Issue. 60, DOI:10.1186/s40537-019-0197-0.
- 80. Neeyati Anand, Shallu Sehgal, Manisha Agarwal, Riya Sehgal, Sanchit Anand, Arun Bashambu, "FEATURE SELECTION USING BIO INSPIRED ALGORITHMS", International Journal of Psychosocial Rehabilitation, 2020, Vol. 24, Issue. 6, Pp. 4824-4846, DOI:10.37200/IJPR/V24I6/PR260474.
- 81. Y. Chen, L. Zhu, P. Ghamisi, X. Jia, G. Li and L. Tang, "Hyperspectral Images Classification With Gabor Filtering and Convolutional Neural Network", IEEE Geoscience and Remote Sensing Letters, 2017, Vol. 14, Issue. 12, Pp. 2355-2359, DOI: 10.1109/LGRS.2017.2764915.
- 82. S. Aljahdali, A. Ansari and N. Hundewale, "Classification of image database using SVM with Gabor Magnitude", 2012 International Conference on Multimedia Computing and Systems, 2012, Pp. 126-132, DOI: 10.1109/ICMCS.2012.6320228.
- 83. R Kusumawati1, A D 'arofah2and P A Pramana3, "Comparison Performance of Naive Bayes Classifier and Support Vector Machine Algorithm for Twitter's Classification of Tokopedia Services", Journal of Physics: Conf. Series, 2019, Vol. 1320, Issue. 012016, DOI:10.1088/1742-6596/1320/1/012016.
- 84. Ali Allahverdipoor, Farhad Soleimanian Gharehchopogh, "An Improved K-Nearest Neighbor with Crow Search Algorithm for Feature Selection in Text Documents Classification", Journal of Advances in Computer Research, 2018, Vol. 9, Issue. 2, Pp. 37-48.

- 85. Freitas D, Lopes LG, Morgado-Dias F, "Particle Swarm Optimisation: A Historical Review Up to the Current Developments", Entropy 2020, Vol. 22, Issue. 362, DOI:10.3390/e22030362.
- 86. K.Maheswari, "Classification of Twitter Data Set using SVM and KSVM", International Journal of Pure and Applied Mathematics, 2018, Vol. 118, Issue. 7, Pp. 675-680.
- 87. Gudder S, "What Is Fuzzy Probability Theory?", Foundations of Physics, 2000, Vol. 30, Pp.1663–1678, DOI:10.1023/A:1026450217337.
- 88. Guixiang Wang, Yifeng Xu, Sen Qin, "Basic Fuzzy Event Space and Probability Distribution of Probability Fuzzy Space", Mathematics 2019, Vol.7, Issue.542, DOI:10.3390/math7060542.
- 89. L. A. ZADEH\*, "Probability Measures of Fuzzy Events", Journal of Mathematical Analysis and Applications, 1968, Vol. 23, Pp. 421-427.
- 90. Abdullah Gubbi, Mohammad Fazle Azeem, Mohammed Rafeeq, Shoaib Kamal, "Fuzzy Shannon Entropy for Face Recognition", International Journal of Innovative Technology and Exploring Engineering (IJITEE), 2019, Vol. 8, Issue. 6S4, ISSN: 2278-3075.
- 91. Mamta Bansal Madasu Hanmandlu, "A new entropy function for feature extraction with the refined scores as a classifier for the unconstrained ear verification", Journal of Electrical Systems and Information Technology, 2017, Vol. 4, Issue.1, Pp. 135-158, DOI:10.1016/j.jesit.2016.10.006.
- 92. Andri Kurniawan, Tito Waluyo Purboyo, Anggunmeka Luhur Prasasti, "Implementation of Image Compression Using Discrete Cosine Transform (DCT) and Discrete Wavelet Transform (DWT)", International Journal of Applied Engineering Research, 2017, Vol. 12, Issue. 23, Pp. 13951-13958, ISSN 0973-4562.

- 93. E. Anupriya, Sachin Soni, Amit Agnihotri, Sourabh Babelay, "Encryption using XOR based Extended Key for Information Security A Novel Approach", International Journal on Computer Science and Engineering, 2011, Vol. 3 Issue. 1, Pp. 146-154, ISSN: 0975-3397.
- 94. B. Schneier, APplied Cryptography: Protocols, Algorithms, and Source Code in C, JohnWiley & Sons, New York, NY, USA, 2nd edition, 1996.
- 95. Sandeep Draksharam, Dheeraj Katravulapalli, Rohith Krishna, K,Thanikaiselvan.V, "Analysis of Hybrid Chaotic Image Encryption", Vol.18, 2018, IEEE 697-703.
- 96. Mohit Kumar, Akshat Aggarwal, Ankit Garg, "A Review on Various Digital Image Encryption Techniques and Security Criteria", International Journal of Computer Applications, 2014, Vol. 96, Issue.13, ISSN: 0975-8887, DOI: 10.5120/16854-6720.
- 97. Nidhal Khdhair El Abbadi, Samer Thaaban Abaas, Ali Abd Alaziz, "New Image Encryption Algorithm Based on Diffie-Hellman and Singular Value Decomposition", International Journal of Computer Applications, 2016, Vol. 5, Issue.1, Pp.197-201, DOI 10.17148/IJARCCE.2016.5147.
- 98. Yicong Zhou, Karen Panetta, Sos Agaian",Image Encryption Using Binary Keyimages", Proceedings of the 2009 IEEE International Conference on Systems, Man, and Cybernetics, 2009, Pp.4569-4574, DOI: 10.1109/ICSMC.2009.5346780.
- 99. Prarthana Madan Modak, Dr. Vijaykumar Pawar, "A Comprehensive Survey on Image Scrambling Techniques", International Journal of Science and Research, 2015, Vol. 4, Issue. 12, Pp. 814-818.
- 100. L. Kocarev, G. Jakimoski, T. Stojanovski, and U. Parlitz, "From chaoticmaps to encryption schemes", in Proceedings of the IEEE International Symposium on Circuits and Systems (ISCAS '98), 1998, Vol. 4, Pp. 514–517, DOI: 10.1109/ISCAS.1998.698968.

- 101. T. Sivakumar, K. Gayathri Devi, "Image Encryption using Block Permutation and XOR Operation", International Journal of Computer Applications 2017, Vol. 160, Issue. 9, ISSN: 0975 8887.
- 102. Rinki Pakshwar, Vijay Kumar Trivedi, Vineet Richhariya, "Image Encryption Using Random Scrambling and XOR Operation", International Journal of Engineering Research & Technology (IJERT), 2013, Vol. 2, Issue. 3, ISSN: 2278-0181.
- 103. D.Ratna Kishore, D.Suneetha, G.G.S.Pradeep, "An Improved Method of Dna Data Encryption using Xor Based Data Segments", International Journal of Recent Technology and Engineering (IJRTE), 2019, Vol. 8, Issue. 1, ISSN: 2277-3878.
- 104. C. E. Shannon, "Communication theory of secrecy systems", The Bell System Technical Journal, Vol. 28, Issue. 4, Pp. 656–715, 1949.
- 105. Andik Setyono, De Rosal Ignatius Moses Setiadi, "Securing and Hiding Secret Message in Image using XOR Transposition Encryption and LSB Method", Journal of Physics: Coference Series, 2019, Article ID: 012039, DOI:10.1088/1742-6596/1196/1/012039
- 106. N. K. Pareek, V. Patidar, and K. K. Sud, "Discrete chaotic cryptography using external key", Physics Letters, Vol. 309, Issue. 1-2, Pp. 75–82, 2003.
- 107. X. Wang and L. Teng, "An image blocks encryption algorithm based on spatiotemporal chaos", Nonlinear Dynamics. An International Journal of Nonlinear Dynamics and Chaos in Engineering Systems, 2012, Vol. 67, Issue. 1, Pp. 365–371.
- 108. D. Xiao, X. Liao, and P. Wei, "Analysis and improvement of a chaos-based image encryption algorithm", Chaos, Solitons & Fractals, 2009, Vol. 40, Issue. 5, Pp. 2191–2199.
- 109. S. Behnia, A. Akhshani, H.Mahmodi, and A. Akhavan, "A novel algorithm for image encryption based on mixture of chaotic maps", Chaos, Solitons & Fractals, 2008, Vol. 35, Issue. 2, Pp. 408–41.

- 110. O.Mirzaei, M. Yaghoobi, and H. Irani, "A new image encryption method: parallel sub-image encryption with hyper chaos", Nonlinear Dynamics, 2012, Vol. 67, Issue. 1, Pp. 557–566, DOI 10.1007/s11071-011-0006-6.
- 111. Y.Wang, K.-W.Wong, X. F. Liao, and G. R.Chen, "A new chaos based fast image encryption algorithm", APplied Soft Computing, 2011, Vol. 11, Issue. 1, Pp. 514–522, DOI:10.1016/j.asoc.2009.12.011.
- 112. A. I. Ismail, A. Mohammed, and D. Hossam, "A digital image encryption algorithm based a composition of two chaotic Wavelet function map", International Journal of Network Security, 2010, Vol. 11, Issue. 1, Pp. 1–10,
- 113. R. Rhouma and S. Belghith, "Cryptanalysis of a new image encryption algorithm based on hyper-chaos", Physics Letters, Section A: General, Atomic and Solid State Physics, 2008, Vol. 372, Issue. 38, Pp. 5973–5978, DOI:10.1016/j.physleta.2008.07.057.
- 114. X.-F. Li, K. E. Chlouverakis, D.-L. Xu Lorenz, Chen, "Nonlinear dynamics and circuit realization of a new chaotic flow: a variant of Nonlinear Analysis Real World Applications", An International Multidisciplinary Journal, 2009, Vol. 10, Issue. 4, Pp. 2357–2368, DOI:10.1016/J.NONRWA.2008.04.024.
- 115. J. F. Zhao, S. Y. Wang, Y. X. Chang, and X. F. Li, "A novel image encryption scheme based on an improper fractional-order chaotic system", Nonlinear Dynamics, 2015, Vol. 80, Issue. 4, Pp. 1721–1729, DOI: 10.1007/s11071-015-1911-x.
- 116. X. Wu, H. Wang, and H. Lu, "Modified generalized projective synchronization of a new fractional-order hyperchaotic system and its aPplication to secure communication", Nonlinear Analysis. RealWorld APplications, 2012, Vol. 13, Issue. 3, Pp. 1441–1450, DOI: 10.1016/j.nonrwa.2011.11.008.
- 117. O. Mannai, R. Bechikh, H. Hermassi, R. Rhouma, and S. Belghith, "A new image encryption scheme based on a simple firstorder time-delay system with aPpropriate

- nonlinearity", Nonlinear Dynamics, 2015, Vol. 82, Issue. 1, Pp. 107–117, DOI: 10.1007/s11071-015-2142-x.
- 118. Q. Liu, P.-Y. Li, M.-C. Zhang, Y.-X. Sui, and H.-J. Yang, "A novel image encryption algorithm based on chaos maps with Markov properties", Communications in Nonlinear Science and Numerical Simulation, 2015, Vol. 20, Issue. 2, Pp. 506–515, 10.1016/j.cnsns.2014.06.005.
- 119. Xiao-yi Wang, Yi Yang, Yu-ting Bai, Jia-bin Yu, Zhi-yao Zhao, Xue-bo Jin, "Fuzzy Boost Classifier of Decision Experts for Multicriteria Group Decision-Making", Complexity, 2020, Vol. 2020, Article ID 8147617, Pp.1-10, DOI:10.1155/2020/8147617.
- 120. Tianqi Chen, Carlos Guestrin, "XGBoost: A Scalable Tree Boosting System", SKDD '16: Proceedings of the 22nd ACM SIGKDD International Conference on Knowledge Discovery and Data Mining, 2016, Pp.785–794, DOI:10.1145/2939672.2939785.
- 121. V. Ayumi, "Pose-based human action recognition with Extreme Gradient Boosting", 2016 IEEE Student Conference on Research and Development (SCOReD), 2016, Pp. 1-5, DOI: 10.1109/SCORED.2016.7810099.
- 122. Xianghai Xu, Xuan Wang, Zhiqing Sun, Shouxiang Wang, "Face recognition technology based on CNN, XGBoost, model fusion and its aPplication for safety management in power system", International Conference on Smart Grid and Energy Engineering, 2020, Vol.654, DOI:10.1088/1755-1315/645/1/012054.
- 123. The dataset downloaded from http://www.cbsr.ia.ac.cn/english/Gait%20Databases.asp link.

# LIST OF PUBLICATIONS

S.No	TITLE OF THE PAPER	NAME OF THE JOURNAL	CITE SCORE	INDEXED
1	Interoperability in smart home network	Lecture Notes in Electrical Engineering, 2020, Springer, book series (LNEE, Vol. 637, pp:69-79)	0.5	SCOPUS- UGC
2	The internet of things routing security	Lecture Notes in Electrical Engineering, 2020, Springer, book series (LNEE, Vol. 637, pp:603-612)	0.5	SCOPUS- UGC
3	The Appraised Structure for Improving Quality in the Compressed Image using EQI-AC Algorithm"	Advances in Intelligent Systems and Computing, 2021, Springer, book series (	0.9	SCOPUS- UGC
4	XORDCT- A Chaotic method for image encryption and decryption	Advances in Intelligent Systems and Computing, 2021, Springer	0.9	SCOPUS- UGC
5	Fuzzy Probability based Person recognition in Smart Environments	Journal of Intelligent and Fuzzy Systems, 2021, IOS Press	1.854	SCI
6	Thresholding images using Binarization and Top- Bottom Agglomerative Clustering Hierarchy (BTTBACH) by Frame differencing Method	International Journal of Advanced Science and Technology (Communicated)	communicated	-
7	Selection, Optimization and Classification of Augmented Gait Energy Image Features using Bayesian filters for Person Recognition	Journal of Intelligent and Fuzzy Systems (under review)	communicated	-

# Interoperability in Smart Living Network—A Survey



M. Durairaj and J. Hirudhaya Mary Asha

**Abstract** Embedded systems or embedded devices are the basic hardware needed for Internet of things (IoT). The "Internet" and "Things" are merged together to make them work as a powerful technology called the Internet of Things (IoT). The IoT is the bombardment of the real-world objects into Internet-based things that can exchange massive amount of data with minimal human interventions. However, the security and privacy concepts of infrastructural engineering are highly critical. Smart IoT projects with smart devices are worldwide known. Smart living is a residence filled with technology that processes the information expected to respond to the needs of the occupants. It promotes the locator comfort, convenience, and security through the technology. Smart devices with the IoT services convert the raw data, read from the home sensors and the actuators, and respond with operational commands to control the home network or home appliances technology from anywhere with the help of Internet. Devices such as smartphones, tablets, and personal computers are used to communicate with these technologies. The home technology highly depends on the interoperability among the communication system architecture to achieve security. In this paper, a survey is done on how the interoperability is built with the efficient use of power energy in the existing smart living.

**Keywords** Internet of Things (IoT) · Energy · Interoperability · Security

### 1 Introduction

Today, humans are addicted to technologies for their daily chores. Every household has more devices connected to the Internet with a uniquely assigned IP address,

M. Durairaj · J. Hirudhaya Mary Asha (⋈)

Assistant Professor, Department of Computer Science, Bharathidasan University, Tiruchirapalli, Tamil Nadu. India

e-mail: hirudhaya\_ashaa20@yahoo.co.in

J. Hirudhaya Mary Asha

Research Scholar, Department of Computer Science, Bharathidasan University, Tiruchirapalli, Tamil Nadu, India

© Springer Nature Singapore Pte Ltd. 2020 V. Bindhu et al. (eds.), *International Conference on Communication, Computing and Electronics Systems*, Lecture Notes in Electrical Engineering 637, https://doi.org/10.1007/978-981-15-2612-1 7 a combination of numbers used to locate the devices on the network. The operational messages routed to the devices are completely controlled and monitored via the Internet. The Internet follows some standardized protocols designed suitable for information and communication facilities [1, 2]. People can operate the household items from the outdoor location and manage smart communication between devices and application by linking the perfect architecture [3]. In M2H or M2M communication, a number of devices with varying levels of complexity can transmit through a gateway. IoT devices route information with different energy levels to the connected gateway at the same time [4]. Various technologies such as machine learning, pervasive computing, and artificial intelligence are used to recognize and record the activity of the people in their daily life. The research community focuses on the technical possibilities to be done and also the lack of interoperability of smart living devices.

### 2 Related Works

The home we live in or the place we work can act smart with automation control systems. Smart units of home are connected together with a user interface for interacting with the home appliances [1]. A "smart living" can be defined as a residence filled with technology expected to respond to the needs of the occupants. To promote the home occupant's comfort, convenience, and security, interfaces such as gateway or middleware are built inside smart home. Smart living network is constructed with three types. (1) through wired home electric line network, (2) through separate physical line network for signal transporting, and (3) through a wireless network. The wired networks have their own strength and weakness to connect the source and destination, but the wireless networks provide more advantages than the other two. Smart sensors are designed to sense gas leakages, temperature, recognize the face, energy consumption, humidity, control television, door lock status, doorbell, refrigerator storage sensors, light intensity, smoke, etc., continuously in regular intervals within range and send alerts to the authorized user [2].

A report is released by "TELECOMMUNICATION ENGINEERING CENTRE" that explains the year-wise changes in how the society adopted to the automation of smart living in their everyday life [5]. Using the data sent by the sensors, specialized software or intelligent processing agents trigger actions in the environment by means of actuators. For example, the sensor can smell smoke by air sampling technique, and if any smoke is detected by the sensor, it warns the proprietor via SMS and sends alerts to the nearby fire station [3]. The middleware is used for their inter-communicability [4]. A smart living control can handle enormous heterogeneous devices in the homes and provide user-oriented services like monitoring adult, elders, or kids by using appropriate algorithms [6, 7]. Smart living is constructed with inter-networks of three blocks [8]. They are:



Fig. 1 Model picture of smart living [8]

- 1. Home Automation System (HAS), an outline that shows the inter-linking of home appliances (e.g., refrigerator, heaters, lights, televisions, and so on)
- 2. Home Controlling System (HCS), an application, which creates automated commands based on the data sensed by the sensor attached to home appliances and forwards the commands to the actuators to perform some operation.
- 3. Home Network System (HNS), a complete framework linkage of HAS and HCS communication to exchange information [8] (Fig. 1).

# 3 Home Framework Designing

The smart living is the projected output gained from the interaction of hardware and software. While designing smart living, there are three main concepts to be considered. They are smart objects participated in the device layer, hardware infrastructure that gives smart capabilities to the object, and finally software layer used to activate the smart capability [9]. Experts are arguing with the smart living functionality that seems to be a better system for managing everyday life. So, the instruments used are goal-oriented part for next-level development [10]. The following chart predicts the dimensional growth of technology in home from 1970 to 2025 [11] (Fig. 2).

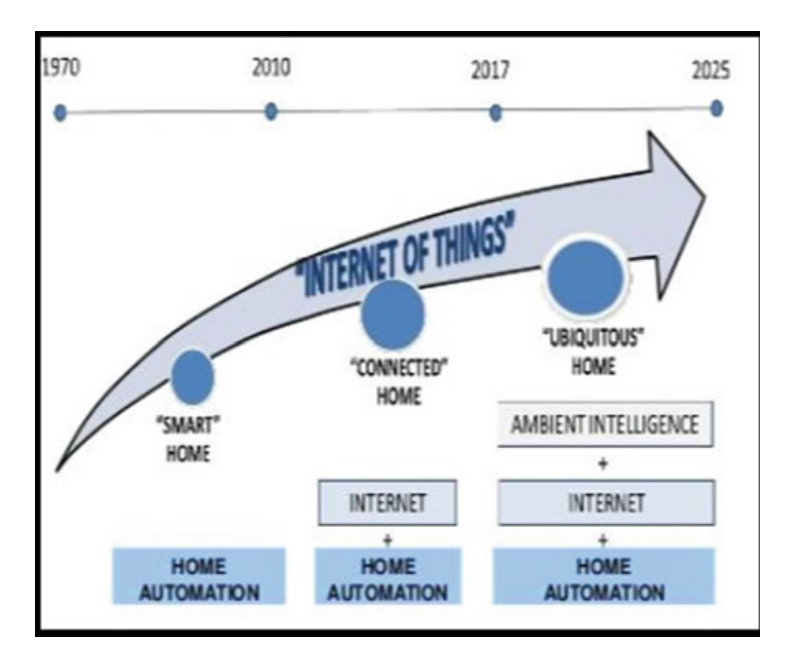


Fig. 2 Growth of smart living automation

### 3.1 Middleware or Gateway

Middleware is the part of the IoT system architecture which stands between the devices and application layer for providing services by effective communication. It is a software interface designed to transfer messages or queries between the device end and the user application end [12]. The server application detects the client's geographical location and performs concurrent processing, balancing load and managing transactions by sharing client requests to multiple servers and providing fast access to resources using cyber security [13]. Different middleware types are used for connecting applications, web and cloud services for trigger-specific functions. Other components can communicate regardless of their medium using messaging frameworks like Simple Object Access Protocol (SOAP), web services, Representational State Transfer (REST), or JavaScript Object Notation (JSON) [12, 14–19].

### 3.2 Communication Protocols

The smart living devices are designed to interface with low-bandwidth network than higher bandwidth. The Institute of Electrical and Electronics Engineer (IEEE) working group enhanced the standards supporting M2M communication. In the local home network, different devices are connected with technologies to forward information in order to trigger the action. The wireless sensor networks (WSN) for the home

are composed of numerous sensors and connected with different communication technologies [20]. They are as follows:

### **RFID**

Radio frequency identification device (RFID) tags are like wireless microchips attached to the home objects or things. RFID has some in-built power and computational capacity, storage, and an antenna for connecting with the radio signal. The tags are read by the RFID reader. The RFID tags and readers can communicate via radio frequency waves to sense, detect, and communicate with the environment [2, 21, 22] (Table 1).

### **IEEE 802.11-WiFi**

WiFi uses global 2.4 GHz UHF and 5 GHz SHF ISM radio bands. 802.11b, 802.11g, and 802.11n activate on 2.4 GHz ISM band [20, 23, 24] (Table 1).

### **IEEE 802.15.4—ZigBee**

ZigBee supports services like home network start-up, routing of messages in multihop model, and management of connection or disconnection of the nodes in the network. Low-power energy consumption, cheap and easy installation procedure has no fixed network size and message routing [14, 20] (Table 1).

#### Z-Wave

In Z-Wave, each device has an identification code. The controller in the network recognizes the devices and determines its location by an embedded code. Then, the controllers increment the network routing table of representing the arrival. The Z-Wave protocol uses the Source Routing Algorithm (SAR) to route the messages in the fastest route. The sensor gateway/actuator gateway collects internal house data from sensors using Z-Wave. It operates between 868 and 900 MHz [14, 20] (Table 1).

### **IEEE 802.15.1—The Bluetooth Low Energy (BLE)**

BLE is the latest version of the Bluetooth 4.0 specifications. It is highly efficient on low-power sensors. The frequency bandwidth of BLE is same as the classic Bluetooth protocol, but BLE modulation is slightly different which results in maximum signal strength [5, 25] (Table 1).

### IEEE802.11ah—HaLow

HaLow is a low-cost WiFi standard specifically designed for IoT applications like smart living and smart grid automation with low cost of implementation with less power consumption. This standard provides greater flexibility of supporting more than 8000 devices on a single application for communication with capacity to cover different distance ranges [12, 14–19] (Table 1).

Wireless technology	Frequency used	Range	Data rate	Network topology
RFID	100 kHz to 5.8 GHz	0–3 m	640 Kbps	P2P
Bluetooth	2.5 GHZ	Up to 100 m	1–3 Mbps	Star, P2P
BLE	2.5 GHZ	Up to 100 m	1 Mbps	P2P, star
ZigBee	2.5 GHZ	10–100 m	250 Kbps	P2P, star, tree, mesh
WiFi	2.5 GHZ	150–200 m	54 Mbps	P2P, star
Z-Wave	850–950 MHz	100 m	9.6–100 Kbps	Mesh
HaLow	900 MHz	1.5 km	18 Mbps	Mesh, P2P, tree

 Table 1 Consolidated overview of communication protocol

### 3.3 Home API

The application programming interfaces or APIs are the points of interaction (POI) between the smart devices and the Internet. Web services are the APIs designed for Internet of things (IoT). A web service is software that any application can parse it. Connected devices access the web services via address of the web API that has developer registration and API key control. The interfaces can be built using different languages such as SOAP, REST, or XML/JSON [25, 26].

# 3.4 Service Projects

There are numerous services offered by IoT projects. Some of the main services are specification, design, and provision service.

### Monitoring home locators

Sensors are fixed for monitoring the physiological and behavioral parameters of the person continuously such as heart rate, blood pressure, mobility, and emotional and mental state of the person residing inside the house. Secure connection is established by decision-making algorithms and transmitting data via wireless body communication networks. Projects such as motion detection, location tracking, facial expression, reading urine, and sweat of the elderly or people with disability are highly possible in IoT environment today. These come under the type of provision services [11, 13, 27].

### Surveillance and security systems

In smart living, cameras, alarms and locks are used to block unknown persons entering the home and allowing an authorized person to access the devices inside the home and make decisions of the personalized services available. It is possible to analyze the images through face recognition algorithm and cryptographic keys [15]. The

camera sensor tracks the happenings of home, especially useful for monitoring from far location.

### **Gesture Recognition Project**

Gesture or hand movement models are stored in the middleware database for authorization process [20]. The gestures which are stored for authenticity are recognized using algorithms specially designed for template matching and control home things remotely. These algorithms compare the actual image with the template sign to find the match. In order to recognize the characters, numbers and objects templates are used. The templates are searched from the database based upon the size of the image.

### Indoor positioning energy efficiency projects

Devices not linked directly with the middleware use some software proxies for connecting. The power meter is such a proxy used for linking devices done with the user mobile platform and middleware for analyzing, monitoring, and controlling the device. Readymade projects such as semantic smart metering and semantic web technology are used to link power-related data semantically. This project is used for public buildings and private houses. Nowadays, power banks, smart grids, and solar energy are used to replace electricity used for smart living. Environmental pollution could also be avoided [26].

### **Energy Management**

Household energy usage is one of the major impacts on the world's energy consumption [5, 11, 13, 20, 27, 28]. The home system with smart capability consumes more energy than normal houses. The energy management of home is how, when, and where the home appliances are to be activated, deactivated, and controlled [20, 29].

# 4 Proposed Interoperability in Living Network System

Smart living is an integration of various physical sensors and communication technology. Choosing the right communication protocol between devices improves the overall system performance [26]. Interoperability is the communication trade-off between heterogeneous devices. In the architecture of living network system (see Fig. 3), devices are arranged in the physical layer which forwards the event happens inside the home through the communication protocols and reaches the routers. The routers route the messages to the API. Depending upon the user response, the API triggers the action in the living system through the intermediate middleware [26].

A good interoperability is established by following good protocols in each and every layer of the living system network. No two layers allotted to do same job. A relay of work shuffled in the architecture. The communication between layers takes place through the communication protocols, application programming interface protocols, and the gateway protocols. Uninterrupted power is supplied to the home network to avoid interruption. The devices involved in this network have limited power storage

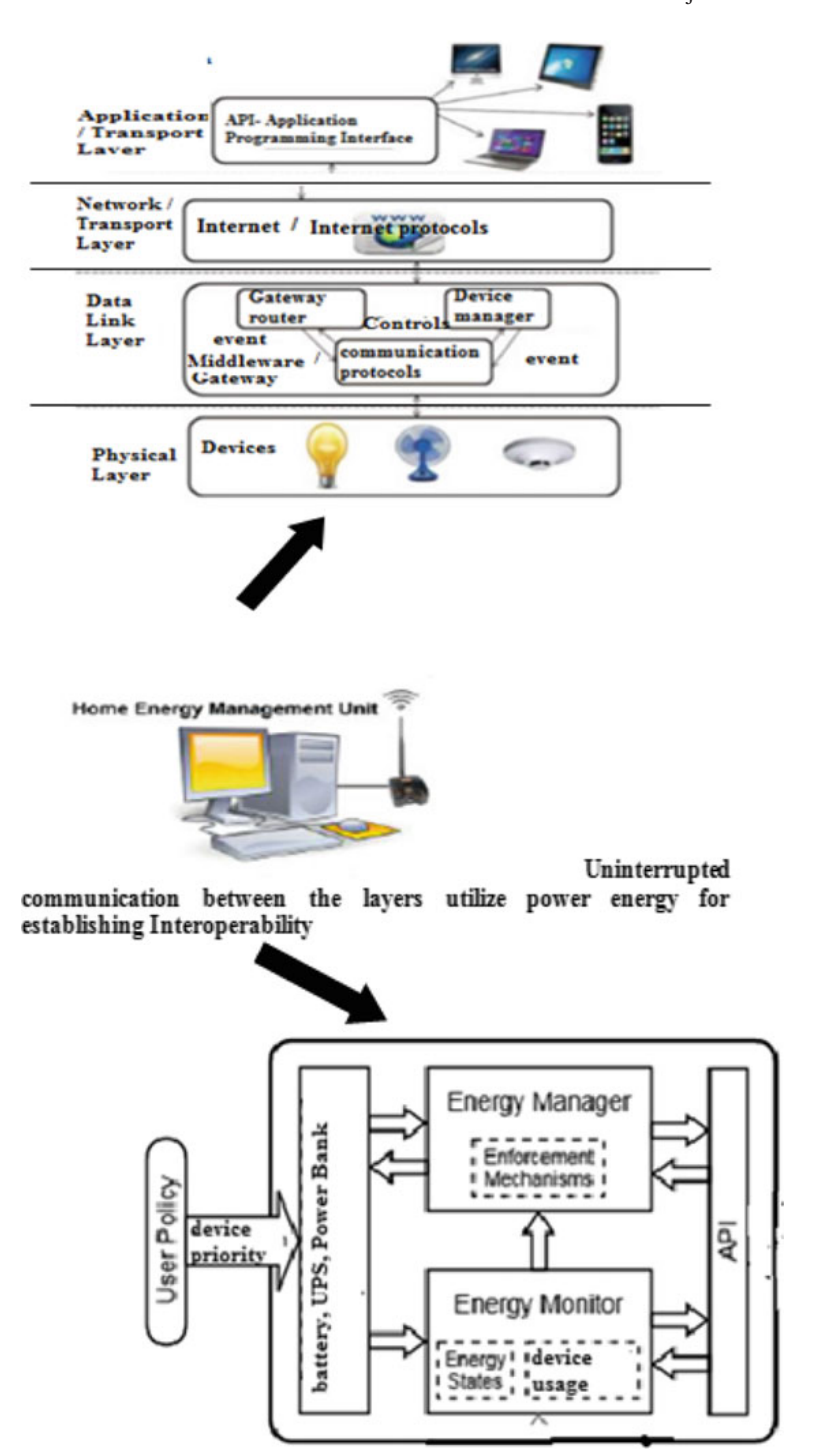


Fig. 3 Proposed smart living network system with efficient use of power energy to avail interoperability

facility. Due to the mobility of the locators, location-based search is helpful, so there is a need of battery backup to avoid interruption from outside. If all the layers are united finely in the network but still has a huge loss of energy, then the entire network is unnecessary one. The energy supplied to every device in the network is based on the preferences of the user. Automatic supply of power energy to the device is dynamic based on the time changes (e.g., door sensor and camera of indoor and outdoor are preferred more than fan and air conditioner in the far location).

The energy manager is a component involved in energy management application. It depends on the communication from the power meter, and the middleware in the energy unit translates the messages between the participating device and the API, which are designed for energy management. If the external power energy is not available, the device can get charge from the artificial power source such as UPS battery. From the energy management API, the user can able to be aware of the energy state and get information based on the device energy consumption, and based on this locator, the devices consume power. It is concluded from the proposed smart living network that power energy is efficient for the working condition of the framework interoperability. Based on the range of communicating distance, suitable protocols such as ZigBee and HaLow are highly used nowadays for smart living mesh network [25].

### 5 Research Consideration

The sensors are the spies used to gather real-life scenario and trigger action accordingly, to provide security and safety to the locators. It is necessary to find the user-centric, low-cost, innovative, interoperable, and integrated home environment by focusing on industry standards. Middleware or building gateway is the syntactic and semantic perspective of the project. Interfaces involved must improve the interoperability among the participating layers. Designing and controlling home smartly improves the quality of life and avoids thefts by the timely information exchange in a critical situation; intimation of leakage of gas or fire is done automatically by enhancing the routing protocols involved in the network system for interoperability.

### 6 Conclusion

The invention of the information communication technology has brought major changes in our everyday life. Smart living has a high potential in the present and future business sector platform. Various impacts noted on intelligent living places such as complexity in construction, inflexibility in connection, power energy demands, inter-operability problem among the devices, lack of managing appliances are considered as the key barriers to their adoption. Numerous researches are undertaken at IoT projects, but confidence building on smart living is still very low for the users because

of the cost, safety, and security risks. Initially and very importantly, home appliances require fine connecting gateway and the server requires high energy harvesting techniques and interoperability features for enhanced continuous flow of interaction more than security constraints. This paper acknowledged the need of power energy to establish interoperability supported by well-designed and flexible protocol standards that can accurately and continuously infer the physiological activities and patterns of sensed data.

### References

- Muntjir, M., Rahul, M., Alhumyani, H.A.: An analysis of internet of things (IoT): novel architectures, modern applications, security aspects and future scope with latest case studies. Int. J. Eng. Res. Technol. (IJERT) 6(06) (2017)
- 2. Ashton, K.: That internet of things thing. RFID J. (1991)
- Malche, T., Maheshwary, P.: Internet of Things (IoT) for building Smart living System. I-SMAC-2017
- 4. Balevi, E., Al Rabee, F.T., Gitlin, R.D.: ALOHA-NOMA for massive machine-to-machine IoT communication. arXiv preprint arXiv:1803.09323 (2018)
- Lin, H., Bergmann, N.W.: Iot Privacy and Security Challenges for Smart living Environments. Information 7, 44 (2016)
- 6. Telecom ITU.: Standardization sector recommendation of ITU (1996)
- Barsocchi, P., Calabrò, A., Ferro, E., Gennaro, C., Marchetti, E., Vairo, C.: Boosting a low-cost smart living environment with usage and access control rules. Sensors 2018, Published: 8 June 2018
- 8. Yun, M., Yuxin, B.: Research on the architecture and key technology of IOT applied on the smart grid", Advances in energy engineering. In: (ICAEE) International Conference, June 2010 [4]
- Wang, H., Saboune, J., El Saddik, A.: Control your smart living with an autonomously mobile smart phone. In: IEEE International Conference on Multimedia and Expo Workshops (ICMEW), pp. 1, 6, 15–19 July 2013
- Byun, J., Hong, I., Lee, B., Park, S.: Intelligent household LED lighting system considering energy efficiency and user satisfaction. IEEE Trans. Consum. Electron. 59(1), 70–76 (2013)
- 11. Barsocchi, P., Calobro, A.: Boosting a low-cost smart living environment with usage and access control rules. Sensors 2018
- 12. Muntjir, M., Rahul, M., Alhumyani, H.A.: Architectures, modern applications, security aspects and future scope with latest case studies. IoT in Latest Trends Int. J. Eng. Res. Technol. (IJERT), JERTV6IS060238, 6(06) (2017)
- 13. Attaran, M., et.al.: Critical success factors and challenges of implementing RFID in supply chain management. Supply chain Operating Management (2012)
- 14. Solaimani, S., Keijzer-Broers, W., Bouwman, H.: What we do and don't know about the smart living: an analysis of the smart living literature. Indoor, and Build Environment (2013)
- Hargreaves, T., Wilson, C.: Analytical Framework for Research on Smart livings and Their Users. Springer, Berlin (2017)
- Wenbo, Y., Quanyu, W., Zhenwei, G.: Smart living implementation based on internet and WiFi technology. In: Proceedings of the 34th Chinese Control Conference, 28–30 July 2015, Hangzhou, China
- 17. Li, M., Lin, H.-J.: Design and implementation of smart living control systems based on wireless sensor networks and power line communications. IEEE Trans. Ind. Electron. **PP**(99), 1, 1 Dec. 2014

- 18. Haradaya, H., Mizutaniy, K., Fujiwaray, J.: IEEE 802.15.4g Based Wi-SUN communication systems. IEICE Trans Commun. **E100–B**(7) (2017)
- 19. Baños-Gonzalez, V., Afaqui, M.S., Lopez-Aguilera, E., Garcia-Villegas, E.: IEEE 802.11ah: a technology to face the IoT challenge. Sensors **16** (1960)
- 20. Bitterman, N., Shach-Pinsly, D.: Smart Living- a Challenge for Architects and Designers Architectural Science Review. Taylor & Francis (2015)
- 21. Vanus, J., Cerny, M., Koziorek, J.: The Proposal of the Smart living Care Solution with KNX Components. 978-1-4799-8498-5/15/\$31.00 ©2015 IEEE
- 22. Fathany, M.Y., Adiono, T.: Wireless protocol design for smart living on mesh wireless sensor network. In: 2015 International Symposium on Intelligent Signal Processing and Communication Systems (ISPACS) 9–12 Nov 2015
- 23. Hsu, Y.-L., Chou, P.-H., Chang, H.-C.: Design and implementation of a smart living system using multi sensor data fusion technology. Sensors 17, 1631 (2017)
- 24. Telecommunication Engineering Centre, Department of Telecommunications, Ministry of Communications, Government of India, Technical Report on M2M enablement in Smart livings, TEC-TR-IoT-M2M-007-01, R1.0 release, 31/03/2017
- 25. K"uhn, E., Prellwitz, M., Rohrer, M., Sieck, J.:"A distributed middleware for applications of the internet of things. In: The 7th IEEE International Conference on Intelligent Data Acquisition and Advanced Computing Systems: Technology and Applications, 12–14 Sept. 2013, Berlin, Germany
- 26. Son, H., Tegelund, B., Kim, T., Lee, D.: A distributed middleware for a smart living with autonomous appliances, 0730-3157/15 \$31.00 ⊚. In: 2015 IEEE, 39th Annal International Computers, Software & Applications Conference
- 27. Mocanu, I., Florea, A.M.: A Multi-Agent System for Human Activity Recognition in Smart Environments. Springer, Berlin (2011)
- 28. Gajewski, M., Batalla, J.M., et.al.: A Distributed IDS Architecture Model for Smart Living System. Springer, 30 Aug. 2017
- 29. Fuller, J.D., Ramsey, B.W.: Rogue Z-Wave controllers: a persistent attack channel. In: 40th IEEE Annual conference on Local Area Networks (2015)

# The Internet of Things (IoT) Routing Security—A Study



M. Durairaj and J. Hirudhaya Mary Asha 🕒

Abstract Internet of things (IoT) is the finest metric following technology that turns the attention of the people throughout the world. IoT is a global connecting network that allows people to connect with each other largely. It is a challenging technology due to its complex environment and resource-dependent features. Different surveys depict that there may be several billions of IoT users by 2020. There are numerous companies that offer IoT services. Nowadays, the security of an IoT feature is an issue which is non-measurable in nature. Different research works are being performed to find the optimal solution to provide security of IoT. IoT requires less human commanding and controls which results in vulnerability due to hacking. In this paper, the literature is reviewed based on the types of routing attacks in wireless sensor network interface layer communication and classified the attacks that disturb the communication. These attacks are classified as attacks on topology, resources, and traffic. Based on the classification of attacks, countermeasures are suggested to protect the routing standard for the IoT environment.

**Keywords** Internet of things · Wireless sensor network · Security attacks · Routing protocols · Resource attacks · Traffic attacks

### 1 Introduction

Because of the increasing usage of wireless sensor network (WSN) technology and the Internet of things (IoT) application, more sensors and wireless communication technologies are used. The IoT applications are used in military, people's livelihood, industry, education, commerce, and other fields. The IoT devices can be remotely

M. Durairaj · J. Hirudhaya Mary Asha (⋈)

Assistant Professor, Department of Computer Science, Bharathidasan University, Tiruchirapalli, Tamilnadu. India

e-mail: hirudhaya\_ashaa20@yahoo.co.in

J. Hirudhaya Mary Asha

Research Scholar, Department of Computer Science, Bharathidasan University, Tiruchirapalli, Tamilnadu, India

© Springer Nature Singapore Pte Ltd. 2020 V. Bindhu et al. (eds.), *International Conference on Communication, Computing and Electronics Systems*, Lecture Notes in Electrical Engineering 637, https://doi.org/10.1007/978-981-15-2612-1 58

#### 9 000 ■ Fixed Satellite, Other 8 000 LPWA **■ WPAN/WLAN** 7 000 Cellular ■ Cellular 6 000 ■ LPWA 5 000 Satellite, others 4 000 WPAN/WLAN 3 000 2 000 1000 Fixed 0 2015 2018 2019 2020 2017 2021

# Number of connected devices/things by technology worldwide from 2015 to 2021 (in millions)

Fig. 1 Number of devices connected

controlled from anywhere to control the home or processes carried out at office. The devices may be wearable accessories or may be larger machines. Each IoT device contains chip like sensor embedded within it. The problems of information security field such as virus attack, data damage, hacker intrusion, malicious code attacks, replication of data attacks, and certain other issues will be very serious for the damage and data losses in the network. The IoT devices followed some standard protocols for sharing information among the devices which are connected in the network. The architecture of the IoT network is constructed based on the communication. Due to some vulnerabilities, the information stored in the network faces great challenges. The defense mechanisms such as encryption and authentication are traditional sources available for ensuring security. Intrusion detection is a new security-enhancing technology which is an active research in the field of network security. Detecting and promoting countermeasure for tackling the drawback of existing traditional security defense technology. The bar chart (see in Fig. 1) shows the number of devices connected by technology among the year 2015–2021 [1].

The research proposed had included the location information in the sensor nodes, which validates the location identity information.

### 2 Related Works

The connection of the Internet of things tends to increase the income of the society [2]. It is a technology-based economic improvement. The Internet of things (IoT) is called distributed and decentralized systems since this technology built things based on the place which is actually located and service established at the destination network [3]. The correlation between different entities achieves a common goal [3]. There are various attacks which highly affects the nodes in the connected network.

The power consumption levels of the connecting devices are important to distinguish the signals of the distributed devices connected to the gateway [1, 4].

An authentication authorization accounting (AAA) communication system [5] is designed to find how much bandwidth consumed by device during communication throughput. It is difficult to provide data access rights' level to different people based on the bondage of commitment in the privacy policy. Thus, authentication checking is forced by introducing a new framework for reducing the insider attack in the industrial Internet of things (IIoT) [6]. If one or more clients request to modify the same data/file, it must be discovered previously else the data/file would prone to attacks [7, 8]. To avoid critical issues in the connecting devices, the scheduling of task must be done better [9–11]. Security challenges in IoT are as follows.

### 2.1 Authentication and Integrity

Integrity promises user rights to access or modify data. The data must be accurate and consistent throughout its routing life cycle. Authentication provides the customer an individual or personal secret key as an opener to access the IoT network [5]. Nowadays, various algorithms are followed to make the sensors to respond at real time.

### 2.2 Access Control for Ensuring Security

Authorization allows the nodes to access different resources based on their access rights. Access control mechanisms check and guarantee the rights of an individual [7]. For verifying access, every IoT node follows some mechanisms different from other nodes for connected in the same network [8, 9]. After the authentication checking, the needed data must be available at the right time in the network routing. Redundancy is the appropriate method to ensure the availability of data [11, 12].

# 2.3 Privacy and Confidentiality

The private information of the people like health data is recorded by the integration of heterogeneous objects. Intruding is a threat to people's privacy. In the IoT world, the nodes connecting in the network can collect one own's data without their knowledge [10]. In the communicating network, the transmitted data must be accessed and read only by the authorized individuals or parties.

### 3 IoT Routing Attacks

The IoT devices connected to the network route are prone to various attacks. The attack happens highly which degrades the network performance. Based on the attacking features, the major attacks and the way it affects the routing is described [13–32] and tabulated (see Table 1). A survey was taken on various attacks which takes place in the routing. The types of attacks occurring in the network layer of IoT communication are as follows:

- Sinkhole attack
- Sybil attack
- Clone ID attack
- Selective forwarding attack
- Hello flooding attack
- Local repair attack
- Wormhole attack
- Denial-of-service attack
- Blackhole attack
- Rank attack
- Neighbor attack
- Version number attack.

## 3.1 Grouping of Attacks

IoT infrastructure or network layer attacks are grouped based on their impact on the network routing, such as attacks against resources, attacks against topology, and attacks against traffic.

### Attacks against resources.

In the wireless network routing, the attacker node attempts to destroy the resources that blocks the routing link of this network and also the lifetime availability of the network is reduced. This resource attack will waste the node energy and control overhead. Attacks occur on resources in two ways.

- (1) **Direct attack**—attacker node generates overload directly.
  - Flooding attacks
  - Routing table overload attacks in storing mode.
- (2) **Indirect attack**—attacker node generates large traffic indirectly. This attack disrupts the route with multiple identities. Some indirect attacks are
  - Increased rank attacks
  - Version number attacks
  - Sybil attack.

 Table 1
 Techniques available for IoT routing attacks

Techniques for overcoming attacks	Authors	Description of techniques
IDS [33]	Linus Wahlgren et al.	IDS: Intrusive IDS systems capture network traffic and perform analysis by comparing the captured data with the intrusion detection definitions stored by the user
Version number and rank authentication (VeRA in RPL) based solution [28]	Kelpen et al.	Initialization and version number update are the two steps recommended in VeRA. VeRA supports cryptographic security RSA; in this, the nodes use Pk as a public key and Sk as a private key known only to the DODAG root
Trail [34]	Heiner Perrey et al.	Trail is recommended for authentication of the topology. The base node of the tree acts as a true sender where each node linked with base node in tree topology. Trail uses cryptography tests for identifying the topology attacker
Heartbeat protocol [33]	Linus Wallgren et al.	In heartbeat protocol, Internet Control Message Protocol version 6 (ICMPv6) request is a message sent by a node from border router to discover neighbor
Parent fail-over [32]	SukhwinderSharma et al.	The DIO message sent by the node contains the parent node hash value, unheard node set, and the number of hops in the destination path
RPL's global and local repair mechanism [23]	Gill et al.	RPL protocol is an error handling mechanism used for the resource-constrained environment
Rank authentication [32]	Sukhwinder Sharma et al.	According to this method, rank value must be incremented for every hop. For calculating rank value, a hash function is xr+1 = h (xr) function is used

(continued)

7D 11 4	( ( 1)	
Table 1	(continued)	

Techniques for overcoming attacks	Authors	Description of techniques
Merkle tree authentication [35]	Li et al.	Merkle tree checks security with cryptographic tests. Each node in the network is accepted with its authentication path information (API)
Svelte [34]	Raza et al.	Svelte is an RPL-based IDS for IoT. It has three modules (1) LoWPAN mapper which traces the RPL network using border router and connects LoWPAN networks to other RPL networks (2) Intrusion detection metric finds the intrusion (3) Firewall for filtering traffic

### Attacks on Topology.

The attacker node attempts to intercept the network route, modify the data, and forward the data to the base station [18]. Some topology attacks are

- Routing table falsification attacks
- Sinkhole attacks
- Wormhole attacks
- Routing information replay attacks
- Worst parent attacks
- Blackhole attacks.

### Attacks on Traffic.

The traffic attacks consume the resources of the network so that the important requests will not be notified due to the lack of resources for either routing or process the work, such as bandwidth and receiving buffer at the server end [19]. Some traffic attacks are

- Sniffing attacks
- Misappropriation attacks
- Decreased rank attacks
- Identity attacks.

# 4 Proposed Work Discussing the Attacks and Techniques Which Addresses the IoT Attacks

IoT is an environment where numerous devices communicate with the help of communication technology. After reviewing literature here, a collection of techniques is proposed for addressing the routing attacks. Protocols like RPL's global and local repair mechanism, IDS, heartbeat protocol, parent fail-over, trail, rank authentication techniques, Merkle tree authentication, a Svelte technique for handling network layer routing attacks.

Different IoT routing attacks and the drawbacks of that routing attacks and the overcoming techniques are discussed, and their possible outcomes are also proposed here in (Table 2).

### 5 Future Research Direction

There is a high demand for structuring an applicable solution to secure essential routing metrics. The Internet of things protocol against attacks like sinkhole attacks, blackhole attacks, selective forwarding attacks and grayhole attacks, version number manipulation attacks should be sorted out and concerned during every IoT evaluation criteria. It is meaningful and useful in investing time to develop various threats overcoming models that faces the routing standard of IoT and its application areas. The standards designed for Internet of things routing do not specify how the node authentication and secured connection mechanisms could be designed. With the increasing feature and usage of IoT projects worldwide, there is a perceptual need for designing secure routing protocols. To design, develop, and implement a secure protocol, which is said to be the undying security goals, all the above-mentioned criteria should be considered.

### 6 Conclusion

The Internet of things (IoT) focuses more on deploying low power and lossy networks in order to run highly critical communication among the devices and their interconnection to the wireless technology. In this paper, a classification of the attacks is presented and protocol types are also listed. The attacks on resources decrease the network lifetime by generating fake control messages or by building loops of messages. The attacks on topology make the coverage of network to a sub-optimal configuration or node isolation. Finally, attacks on network traffic make a good node to be captured by the malicious node and destroy the larger part of the traffic. From the review of the literatures, comes to know that IDS based system finds the rank attacks and VeRa attack, where TRAIL techniques prevents the Rank attack by minimizing

 Table 2
 Routing attacks and its survey

Attack types	Drawbacks of attacks	Techniques for the counter-attack	Possible outcome
Rank attack [20] Hashem et al.	Degrades network performance generates non-optimal loop     Packet delay	IDS [33], VeRA-based solution, trail [34]	Network overhead time is minimized
Selective forwarding [21] Airehrour et al.	Disturbs routing path and intrudes any protocol	Heartbeat protocol [33]	Creating a dynamic path between parent and children
Sinkhole [22] Tiwari et al.	• Altering the ranking field of the destination information message (DIM)	Parent fail-over method [22, 32], rank authentication technique [22]	The density of the network is increased
Hello flooding [23] Gill et al.	Creates legitimate traffic	RPL's global repair mechanism	Minimizes communication overhead
Worm hole [24] Ghugar et al.	Due to this attack, network route topology is disrupted and creates a traffic flow	Merkle authentication [35]	Provides resiliency
Sybil and Clone ID [25] Thomas et al.	The legitimate nodes are denied access to reserved resources	RPL local repair[36–38]	Reduces traffic and makes resources available
Denial of service [26] Yujie et al.	Nodes request more resources with fake identity and creates traffic	IDS solution [33]	Reduces traffic
Black hole [27] Singh et al.	<ul> <li>Publish wrong fake route as a trusted route</li> <li>Dropping the packets instead of forwarding</li> </ul>	Svelte [34], parent fail-over [32, 39]	Overhead is small enough with limited energy and memory capacity
Version number [28, 29] Kelpen et al.	Increases the control overhead     Low packet delivery that drains battery energy	VeRA [28, 35]	Prevents node from increasing the version number and decreased rank values illegitimately
Local repair control overhead [29, 39] Azzuhri et al.	Affect the network performance by control and routing traffic	Finite state machine-based IDS system solution [40]	Network overhead time is optimized

the network-overhead time. Likewise, parent fail-over technique detects the sinkhole attack, but Svelte technique only can filter the unwanted traffic and helps to avoid the sinkhole attack. As a final prediction, insecure routing plays a major impact in the IoT network and the entire network functioning must be safe by finding a universal solution applicable to all the present and future routing attacks.

### References

- Akpakwu, G.A., et al.: A survey on 5G networks for the Internet of Things: communication technologies and challenges. IEEE Access 6: 3619–3647 (2018)
- 2. Vermesan, O., et al.: Internet of things strategic research roadmap. In: Internet of Things-Global Technological and Societal Trends, vol. 1.2011, pp. 9–52 (2011)
- 3. Roman, R., Zhou, J., Lopez, J.: On the features and challenges of security and privacy in the distributed internet of things. Comput. Netw. **57**(10), 2266–2279 (2013)
- 4. Balevi, E., Al Rabee, F.T., Gitlin, R.D.: ALOHA-NOMA for massive machine-to-machine IoT communication. arXiv preprint arXiv:1803.09323 (2018)
- 5. Zhou, R., et al.: File-centric multi-key aggregate keyword searchable encryption for industrial internet of things. IEEE Trans. Ind. Inf. (2018)
- Silva, E.F., Muchaluat-Saade, D.C., Fernandes, N.C.: ACROSS: a generic framework for attribute-based access control with distributed policies for virtual organizations. Fut. Gener. Comput. Syst. 78: 1–17 (2018)
- 7. Huotari, S., Rothstein, K.M.: Mechanism for executing server discovery. U.S. Patent No. 9,871,872, 16 Jan 2018
- Kogias, D.G., et al.: Realizing the wireless technology in the Internet of Things (IoT). In: Emerging Wireless Communication and Network Technologies. Springer, Singapore, pp. 173–192 (20118)
- 9. Jiang, Y., Huang, Z., Tsang, D.H.K.: Challenges and solutions in fog computing orchestration. IEEE Netw. **32**(3): 122–129 (2018)
- Rao, A.P.: Adaptive control strategies for task scheduler using the Internet of Things. In: Exploring the Convergence of Big Data and the Internet of Things. IGI Global, pp. 129–140
- 11. Morabito, R., et al.: Consolidate IoT edge computing with lightweight virtualization. IEEE Net. **32**(1): 102–111 (2018)
- 12. Silva, B.N., Khan, M., Han, K.: Internet of things: a comprehensive review of enabling technologies, architecture, and challenges. IETE Techn. Rev. 35(2), 205–220 (2018)
- 13. Restuccia, F., D'Oro, S., Melodia, T.: Securing the Internet of Things: new perspectives and research challenges. arXiv preprint arXiv:1803.05022 (2018)
- 14. Wang, H., Zhang, Z., Taleb, T.: Special issue on security and privacy of IoT. World Wide Web **21**(1), 1–6 (2018)
- 15. Osanaiye, O., Alfa, A.S., Hancke, G.P.: A statistical approach to detect jamming attacks in wireless sensor network. Sensors 18(6), 1691 (2018)
- Weekly, K., Pister, K.: Evaluating sinkhole defense techniques in RPL networks. In: 2012 20th IEEE International Conference on Network Protocols (ICNP), pp. 1092–1648, 14 Feb 2013
- 17. Gao, S., et al.: Security threats in the data plane of software-defined networks. IEEE Netw. (2018)
- 18. Feng, Y., et al.: Vulnerability of traffic control system under cyber-attacks using falsified data. Transportation Research Board 2018 Annual Meeting (TRB) (2018)
- Valanarasu, M.R.: Smart and secure IoT and ai integration framework for hospital environment.
   J. ISMAC 1(03):172–179 (2019)
- 20. Airehrour, D., Gutierrez, J., Ray, S.K.: A trust-based defense scheme for mitigating blackhole and selective forwarding attacks in the RPL routing protocol. Aust. J. Telecommun. Dig. Econ. **6**(1), 41 (2018)

- 21. Tiwari, R., Saxena, T.: A review on Sybil and sinkhole of service attack in VANET. Recent Trends Electron. Commun. Syst. 5(1) 7–11 (2018)
- 22. Gill, R.K., Sachdeva, M.: Detection of hello flood attack on LEACH in wireless sensor networks. In: Next-Generation Networks, pp. 377–387 (2018)
- 23. Ghugar, U., Pradhan, J.: Intrusion detection system in wireless sensor networks for wormhole attack using trust-based system. In: Handbook of Research on Information Security in Biomedical Signal Processing. IGI Global, pp. 198–209 (2018)
- 24. Thomas, A., Gireesh Kumar, T., Mohan, A.K.: Neighbor attack detection in the internet of things. In: Advanced computational and communication paradigms. Springer, Singapore, pp. 87–196 (2018)
- 25. Yujie, Z.H.A.O., et al.: Techniques for automatically mitigating denial of service attacks via attack pattern matching. U.S. Patent No. 9,912,678. 6 Mar 2018
- 26. Singh, M.M., Mandal, J.K.: Impact of black hole attack on the reliability of mobile ad hoc network under DSDV routing protocol. Int. J. Syst. Control Commun. 9(1), 20–30 (2018)
- Kelpen, K., Simo, H.: Privacy and data protection in the domain name system. Privatheit und selbstbestimmtes Leben in der digitalen Welt. Springer Vieweg, Wiesbaden, pp. 253–302 (2018)
- 28. Azzuhri, S.R., et al.: Towards a better approach for link breaks detection and route repairs strategy in AODV protocol. Wireless Commun. Mobile Comput. (2018)
- Devibala, K., et al.: Neighbor constraint traffic centric distributed sinkhole detection and mitigation approach for quality of service improvement in wireless sensor networks. In: Industry Interactive Innovations in Science, Engineering, and Technology. Springer, Singapore, pp. 357–366 (2018)
- 30. Cho, J.-H., Chen, R.: PROVEST: provenance-based trust model for delay tolerant networks. IEEE Trans. Dependable Secure Comput. **15**(1), 151–165 (2018)
- 31. Sharma, S., Bansal, R.K., Bansal, S.: Issues and challenges in wireless sensor networks. In: 2013 International Conference on Machine Intelligence Research and Advancement (2013)
- 32. Le, A., Loo, J., Luo, Y., Lasebae, A.: Specification-based IDS for securing RPL from topology attacks (2011)
- 33. www.postscapes.com/internet-of-things-protocols/
- 34. Perrey, H., Landsmann, M., Ugus, O., Wahlisch, M., Schmidt, TC: TRAIL: topology authentication in RPL. ACM 978-1-4503-1169-4 (2016)
- 35. Raza, S., Wallgren, L., Voigt, T.: SVELTE: real-time intrusion detection in the Internet of Things. Ad Hoc Netw. (2013)
- 36. Patil, M., Biradar, R.C.: A survey on routing protocols in wireless sensor networks. 978–1-4673-4523-1/12/\$31.00 ©2012. IEEE
- 37. Li, H., Lu, R., Zhou, L., et al.: An efficient Merkle-tree-based authentication scheme for smart grid (2013)
- 38. Wikipedia: Wikipedia: the free encyclopedia. Retrieved from https://www.wikipedia.org/(2017)
- 39. Thubert, P., et al.: Co-existence of a distributed routing protocol and centralized path computation for deterministic wireless networks. U.S. Patent No. 9,882,804, 30 Jan 2018
- 40. Mihovska, A., Sarkar, M.: Smart connectivity for the Internet of Things (IoT) applications. In: New Advances in the Internet of Things, pp. 105–118. Springer, Cham (2018)



# The Appraised Structure for Improving Quality in the Compressed Image Using EQI-AC Algorithm

M. Durairaj and J. Hirudhaya Mary Asha<sup>(⊠)</sup>

Department of Computer Science, Bharathidasan University,
Tiruchirapalli, Tamilnadu, India
durairaj.bdu@gmail.com, hirudhaya ashaa20@yahoo.co.in

**Abstract.** The electronic form of data is compressed practically using techniques to acquire information which are not redundant is called image compression. After compression, the image gains high visual quality with reduced bit rate compared to the raw image. In the Internet of Things (IoT) environment, efficient transmission and storage of images are required for security purposes. Block splitting (BS) and discrete cosine transform (DCT) is applied initially on the raw images to reduce the actual bit rate which minimizes the mean square value (MSE) and the noise in the near-constant region. In this paper, EQI-AC (Enhanced Quality Image After Compression) algorithm is used to enhance contrast, intensity and brightness of the compressed image, which is balanced, for visualization. Peak signal noise ratio (PSNR) values are calculated and found that 1/3rd of the psnr value is decreased comparing to the original image as displayed in Table 1. Structure similarity index (SSIM) values are calculated and found that there is slight degrade from 0.01 to 0.1 range in the quality of the compressed image compared to the original image.

**Keywords:** Raw image · Compressed image · JPEG · Enhanced image · Balanced for visualization

### 1 Introduction

In order to make our living environment productive and smart, the evolution of smart homes takes place. Every people spend their day-to-day life maximum at their school, colleges and their workplace. So for their convenience, apartment homes had been bought to the use, where there is a collaboration of people in a single colony. Hence in order to preserve the feeling of safety, technologies that include several sensors along with the machine learning techniques could be adapted to identify, detect and respond to the potential threats. But this system is said to be stand-alone security-based used for many years and they could not be capable of obtaining or working through the plenty of information, which is provided by the sensors combined all over the building that is not capable of providing the right information. Hence smart doors could be designed that does the face recognition serving as the video surveillance system. Since the storage of the device increases and it will not suffice if we did not compress the video file although hard disk of capacity 2 Terabytes are used. The aim of this paper is to

<sup>©</sup> The Editor(s) (if applicable) and The Author(s), under exclusive license to Springer Nature Switzerland AG 2021 J. I.-Z. Chen et al. (Eds.): ICIPCN 2020, AISC 1200, pp. 201–217, 2021.

compress the image captured from the video using EQI-AC algorithm and enhancing brightness, contrast and intensity. Every image should be represented in the appropriate value of brightness and contrast for human eye visualization. Brightness refers to the limited darkness needed to visualize the image. If the brightness value of the image is high as usual, the white color ratio of pixels is dripped, if the brightness value of the image is low, the black color ratio of the pixels is dripped and hence the actual details of the image will be destroyed. Contrast means the percentage of color or grayscale representation exists in images. The level of contrast helps to differentiate the object. If the contrast value of the image is set high as compared to average, the black color in the pixels become too black and the white color in the pixels become too white. If the contrast value is set as low, the pixels of the image fades. So the contrast and brightness are the parameters used to measure the intensity of the image. The proposed system of this paper focuses more on contrast and brightness level of the compressed image compared to the raw image. JPEG (Joint Photographic Experts Group) is an international standard for continuous-tone still image compression both the color and the grayscale and helps with the large varieties of application. This standard is now in progress with the JPEG XS that forms a solution for the interoperable solution for visually lossless compression, low-latency and light-weight.

### 2 Related Work

The smaller digital camera with maximization of picture elements tends to rise a critical problem. A novel method had been implemented in [1] for the detection and elimination of aberration in the images. The refractive effects of the lens tend to affect the optical systems by causing aberration. Chromatic aberration is of two types: lateral aberration - the occurrence of geometry shift or the displacement occurs among each color components that are well focused and longitudinal aberration - blurring of images occurs due to the foci of several color components. The color variation occurs on every transition region and the variation of the RGB is given as (226, 210, 200) to (71, 30, 40). Z(p) is the transition region retrieved from the pixel set l(p) and r(p) (the color varies from the start point l(p) and ends at r(p)). The chromatic aberration is not seen at the normal edges, where the chromatic correlation exists. Then the gradient operation is applied in detecting the color intensity variation with the special operators. The proposed algorithms in [1] will separate the data for processing in both the vertical and in the horizontal direction. The transition region is determined with the search procedure that involves 3 steps:

1) The initial point p is obtained by incrementing the pixel location j, which is kept initially at 1. This is done till the green gradient magnitude becomes greater than or equal to T. This is given as,

$$j \leftarrow j+1$$
, while  $|EG(j)| < T$ , 
$$Set p = j, if |EG(j)| > T. \tag{1}$$

The location of the pixel p should be within the transition area.

2) Next, the transition region Z(p) is calculated by the initial point p to the point m and n, which is the left and the right place of the transition width. At the initial point p, the largest gradient value between R, G and B with the similar edge G is given by,

$$H(x|p) = Max \{s(p) ER(x), s(p) EG(x), s(p) EB(x)\}$$
 (2)

3) Then the next transition value search begins at r(p) + 1 with the gradient value.

The chromatic aberration is detected and eliminated for the individual signals by conducting the pixel search within the transition region. In this proposed method [1], the color fringes are eliminated directly from the given image. This algorithm also reduces the computation of parameter estimation process complexity. In [2], the influence of chroma sub-sampling on the apparent video quality had been analyzed subjectively. The video codecs used in this paper belongs to H.264/AVC and H.265/HEVC (High-Efficiency Video Coding) that is commonly used. The process of image encoding with the implementation of lower resolution for chroma information is termed as chroma subsampling (the concentration is provided more to chroma information rather than luma). The visual systems of the human have a minimum sensitivity to the color details. The evaluation of the video quality depends on two important factors. The perceived quality of an image obtained from the observers or people, who rate the quality of the video by watching them is termed as subjective quality assessment. This is the most fundamental way in determining the quality of the video that is termed as Quality of Experience (QoE). The duration is the drawback of this method but the accuracy quality could be enhanced. This method is further divided as single and double stimulus methods. The objective quality assessment is not concentrated when compared to the subjective type. Then the coding procedure is carried out with the FFmpeg tool, where the chroma sub-sampling is done at the test video sequence with the change in the resolution carried out from UHD to FHD. This procedure is carried out at all the test sequences. Then, the encoding process takes place and all the sequences are encoded to H.264/AVC and H.265/HEVC standard for the compression. "Bund Nightscape" and the "Construction Field" are denoted as the sequences with the low SI and TI values that have low MOS score and bit rates [2].

The modification of the luminance quantization table with the enhanced JPEG compression algorithm with two most important components are considered in the quantization table namely chrominance and luminance. As stated in the previous work, luminance table changes could not be detected by the human visual system easily. Different image color had been chosen that utilizes Baboon, Pepper, Brick-house etc. The modified performance JPEG is assessed by peak signal and noise ratio (PSNR), compression ratio (CR) and mean square error (MSE). The proposed JPEG algorithm is shown in Fig. 1. Due to the modification of quantization table, the PSNR, CR and MSE values had been improved by the proposed JPEG algorithm [3].

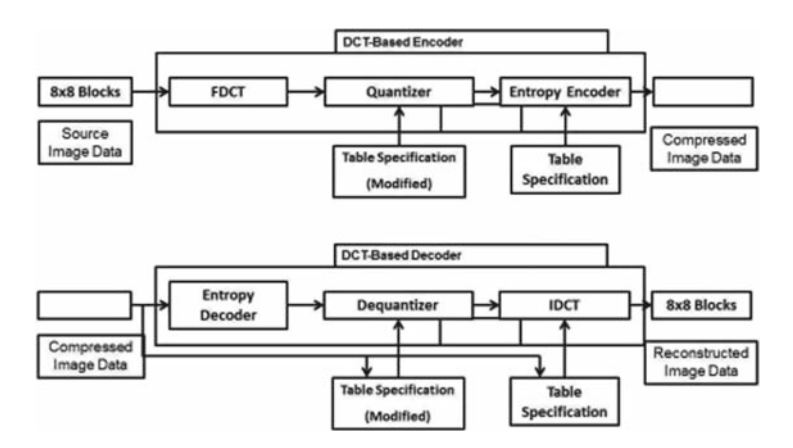


Fig. 1. DCT based encoder and decoder processing stages in JPEG image compression algorithm [3]

The most important process of capturing, storing, sharing, rendering and utilizing the images belongs to the standards that include JPEG, JPEG 2000, JPEG XT and JPSearch. In [4], the archiving and digitization application with these standards had been presented with certain efforts of ongoing standard. The author had also stated the advancement of each of these standards. Among these, JPEG 2000 has good compression efficiency with the versatility and good rate-distortion control. This standard could be adapted in the field of satellite imaging, medical imaging, digital cinemas and many more due to their wavelet-based compression technique. By piggybacking with the other standards, JPEG XT finds its application into the widen consumer markets with the advanced functionalities. These standards play a role in the portability of image, searching and accessing the image along with the metadata handling. The images are stored in the personal devices, social media and online repositories. Due to this wide growth of image data, interoperability should be supported among the systems. This could be possible with the JPSearch that helps in search and retrieval of still images. Certain ongoing activities include JPEG PLENO and JPEG LS that should support low-latency along with the new image modalities.

The reduction of data correlation is the basic idea behind the development of data compression techniques. Discrete Cosine Transform (DCT) is used that transfers the data from the time domain to the frequency domain. But the image at higher frequency is not clearly visible to the human vision due to the low sensitivity. In case of video captured with the 3-D space, reduction of time correlation along with the spatial correlation is necessary. Motion Estimation (ME) method had been proposed in [5] in which the past and the new evolving frames are compared to get the similar parts. Then the time correlation factor is reduced by replacing the image with the Motion Vector (MV). The compression standard in this paper includes JPEG and MPEG respectively.

The detection of Contrast Enhancement (CE) with the laundering attacks is said to be a very difficult task. The CE detectors had been misleading by the compression standard JPEG that is found to be a detrimental laundering attack. In paper [6], compression standard JPEG had been utilized along with the adaptive histogram (AH) to determine the CE by means of training a JPEG-aware SVM detector with the color SPAM feature. Results have also been estimated based on this SVM trained detector and this works well with the imposed Quality factor (QF) along the compressed images under tests. If this QF factor could not be determined from the image then idempotency properties of JPEG compression for extracting QF could be adapted. The enhancement in the contrast is done by Contrast-Limited implementation of AHE (CLAHE). Then the SVM classifier was given with 1372 dimensional features that are determined from the color images. The parameters of the Gaussian kernel were obtained by 5-fold cross-validation. This approach could also be adapted with the Convolutional Neural Networks (CNN) that could provide higher significant results in many applications.

To detect the presence of histogram equalization, a novel machine learning concept had been proposed in this paper [7] and the statistical parameters of DC Discrete Cosine Transform (DCT) coefficients are considered. The features used for the classification of original and histogram equalized image is done by the Gaussian Mixture Model (GMM) statistical parameters. The accuracy is obtained with the SVM classifier that classifies the original and histogram equalized images.

Enhancing the contrast of the image could be possible with the Contrast-Limited implementation of AHE (CLAHE). In Adaptive Histogram Equalization (AHE), an image will be sub-divided into several tiles and the enhancement will be carried out by applying HE to every individual tiles that concentrates on every small details by improving the image local contrast. Sometimes, AHE could increase the amplification noise factor that could be prevented by CLAHE in the relative homogenous region. Prior to the cumulative distribution function (CDF) computation, the above procedure will be carried out that could clip the histogram at the particular value. The function of slope transformation will be limited that obtains the contrast amplification. This slope transformation function will be estimated by the CDF. Clip limit is said to be the clipped value of the histogram and this will rely on the histogram normalization value as well as the default neighborhood region size  $8 \times 8$  [10, 11]. The RGB image will be converted to HSV color space in spite of applying the CLAHE directly for each channel that color result in the improper color balance and also produces unbalanced image presentation. By converting the image to HSV color space, the above cons could be avoided and the CLAHE could be applied focusing on the luminance channel. After this process, the image will be converted again back to the original RGB domain image forgeries are highly possible due to the contrast enhancement inconsistency.

A novice method had been introduced in [9] to analyze the contrast enhancement for the particular image. According to this method, mapping is done among the pixel values and also a distinct characteristic is introduced to the histogram of the image pixel. The method is said to be highly robust that considers the additive noise perturbations that affects the contrast enhancement.

### 3 Novel Structure Addressing Image Compression

The clarity and certain features of the images are not guaranteed during the image compression technique done by JPEG standard. Hence the below technique should be carried out to enhance the quality and control over the image that could be better than the source image.

### 3.1 Color Space Conversion from RGB to YCbCr

The RGB color representation of the image is converted in the form of Luminance (Y) and Chrominance (Cb & Cr) in order to achieve the delicacy and for interpreting the spatial content better for an image since human visual system is more sensitive to luminosity [12]. This methodology is done by the JPEG compression standard to limit the amount of information stored in the image. Usually, the color of the image could be represented by RGB and the transformation to Y, the luminosity component will enhance the intensity and the brightness of the pixels in the image. Cb and Cr represent the chrominance of the color blue and green respectively. Through this conversion, high compression could be achieved and this is mathematically represented as,

$$[Y\,Cb\,Cr] = [R\,G\,B] = \begin{bmatrix} 0.299 & 0.169 & 0.499 \\ 0.5870 & 0.3310 & 0.418 \\ 0.114 & 0.500 & 0.081 \end{bmatrix}$$

### 3.2 Chrominance Components - Sub-sampling Process

Our human visual system is composed of rods and cons. Rods indicates the brightness and cons detect the color sensitivity [13]. The density of the rods is very high when compared to the cons that make them go well with the brightness rather than the color. This concept had been utilized by the JPEG standard in reducing the spatial resolution of the chrominance components. The subsampling process takes place on the Cb and Cr chrominance components formed due to the color transformation. The advantage of this method is that humans do not have effective diligence to find chrominance changes [14]. Every horizontal and the vertical components will be removed from the image with the JPEG standard that results in the subtraction of 3/4 of the information from each of these components [15]. In simple words, certain pixels could be merged that have the same chrominance values done at a factor of 2 in both the vertical and horizontal directions.

### 3.3 Block Splitting

The entire matrix will be sub-divided into the smaller individual matrix of 8X8. These sub-matrices is said to be known as the blocks. After this splitting process, it is necessary to fill the empty block by pixel edge data.

### 3.4 Discrete Cosine Transformation

The redundancy in the image data is removed by applying DCT in every pixel block. For lossy image compression, DCT is the best-adapted method due to their robust energy compaction [16]. DCT will store a large amount of data with the low-frequency component and the rest of the smaller data will be stored at a low bit rate level. DCT transformation formula is given as:

$$F_{u,v} = \frac{c(u)c(v)}{4} \sum_{x=0}^{7} \sum_{y=0}^{7} f(x,y) \cos \frac{(2x1)u\pi}{16} \cos \frac{(2x1)v\pi}{16}$$

Where,

$$C(w) = \begin{cases} \frac{1}{\sqrt{2}} for \ w = 0\\ 1: for \ w = 1, 2, \dots 7 \end{cases}$$
 (3)

u, v – spatial frequencies in both horizontal and vertical direction and the integers should be in the range of  $0 \le u < 8$ 

$$F u$$
,  $-$  DCT coefficient at the coordinates  $(u, v)$  (4)

f(x, y) – the value of the pixel at the coordinates (x, y).

The information regarding the image file should be obtained before performing the DCT transformation [17]. The information file consists of the pixel value in terms of integers ranging from 0–255 that is divided in 8X8 matrix block and then DCT is applied in every block of data. Before transforming the image to the frequency domain, JPEG should subtract 128 to all the pixel value of the image in order to minimize the DC coefficient size. After DCT transformation it is found that 90% of the data will fall below the lower frequency component. In order to enhance the compressed image, CLAHE metric is applied to the images.

### 3.5 CLAHE Transformation on Images

In order to reduce noise in the near-constant region Contrast Limited AHE (CLAHE) is adapted that works better with adaptive histogram equalization by limiting the contrast amplification factor thereby reducing the noise factor. The contrast amplification in CLAHE is given by the transformation function slope for the sufficient pixel value. This will be proportional to the slope of neighborhood cumulative distribution function (CDF) and hence to the histogram of that particular pixel value. Prior to the CDF computation, the histogram amplification will be clipped at a predefined value thereby limiting the transformation function and CDF slope. This clip limit value depends on the size of the neighborhood region. The clip limit amplified value lies at a range of 3 and 4. This does not eliminate the histogram value rather it will distribute the values to the histogram bins (Fig. 2).

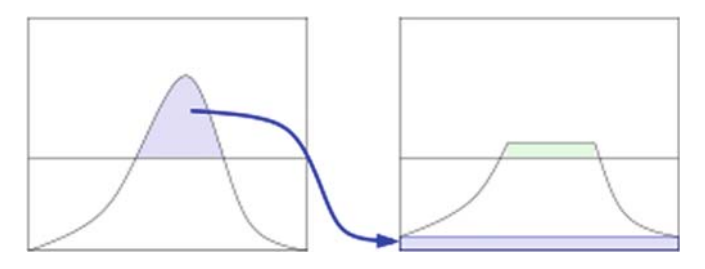


Fig. 2. Clip limit of the histogram value

In the above figure, it is seen that range above the clip limit will be pushed to the bin through the redistribution process (shaded in green color) that results in the effective clip limit of an exact value. This redistribution process could be repeated until the prescribed effective value is obtained. Hence the only one difference that separated CLAHE with AHE is that an extra procedure should be carried out to clip the histogram prior to the mapping function of CDF computation [18]. An optimal parameter should be considered with CLAHE that specifies the level to be clipped for the histogram. At the initial stage, clipping operation is not done. The range of the clip value validity will be 1 to 1/bins. Clipping is not a straight forward method since the excess portion after clipping should be redistributed among the other bins. This could increase the histogram clipping level [18]. Therefore, this process should be carried out at the lower range of the specific clipping level. This tends to maintain the clip level equal to the histogram at the maximum level during the redistribution process. To determine the clipping point, the binary search method should be adapted as mentioned in [18]. From Eq. (1), (2), (3), (4), the image is transformed and compressed using EQI-AC algorithm.

# 4 Methodology

Based on the novel structure addressing image compressing, EQI-AC algorithm is found for compressing and enhancing the raw image. Every horizontal and the vertical components will be removed from the image with the JPEG standard that results in the subtraction of 3/4 of the information from each of these components. Certain pixels could be merged that have the same chrominance values done at a factor of 2 in both the vertical and horizontal directions. The entire matrix will be sub-divided into the smaller individual matrix of  $8 \times 8$ . These sub-matrices is said to be known as the blocks. After this splitting process, it is necessary to fill the empty block by pixel edge data. The redundancy in the image data is removed by applying DCT in every pixel block. After the DCT transformation, CLAHE metrics are applied. The following EQI-AC algorithm is used to improve the color, brightness and intensity of the compressed image. The raw images of varying size are selected automatically and stored in the temporary folder and considered for compression. For compressing the raw images, the folder which contains the raw images are imported as an input to the source codes. For example.png files are compressed and saved with.jpg extension. The dataset of nearly 98 images is given as an input to the source codes for compression. From the Table 1, it is easy to visualize the extension of the input file and its actual file size and what is the extension of the saved output file and its compressed file size.

### 4.1 Pseudocode for EQI-AC Algorithm for Image Compression with Enhanced Quality

Input: Raw images with .png Extention

#### Output: Compressed images with enhanced colour, brightness and intensity

- Step1: Take an image and divide it up into 8-pixel by 8-pixel blocks. If the image cannot be divided into 8-by-8 blocks, then you can add in empty pixels around the edges, essentially zero-padding the image.
- Step 2: For each 8-by-8 block, get image data such that you have values to represent the color at each pixel.
  - Step 3: Take the Discrete Cosine Transform (DCT) of each 8-by-8 block.
- Step 4: After taking the DCT of each block, multiply the block by a mask called matrix value that will zero out certain values from the DCT matrix.
- Step 5: Finally, to get the data for the compressed image, take the inverse DCT of each block. All these blocks are combined back into an image of the same size as the original.
  - Step 6: Now we have the compressed Images.
- Step 7: Calculate a grid size based on the maximum dimension of the image. The minimum grid size is 32 pixels square.
- Step 8: If a window size is not specified chose the grid size as the default window size.
- Step 9: Identify grid points on the image, starting from top-left corner. Each grid point is separated by grid size pixels.
- Step 10: For each grid point calculate the cdf of the region around it, having area equal to window size and centered at the grid point.
- Step 11: After calculating the mappings for each grid point, repeat steps 6 to 8 for each pixel in the input image.
- Step 12: For each pixel find the four closest neighboring grid points that surround that pixel.
- Step 13: Using the intensity value of the pixel as an index, find its mapping at the four grid points based on their cdfs.
- Step 14: Interpolate among these values to get the mapping at the current pixel location. Map this intensity to the range [min:max) and put it in the output image.
- Step 15. Thus, output images formed are of high quality when compared to the JPEG Compressed Images.

Step 16: Stop the process

#### 4.2 Flowchart for EQI-AC Algorithm Methodology

See Fig. 3

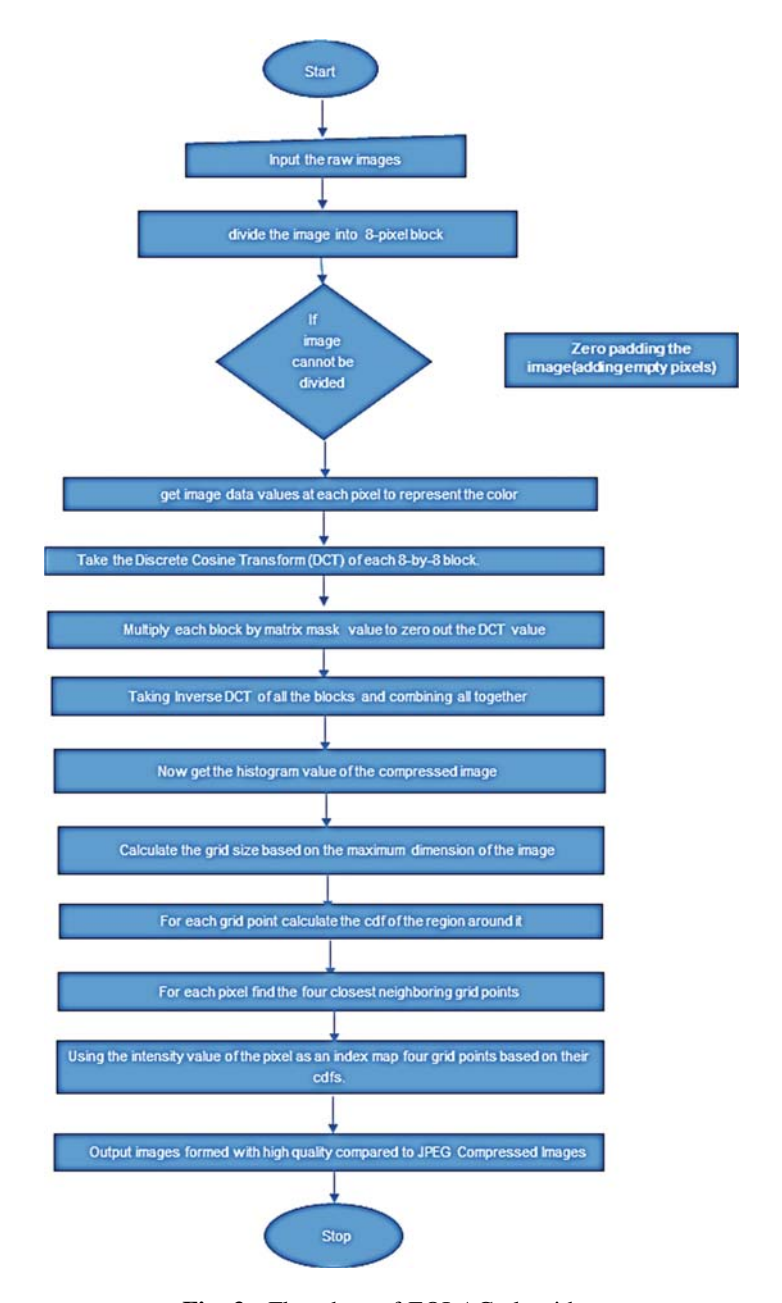


Fig. 3. Flowchart of EQI-AC algorithm

#### 5 Results and Discussion

The contrast, brightness and intensity of the raw image is changed for human visualization and represented in the chart. The size of the raw image and the size of the compressed images are compared and tabulated below (Table 1).

**Table 1.** Compression table shows the name of the raw image, its actual size, the compressed image with its shrunk file size.

S.	Raw image name	Raw	Compressed image name	Compressed
no		image size		image size
1	1.06mag-06firstwords-t_	182.9 KB	1.06mag-06firstwords-t_CA0-	41.3 KB
	CA0-articleLarge-v2.png		articleLarge-v2.jpg	
2	1.forest4_612251.png	435.0 KB	1.forest4_612251.jpg	155.0 KB
3	10.Untitled-design-9-796x417.png	189.9 KB	10.Untitled-design-9-796x417.jpg	136.1 KB
4	10.forestsmain.png	2.7 MB	10.forestsmain.jpg	742.9 KB
5	11.csm_Finland_forest_by_	669.9 KB	11.	184.3 KB
	Ninara_flickr_42b14a06aa.png		csm_Finland_forest_by_Ninara_flickr_	
			42b14a06aa.jpg	
6	11.when-will-little-people-big-world-	320.4 KB	11.when-will-little-people-big-world-	86.7 KB
	return-1546445203.png		return-1546445203.jpg	
7	12.730_ThinnedForest_	826.8 KB	12.730_ThinnedForest_Unthinned	275.2 KB
	UnthinnedForest_background.png		Forest_background.jpg	
8	12.bianca-devins.png	2.0 MB	12.bianca-devins.jpg	765.6 KB
9	14.inner_slider.png	2.1 MB	14.inner_slider.jpg	637.0 KB
10	15.FOD.png	1.1 MB	15.FOD.jpg	351.5 KB
11	15.denis5-1-400x400.png	180.7 KB	15.denis5-1-400x400.jpg	37.1 KB
12	16.theni%20forest.png	767.0 KB	16.theni%20forest.jpg	202.9 KB
13	17.ron-golden-1.png	275.8 KB	17.ron-golden-1.jpg	208.1 KB
14	18.river.png	429.8 KB	18.river.jpg	102.1 KB
15	19.aboutus-our-people-tab-careers.png	132.4 KB	19.aboutus-our-people-tab-careers.jpg	127.0 KB

The following chart shows the size chart of how the raw image is compressed (Fig. 4).

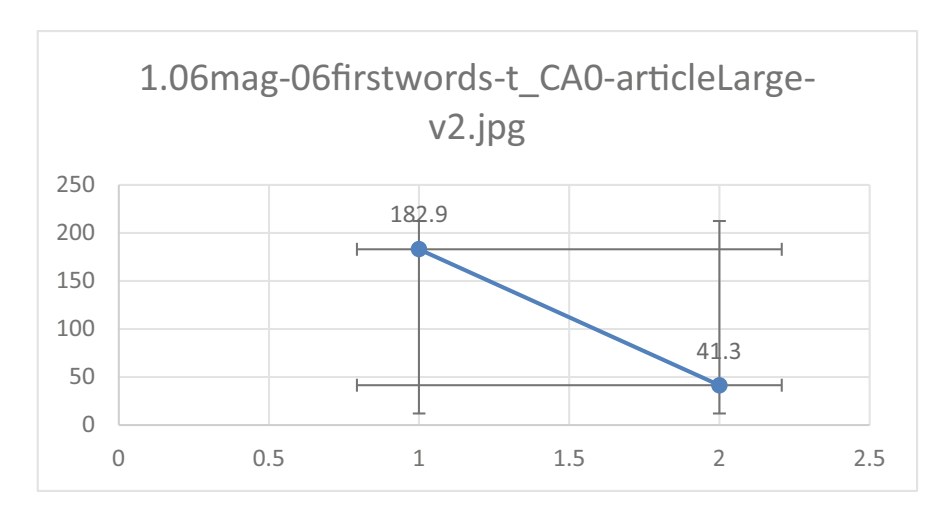


Fig. 4. shows how the image is compressed from 182.9 kb size to 41.3 kb size.

#### 5.1 PSNR

For measuring the quality of the compressed image, MSE (Mean Square Error) and PSNR values are calculated. Peak Signal Noise Ratio (PSNR) is the rational value calculated between the signal or original data and the noise or error which corrupts or affects the quality of the image after compression. The Quality comparison table is drawn to display how the compressed image is enhanced and its PSNR values are quoted in Table 2.

S.	Compressed Image Name	Compressed	PSNR for	PSNR for image
no		image size	compressed image	enhanced using EQI-AC
1	1.06mag-06firstwords-t_CA0-articleLarge-v2.jpg	41.3 KB	42.01572425	33.5922751
2	1.forest4_612251.jpg	155.0 KB	31.03455893	28.37294619
3	10.Untitled-design-9-796x417.jpg	136.1 KB	37.53878891	28.67509408
4	10.forestsmain.jpg	742.9 KB	39.03112413	28.15049873
5	11.	184.3 KB	32.27701443	28.21003005
	csm_Finland_forest_by_Ninara_flickr_42b14a06aa. jpg			
6	11.when-will-little-people-big-world-return- 1546445203.jpg	86.7 KB	36.29536386	29.16766387
7	12.730_ThinnedForest_UnthinnedForest_background.	275.2 KB	32.2505882	28.55379357
8	12.bianca-devins.jpg	765.6 KB	49.48272976	28.37872612
9	14.inner_slider.jpg	637.0 KB	34.09973061	28.35485278
10	15.FOD.jpg	351.5 KB	31.60122669	28.16294106
11	15.denis5-1-400x400.jpg	37.1 KB	40.55023649	30.59407807
12	16.theni%20forest.jpg	202.9 KB	38.95896213	28.21869
13	17.ron-golden-1.jpg	208.1 KB	33.83155675	28.44046449
14	18.river.jpg	102.1 KB	42.87173892	28.49909941
15	19.aboutus-our-people-tab-careers.jpg	127.0 KB	37.69856963	30.45363582

Table 2. Quality comparison table with PSNR values

The below bar chart is the graphical representation for the PSNR value of the compressed image and the PSNR value of the enhanced image by applying EIQ-AC algorithm. From the output images it is visibly seen that the color, contrast and intensity of the given images are enhanced (Fig. 5).

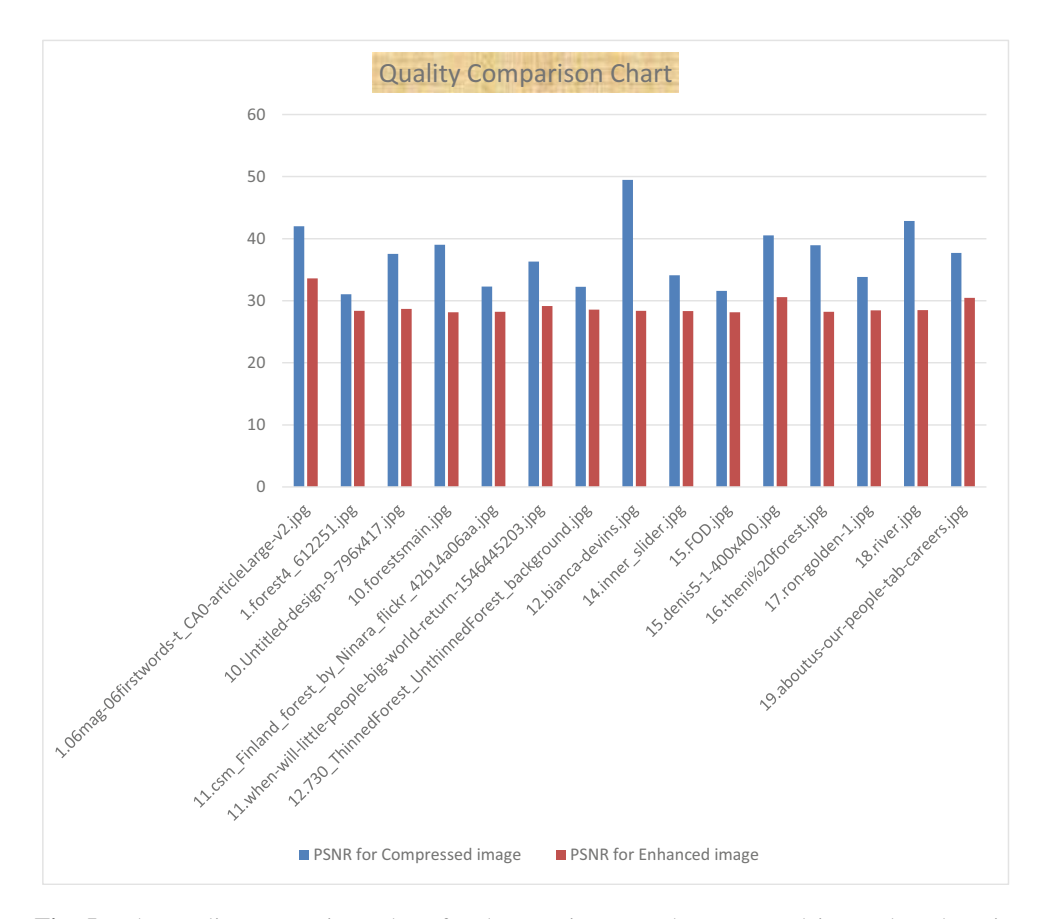


Fig. 5. The quality comparison chart for the raw image and compressed image based on its PSNR value.

#### **5.2 SSIM**

Structure Similarity Index is the quality measure used to find the similarity quality between two same images, the raw image and the compressed image. The following table shows the structural similarity between the 15 raw images taken as a sample input for compression (Table 3).

S.	Compressed image	SSIM value of compressed	SSIM value of EQI-AC applied
no		image	image
0	1.06mag-06firstwords-t_CA0-articleLarge-v2.jpg	0.993276488	0.967669013
1	1.forest4_612251.jpg	0.980494321	0.831007905
2	10.Untitled-design-9-796x417.jpg	0.976760044	0.818730254
3	10.forestsmain.jpg	0.988178904	0.723306708
4	11.csm_Finland_forest_by_Ninara_flickr_42b14a06aa.jpg	0.97671113	0.808361255
5	11.when-will-little-people-big-world-return-1546445203.	0.97784198	0.863056503
	jpg		
6	12.730_ThinnedForest_UnthinnedForest_background.jpg	0.970369237	0.794251695
7	12.bianca-devins.jpg	0.99559195	0.86142213
8	14.inner_slider.jpg	0.992146256	0.85905047
9	15.FOD.jpg	0.964105035	0.762102643
10	15.denis5-1-400x400.jpg	0.991242482	0.899955901
11	16.theni%20forest.jpg	0.992998901	0.842987241
12	17.ron-golden-1.jpg	0.944776986	0.776488431
13	18.river.jpg	0.990599087	0.828948821
14	19.aboutus-our-people-tab-careers.jpg	0.970074594	0.881192121
15	2.forestblog3.jpg	0.971007348	0.773670275

Table 3. The structure similarity index of the compressed image and enhanced images

The below chart (Fig. 6) graphically shows how the EQI-AC applied image having the similarity with the compressed image.



Fig. 6. The structure similarity index chart for the above table

#### 6 Output

The following images shows how the raw images and the enhanced images are differed in contrast, brightness and intensity before and after applying EQI-AC algorithm for compression. Here the enhanced output of the 6th image, 12th image and 98th image of the dataset are displayed for the reference (Fig. 7).



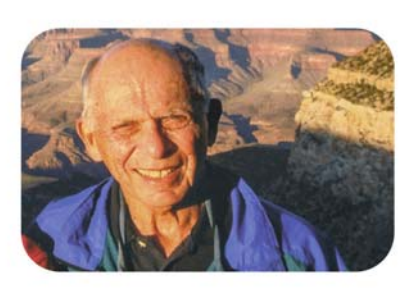
raw image. 6th image in the dataset



EQI-AC algorithm applied enhanced image



12th raw image of the dataset



EQI-AC algorithm applied enhanced image



98th image of dataset



EQI-AC algorithm applied enhanced image

Fig. 7. Compressed image with JPEG standard and CLAHE

#### 7 Conclusion

While attempting image compression, the size of the image decreases been a fact, Using EQI-AC algorithm, the file size is reduced and the quality of the image is also improved. By calculating the PSNR & SSIM of the original images, it is acceptable that the image color, contrast and intensity of the image is improved even after compression. In this paper, EQI-AC (Enhanced Quality Image After Compression) algorithm is used to enhance contrast, intensity and color of the compressed image, which is balanced, for visualization. Peak signal noise ratio (PSNR) and Structure similarity index (SSIM) is also calculated to prove that there is only a slight degrade in the quality of the compressed image compared to the original image.

#### References

- 1. Chung, S.-W., Kim, B.-K., Song, W.-J.: Removing chromatic aberration by digital image processing. Opt. Eng. **49**(6) (2010). https://doi.org/10.1117/1.3455506
- 2. Uhrina, M., Bienik, J., Mizdos, T.: Chroma subsampling influence on the perceived video quality for compressed sequences in high resolutions. Digit. Image Process. Comput. Graph. **15**(4) (2017). https://doi.org/10.15598/aeee.v15i4.2414
- 3. Alam, L., Dhar, P.K., Hasan, M.A.R., Bhuyan, M.G.S., Daiyan, G.M.: An improved JPEG image compression algorithm by modifying luminance quantization table (2019)
- 4. Temmermans, F., Bruylants, T., Schelkens, P., Ebrahimi, T.: An introduction to JPEG standards for digitization and archiving applications (2009)
- 5. Barni, M., Nowroozi, E., Tondi, B.: Detection of adaptive histogram equalization robust against JPEG compression (2018). https://doi.org/10.1109/iwbf.2018.8401564
- Chen, Z., Zhao, Y., Ni, R.: Detection for operation chain: histogram equalization and ditherlike operation. KSII Trans. Internet Inf. Syst. 9(9), 3751–3770 (2015). ISSN 1976-7277. https://doi.org/10.3837/tiis.2015.09.026
- Cozzolino, D., Gragnaniello, D., Verdoliva, L.: Image forgery detection through residualbased local descriptors and block-matching. In: 2014 IEEE International Conference on Image Processing (ICIP), pp. 5297–5301. IEEE (2014)
- 8. Pizer, S.M., Amburn, E.P., Austin, J.D., Cromartie, R., Geselowitz, A., Greer, T., ter Haar Romeny, B., Zimmerman, J.B., Zuiderveld, K.: Adaptive histogram equalization and its variations. Comput. Vis. Graph. Image Process. **39**(3), 355–368 (1987). ISSN 0734-189X. https://doi.org/10.1016/S0734-189X(87)80186-X
- Cao, G., Zhao, Y., Ni, R.: Forensic estimation of gamma correction in digital images. In: 2010 17th IEEE International Conference on Image Processing (ICIP), pp. 2097–2100. IEEE (2010)
- 10. Cao, G., Zhao, Y., Ni, R., Li, X.: Contrast enhancement-based forensics in digital images. IEEE Trans. Inf. Forensics Secur. 9(3), 515–525 (2014)
- Barni, M., Fontani, M., Tondi, B.: A universal technique to hide traces of histogram-based image manipulations. In: Proceedings of the on Multimedia and Security, pp. 97–104. ACM (2012)
- De Rosa, A., Fontani, M., Massai, M., Piva, A., Barni, M.: Second-order statistics analysis to cope with contrast enhancement counter-forensics. IEEE Sig. Process. Lett. 22(8), 1132– 1136 (2015)

- 13. Pan, X., Zhang, X., Lyu, S.: Exposing image forgery with blind noise estimation. In: Proceedings of the Thirteenth ACM Multimedia Workshop on Multimedia and Security, pp. 15–20. ACM (2011)
- 14. Li, H., Luo, W., Qiu, X., Huang, J.: Identification of various image operations using residual-based features. IEEE Trans. Circuits Syst. Video Technol. 28, 31–45 (2016)
- 15. Singh, N., Gupta, A.: Analysis of contrast enhancement forensics in compressed and uncompressed images. In: 2016 International Conference on Signal Processing and Communication (ICSC), pp. 303–307. IEEE (2016)
- 16. Barni, M., Nowroozi, E., Tondi, B.: Higher-order, adversary-aware, double jpeg-detection via selected training on attacked samples. In: 2017 25th European Signal Processing Conference (EUSIPCO), pp. 281–285, August 2017
- Bestagini, P., Allam, A., Milani, S., Tagliasacchi, M., Tubaro, S.: Video codec identification.
   In: 2012 IEEE International Conference on Acoustics, Speech and Signal Processing (ICASSP), pp. 2257–2260. IEEE (2012)
- 18. Fridrich, J., Kodovsky, J.: Rich models for steganalysis of digitalimages. IEEE Trans. Inf. Forensics Secur. **7**(3), 868–882 (2012)
- Verdoliva, L., Cozzolino, D., Poggi, G.: A feature-based approach for image tampering detection and localization. In: 2014 IEEE International Workshop on Information Forensics and Security (WIFS), pp. 149–154. IEEE (2014)
- Goljan, M., Fridrich, J., Cogranne, R.: Rich model for steganalysis of color images. In: 2014 IEEE International Workshop on Information Forensics and Security (WIFS), pp. 185–190. IEEE (2014)
- 21. Kodovsky, J., Fridrich, J., Holub, V.: Ensemble classifiers for steganalysis of digital media. IEEE Trans. Inf. Forensics Secur. **7**(2), 432–444 (2012)



### ExclusiveOR-Discrete Cosine Transform-A Chaotic Algorithm for Image Encryption and Decryption

M. Durairaj and J. Hirudhaya Mary Asha<sup>(⊠)</sup>

Department of Computer Science, Bharathidasan University, Tiruchirappalli, Tamilnadu, India

durairaj.bdu@gmail.com, hirudhaya ashaa20@yahoo.co.in

Abstract. Image encryption is an operative method to shield images or videos from disrupting, while transporting them in a shared link for security reasons. The security levels are increased by applying various algorithms. In this literature, image encryption is done with chaotic methods. Chaotic representation like XOR representation is used to scramble the image data in a pixel by pixel limit. The input image is scrambled using P Fibonacci-XOR transform with masking coefficients and Discrete Cosine Transform (DCT). Later, the scrambled images got unscrambled by applying the inverse of the applied function. As a result, Chaotic concepts avoids iteration of the image data by the unintended persons and the performance of the ExclusiveOR-Discrete Cosine Transform XORDCT algorithm is analyzed by PSNR, NPCR, UACI and Correlation coefficient factors.

**Keywords:** Compressed image · Discrete Cosine Transform (DCT) · XOR transform · Masking coefficients · Inverse operation · Image scrambling and unscrambling

#### 1 Introduction

Secret communication is expected between the users to ensure privacy. The contents may be hide from exposing to the public and delivered via authentication acknowledgement. Unintended persons may intercept our messages in order to aware of it or destroy it. Many encryption algorithms are found and suggested in the past. Thus, hiding messages are serious problem to consider. XOR Cipher encrypts image data using mathematical parameters for making the encryption stronger [1]. XOR cipher combines matrix data of an image with a random key to make the process highly efficient and unbreakable. Chaos based scrambling gives more number of permutation to re-align the pixels of the image which can be non-recognizable and dis-order. Chaosbased algorithms are simple and highly secured to adopt. The chaotic or mathematical formulae are widely applied in image diffusion and image confusion [2]. The P-Fibonacci XOR operation is applied for scrambling the image. These mathematical techniques are called scrambling techniques follows randomization using numerical data of the image but unchanging the actual representation of the image data.

P-Fibonacci XOR transformation is the technique. This encryption process is formulated by giving the hash value of the raw image and compressed image as input. Transformation in the image data is done using DCT (discrete cosine transform) [2]. Encryption process encodes the original image using cipher key and the decryption process reverses the encryption to get the original image back. There are two methods Confusion and Diffusion to perform encryption. The masking key and image is confused and rearranged in the distribution process [3]. High redundant pixels in the image have strong correlations in the encrypted image also. Chaos based iterations are applied [5–13]. Chaotic system have two types of integer order, the proper fractional-order and improper-fractional order. Parameters of the matrix image data are arranged in fractional orders. While transferring secret image or text, the density of the image pixel and security of the data are interrelated [17, 18].

#### 2 Related Works

Due to the in-determinant rise in digital communication, manifold technologies are used to transfer private particulars like images and videos. Every individual, companies and officials use encryption methods. Encrypting or transforming the data into an altered format is a constructive method to protect images or videos. The authorized users can decode encrypted objects [1]. Many applications required security as a basement for shielding privacy to hide confidential commercial matters. Authorization is allocated to others via fingerprint matches, iris matches etc., are such type of security applications. Depends upon the expecting security, the data can be either partially or fully altered by following different Technologies [2]. Fresnel Transform (Fr-T) were used to transform the input image [3, 4]. Fractional and Fourier Transform (Fr-FT) are followed to scramble the image input [5–7]. Spatial domain calculus is used to protect data with high security and high quality. Naïve-based algorithms assume the data stream to encrypt the data [8]. Des (Data Encryption Standard) encrypts data part of the sequence [9] Without scrambling the input, AES (Advanced Encryption Standard) method performs expandable output [10-12]. Chaos or mathematical systems use numeric data and provide results with real numbers which guide the algorithm for scrambling [13–18]. Recursive routines like Fibonacci sequences encrypt images with less security [19, 20]. The efficiency and security of the encryption process are improved using P-Fibonacci transform sequence and P-recursive function [21, 22]. Permutation changes the pixel values of image blocks vulnerable to plain-text attacks [23, 24]. Exclusive-OR functions followed for bit plane encryption [25]. In handheld devices, transforms are done using Asynchronous standards for encryption (AES). Images are arranged with matrix of pixels of Red Green Blue color. Each color value starts from 0 to 255 for each bit. Base picture based method is similar to the random matrix based methodology. Here, instead of generating the random matrix, we take a base picture and extract the pixel values from it and use it to XOR each value in the other picture matrix. If the size of the base picture is smaller than the size of the original picture, we repeat the same values from start as in a loop [26].

69	R: 68	R: 70	R: 71	R: 73	R: 76	R: 74	R: 71	R: 72	R: 76	R:
44	G: 43	G: 43	G: 44	G: 43	G: 43	G: 41	G: 42	G: 44	G: 54	G:
68	B: 70	B: 72	B: 70	B: 66	B: 65	B: 69	B: 70	B: 67	B: 61	B:
70	R: 71	R: 71	R: 69	R: 70	R: 69	R: 72	R: 87	R:110	R:128	R:1
45	G: 44	G: 44	G: 42	G: 43	G: 41	G: 46	G: 64	G: 90	G:116	G:1
73	B: 70	B: 67	B: 65	B: 67	B: 67	B: 62	B: 55	B: 51	B: 41	B:
74	R: 72	R: 70	R: 69	R: 74	R: 81	R:102	R:132	R:148	R:151	R:1
42	G: 44	G: 44	G: 43	G: 49	G: 64	G: 90	G:121	G:138	G:144	G:1
75	B: 73	B: 70	B: 68	B: 64	B: 54	B: 40	B: 30	B: 25	B: 19	B:
71	R: 72	R: 75	R: 92	R:115	R:130	R:143	R:152	R:151	R:153	R:1
44	G: 44	G: 47	G: 70	G: 96	G:118	G:133	G:140	G:143	G:148	G:1
69	B: 66	B: 62	B: 53	B: 44	B: 23	B: 11	B: 11	B: 13	B: 18	B:
68	R: 75	R:103	R:129	R:135	R:145	R:151	R:153	R:157	R:164	R:1
44	G: 56	G: 09	G:120	G:126	G:135	G:141	G:143	G:145	G:150	G:1
62	B: 53	B: 47	B: 42	B: 27	B: 15	B: 7	B: 8	B: 15	B: 15	B:
78	R:115	R:136	R:131	R:142	R:151	R:153	R:157	R:160	R:164	R:1
59	G:102	G:128	G:126	G:133	G:142	G:143	G:146	G:150	G:155	G:1
48	B: 45	B: 37	B: 12	B: 11	B: 18	B: 13	B: 10	B: 18	B: 30	B:
118	R:135	R:128	R:161	R:153	R:151	R:153	R:160	R:163	R:165	R:1
105	G:127	G:124	G:133	G:143	G:143	G:145	G:151	G:154	G:154	G:1
40	B: 29	B: 14	B: 7	B: 7	B: 6	B: 9	B: 19	B: 24	B: 21	B:

Fig. 1. Shows how the images are represented in matrix form

From the above Fig. 1, can aware of how the images are represented in matrix form. The matrix form of an image is transformed using DCT(discrete cosine transform) and the output is XORed with the masking coefficients to get the scrambled image.

#### 2.1 P-Fibonacci Transform Function

P-Fibonacci transforms method is used to select an initial sequence from the inputted image matrix. Let, consider some of the properties of the P-Fibonacci transform properties for selecting the input sequence. To encrypt the image, the pixel location of the images is scrambled initially using P-Transform series.

Definition 1.1: The Fibonacci sequence is a recursive function

$$f(p) = \begin{cases} 0 & p < 0 \\ 1 & 1 \\ f(p-1) \wedge (p-2)^2 & p > 0 \end{cases}$$
 (1)

Where, p is an indexing parameter of the Fibonacci XOR transform sequence. This parameter is used to mark the distance vector. From the Eq. (1), the Fibonacci sequence changes with the difference in the values of p and calculated by representing the image data in binary form, the result will be true or 1 if either bit of data is 1 otherwise false [19, 20].

Definition 1.2: Fibonacci sequence generator is formed by

$$Fn = Fn - r + \dots + Fn - s \pmod{q} \text{ where } r > s > 0$$
 (2)

Initially, two elements are needed to find the next element in the sequence. From the previous expression, the value of r and s must be set greater than 0. Adding all the terms, the nth term of the function is calculated. The interest of function Fn is calculated by the power of two that is,

Definition 1.3: Golden spiral-ratio is continued based on Eq. (2). to select the next term of the fibonacci series. The Fibonacci sequence varies depending on the p and q value. Fibonacci series is an infinite series of integer numbers, where each term is the sum of the two previous term. The total pixel ratio of an image is found by the summing of the pixel values of the whole image are called the Fibonacci-golden ratio. It is represented mathematically with p and q where p > q > 0,

$$q = 2^{q} \tag{3}$$

$$p/q = (p+q)/p = 1.6180339887498948420...$$
 (4)

If p = 0, the Fibonacci-0 coding sequence is a power sequence of 2 that 1, 2, 4, 8, 16, If p = 1, the Fibonacci-1 coding sequence is the classical Fibonacci sequence 1, 1, 2, 3, 5, 8, 13, 21,...

If p > 1, the Fibonacci-2 coding sequence is a recursive function [21–23] (Figs. 2 and 3).

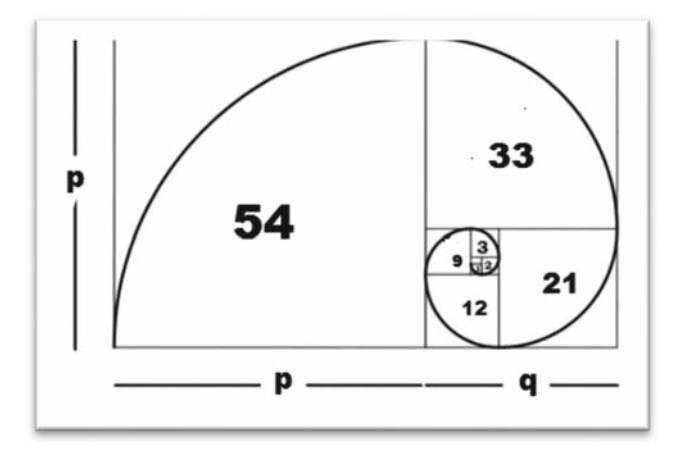


Fig. 2. The golden spiral representation of an equation





golden spiral of ashfordoaks-primary-8.png

Fig. 3. Golden ratio spiral representation of the taken inputs

#### 3 Proposed Methodology-XORDCT Transform

XOR cipher is an encrypting method used to make cipher image and hard to find by the intruders. Every character of the image can be scrambled by applying the XOR operation using a given cipher key. To descramble the encrypted image, reapply the XOR function along with the cipher key.

#### Proof

Let the secret image is represented as I. Based on the Fibonacci series concept, an image is splitted into sequence of images such as I1, I2, I3,....In. The XOR operator in the source side transforms the inputted single secret image into set of images before transmitting it to the destination side. The masking coefficients are discovered by performing discrete cosine transform (DCT) on the input image. The XOR-ed result of the input images are,

$$R <= \Sigma \{I1 \oplus I2 \oplus I3, \dots \oplus In\}$$
 (4)

Where R and  $\sum$ {.} denotes the coefficients for masking the input images. The masked image is represented as Mi and

$$Mi = M1, M2, M3,...Mn$$
 (5)

The masked image Mi is XOR - ed using the Ii and R. Likewise Mi = Ii  $\oplus$  R (6)

Where i = 1, 2, 3,...n. Then the masked images Mi are formed and transmitted to the destination side. After receiving, the destination part joins all the masked images M1, M2...Mn and perform the XOR to recover the original input image.

$$\overline{Ii} = Mi \oplus \bar{R}$$
 (7)

Theorem 1

The XOR sequence is reversible if and only if  $R = \bar{R}$ .

Proof: The P-fibonacci XOR sequence is reversible if it satisfies  $Ii = \overline{Ii}$ , where i = 1, 2, ...n. This condition is solved when  $Ii = \overline{Ii}$  then

$$\overline{li} = Mi \oplus \bar{R}$$
 (8)

From the above equation know that, Mi = Ii  $\oplus$  R, where i = 1, 2,...n then

$$\overline{li} = \operatorname{Ii} \oplus \operatorname{R} \oplus \overline{R} \qquad \text{(substitute Eq.(9) here)}$$
 (9)

whereas Ii  $\oplus$  0 =  $\overline{Ii}$ .

By using the XOR property  $\overline{R \oplus \overline{R}} = 0$  multiply both side by  $\overline{R}$ 

R 
$$\oplus \bar{R} \oplus \bar{R} = 0 \oplus \bar{R}$$
 and  $0 \oplus \bar{R} = \bar{R}$ , (10)

The above equation is simplified as  $R = \bar{R}$ 

Now the value of 
$$\bar{R} = \sum \{ I1 \oplus I2 \oplus \dots \text{In } \oplus \underbrace{R \oplus R \oplus R}_{\text{n is odd}} \}$$
 (11)

Finally  $R \oplus \bar{R} = 0$  equals  $R = \bar{R}$ . If the masking coefficients are identical for both encryption and decryption, the process is reversible.

Theorem 2

The process is reversible, if n is even number.

Proof: If n is even number, the masking coefficient is

$$\bar{R} = \sum \{M1 \oplus M2 \oplus \ldots \oplus Mn\}$$
 By fact (12)

 $Mi = Ii \oplus R$  (Mi- masking coefficient) Where R can be written as

$$\bar{R} = \sum \{I1 \oplus I2 \oplus \ldots \oplus In \oplus Rn\}$$
 By regrouping of R (13)

$$\bar{R} = \sum \{ I1 \oplus I2 \oplus \ldots \oplus In \oplus \underbrace{R \oplus R \oplus \ldots \oplus R}_{\text{niseven}} \}$$
 (14)

(15)

 $\bar{R} = \sum \{I1 \oplus I2 \oplus \ldots \oplus In \oplus 0\}, \text{ Where } R \oplus R \oplus \ldots \oplus R = R \oplus R = 0\} \text{ it can be rewritten as } \sum \{I1 \oplus I2 \oplus \ldots \oplus In\}$ 

The value of  $\bar{R}$  is equal to the value of R. (i.e.)  $\bar{R} = R$ . If n is odd number, the recovered masking coefficient  $\bar{R}$  is calculated as

$$\bar{R} = \sum \{M1 \oplus M2 \oplus \ldots \oplus Mn\}$$

Initially M1 = Ii  $\oplus$  R then  $\bar{R}$  can be rewritten as

$$\bar{R} = \sum \{ I1 \oplus R \oplus I2 \oplus R \oplus \ldots \oplus In \oplus R \}$$
 (16)

By using XOR property  $\underbrace{R \oplus R \oplus \ldots \oplus R}_{\text{n is odd}} = R \oplus R \oplus R = 0 \oplus R = R$ 

The value of  $\bar{R}$  can be formed by  $\bar{R} = \sum \{I1 \oplus I2 \oplus \ldots \oplus In \oplus R \oplus R \oplus \ldots \oplus R\}$ 

$$\bar{R} = \sum \{ I1 \oplus I2 \oplus \ldots \oplus In \oplus R \} \tag{17}$$

The  $\bar{R}$  is not identical to original R. From comparing Eq. (11) and Eq. (17) it is clear that  $\bar{R}$  is identical to R when the inputted images are scrambled into even number of images. Thus scrambling the image is an alternative choice for enhancing the security of the image. The images are altered in unreadable mode. The original image of the jpeg format is transformed using a Discrete Cosine Transform (DCT).

The coefficients of the image are formed by the 2D P-Fibonacci XOR Transform. The parameters of P-Fibonacci XOR transform are p and i. Lossless image scrambling method is build using P-Fibonacci XOR transform.

#### **Encryption Using XORDCT Algorithm**

- Step 1: Based on Fibonacci series, The image Ii is converted to three color components: R, G, B such as 'n' number of shared images I1, I2, I3,...In, before sending to the destination.
- Step 2: Apply DCT to each color component and combining together all components. (Ii = I1  $\oplus$  I2  $\oplus$  I3  $\oplus$  ... $\oplus$ In)
- Step 3: XOR-ing the matrix component of an image for calculating the masking coefficient R (R <=XOR (Ii))
- Step 4: The shared images Mi are scrambled by XOR-ing the Ii and R. (Mi  $\leq$  Ii  $\oplus$  R)
- Step 5: If the scrambled images have 'n' odd shared images then the original image is ir-reversible otherwise reversible.
- Step 6: The scrambled images are got.

#### **Decryption Using Inverse- XORDCT Algorithm**

- Step 1: The destination module XOR-ed the scrambled image with the masking coefficient Mi.
- Step 2: Calculate the XOR inverse function for the masking coefficient matrices of an image  $\bar{R}$ . ( $\bar{R} < = (M1 \oplus M2 \oplus M3 \oplus ... \oplus Mn)$ )
- Step 3: After that apply inverse DCT to each color component and combining together all components.  $(\overline{Ii}=Mi\oplus \bar{R})$
- Step 4: Recovering the color components together to get the original R:G:B image.
- Step 5: The actual image is reconstructed.

#### 3.1 Block Diagram of XORDCT Algorithm

The image compressed using EQIAC algorithm is taken as an input for XORDCT encryption algorithm (Fig. 4).

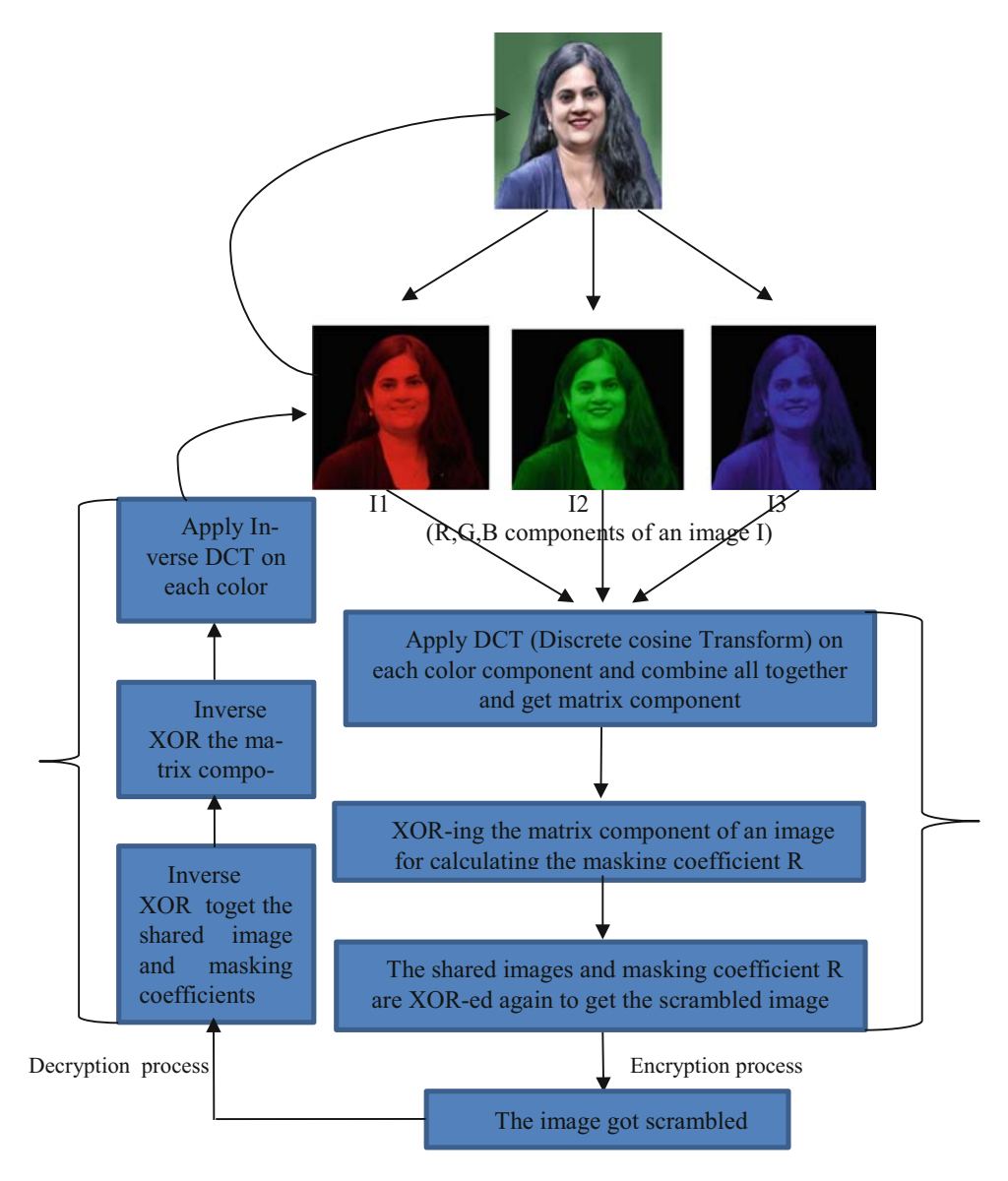


Fig. 4. Block diagram of XORDCT algorithm

#### 4 Experimental Results

#### 4.1 Statistical Result Analysis

Here more than 95 images are considered. First of all, consider an image which we want to encrypt. Initially convert the image into a binary data which want to encrypt. The image with .png format is taken for compression. The iteration made in the images are seen visually. In order to quantify the encryption process two metrics are used.

#### 1. Net Pixel Change Ratio (NPCR)

Change in the rate of the pixel number comparing the original and the encrypted image.

NPCR = 
$$\frac{1}{MxN} \sum_{i=1}^{M} \sum_{j=1}^{N} D(i,j) x 100\%$$
 (18)

where 
$$D(i, j) = 0$$
 when  $C1(i, j) = C2(i, j)$   
 $D(i, j) = 1$  when  $C1(i, j) \neq C2(i, j)$ 

The parameters C1 be the original image and C2 be the modified image, D be the array used for storing the image size before and after encryption M and N are the height and width of the images. NPCR is used to analyze the image and find the bit change by comparing pixel by pixel.

#### 2. Unified Average Changing intensity (UACI)

This metric is used to measure the average of the intensity differences in pixels of the raw image and the original images.

UACI = 
$$\sum_{i=1}^{M} \sum_{j=1}^{N} \frac{|(C1(i,j) - C2(i,j))|}{255} x \frac{100\%}{M \times N}$$
 (19)

#### 3. Correlation coefficient analysis

The pixels of the encrypted image is intercorrelated with others. The correlation exists in the adjacent pixels can be used by the intruder for creating the sequence of the image. The range of the correlation coefficient lies within -1 and +1.

$$Cov(\alpha, \beta) = \frac{1}{N} \sum_{i=1}^{N} (\alpha i - E(\alpha))(\beta i - E(\beta))$$

$$r\alpha\beta = \frac{Cov(\alpha, \beta)}{\sqrt{\sqrt{D(\alpha)}}\sqrt{D(\beta)}}$$

$$D(\alpha) = \frac{1}{N} \sum_{i=1}^{N} (\alpha i - E(\alpha))^{2}$$

$$E(\alpha) = \frac{1}{N} \sum_{i=1}^{N} \alpha i$$
(20)

The correlation covariance of the original image and the encrypted image is calculated using  $Cov(\alpha,\beta)$  and  $D(\alpha)$  is the variance range value of the image and  $E(\alpha)$  is assumed as the mean deviation of the image pixel values (Tables 1 and 2).

Table 1. UACI and NPCR value of the taken input image

Image	Image Name	NPCR (in %)	UACI (in %)
6	Image A-img-people-Abha-Mishra.jpg	99.585	28.621
	Image B-ron-golden-1.jpg	99.6078	50.1931
	Image C-ashford-oaks-primary-8.jpg	99.6094	27.4092

Table 2. Correlation coefficient of original image and cipher image.

(img-people	-Abha-Mishra.jpg)			
	Horizontal	Vertical	Diagonal	Counterdiagonal
Original image	0.972953	0.970462	0.916925	0.938441
Encrypted image	$-4.097226 \times 10^{-5}$	$1.158832 \times 10^{-4}$	$4.620716 \times 10^{-5}$	$4.539076 \times 10^{-4}$
(ron-golden-	·1.jpg)			
	Horizontal	Vertical	Diagonal	Counterdiagonal
Original image	0.915352	0.922622291	0.868221	0.857255
Encrypted image	$-3.811868 \times 10^{-6}$	$-7.131676 \times 10^{-4}$	$-9.372164 \times 10^{-4}$	$-3.496642 \times 10^{-4}$
(ashford-oak	cs-primary-8.jpg)			
	Horizontal	Vertical	Diagonal	Counterdiagonal
Original image	0.94514	0.950725	0.919702	0.937272
Encrypted image	-0.001678	$3.514572 \times 10^{-4}$	$-9.329940 \times 10^{-4}$	$-4.626904 \times 10^{-5}$

#### 4. PSNR and MSE analysis

It is the ratio between the original image (signal) and the encrypted image (noise). PSNR scale is used to represent the signal. It is calculated by

$$PSNR = 20 \times \log_{10} \frac{(255)}{\sqrt{MSE}} dB$$

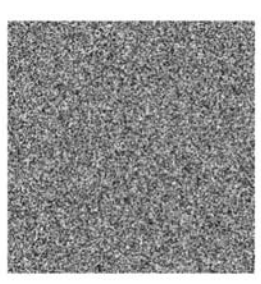
Where MSE is the average of the errors  $MSE = \sum_{i=1}^{M} \sum_{j=1}^{N} \frac{[R(i,j) - S(i,j)]}{MxN}$ Where R(i, j) is the pixel value of the taken input image, S(i, j) is the pixel value of the encrypted image (Table 3).

Table 3. Shows the MSE and PSNR of the input image, encrypted image and decrypted image

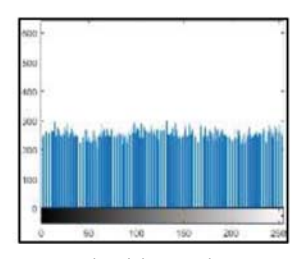
Image	Image Image name		PSNR for decrypted image
Image A- img-people-Abha-Mishra.jpg		0.2698	28.621
	Image B-ron-golden-1.jpg	0.2711	50.1931
	Image C-ashford-oaks-primary-8.jpg	0.2013	27.4092

a) Image A (original)

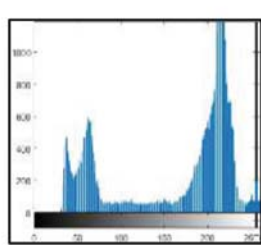
d. Graphical result



b) Image A (encrypted)



c) Image A (Decrypted)



--Pixel intensity-----

d) Histogram of original imageA decrypted imageA

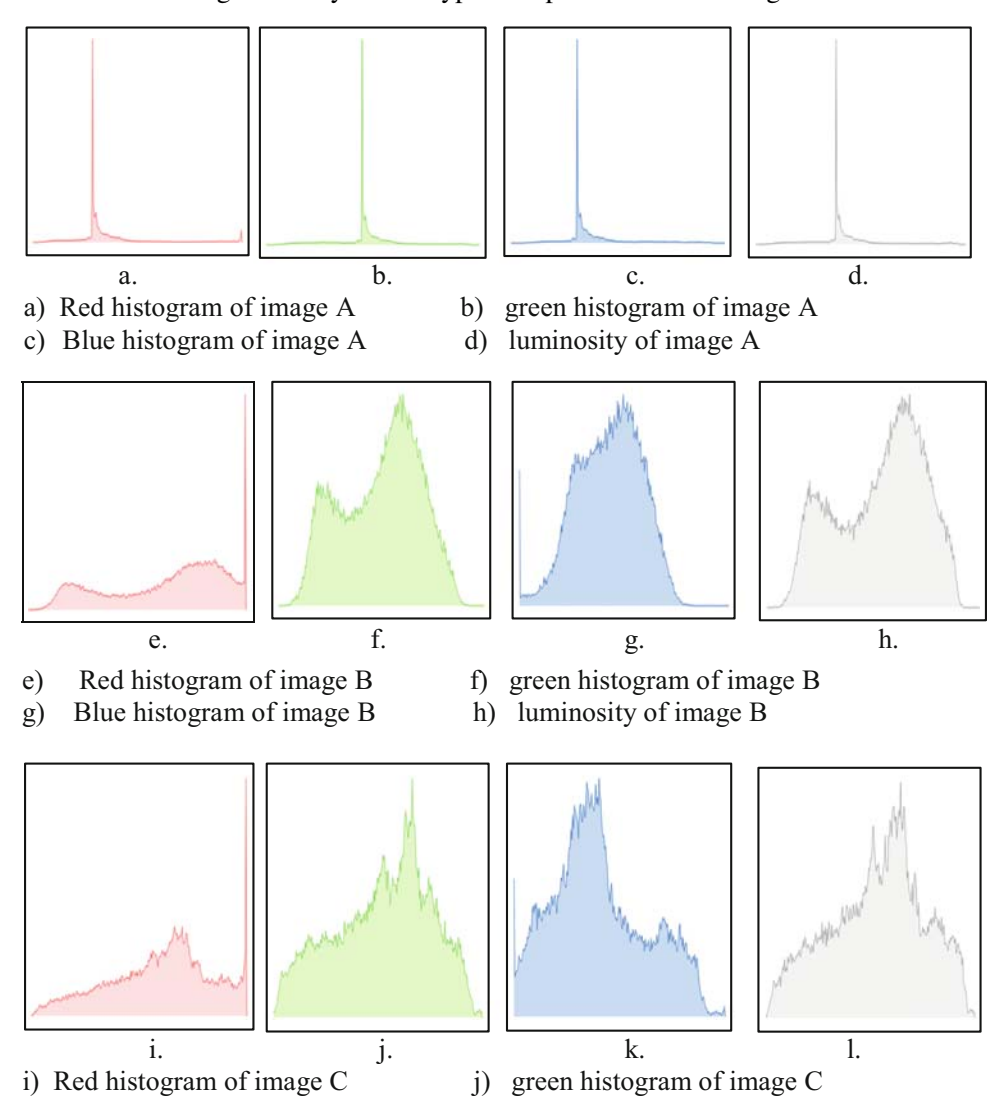
No of pixels

- e) Histogram of encrypted imageA
- f) Histogram of

#### d. Histogram analysis

k) Blue histogram of image C

An image can be represented graphically using the intensity values of the pixels as their axis values. Histogram analysis is a type of representation of image format.



1) luminosity of image C

#### 5 Conclusion

An image is scrambled using Fibonacci series, XOR operation, masking coefficients and DCT (discrete cosine transform). XORing the image matrix component makes changes in the input also brings drastic variation in the encrypted image. The masking coefficients used in this experiment is also XORed to bind more with the input data. The working feature of the encryption and decryption algorithm is experimented and described in this literature. he Experimental results of all the images (image A, image B, image C) are tabulated in this literature. Depends on the ratio of the color accommodated in the image, the PSNR, UACI, NPCR and correlation coefficients varied. From the experimental results, UACI of the taken image is calculated as 30% and NPCR of the taken image is 90%. It is clear that XORDCT algorithm is suitable for encryption and avoids attacks which violates security brute-force attacks.

#### 6 Future Enhancement

In future, this algorithm can be used in real-time devices used in smart homes, smart environments, which uses audios and videos as a primary key for security. The presented algorithms enables high security for secret and confidential data transfer. It can be applicable for text message transferring also. It can be adapted with face recognition algorithms to store images in large databases like cloud for future references.

#### References

- 1. Kadhim, Q.K.: Image compression using discrete cosine transform method. Int. J. Comput. Sci. Mobile Comput. 5(9), 186–192 (2016)
- 2. Anupriya, E., Soni, S., Agnihotri, A., Babelay, S.: Encryption using XOR based extended key for information security a novel approach. Int. J. Comput. Sci. Eng. **3**(1), 146–154 (2011). ISSN: 0975-3397
- 3. Schneier, B.: Applied Cryptography: Protocols, Algorithms, and Source Code in C, 2nd edn. Wiley, New York (1996)
- 4. Daemen, J., Rijmen, V.: The Design of Rijndael: AES-The Advanced Encryption Standard. Springer, Germany (2002)
- 5. Draksharam, S., Katravulapalli, D., Rohith Krishna, K., Thanikaiselvan, V.: Analysis of hybrid chaotic image encryption, vol. 18, pp. 697–703. IEEE (2018)
- 6. Kumar, M., Aggarwal, A., Garg, A.: A review on various digital image encryption techniques and security criteria. Int. J. Comput. Appl. (0975 8887), **96**(13) (2014)
- El Abbadi, N.K., Abaas, S.T., Alaziz, A.A.: New image encryption algorithm based on Diffie-Hellman and singular value decomposition. Int. J. Comput. Appl. (0975 – 8887), 96 (13), 19–26 (2014)
- 8. Zhou, Y., Panetta, K., Agaian, S.: Image encryption using binary key-images. In: Proceedings of the 2009 IEEE International Conference on Systems, Man, and Cybernetics, vol. 09, pp. 4569–4574 (2009)
- Modak, P.M., Pawar, V.: A comprehensive survey on image scrambling techniques. Int. J. Sci. Res. 4(12), 814–818 (2015)

- 10. Kocarev, L., Jakimoski, G., Stojanovski, T., Parlitz, U.: From chaoticmaps to encryption schemes. In: Proceedings of the IEEE International Symposium on Circuits and Systems (ISCAS 1998), pp. 514–517. IEEE, Monterey (1998)
- 11. Shannon, C.E.: Communication theory of secrecy systems. Bell Syst. Tech. J. **28**(4), 656–715 (1949)
- 12. Pareek, N.K., Patidar, V., Sud, K.K.: Discrete chaotic cryptography using external key. Phys. Lett. A **309**(1–2), 75–82 (2003)
- 13. Wang, X., Teng, L.: An image blocks encryption algorithm based on spatiotemporal chaos. Nonlinear Dyn. Int. J. Nonlinear Dyn. Chaos Eng. Syst. **67**(1), 365–371 (2012)
- 14. Xiao, D., Liao, X., Wei, P.: Analysis and improvement of a chaos-based image encryption algorithm. Chaos, Solitons Fractals **40**(5), 2191–2199 (2009)
- 15. Wang, X.-Y., Bao, X.-M.: A novel block cryptosystem based on the coupled chaotic map lattice. Nonlinear Dyn. **72**(4), 707–715 (2013)
- Jakimoski, G., Kocarev, L.C.: Analysis of some recently proposed chaos-based encryption algorithms. Phys. Lett. A 291(6), 381–384 (2001)
- 17. Behnia, S., Akhshani, A., Mahmodi, H., Akhavan, A.: A novel algorithm for image encryption based on mixture of chaotic maps. Chaos, Solitons Fractals **35**(2), 408–419 (2008)
- 18. Mirzaei, O., Yaghoobi, M., Irani, H.: A new image encryption method: parallel sub-image encryption with hyper chaos. Nonlinear Dyn. **67**(1), 557–566 (2012)
- 19. Wang, Y., Wong, K.-W., Liao, X.F., Chen, G.R.: A new chaos based fast image encryption algorithm. Appl. Soft Comput. **11**(1), 514–522 (2011)
- 20. Ismail, A.I., Mohammed, A., Hossam, D.: A digital image encryption algorithm based a composition of two chaotic wavelet function map. Int. J. Netw. Secur. **11**(1), 1–10 (2010)
- 21. Rhouma, R., Belghith, S.: Cryptanalysis of a new image encryption algorithm based on hyper-chaos. Phys. Lett. Sect. A: Gen. Atomic Solid State Phys. **372**(38), 5973–5978 (2008)
- Li, X.-F., Chlouverakis, K.E., Xu, D.-L.: Nonlinear dynamics and circuit realization of a new chaotic flow: a variant of Lorenz, Chen and Lü. Nonlinear Anal. Real World Appl. Int. Multidiscip. J. 10(4), 2357–2368 (2009)
- 23. Zhao, J.F., Wang, S.Y., Chang, Y.X., Li, X.F.: A novel image encryption scheme based on an improper fractional-order chaotic system. Nonlinear Dyn. **80**(4), 1721–1729 (2015)
- Wu, X., Wang, H., Lu, H.: Modified generalized projective synchronization of a new fractional-order hyperchaotic system and its application to secure communication. Nonlinear Anal. RealWorld Appl. 13(3), 1441–1450 (2012)
- 25. Mannai, O., Bechikh, R., Hermassi, H., Rhouma, R., Belghith, S.: A new image encryption scheme based on a simple firstorder time-delay system with appropriate nonlinearity. Nonlinear Dyn. **82**(1–2), 107–117 (2015)
- Liu, Q., Li, P.-Y., Zhang, M.-C., Sui, Y.-X., Yang, H.-J.: A novel image encryption algorithm based on chaos maps with Markov properties. Commun. Nonlinear Sci. Numer. Simul. 20(2), 506–515 (2015)

# Fuzzy probability based person recognition in smart environments

M. Durairaj<sup>a</sup> and J. Hirudhaya Mary Asha<sup>b,\*</sup>
Department of Computer Science and Engineering, Bharathidasan University, Tamilnadu, India

Abstract. Biometric features are used to verify the people identity in the living places like smart apartments. To increase the chance of classification and recognition rate, the recognizing procedure contains various steps such as detection of silhouette from the gait profile, silhouette segmentation, reading features from the silhouette, classification of features and finally recognition of person using its probability value. Person recognition accuracy will be oscillated and declined due to blockage, radiance and posture variance problems. In the proposed work, the gait profile will be formed by capturing the gait of a targeted person in stipulated time to reach the destination. From the profile the silhouettes are detected using frame difference and segmented from the background using immediate thresholding and features are extracted from the silhouette using gray-level covariance matrix and optimized feature set is formed using PSO. These optimized features are fused, trained and classified using nearest neighbor support vectors. The fuzzy probability method is used for recognizing the person based on the probability value of the authentic and imposter scores. The relationship between the CMS, TPR, TNR and F-rate are calculated for 1:1 matcher from the gallery set. The performance of the classifiers are found to be perfect by plotting the DET graph and ROC curve. The proposed fuzzy probability theory is mingled with GLCMPSO and NSFV method for human recognition purpose. The performance of the proposed is proved to be acceptable for recognition with the optimal parameters (Entropy, SSIM, PSNR, CQM) calculation From the work, it is clear that, the rank probability is proportional to the match score value of the silhouette stored in the gallery.

Keywords: Gait cycle, silhouette image, feature detection, feature extraction, feature classification, person recognition using fuzzy probability

#### 1. Introduction

Compound Annual Growth Rate (CAGR) of recognition concepts grows better from 2016 upto now. Smartly secured places are exempted from problems like theft and murder. The invention of new cost effective GPUs, powerful energy back-ups and silhouette profiles helps to focus on designing smart home networks. Recognizing the human by the way of walk is called gait. Gait analysis is a kind of biomet-

ric mechanism, used to notice human without their knowledge. Identifying public using gaits can be followed in apartmental houses, banks, shopping malls, airports etc., Smart residence is an environment with full pledged security. This work detects the movement of human in the smart places with the static surveillance setup. It responds to the superior in real-time and notify the intruder arrival. This setup will prevent the theft or crime in time. The setup raises alarm, if any unnecessary motion detected before the camera. The living places, shopping malls and temples needs surveillance monitoring all over the time to avoid thefts, murder, or any illegal incidents. Targeting or locating the moving object in the captured frames is called the tracking. Difficulties in tracking will

<sup>\*</sup>Corresponding author. J. Hirudhaya Mary Asha, Department of Computer Science and Engineering, Bharathidasan University, Tamilnadu, India. Tel.: +917502364030; E-mail: hirudhaya\_ashaa20@yahoo.co.in.

occur when objects changes it direction faster than the frame rate. Recognition techniques contains tracking sensors to capture the person's significance from distance. In this work, video based silhouette recognition is practiced. Detecting an object through the surveillance video is an ongoing step in security ensuring process. The human recognition procedure consists of 3 steps. They are segmentation of captured frame, tracking the object in the frames, classifying the object based on its similarity and recognizing the person using fuzzy probability value of the membership functions. The gait data are captured with RGBdepth camera and Kinect sensor [1-3]. Silhouettes are detected from the whole image motion by frame difference method. GEI is computed by converting the silhouettes pattern into 2D-grey image and FDEI is GEI updation. Using FDEI the incomplete pixels in the frames of the silhouette pattern are filled and normalized [4, 5]. As the silhouette pixels are not same as the background pixel, so, subtracting the background pixel by pixel is done by immediate thresholding method [6–8]. The input silhouette images are highly complex for processing, so the repetition of pixels in the images are grouped as feature subset. So, texture based features and Shape based features are extracted from the silhouette images using region of interest (ROI) from the silhouette image. These subsets are extracted using Gray level Covariance Matrix (GLCM) [9-11] and reduced by the Particle swarm optimized (PSO) algorithms. In terms of human recognition, dynamic postures increases the challenge of analysis. Gait changes with respect to velocity. Features collected from the silhouette image by GLCM (Gray level Co-variance matrix) and region of interest (ROI) are optimized by PSO to select the best features from the feature list [12, 13]. In some cases, pattern of a silhouette belongs to one or more cluster. Fuzzy clustering helps to classify the pattern more meaningfully. Clustering or grouping patterns unite patterns of same silhouette. Fuzzy probability is followed to select best match from the template gallery [14-19]. The pixels of template image and captured images are matched by their corresponding probability [20]. Section 2 describes the block diagram of the proposed work. Section 3 describes the preliminaries of fuzzy probability. Section 4 describes the related works regarding person recognition through their silhouettes and gait specification. Section 5 describes the proposed methodology for person recognition and section 6 describes the conclusion of the work done. Section describes the future work.

#### 2. Block diagram of the proposed system

Figure 1 shows the block diagram of the proposed work. The gait images captured through the camera are saved and frame difference (FDAI) is found using weighted average method and automatic immediate thresholding is applied to segment silhouette from the image and the silhouette features are extracted using gray level co-variance and optimized using Particle swarm optimization method. The person can be recognized using the fuzzy probability method using the scores of the features [5, 8].

#### 3. Preliminaries of Fuzzy probability

Let P be the probability measure for the fuzzy set X.  $P(x_i)$  denotes the probability of  $x_i$ , where  $x_i \in X$ . Likewise A be the fuzzy set representing the fuzzy event.  $A = \{x, \mu_A(x) | x \in X\}$ . The degree of membership of  $x_i$  is represented by  $\mu_A(x_i)$ .

**Definition 3.1.** Let A, B be two fuzzy sets.

(a) The complement of A is denoted by A<sub>c</sub>.

$$A_c(x) = 1 - A(x)$$
 where  $x \in X$ .

(b) The intersection of fuzzy sets will also be a fuzzy set defined by

$$(A \cap B)(x) = T(A(x), B(x))$$

(c) The union of fuzzy sets will also be a fuzzy set defined by

$$(A \cup B)(x) = S(A(x), B(x))$$

where A and S are associative in each argument.

**Definition 3.2.** Let X, Y are the two fuzzy random variable. If X and Y are independent then each random variable in the set are also independent.

P(Y = y | X = x) == P(Y = y), for all x, y. where P be the probability

#### 4. Related works

From the previous researches, It was found that every individual has own unique walking style (gait), fingerprints and iris. While attempting to recognize the person with their biological feature, clothes, shoes, angel of capturing, distance between the person and device plays the major role in misidentification. The following works shows how the features of objects are collected for recognition.

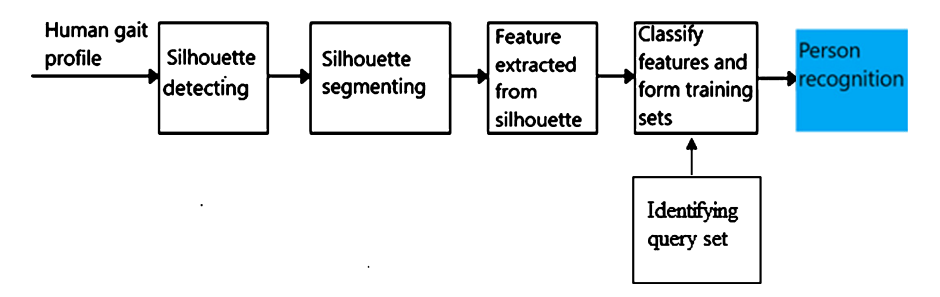


Fig. 1. Block diagram of proposed work.

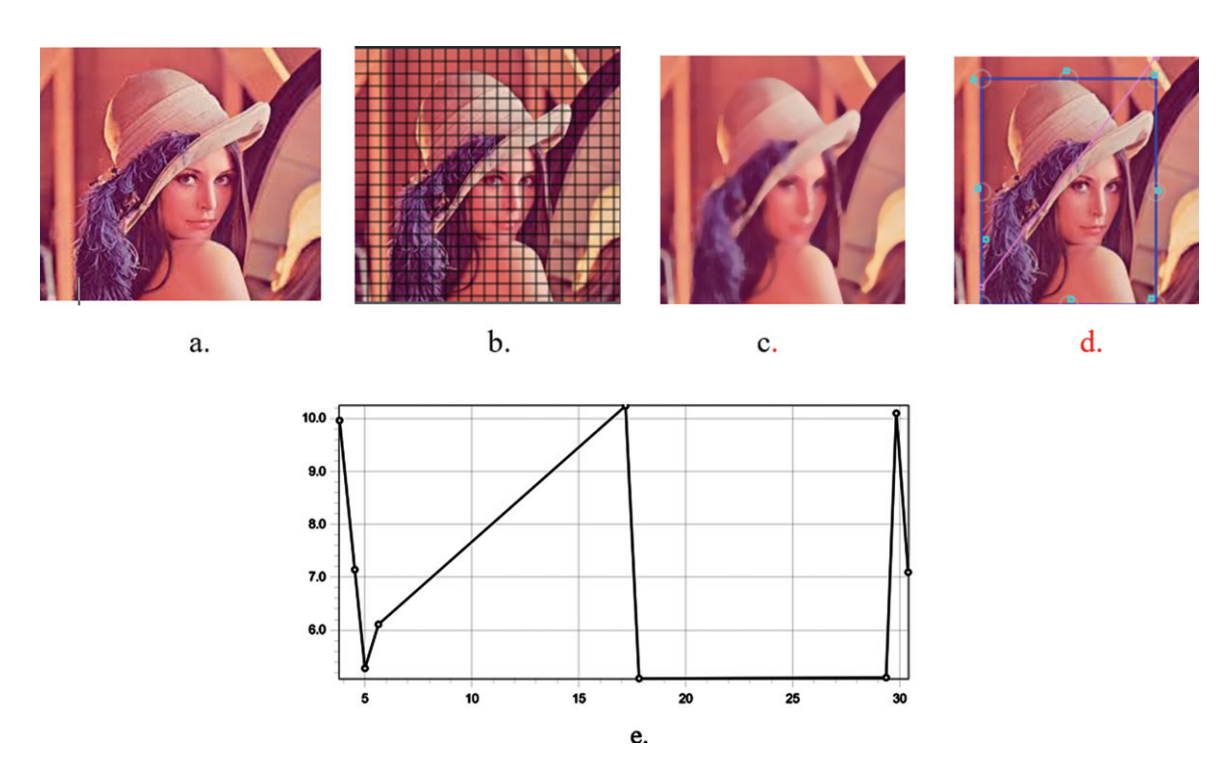


Fig. 2. a) lena.jpg input image, b) Dividing the Lena.jpg into blocks using edge histogram descriptor, c) mean average filter applied image, d) the X and Y selected 135degree diagnal, e) Line chart for the image with X and Y values using the below data. X-data used: [3.813,4.525,5,5.633,17.184,17.816,29.367,29.842,30.396] Y-data used: [9.966,7.144,5.279,6.11,10.241,5.086,5.103,10.102,7.095].

The gait of the person is captured using Kinect sensor, then the joints of the gait were allotted an unique rank number. Background substraction method is used to detect the person in the video sequence and Gaussian mixture model is used to segment the person image and PCA is used for averaging the video frames and classification is done using SVM vectors and Fisher component to recognize the person, LIBSVM is a software used to query the database [1, 2]. Features of movable places are segmented and saved as GEI and the pixel values of that area

more than threshold value are saved as features using PCA in [3]. The silhouettes are the segmented pieces used to recognize person using its similarity score in [4]. From the silhouettes unique features like clothes and the properties carried are extracted using Haralick features in [5]. The horizontally or vertically divided GEI needs K-Nearest Neighbor method for classifying the features. From [1, 2] the image features are ranked. Signal to Noise Ratio value is used for ranking and SVM, decision-tree and K-Nearest Neighbor are united to produce 98% accuracy. In [7],

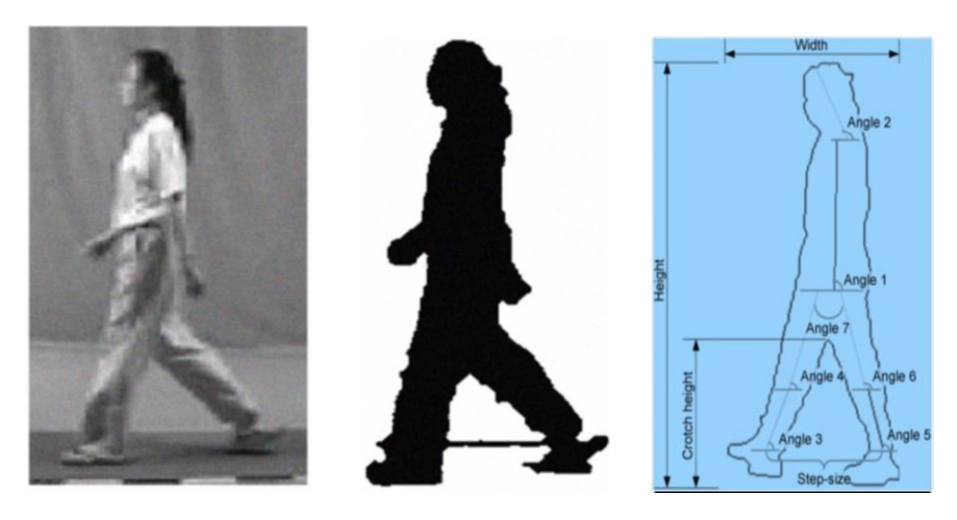
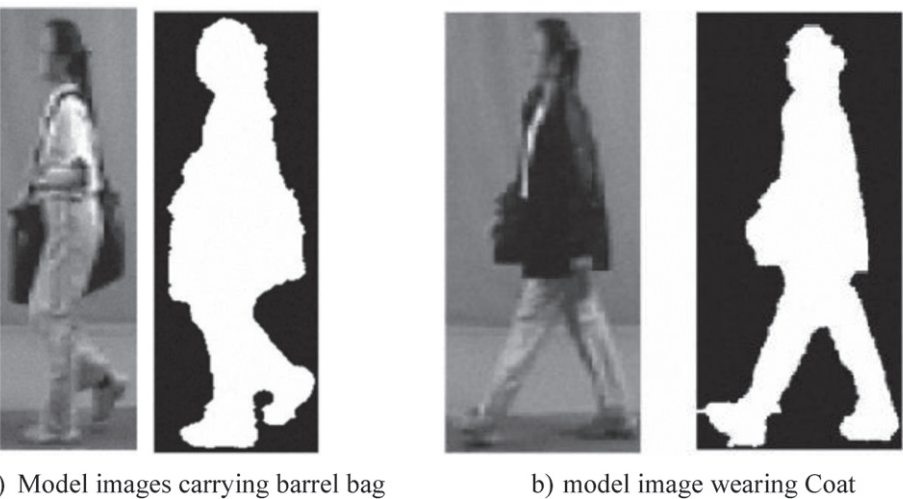


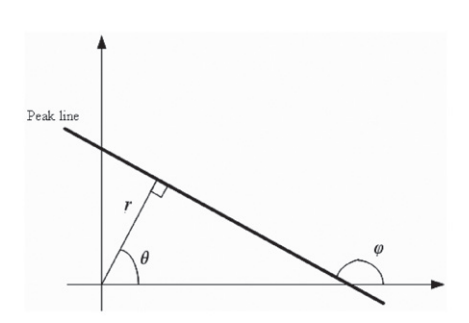
Fig. 3. The model silhouette is marked with angles for extracting features.



a) Model images carrying barrel bag



c) Person wearing shoulder bag



d) The angle of the silhouettes

Fig. 4. a), b), c) shows the model silhouettes of the captured video and d) shows the angle formed from the silhouette.

segmentation types are described in detail such as region based segmentation and edge based segmentation techniques. Depends on the features of image and similarities techniques are selected. Biometric systems are deployed for safety and security purposes using the features of face or gait used for detection and recognition. In [8] Back propagation method is used to learn the face features to recognize the person with an accuracy of acceptance ratio. For any type of image either it is a human image or medical image, extracted features only helps to differentiate between the original and fake. From [9] Classification reliability depends on the feature segmentation method and extracted features. Co-occurrence Matrix values are also used to extract features from the images. The fuzzy probability distribution [10] is explained how the preliminaries are helpful to find the probability of the random variable assumed. The probability value of the random variables must be filtered upon interests, In [11], five filtration methods with various probabilities are united to form a new filter with selected features, classified features and the time needed for execution. The average distance of the selected region [12] data to the neighbor is calculated and classified. The data with minimum distance is found using Euclidean measure. Each individual data are formed as a single class [13]. Classifying each data individually and cluster them to make a framework for tracking the objects using the Gaussian and Bayesian algorithm. Inorder to recognize a person, features are extracted based on appearance or model are discussed in [14]. An object detection from video surveillance is presented in [15]. The algorithm proposed in [15] uses DCT for compression of video, and correlational coefficients are used for detection of object and Bayesian rule is followed for locating the object. Features extracted from the image are considered for recognition. In [16] a silhouette feature based human action recognition is performed. The extracted features are used for learning the model. The training phase has many key poses used to recognize human action. In [17, 18] the stages involved in the biometric recognition system are discussed. Various levels of methods are united in biometric systems to provide better sensing and processing systems for human recognition. A sequential platform that collects data that meets the identification, the database profile trained for processing and operation and the parameters initially set to obtain the result of identification are highly suggested in [19]. But From [20], feature selection method is described to found the percentage of body fat. Finally feature selection

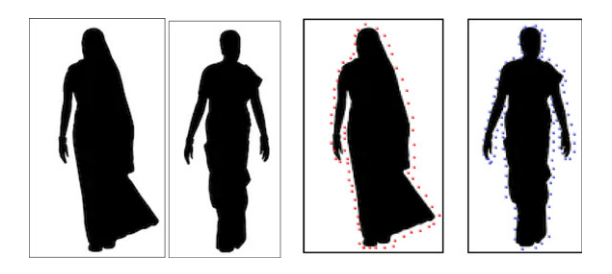


Fig. 5. The model silhouttes with different dresses that gait features cannot be captured correctly because of the clothes wored by the person.

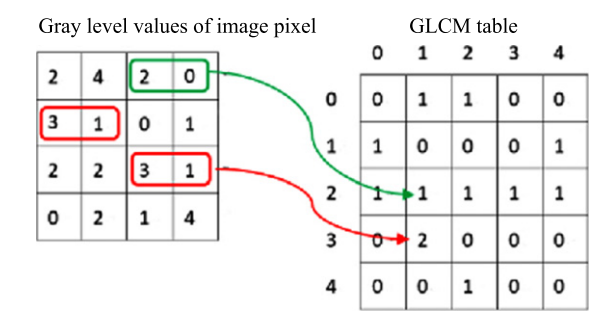


Fig. 6. the output of the silhouette image pixel values stored in left side table and its corresponding covariance matrix saved in GLCM table.

is the important task have to done before recognition. The ability to optimize features that satisfies the requirement is an challenging task.

### **5. Proposed Methodology for person recognition using gait images**

In fact each and every person have their own style of walk and walking speed. For this research, gait cycles stored in the National Laboratory of Pattern Recognition (NLPR) gait database and CASIA gait database are used. Human recognition for smart home safety is planned in 5 steps. This initial step was modeled by collecting human gait through the Grid-eye sensor fixed with the RGB-depth camera. The gait profile contains the number of images captured within the certain period as like in [1].

#### 5.1. Grid eye sensor

The Grid-eye Infrared thermopile sensor is used to detect the human. The silicon lens is attached with sensor for image formation. It detects the human using infrared radiation. The thermopile sensors con-

sists of numerous thermocouples arranged in 8\*8 series of grid without contact with each other for measuring temperature. Each and every thermopile records temperature value. Thus overall 64 temperature values are stored. Grid-eye extends its view to 60° in both horizontal and vertical directions upto 5 meters. The Grid-eye sensor is used to detect human at stationary position.

#### 5.1.1. RGB-depth camera

Grid-eye sensor attached with RGB-depth camera to capture the gait based on the movement and estimating the 3-D view of the human body joints without any locating bounding boxes. If anybody walks before the camera, the infrared radiations detect the human and wakes up the camera to capture the pose depth. The camera is placed at 1 meter from the floor distance to capture all parts of the body. The gait cycle (gait profile) consists of person gait details captured in 11 focus view based on variations such as angle, clothes wearing and carrying properties are considered [1–3].

### 5.2. Image averaging or Silhouette detection using frame difference method

Gait cycle:

Frames are the patterns captured and grouped together as one gait cycle. A gait cycle is the full walking pattern of an individual. A walking pattern is the oscillation of the legs from floor to up marching. Frame rate depends on the number of frames captured in the specific duration. Frame differencing is the method used to find the average image from all the captured image.

### 5.2.1. Pseudocode for Frame difference average image (FDAI) function

Frame Difference Average Image method (FDAI) fills the incomplete pixels in the silhouette pattern using the membership values of the clusters [4, 5].

*Input*: All the captured images are given as input *Output*: Average image

Step 1: Each images are splitted into two parts. Pixels occupied in the object and pixels outside the object within the image. Silhouette models are represented as D (x, y, t). So, D  $\in$  I and x and y are the coordinates of the image, and t is the index of the frames.

Step 2: Average energy image (A) finding: It converts the silhouettes into 2D-grey image. It is

computed by

$$A(x, y, t) = \frac{1}{N} \sum_{t=1}^{N} D(x, y, t), \qquad (1)$$

Where N is the total number of frames in the captured video.

Step 3: If the segmented silhouette are not smooth, because of the noise or uneven edges and fake spots, the normalization factor q is applied to the extracted silhouettes for smoothing the edges. Then q is computed by,

$$q = \frac{1}{n^2} \sum_{i=1}^{n} \sum_{j=1}^{n} |Pi - Pj|$$
 (2)

Where n is the number of points normalizing the pixels P, i and j be the starting and ending pixel number.

Step.4: The smooth silhouettes  $F_s(x, y, t)$  are calculated by

$$F_s(x, y, t) = \begin{cases} 0 \text{ if } A(x, y, t) \ge A(x, y, t - 1) \\ A(x, y, t - 1) - A(x, y, t), \text{ Otherwise} \end{cases}$$
(3)

Step 5: Using Eqn. (2) and (3), FDAI is calculated by

$$F_d(x, y, t) = F_s(x, y, t) + g(x, y)$$
 (4)

Using FDAI (F<sub>d</sub>) the unique differences noted in the images are averaged and normalized.

## 5.3. Edge detection and segmentation using wavelet transform automatic thresholding (WT-AT)

The wavelet transform method is used to detect the edges of the average image. Using the histogram of the image, the image details are highlighted. The difference between the white and gray values of the image pixels are used to calculate the gradient value. The gradients are calculated in all the four directions without missing the edge points. Later automatic thresholding method is used to calculate the threshold of the image histogram. The ratio of the total number of pixels in a block is used to set the initial threshold. The area located on the sides of the selected threshold are fixed as the max and min value [6–8, 21]. Here, immediate thresholding method is employed for silhouette segmentation

#### 5.3.1. Pseudocode for WT-AT method

- Step 1: The histogram value of the average image F<sub>d</sub> is taken as an initial threshold value T
- Step 2: divide the image  $F_d$  into S1 and S2 based on the threshold value
- Step 3: Calculate the intensity value I1 for image S1 and intensity value I2 for image S2 and In for Sn.
- Step 4: If I1 < T, the pixels of an silhouette area is replaced with a black pixel and if I1 > T, silhouette pixels are replaced with white pixels.
- Step 5: Calculating the average mean M1 and M2 of the two images S1 and S2 with their corresponding thresholds
- Step 6: Calculate the new threshold value T1 by averaging M1 and M2.
- Step 7: If T1 lies within the specified block, select the region for segmentation or else apply T1 as the new threshold value to the original image
- Step 8: restart the process to select the new threshold or stop the selection

#### 5.4. Features of the silhouette

Features are special notable fragments. For images, edges, corners, blobs and ridges are the types of features practiced for years. Features remain static to the transformation operation like rotation, translation and scaling. Texture features are splitted by regions of interest and specified by the scattering of energy level of neighborhood pixel. Refer Table 1 for the features noted from the given silhouettes. From that some of the features are described below.

#### 5.4.1. Area

Area is the number of pixels in the specified image region [9, 10].

#### 5.4.2. Bounding box

The height and width of the silhouette is calculated by the rectangular box bounded over the silhouette. The height of the box directly proportional to the height of the silhouette and vice-versa the width [9, 10].

#### 5.4.3. Eccentricity

It refers to the correlational distance between the centroid and its major axis length. Example, The footstep length is the distance between the left leg and right leg while walking [9, 10]. It is found using the

Euclidian distance (see in Fig. 3). To find the thigh angle,

$$Angle 7 = Angle 6 - Angle 4 \tag{5}$$

#### 5.4.4. Euler Number

It refers to the difference between the number of segments and the number of joints in the image region. Example, dividing the silhouettes based on anatomy. So, silhouettes are segmented into 10 body segments based on the human anatomy. Based on the centroid, the upper human parts appeared above the centroid is the head, neck and torso. The lower human parts appeared below the centroid is the hip, legs and feet. Further, they are divided into right side hip with thigh, right leg knee to foot joint, right foot joint to floor, left side hip with thigh, left leg knee to foot joint, left foot joint to floor (see in Fig. 3).

#### 5.4.5. Extent

It refers to the correlation of the pixels in the image region to the pixels in total bounding box.

Example, if the targeted region is the human face, quality silhouettes of facial profiles are referred. Duplicating the captured silhouette by shifting the targeted region to left, up and then down relatively proportional to the actual area of the template silhouette. Then place the duplicated silhouettes over the template silhouette and extract the excess region over the silhouettes [11].

#### 5.4.6. Convex Area

The total number of pixels present in the image outcurve. Example, the property the person carried along with them [11].

#### 5.4.7. Orientation

It refers to the angle between the x-axis and sits corresponding y-axis [11]. Example, the foot-step length of the person, marching length, marching speed, pulse and hip angles are used for gait analysis (see in Fig. 4)

#### 5.4.8. Solidity

It specifies the proportion of the pixels in the skeletal outcurve of the image region. It is calculated as the ratio of the total area and the convex area. Example, silhouettes of the people wearing different dresses based on the climatic condition and the culture they related. Thus the dressing practice highly affects the recognition accuracy [11].

#### 5.5. Feature Extraction using Grey level Co-variance matrix based on the area of interest

Texture based features are described from the silhouette image using edge histogram descriptor. The feature subsets are extracted using Gray level Covariance Matrix (see in Fig. 6) and reduced by Particle swarm optimized (PSO) algorithms. The GLCM is used to find the distance between the blocks of image, the location angle relationship of blocks and to calculate he occurrence of gray-level pixel in all the direction either horizontal, vertical, diagonal or adjacent. The image features or blocks composed of individual particles or pixels. Each particles has attribute value which are directly or indirectly depends on the behaviour and location of the particle.

### 5.5.1. Pseudocode for best feature selection using GLCMPSO

Input: Features extracted and optimized from the image

Output: best features are filtered

Step 1: define each block in terms of i, j matrix using GLCM and find the number of times the pixel occurs in specific location of blocks

Step 2: make the GLCM symmetric by adding the matrix with its transpose

Step 3: normalize the GLCM by dividing each element by the sum of all elements

$$\sigma(x, y) = \frac{1}{n-1} \sum_{i=1}^{n} (x - \bar{x}) (y - \bar{y})$$

Step 4: Initialize each feature with random position and their velocity within the block

Step 5: Define the feature subset f and its boundary as min and max, where f = 1, 2..., n

Step 6: For best feature selection:  $P_f$ ,  $V_f$ , the local feature  $L_f$ , global feature  $G_f$  and nearest neighbour  $N_f$  are combined together to get  $U_f$ . Where,

$$U_f = WV_f + \rho 1 \text{r1} (G_f - P_f) + \rho 2 \text{r2} (L_f - P_f) \dots$$
(7)

The coefficients W,  $\rho 1$ ,  $\rho 2$  adds weightage to the global feature and local feature which determines the new velocity. The parameters r1 & r2 are the random vectors with values lies between 0 & 1.

Step 7: Update the new position of the particle, Hence  $NP_f = P_f + V_f$ If  $NP_f < P_f$  then resume the local feature as  $Np_f \leftarrow P_f$ If  $P_f < G_f$  then resume the global feature as  $G_f \leftarrow NP_f$ 

Step 8: Continue the steps 6 and 7 until the best position found for selecting the feature.

In the output of the GLCM table, element (2,0) contains the value 1 because there is only one occurrence of the feature in the input image. GLCM (3,1) contains the value 2 because there are two occurrence of the horizontally adjacent pixels. The features extracted using GLCM are listed in Table 1. The optimized output of GLCMPSO method are listed in Table 2.

#### 5.6. Classification of feature subset

Images are made up of numerous pixels with various color combination. The correlation value and locational relationship angles are considered for grouping the features. The features are classified for ease the recognition part. In the feature learning method K-nearest neighbor method is used to train noisy large data. For every new blocks, objective function called distance D is generated, approximated and applied to the neighborhood. The disadvantage of Support Vector algorithm forced to find the distance of each training blocks or features. In the feature classification part, the distance of the N-vectors of the blocks are grouped and formed a similarity function k which would nearly closer to the feature vector. The average distance between the newly arrived features and the support feature vectors are also calculated. Based on the distances, the features are grouped as a single class. The accuracy of classification method proposed is compared with the existing and listed in Table 4.

### 5.6.1. Pseudocode for Nearest Support Feature Vector (NSFV) algorithm

Input: Set of features as S, proportional values of each features as M, classification definition as  $\varepsilon$ , training set as R, support vectors as  $SV_i$ . where  $SV_I \in R$  (i = 1, 2, ..., m) and Difference D,

*Output:* multiple features are classified based on their support vector values.

For each feature set do For i, j = 1 to m do If D (SVi, SV<sub>j</sub>)  $< \varepsilon$ 

Table 1
Contains the features detected using edge histogram detector and calculated the value using GLCM

S.No	Feature	Feature name	Calculated value
1	Shape	Area	737
2	Shape	Centroid	114.5726
3	Shape	Bounding Box	84.5
4	Shape	Major Axis Length	70.592
5	Shape	Minor Axis Length	46.2697
6	Shape	Eccentricity	0.7552
7	Shape	Orientation	-67.802
8	Shape	Convex Hull	142.5
9	Shape	Convex Area	1839
10	Shape	Filled Area	1703
11	Shape	Euler Number	<b>–7</b>
12	Shape	Extrema	142.5
13	Shape	Solidity	0.4008
14	Shape	Extent	0.2955
15	Shape	Perimeter	180.4092
16	Texture	Autocorrelation	1.211
17	Texture	Contrast	0.034
18	Texture	Correlation	0.878
19	Texture	Cluster Prominence	32.13
20	Texture	Cluster Shade	0.92
21	Texture	Dissimilarity	0.017
22	Texture	Energy	0.968
23	Texture	Entropy	0.126
24	Texture	Homogeneity	0.993
25	Texture	Sum of Square: Variance	1.1968
26	Texture	Sum Average	2.0841
27	Texture	Sum Variance	4.4117
28	Texture	Sum Entropy	0.116
29	Texture	Difference Variance	0.0348
30	Texture	Difference Entropy	0.0694
31	Texture	Information measure of correlation	-0.6087
32	Texture	Inverse difference normalized	0.9982
33	Texture	Inverse difference moment normalized	0.9995

$$SV_{j} \leftarrow SV_{i};$$

$$Update \ SV_{j};$$

$$SV_{j} = P_{i}$$

$$end \ for$$

DET (Detection Error Trade-off) graph

It plots with FPR in X-axis and FNR as Y. The curve slants closure to the bottom of the graph shows the best recognition performance.

ROC (Receiver operating Characteristic) curve It plots with true positive rate (TPR) in X axis and false positive rate (FPR) in Y axis. The best recognition performance occupies at the top of the plot.

### 5.7. Recognizing person by selecting the best match score of the feature subset

It is difficult to classify and compare person in moving condition with carrying properties. If the carrying condition is also considered as part of recognition, the accuracy and the rate of recognition will be very low. Using the proposed classifier NSFV, the optimized features are initialized as  $P_i$ . The database G with m samples (i = 1, 2,...m). The newly entered image is Q with unknown features Qj (j = 1,2,...,n) having more than one feature not stored before in G. For estimating the CMS, each and every Qj, must be matched with every gallery set and a confident score S for ( $P_i$ ,  $Q_j$ ) are computed for n x m times.

$$S = \{s(Qj.P1), s(Qj.P2), s(P'_j.P3), \dots, s(P'_j.Pm)$$
(8)

The query Qj is assigned the rank  $k_j = K$ . Then the matching feature from G is  $P_i(k)$ . There are K set of n rank estimates and must be one estimate for each query feature Qj. For each query there is one estimate likewise every feature is ranked only if there is correct identity  $C_m$  from the sorted list of gallery.

$$C_{m} = C_{m}(Qj;G) \tag{9}$$

 $\label{eq:table 2} \mbox{Table 2}$  Features extracted from the images using GLCM and optimized (reduced) using particle swarm method

Features found using GLCM	Backpropogation	Swarm Intelligence	Proposed optimized feature set GLCMPSO method
Solidity	Autocorrelation	Autocorrelation	Aut Correlation
Bounding Box	Bounding Box	Bounding Box	Bounding Box
Centroid	Centroid	Centroid	Centroid
Autocorrelation	Cluster Prominence	Cluster Prominence	Cluster Prominence
Contrast	Cluster Shade	Cluster Shade	Cluster Shade
Extent	Contrast	Contrast	Contrast
Orientation	Convex Area	Convex Area	Convex Area
Eccentricity	Convex Hull	Convex Hull	Correlation
Perimeter	Correlation	Correlation	Difference Entropy
Sum Average	Difference Entropy	Difference Entropy	Dissimilarity
Sum of Square: Variance	Difference Variance	Difference Variance	Eccentricity
Correlation	Dissimilarity	Dissimilarity	Energy
Major Axis Length	Eccentricity	Eccentricity	Entropy
Cluster Prominence	Energy	Energy	Extent
Cluster Shade	Entropy	Entropy	Filled Area
Convex Area	Euler Number	Euler Number	Orientation
Extrema	Extent	Extent	Solidity
Filled Area	Extrema	Extrema	Sum Average
Convex Hull	Filled Area	Filled Area	Sum Entropy
Dissimilarity	Homogeneity	Homogeneity	••
Sum Variance	Information measure of correlation	Orientation	
Sum Entropy	Inverse difference normalized	Perimeter	
Minor Axis Length	Orientation	Solidity	
EquivDiameter	Perimeter	Sum Average	
Euler Number	Solidity	Sum Entropy	
Energy	Sum Average	Sum Variance	
Homogeneity	Sum Entropy		
Entropy	Sum Variance		
Difference Variance			
Difference Entropy			
Information measure of correlation			
Inverse difference normalized			
Inverse difference moment normalized			

Table 3
The performance metrics for feature classification accuracy

Metrics	Calculating formula
Accuracy	$\frac{TP + TN}{TP + FP + FN + TN}$
Precision or positive predictive value (PPV)	$\frac{TP}{TP + FP}$
F-rate	2 (Precision * Recall) (Precision + Recall)
Specificity or True negative rate (TNR)	TN TN + FP
Sensitivity or Recall or True positive rate (TPR)	TP TP + FN
False Positive rate (FPR)	FP TN + FP
False Negative rate (FNR)	$\frac{FN}{FN + TP}$
True Positive (TP)	No of pixels correctly identified as silhouettes selected for
True Negative (TN)	No of pixels correctly identified as non silhouettes
False Positive (FP)	No of pixels incorrectly identified as silhouette features
False Negative (FN)	No of pixels incorrectly identified as non silhouette features

Table 4
Comparitive Classification results of the feature classifiers accuracy based on the total number of images used

Classifiers	Total images used	True positive (TP)	True negative (TN)	False Positive (FP)	False Negative (FN)	Precision	TPR	TNR	FPR	FNR	Accuracy	F-rate
K-nearest	45	35	10	10	9	0.7777	0.7954	0.5	0.5	0.2045	0.7031	0.7864
	80	69	11	13	10	0.8625	0.8734	0.4583	0.5416	0.1265	0.7766	0.8679
	100	90	10	6	6	0.9	0.9375	0.625	0.375	0.0625	0.8928	0.8983
SVM	45	39	6	10	8	0.8666	0.8297	0.375	0.0625	0.1702	0.7142	0.8477
	80	74	6	9	6	0.925	0.925	0.4	0.6	0.75	0.8421	0.905
	100	92	8	8	3	0.92	0.9684	0.5	0.5	0.031	0.9009	0.9135
NEAREST SUPPORT	45	41	4	10	8	0.9	0.8367	0.2857	0.0714	0.1632	0.7142	0.8671
FEATURE VECTOR(NSFV)	80	74	6	4	4	0.925	0.9487	0.6	0.4	0.0521	0.9090	0.9367
(hybrid of existing)	100	94	6	3	1	0.94	0.9894	0.666	0.333	0.0163	0.9615	0.964

The probability of rank estimation is Pr(k)(k = 1,...,m). For the query set and the gallery data, the  $P_r(k)$  of the matcher is estimated by

$$P_r(k) = \frac{1}{n} (\#k_j = k) \text{ where } k \in K$$
 (10)

That is, Cumulative match score (CMS) is calculated by the sum of P(k). So,

$$CMS(k) = \sum_{r=1}^{k} P(r)$$
 (11)

where k = 1, 2, ..., m

To identify new feature from the features Qj in the gallery set G, fuzzy rule chooses the highest ranking feature

$$C_m(Qj;G) = \{P_{(1)}, P_{(2),\dots,S_{(m)}}\}$$
 (12)

$$I_d(Qj) = I_d(d1) \tag{13}$$

Then

$$\begin{split} &I_{d}\;(Qj)\;\text{is Identified if }Qj\in\;C_{m}\;(Qj;G)\;\text{and}\\ &I_{d}\;(Qj)\;\text{is Identified if rank}\;K_{i}\;\text{of }Qj< K \end{split} \tag{14}$$

for every new search the authentic scores of the correctly matching feature can be find as better threshold on the imposter scores s  $(Qj,P_i)$  and  $I_d(P_i) \neq I_d(Qj)$  from the database. The relationship between the CMS, TPR, TNR and F-rate from Table 3 is referred for 1:1 matcher from the gallery set.

To select m random match from the gallery of size m:

- 1. The authentic score  $X = s(P_i, Q_j)$  i.e  $P_i \in G$  where  $P_i$  and  $Q_j$  are from same
- 2. Imposter score is Y. For m size gallery there are m-1 imposter scores  $\{Y_1, ..., Y_{m-1}\}$ , i.e.,  $\{s(P_i, Q_j), i = 1, ..., (-1), (+1), ..., n \text{ and } j = 1, ..., (-1), (+1), ..., m\}$ , Though Qj is listed in the gallery but Qj not matching to  $P_i$ .

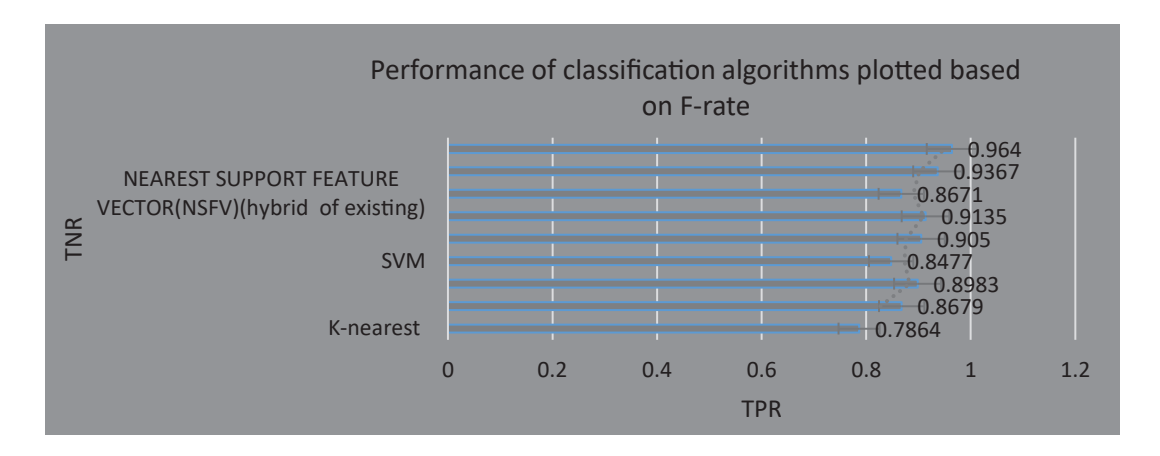


Fig. 7. Clustered chart shows the F-rate performance of NEAREST SUPPORT FEATURE VECTOR(NSFV) classifier compared with svm and k-nearest methods.

Table 5 Accuracy comparision of classifiers used

Classifier	K-nearest	SVM	Nearest Support
performance			Feature Vector (NSFV)
			(hybrid of existing)
Accuracy	0.8928	0.9009	0.9615

In fuzzy system, input, output with two corresponding membership values are derived. Authentic score X and imposter score Y are the two membership values used in fuzzy probability.

#### • If the database size m equals to 2 (m=2)

The newly arriving unknown query feature starts with j=1 (Qj) gives the XY value with authentic score as  $X=s(Qj, P_1)$  and imposter score  $Y=s(Qj, P_2)$ . The probability density function of X is f(x) and the probability density function of Y is g(y). Finally, the probability density function of f(X, Y) for f(X, Y) for f(X, Y) matcher will be f(X, Y)=f(X).

The rank probability of X and Y is calculated as,

$$P(1) = P_r \text{ (rank Qj is 1)} = P_r(X \ge Y),$$
  
 $P(2) = P_r \text{ (rank Qj is 2)} = P_r(Y > X)$ 
(15)

The fuzzy probability values of the silhouette images are chosen for selecting the perfect match from the gallery set. Using the Eq. (1) to Eq. (15) the probability of correct identification and probability of misidentification are found.

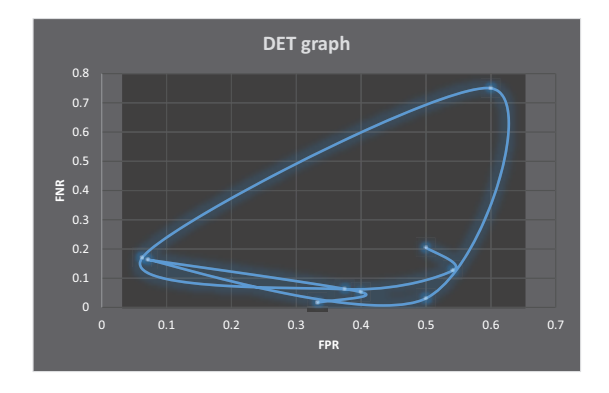


Fig. 8. Shows the performance of Nearest Support Feature Vector (NSFV) classifier through DET graph.

### 5.7.1. Pseudocode for fuzzy probability based person recognition

Algorithm Input: Video dataset containing human silhouettes

Output: human recognized based on best match feature score

- Step 1: Start
- Step 2: Analyzing the gait cycle containing n frames.
- Step 3: Detecting the silhouettes from the gait cycle using FDAI method ← call FDAI function
- Step 4: images are segmented from the gait cycle using Wavelet Transform and automatic Thresholding method ← call WT-AT method
- Step 5: Texture based features are extracted from the image using GLCM and PSO methods ← call GLCMPSO function

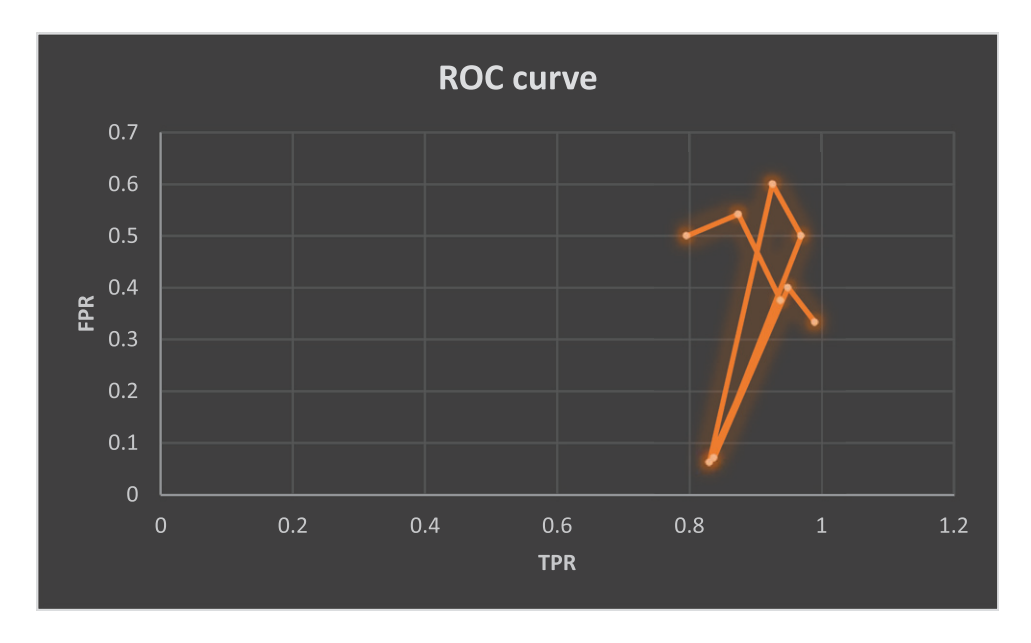


Fig. 9. Shows the performance of the NEAREST SUPPORT FEATURE VECTOR (NSFV) classifier through ROC curve.

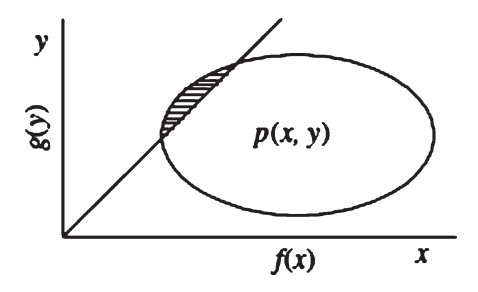
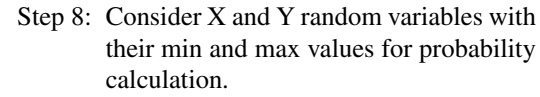


Fig. 10. The probability of misidentification when the size of the database m = 2.

Step 6: The optimized feature lists are clustered and classified based on its repetitive occurrence using Nearest Support Feature Vector (NSFV) ← call NSFV method

Step 7: The classes are labeled depends upon the support vectors k.

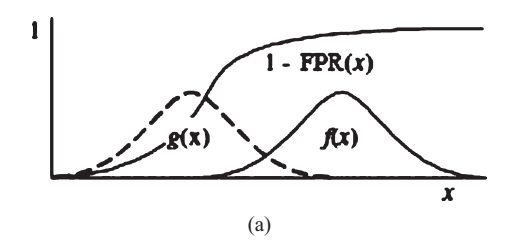


Step 9: The probability difference between the FPR and FNR is considered for recognition.

Step 10: Stop

### 5.8. Performance evaluation

From the Table 1 the values of the features are listed which are found using GLCM method. In Table 2 the shortlisted or optimized features are listed which are found using PSO. In Table 3 the performance metrics of the classifiers are listed. In Table 4 the comparative performance accuracy of the classifiers used are tabulated and found that Nearest support feature vector performs well. In Table 5 the accuracy of the classification algorithm is compared with the existing. In Table 6 Entropy, correlative quality measure, PSNR,



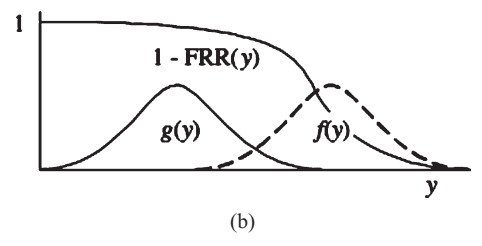
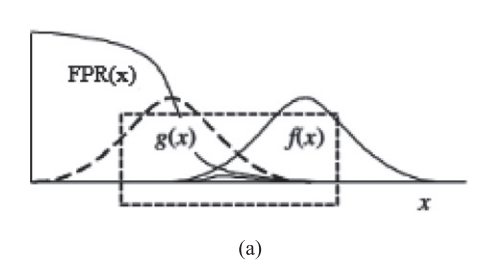


Fig. 11. The probability of correct identification when database size is m = 2 is the integral of f(x)[1-FPR(x)] and g(y)[1-FRR(y)].



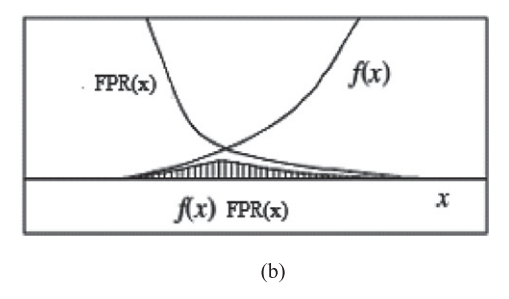
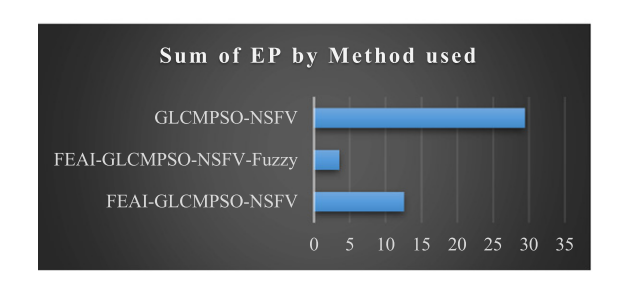


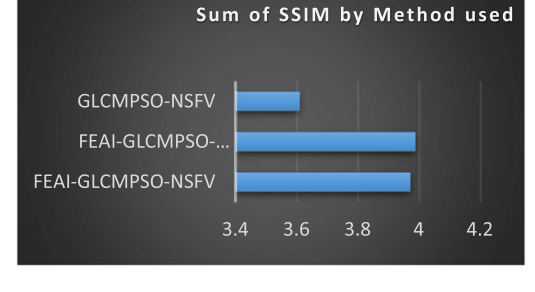
Fig. 12. a and b shows the probability of misidentification is the integral of f(x)FPR(x).

Table 6
Accuracy of Image recognition listed by Optimal parameters

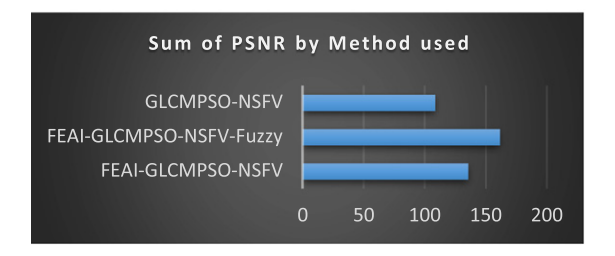
Image	Method used	EP	SSIM	PSNR	CQM
Mishra.jpg	GLCMPSO-NSFV	0.0147	0.9009	43.6937	34.0028
	FDAI-GLCMPSO-NSFV	0.0287	0.9933	34.8725	54.5813
	FDAI-GLCMPSO-NSFV-Fuzzy	0.0041	0.9982	45.9202	57.1044
Lena.jpg	GLCMPSO-NSFV	7.5809	0.9892	22.7278	34.0028
	FDAI-GLCMPSO-NSFV	8.5594	0.9933	27.7099	39.6381
	FDAI-GLCMPSO-NSFV-Fuzzy	1.8632	0.9972	36.9587	44.0911
ron-golden-1.jpg	GLCMPSO-NSFV	7.3568	0.8514	22.456	35.6456
	FDAI-GLCMPSO-NSFV	0.1974	0.9885	35.7556	46.3535
	FDAI-GLCMPSO-NSFV-Fuzzy	0.0059	0.9937	40.7648	47.2322
ashford-oaks-primary-8.jpg	GLCMPSO-NSFV	14.448	0.8668	19.7436	40.115
	FDAI-GLCMPSO-NSFV	3.762	0.9951	37.1563	49.374
	FDAI-GLCMPSO-NSFV-Fuzzy	1.6283	0.9976	37.7187	49.6327



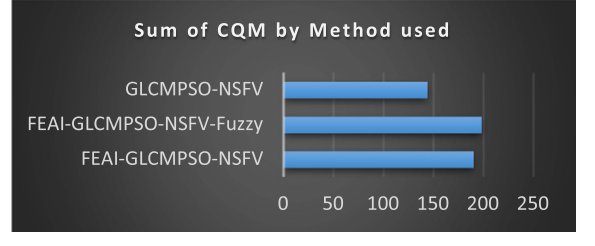
a. Entropy value must be smaller for the recognition algorithms



b. SSIM value must be greater compared to the other recognition algorithms



PSNR value must be greater compared to the other recognition algorithms



d. Correlative coefficient Quality measure value must be greater compared to other recognition algorithms

Fig.13. a, b, c and d shows the results of optimal parameters to prove the accuracy performance of fuzzy probability.

SSIM are calculated to show the performance of the hybrid methods.

### 6. Conclusion

From the proposed work, the person is recognized by the gait. The fuzzy probability method is used for comparing the probability value of the authentic and imposter scores generated from the NEAREST SUP-PORT FEATURE VECTOR(NSFV) algorithm. The relationship between the CMS, TPR, TNR and F-rate are calculated. The performance of the classifiers are found to be perfect and displayed by plotting the DET graph and ROC curve. The identified best classifier will occupies the bottom position in the DET graph and top most position in the ROC curve. If the classification part will be done clearly, the template matching from the gallery set will also be good. Thus the feature match scores are saved with the FPR and FNR values directly proportional to the probability value of the rank allotted to the features. The Proposed Fuzzy probability

### 7. Future work

Fuzzy probability based person silhouette recognition work can be considered for recognizing the person in schools, apartmental houses, shopping malls etc., In future skin texture features and image features are combined to recognize the person so that the recognition accuracy can be improved.

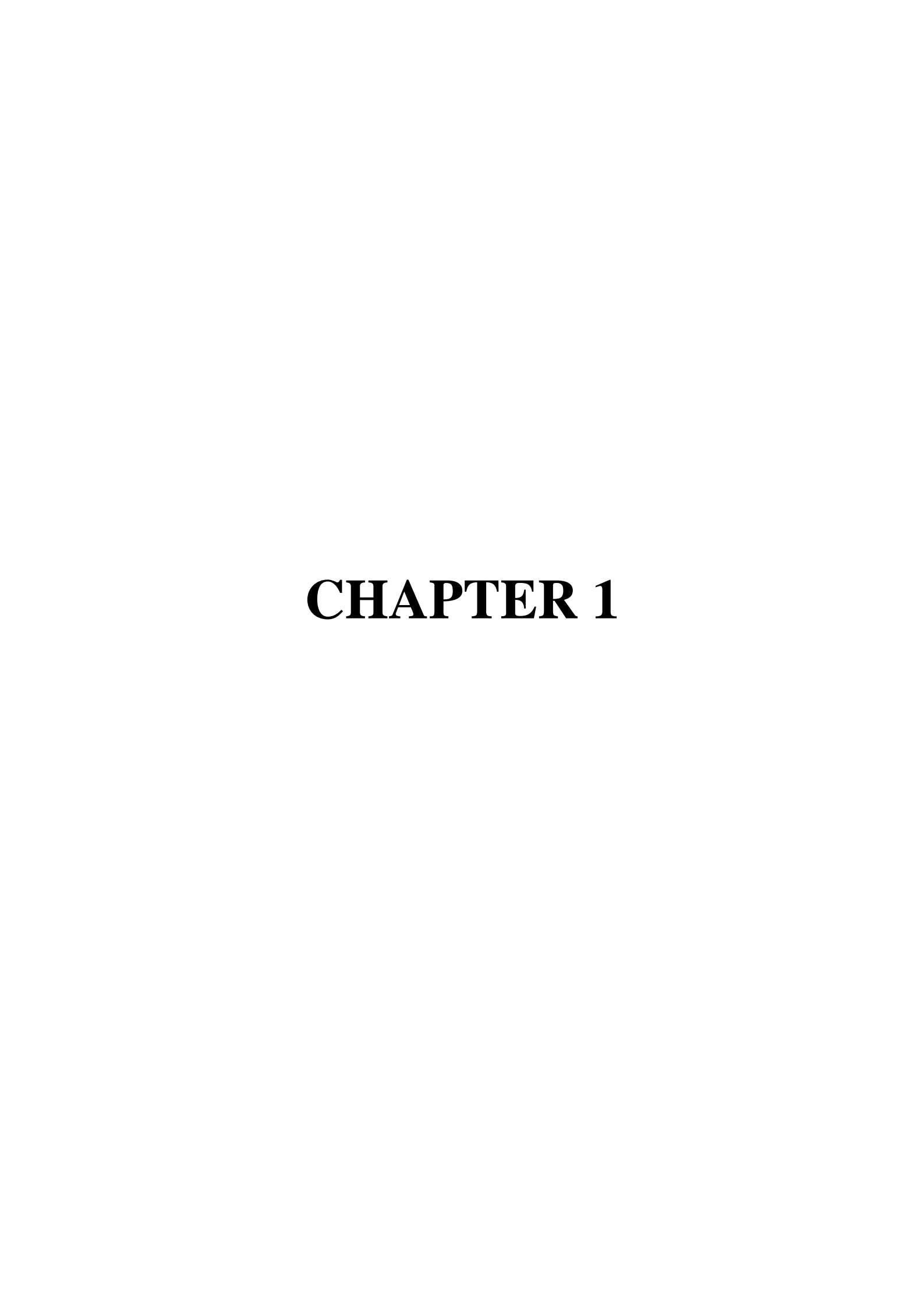
### References

- [1] B.M. Gowtham, K. Harshavardhan, G.C. Mohan, S.A. Nikhil and C. Prathap, Human Identification using Gait Recognition, *International Conference on Communication* and Signal Processing April 6-8, 2017, India, 978-1-5090-3800-8/17/\$31.00 ©2017 IEEE
- [2] O.V. Strukova1, L.V. Shiripova1 and E.V. Myasnikov1, Gait analysis for person recognition using principal component analysis and support vector machines, IV International Conference on "Information Technology and Nanotechnology (ITNT-2018).
- [3] M. Iftikhar, S. Karim, S. Rehman and A. Shaukat, Biometric based human recognition using gait energy images, Proc. SPIE 10649, Pattern Recognition and Tracking XXIX, 106490L (30 April 2018). https://doi.org/10.1117/12.2304737
- [4] N.A. Makhdoomi et al., Human Gait Recognition And Classification Using Similarity Index for various conditions, *IOP Conf. Series: Materials Science and Engineering* 53 (2013), 012069. doi:10.1088/1757-899X/53/1/012069

- [5] A.O. Lishani, L. Boubchir and A. Bouridane, Haralick Features for GEI-based Human Gait Recognition, 978-1-4799-8153-3/14/\$31.00 ©2014 IEEE.
- [6] A.J. Nair, R. Rasheed and K.M. Maheeshma, An Ensemble-Based Feature Selection and Classification of Gene Expression using Support Vector Machine, K-Nearest Neighbor, Decision Tree, Proceedings of the Fourth International Conference on Communication and Electronics Systems (ICCES 2019)IEEE Conference Record # 45898;IEEE Xplore ISBN: 978-1-7281-1261-9
- [7] D. Kaur, et al., Various Image Segmentation Techniques: A Review, *International Journal of Computer Science and Mobile Computing* 3(5) (2014), 809–814.
- [8] S. Tikoo and N. Malik, Detection, Segmentation and Recognition of Face and its Features Using Neural Network, J Biosens Bioelectron 7 (2016), 210. doi:10.4172/2155-6210.1000210
- [9] K.P.S. Shiji and V.S. Dharun, Extraction of Texture Features using GLCM and Shape Features using Connected Regions, *International journal of engineering and technology*, 2016. DOI:10.21817/IJET/2016/V8I6/160806254, Corpus ID: 53692978
- [10] E.D. Habil and T.Z. Nasr, The two scopes of fuzzy probability theory, Algebras Groups and Geometries 27(2) January 2010.
- [11] F. Gowmi, M. Aldasht and H. Tamimi, Efficient Feature Selection using Particle Swarm Optimization: A hybrid filters-wrapper Approach, 2019 10th International Conference on Information and Communication Systems (ICICS), ISSN: 2573-3346
- [12] G. Alimjan, T. Sun, Y. Liang, H. Jumahun and Y. Guan, A New Technique for Remote Sensing Image Classification Based on Combinatorial Algorithm of SVM and KNN, International Journal of Pattern Recognition and Artificial Intelligence 32(7) (2018), 1859012 (23 pages). DOI: 10.1142/S0218001418590127
- [13] N.L. Sowah, Q. Wu and F. Meng, A Classification and Clustering method for tracking multiple objects, Proceeding of IEEE conference on Computing and communication workshop and conference (cows), pp. 537, Jan 2018.
- [14] S.F. Kak, F.M. Mustafa and P. Valente, A Review of Person Recognition Based on Face Model, *Eurasian Journal of Science & Engineering*, ISSN 2414-5629 (Print), ISSN 2414-5602 (Online), Sep 2018. doi: 10.23918/eajse.v4i1sip157 EAJSE
- [15] K. Kalirajan and M. Sudha, Moving Object Detection for Video Surveillance, *The Scientific World Journal*, 2015, Article ID 907469, 10 pages, 2015. https://doi.org/10.1155/2015/907469
- [16] A.A. Chaaraoui and F. Flórez-Revuelta, A Low-Dimensional Radial Silhouette-Based Feature for Fast Human Action Recognition Fusing Multiple Views, Hindawi Publishing Corporation, *International Scholarly Research Notices* 2014, Article ID 547069, 11 pages.
- [17] A.D. Shetty, B.S. Disha and K. Suryanarayana, Detection and Tracking of a Human Using the Infrared Thermopile Array Sensor-Grid -EYE, 2017 International Conference on Intelligent Computing, *Instrumentation and Control Technologies (ICICICT)*, 978-1-5090-6106-8/17/\$31.00 @d2017 IEEE.
- [18] M.O. Oloyede and G.P. Hancke, Unimodal and Multimodal BiometricSensing Systems: A Review, *IEEE* 4 (2016), 2169–3536. DOI: 1109/ACCESS.2016.2614720

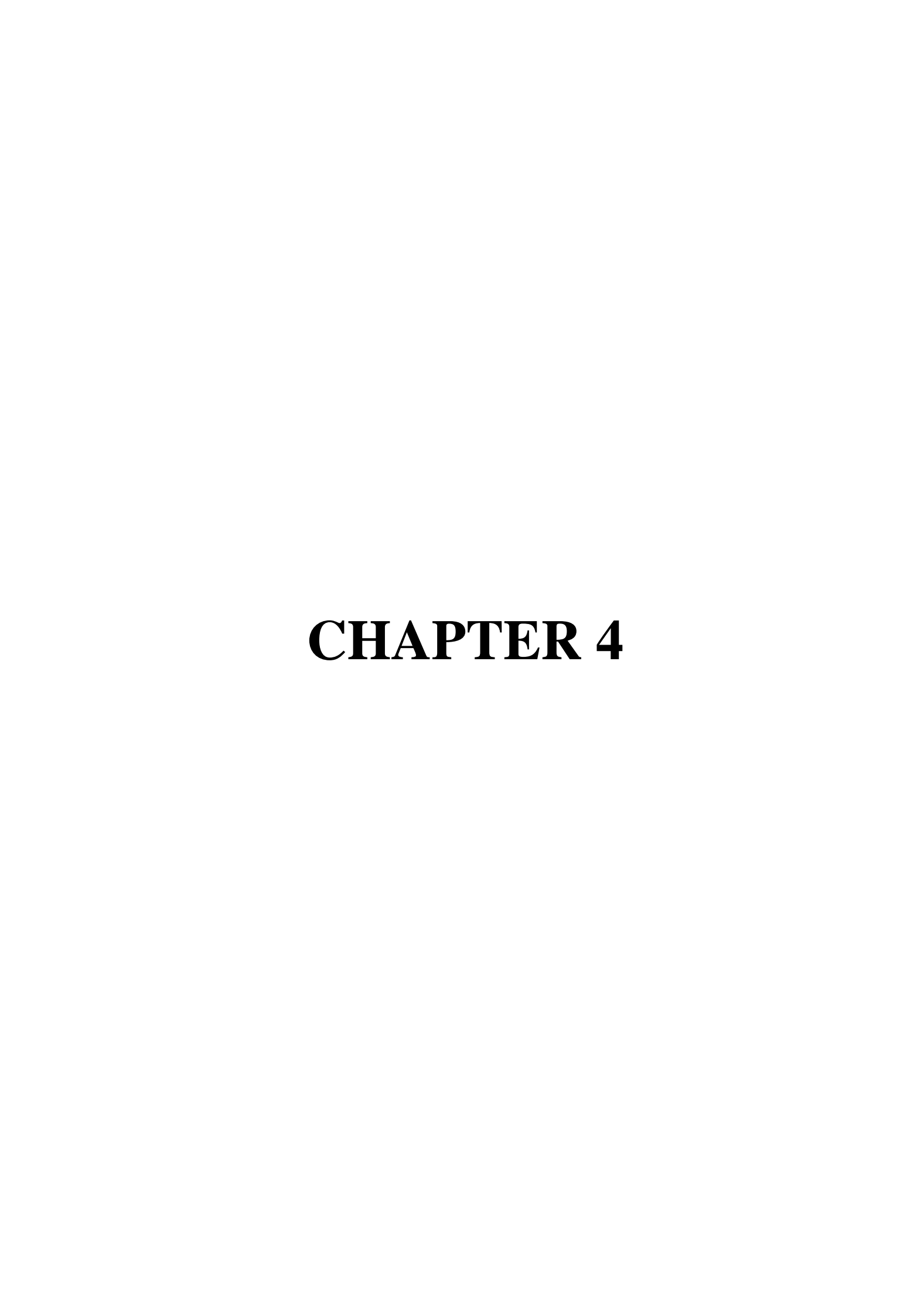
- [19] S. Mahmudova, The Ways of Increasing Quality of Human Recognition in Biometric Network Environment, *International Journal of Intelligent Information Systems* **6**(5) (2017), 56–61. doi: 10.11648/j.ijiis.20170605.11
- [20] A. Adam, Z. Ibrahim, N. Mokhtar, M.I. Shapiai, M. Mubin and I. Saad, Feature selection using angle modulated simulated Kalman filter for peak classification of EEG signals,
- SpringerPlus 5 (2016), 1580. DOI: 10.1186/s40064-016-3277.
- [21] B.B.S. Tawfik and M.M. El-Gazzar, Multiscale edge detection using wavelet transform compared to other methodologies, *International Journal of Mathematics and Computer Applications Research (IJMCAR)*, ISSN 2249-6955, 3(2) (2013), 103–114.

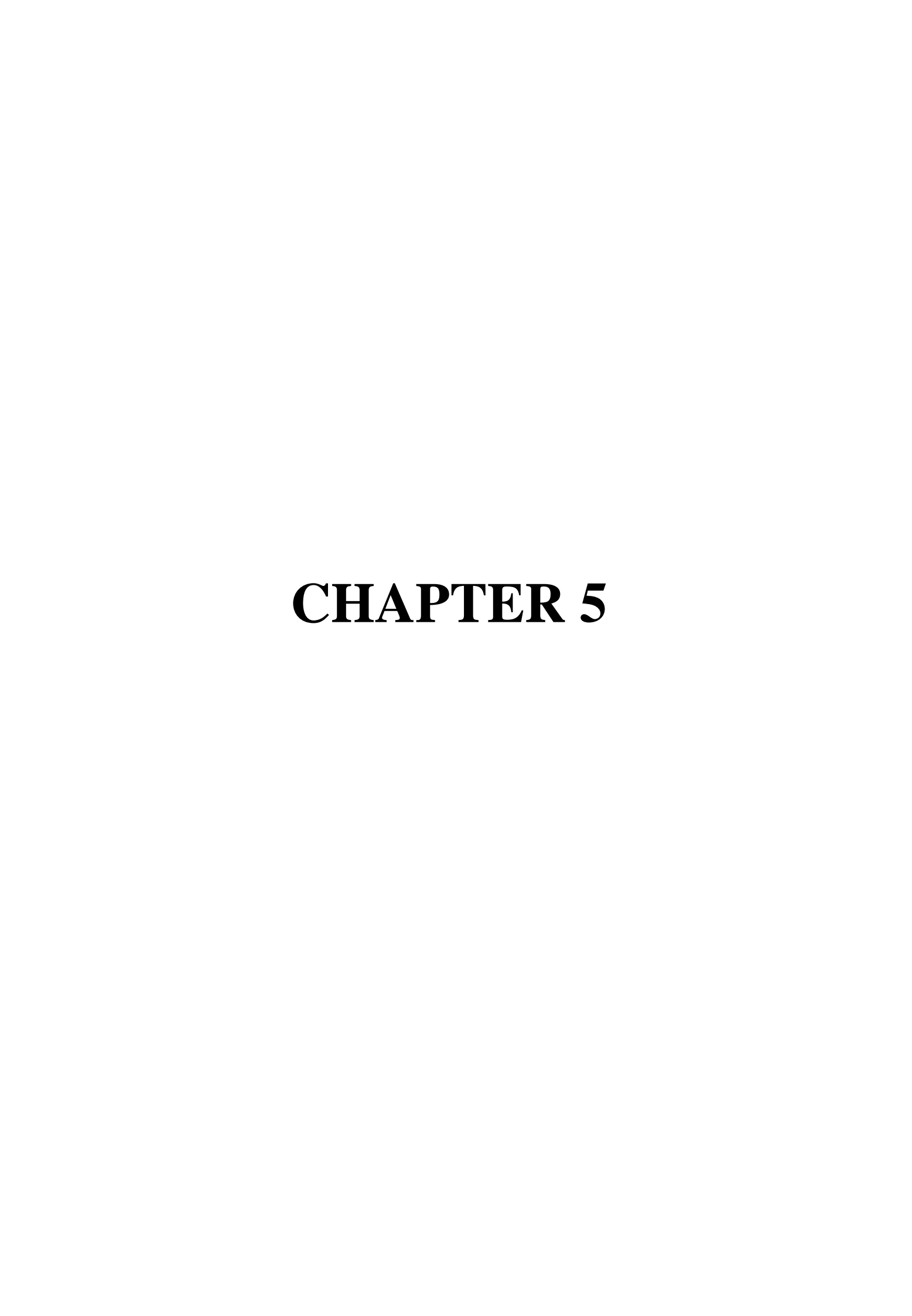


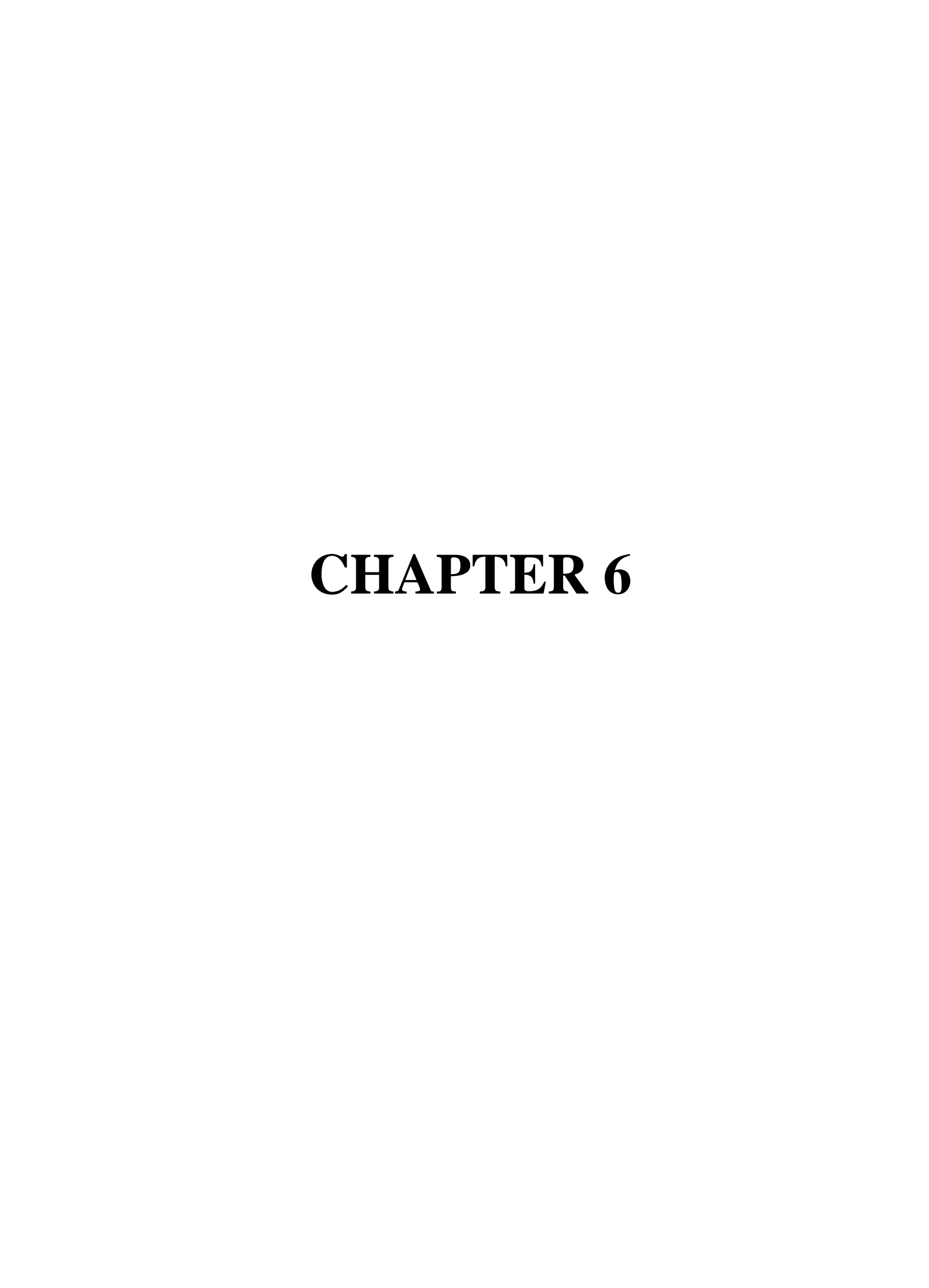


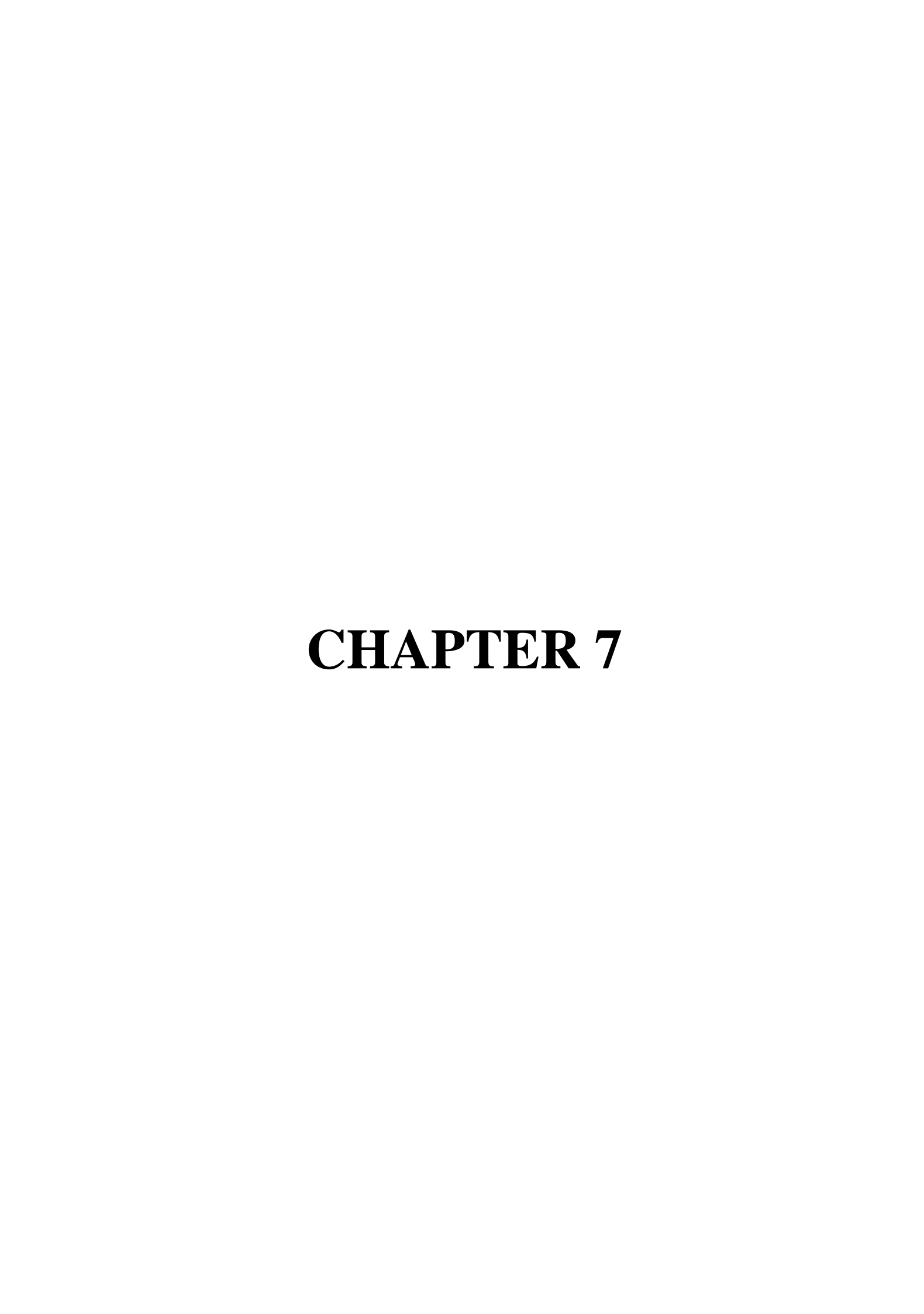
## CHAPTER 2

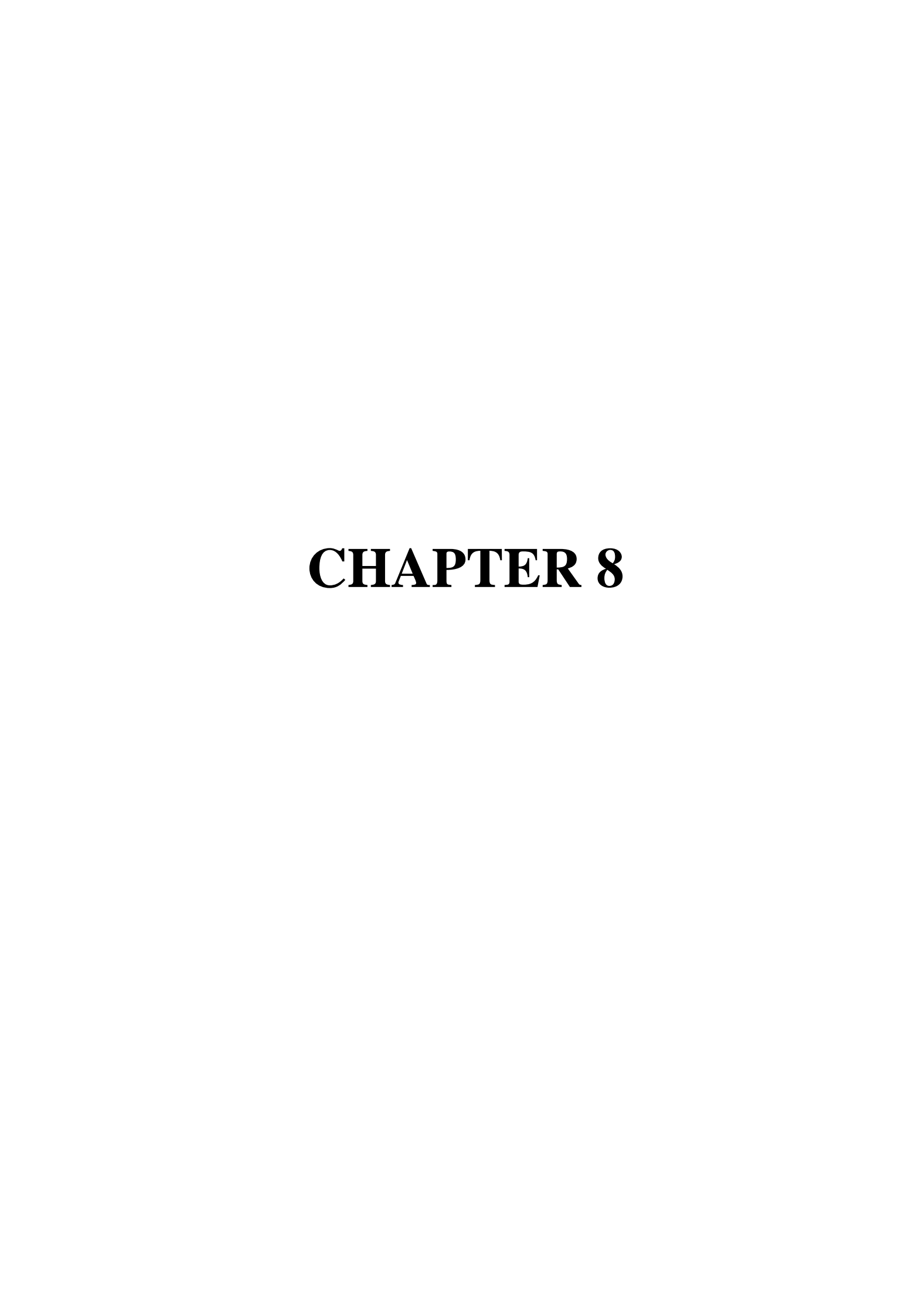
# **CHAPTER 3**

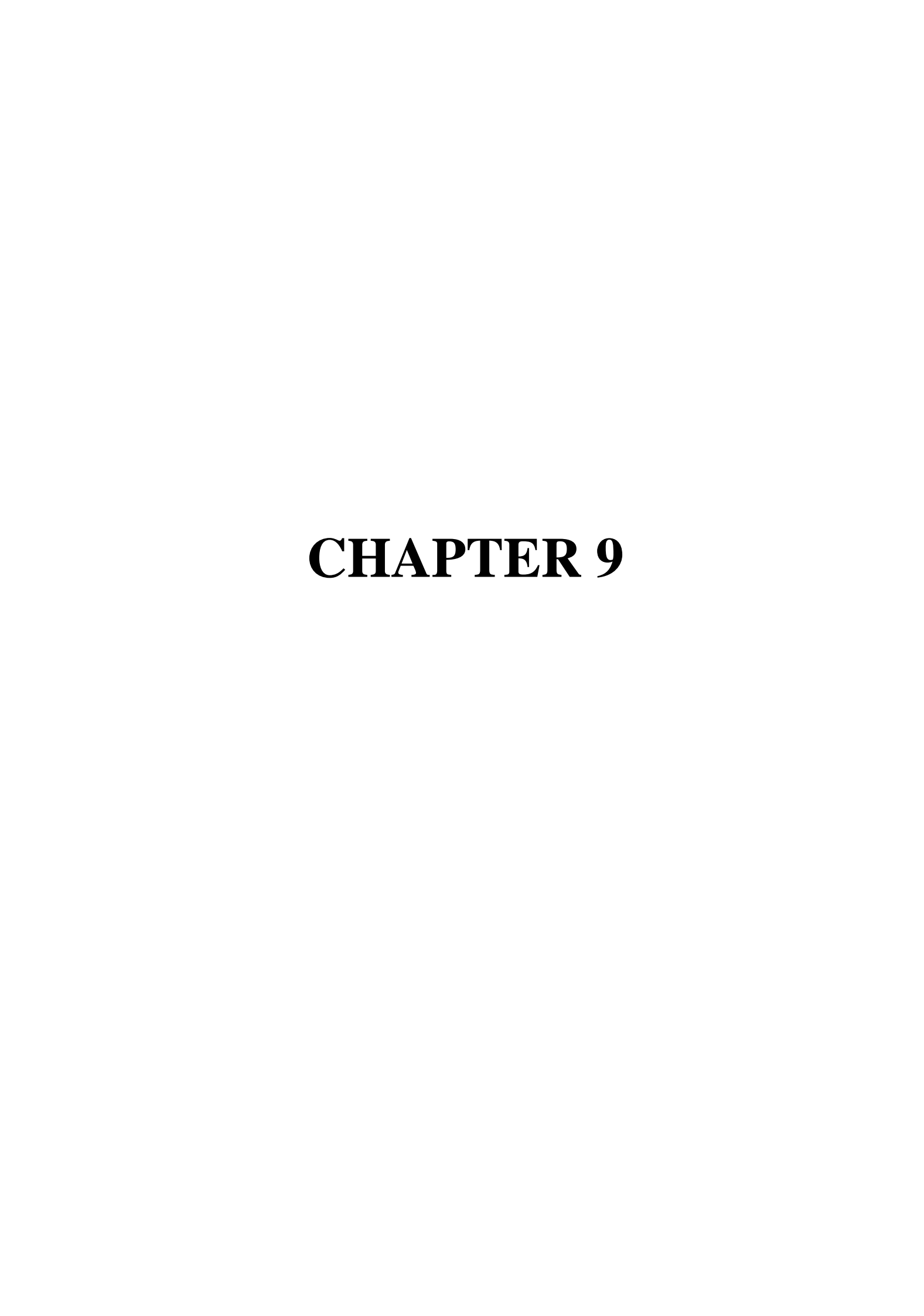












## **CHAPTER 10**

